https://doi.org/10.61092/iaea.c20j-kf6y

INDC(NDS)-0645
Distr. FE

IAEA
International Atomic Energy Agency

INDC International Nuclear Data Committee

FENDL-3 Library

Final Report of the Coordinated Research Project on

Nuclear Data Libraries for Advanced Systems: Fusion Devices

R.A. Forrest
IAEA Nuclear Data Section, Vienna, Austria

C. Kalbach Walker
Duke University, Durham, USA

M. Avrigeanu and V. Avrigeanu
Horia Hulubei National Institute for Physics and Nuclear Engineering,
Bucharest Magurele, Romania

A.V. Ignatyuk
Institute for Physics and Power Engineering, Obninsk, Russia

F. Tárkányi
Institute for Nuclear Research, Hungarian Academy of Sciences, Debrecen, Hungary

A. Trkov
Jožef Štefan Institute, Ljubljana, Slovenia

J. Kopecky
JUKO Research, Alkmaar, Netherlands

U. Fischer
Karlsruhe Institute of Technology (KIT), Germany

December 2013

IAEA Nuclear Data Section
Vienna International Centre, P.O. Box 100, 1400 Vienna, Austria

Selected INDC documents may be downloaded in electronic form from
http://www-nds.iaea.org/publications
or sent as an e-mail attachment.
Requests for hardcopy or e-mail transmittal should be directed to
NDS.Contact-Point@iaea.org
or to:
Nuclear Data Section
International Atomic Energy Agency
Vienna International Centre
PO Box 100
1400 Vienna
Austria

Printed by the IAEA in Austria

December 2013

INDC(NDS)-0645
Distr. FE

FENDL-3 Library

Final Report of the Coordinated Research Project on

Nuclear Data Libraries for Advanced Systems: Fusion Devices

R.A. Forrest
IAEA Nuclear Data Section, Vienna, Austria

C. Kalbach Walker
Duke University, Durham, USA

M. Avrigeanu and V. Avrigeanu
Horia Hulubei National Institute for Physics and Nuclear Engineering,
Bucharest Magurele, Romania

A.V. Ignatyuk
Institute for Physics and Power Engineering, Obninsk, Russia

F. Tárkányi
Institute for Nuclear Research, Hungarian Academy of Sciences, Debrecen, Hungary

A. Trkov
Jožef Štefan Institute, Ljubljana, Slovenia

J. Kopecky
JUKO Research, Alkmaar, Netherlands

U. Fischer
Karlsruhe Institute of Technology (KIT), Germany

ABSTRACT

Details of work carried out by participants of the FENDL-3 CRP are presented. The results of some of these studies have been included in the various parts of the FENDL-3 library, while other parts should be considered for any future updating and improvements of the library.

December 2013

TABLE OF CONTENTS

1. INTRODUCTION

Contents

The main deliverable of the CRP on the development of the FENDL-3 library is, by definition, the set of nuclear data that comprises the library. However, during the course of the CRP several reports and documents were generated and this report presents this work in a single document that enables the work to be preserved and properly reported. A companion report [1] provides details about the various parts of the library and the introduction from that report is reproduced with minor changes in the section below.

History of the FENDL libraries

Nuclear fusion is recognised as a long-term energy source. The IAEA has played an important role in nurturing the work on this future energy source by providing support for the exchange of scientific and technical information on fusion research through conferences, meetings and projects. The most important initiative on fusion research is currently the International Thermonuclear Experimental Reactor (ITER) project, and in order to design this and ensure safe operation a wide range of Nuclear Data information is fundamental. Realisation that the needs of nuclear data for fusion are different from those of fission meant that it was appropriate to produce a specific data library to address these needs.

The Fusion Evaluation Nuclear Data Library (FENDL) was the response of the IAEA to the need for a data library specifically designed for fusion applications. An initial meeting was held in 1989 [2] and, following the creation and testing of FENDL-1 in 1995 [3], work started on FENDL-2. This work culminated in the release of the library FENDL-2 [4] containing evaluations judged to be the best available in February 1997.

Following testing and discussion of the way forward [5], the next version (FENDL-2.1) was released in 2004 [6], and this was extensively used for ITER material studies (ITER Project Management and Quality Programme: Quality Assurance in Neutronic Analyses). It had long been recognised that the neutron fluxes achievable in ITER would not be sufficient to investigate and qualify materials for future fusion power plants, and it would be therefore necessary to construct a facility to test candidate fusion reactor materials under high neutron radiation dose conditions approximating those to be found in a fusion reactor. This facility – International Fusion Materials Irradiation Facility (IFMIF) – involves accelerating high currents (up to 250 mA) of deuterons to 40 MeV and impinging them on a liquid lithium target to produce neutrons. Deuterons that strike elements of the accelerator transport system, as well as various target materials, would induce radioactivity that needs to be considered in the safe operation of this facility as well as in its eventual decommissioning. The status of energy differential deuteron cross section data from a few MeV up to 40 MeV is considered by the IFMIF development community to be inadequate for the purposes of assessing the facility with respect to operational safety and licensing issues. In particular, the FENDL-2.1 library does not contain data for incident charged particles (e.g. protons and deuterons), while the maximum energy for incident neutrons is limited to 20 MeV.

Recognizing these difficulties in March 2006, the International Nuclear Data Committee (INDC) recommended the extension of the FENDL library to cover the nuclear data needs of the IFMIF community. A Technical Meeting aiming at identifying possible detailed objectives for a CRP was held at IAEA, Vienna, on 31 October – 2 November 2007 [7]. The CRP was approved by IAEA Research Program Advisory Committee on December 2007.

As is usual for a CRP there were three Research Coordination Meetings; [8, 9, 10] and these led to the production of the FENDL-3 library.

References for Section 1

[1] R.A. Forrest, R. Capote, N. Otsuka, T. Kawano, A.J Koning., S. Kunieda, J-Ch. Sublet, Y. Watanabe, "FENDL-3 Library – Summary documentation", INDC(NDS)-628, IAEA Nuclear Data Section, December 2012.

[2] V. Goulo, "Proceedings of the IAEA Specialists' Meeting on Fusion Evaluated Nuclear Data Library (FENDL)", INDC(NDS)-223, IAEA Nuclear Data Section, 8-11 May 1989.

[3] A.B. Pashchenko, "Summary Report on IAEA Advisory Group Meeting on Completion of FENDL-1 and Start of FENDL-2", INDC(NDS)-352, IAEA Nuclear Data Section, 5-9 December 1995.

[4] M. Herman, A.B. Pashchenko, "Report on an IAEA Advisory Meeting on Extension and Improvement of the FENDL Library for Fusion Applications (FENDL-2)", INDC(NDS)-373, IAEA Nuclear Data Section, 3-7 March 1997.

[5] R. Forrest, A. Trkov, "Summary Report of an IAEA Consultants' Meeting to Maintain FENDL Library for Fusion Applications", INDC(NDS)-451, IAEA Nuclear Data Section, 10-12 November 2003.

[6] D. Lopez Aldama, A. Trkov, "FENDL-2.1, Update of an evaluated nuclear data library for fusion applications", INDC(NDS)-467, IAEA Nuclear Data Section, December 2004.

[7] R. Forrest, A. Mengoni, "IAEA Technical Meeting on Nuclear Data Library for Advanced Systems - Fusion Devices", INDC(NDS)-525, IAEA Nuclear Data Section, 31 October - 2 November 2007.

[8] A. Trkov, R. Forrest, A. Mengoni, "Summary Report from First Research Coordination Meeting on Nuclear Data Libraries for Advance Systems - Fusion Devices (FENDL - 3)", INDC(NDS)-547, IAEA Nuclear Data Section, 2 - 5 December 2008.

[9] M.E. Sawan, "Nuclear Data Libraries for Advanced Systems - Fusion Devices (FENDL - 3) Summary report from the Second Research Coordination Meeting", INDC(NDS)-567, IAEA Nuclear Data Section, 23-26 March 2010.

[10] M.E. Sawan, "Summary Report from the Third RCM on Nuclear Data Libraries for Advanced Systems - Fusion Devices (FENDL 3)", INDC(NDS)-602, IAEA Nuclear Data Section, 6-9 December 2011.

2. Complete Phenomenological Model for Projectile-Breakup Reactions (Constance Kalbach Walker)

2.1 INTRODUCTION

One of the important goals of the FENDL-3 development project is the inclusion of deuteron-induced reactions in the data library. This will rely heavily on reaction model calculations, but general reaction model codes typically lack a model for the deuteron-breakup mechanism, which makes important contributions at almost all incident energies. The development of a robust projectile-breakup model is, therefore, an important priority for the FENDL-3 Coordinated Research Project.

Projectile breakup is here defined as the emission of a projectile fragment with a fairly narrow energy distribution peaked at an emission energy corresponding to the projectile velocity. These fragments are emitted with an angular distribution that is more sharply peaked toward forward angles than the surrounding and underlying cross section. When the undetected fragment interacts with the target nucleus, it forms a composite system that will then undergo energy equilibration. Particle emission occurring during and after that equilibration will need to be included in reaction model codes.

The question of projectile breakup, however, extends beyond deuterons. The breakup mechanism also makes significant contributions for reactions induced by ^{3}He ions and, at sufficiently high incident energies, by α-particles. Until a model for this mechanism is included in pre-equilibrium-model reaction codes, it is impossible to finalize the benchmarking of these codes for complex-particle-induced reactions. In particular, a definitive assignment of the initial particle-hole configuration in the exciton model cannot be made for complex-particle projectiles, because projectile breakup is expected to significantly reduce the amount of the total reaction cross section going into the main exciton-model equilibration calculations.

Given the importance of the projectile-breakup mechanism, both from a basic physics perspective and for energy applications, a phenomenological breakup model has been developed. It is designed for inclusion in the next release of the Triangle Universities Nuclear Laboratory pre-equilibrium reaction code PRECO and in larger, more comprehensive Hauser-Feshbach model codes such as GNASH and TALYS.

2.2 DATABASE

The model reported here was developed based on data for deuteron, ^{3}He, and α-particle breakup. This yields a more robust and global model than one developed for deuteron breakup alone, because it uncovers the dependence of the breakup reaction on the energy required to separate the projectile into its constituent fragments. Continuum energy spectra measured at a variety of forward angles in a given reaction have been collected from the literature. All of the detected fragments are charged particles, so it will be assumed that neutron fragments follow generally the same systematics as proton fragments, except, of course, that there will be no Coulomb barrier in the exit channel. The data used are summarized in Table I. Other data at lower incident energies are available for ^{3}He and α-particle projectiles, but the breakup peaks, when present, are not distinct enough to be used in this study.

In order to develop a model for projectile breakup, the breakup peak must be differentiated from the underlying continuum cross section. This involves drawing a "background" underneath the obvious breakup peak, where the background is typically the usual pre-equilibrium cross section. This separation process was carried out for all of the spectra analysed and is the greatest source of uncertainty in the present work. Even the assignment of uncertainties to the quantities extracted from the breakup peaks is a subjective process. Fortunately both the peak energies and their widths appear to be generally independent of the emission angle, so data from more than one angle can sometimes be used, thus reducing uncertainties. All analyses are carried out in the laboratory system.

TABLE I: LITERATURE DATA USED IN DEVELOPING THE PROJECTILE BREAKUP MODEL.

Proj.	E_{inc} **(MeV)**	**Targets**	**Ejectile**	**Angles**	**Ref.**
d	14.8	Al, Cu, Zr, Cd, Pt	p	12°-85°	[1]
	14.8	11 others	p	30°	[1]
	15.0	^{62}Ni, Ta	p	23°-120°	[2]
	25.5	Al, ^{62}Ni, Nb, ^{119}Sn, Ta	p	20°-120°	[3]
	27.5	^{57}Fe, ^{116}Sn	p	20°-90°	[4]
	56	Al, ^{58}Ni, ^{90}Zr, ^{118}Sn, Bi	p	9.5°-30°	[5]
	56	9 others	p	9.5°	[5]
	70	^{90}Zr, ^{208}Pb, ^{232}Th	p	20°-90°	[6]
	80	Al, ^{58}Ni	p	20°-90°	[6]
3He	70, 90, 110	^{90}Zr	d	13°-30°	[7]
	70	6 others	d	13°	[7]
	90	11 others	d	13°	[7]
	70, 90	^{90}Zr	p	13°-40°	[7]
	130	Al, Co, Nb, Au	d	7.5°-21°	[8]
α	80	Al, ^{58}Ni, ^{90}Zr	p,d	6°-26°	[9]
	80	Al	t,^{3}He	6°-26°	[9]
	140	Bi	^{3}He	13°-20°	[10]
	160	Al, ^{58}Ni, ^{90}Zr, Bi	p,d,t,^{3}He	6°-26°	[9]

2.3 CENTROID ENERGIES

The simplest estimate of the energy of the breakup peak is that it corresponds to a fragment moving at the projectile velocity, so that $E_0 = E_{inc}\ A_b / A_a$, where A_a and A_b are the mass numbers of the projectile and the detected fragment, respectively, and E_{inc} is the projectile energy in the laboratory system. The actual peak energy can be shifted from this value by Coulomb deceleration in the entrance channel and by Coulomb acceleration in the exit channel. In the case of "dissociative" breakup, where both projectile fragments continue moving forward, the requirement of supplying the projectile's dissociation energy would lower the peak energy, but experimental peak energies for both ^{3}He and α-particle breakup exclude this as being a dominant mechanism. Instead, they point to "absorptive" breakup, in which the non-observed fragment interacts strongly with the target and the observed fragment is largely a spectator. For incident α particles, this observation is confirmed by coincidence measurements [11], so absorptive breakup is here assumed to be the dominant mechanism. Thus the final expression for the peak energies is

$$E_0 = \frac{A_b}{A_a}\,(E_{inc} - C_a) + C_b \qquad (1)$$

where C_a and C_b are the Coulomb barriers in the entrance and exit channels, respectively. The barrier C_a expressed in MeV is given by

$$C_a = 1.44 Z_a Z_A / D_0 \quad (2)$$

where Z_a and Z_A are the atomic numbers of the projectile and target, respectively. A similar expression applies for C_b. Here D_0 is the effective target-projectile separation at the point of interaction and is given in femtometers.

Using the experimental peak positions for the heaviest targets (the ones with the largest Coulomb barriers), estimates of the Coulomb shifts in the peak positions have been used to extract estimates for D_0. These results have been fit with the formula

$$D_0 = r_0 A^{1/3} + 1.2 \text{ fm} \quad (3)$$

where r_0 is an effective radius parameter that depends only on the incident energy, and where the constant 1.2 fm should represent the size of the projectile. Here A is the target mass number, and r_0, like D_0, is given in femtometers. Values of $r_0 = (D_0 - 1.2 \text{ fm}) / A^{1/3}$ were extracted for each breakup channel and incident energy for which adequate data were available, and the results are shown in Fig. 1. The results for the three projectile types seem to generally follow a common trend with incident energy and can be adequately reproduced by the formula

$$r_0 = 1.2 + \frac{5}{1 + \exp(E_{inc}/30)} \quad (4)$$

where the projectile energy E_{inc} is assumed to be given in MeV. The curve in Fig. 1 corresponds to this result. It is assumed that this formula will apply to lighter targets as well, since the data uncertainties do not allow the Z-dependence of r_0 to be probed.

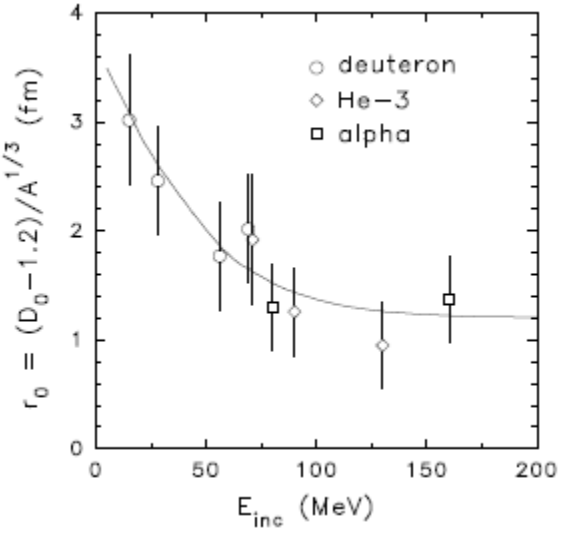

FIG. 1. Effective radius parameter for projectile breakup. The points show the values inferred from the Coulomb shifts in the energies of the breakup peaks in literature data for the indicated projectiles. In each case the results from the heaviest available target were chosen, since these have the largest energy shifts. The solid curve shows the fitted dependence given by Eq. (4). Its asymptotic value is 1.2 fm.

The systematic peak energies for (d,p), (^{3}He,d), and (^{3}He,p) breakup obtained from Eqs. (1)-(4) are shown in Fig. 2 along with the experimental values. Fig. 3 shows the same quantities for α-particle breakup.

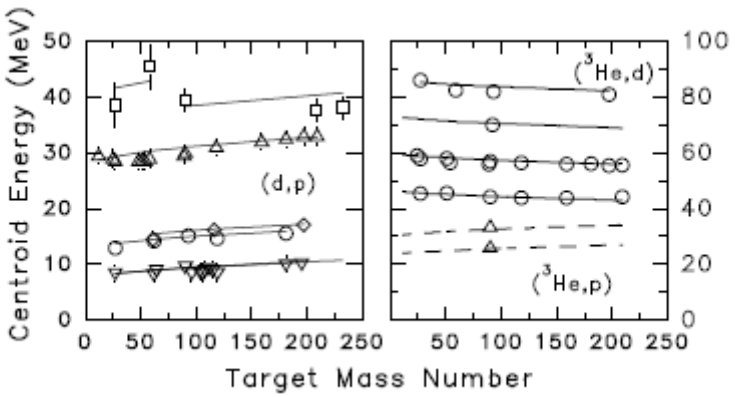

FIG. 2. Experimental peak energies for (d,p), (^{3}He,d), and (^{3}He,p) breakup. The points show the values extracted from the data, while the lines represent the systematic values obtained from Eq. (1). The incident energies for (d,p) are (from the top curve to the bottom) 80, 70, 56, 27.5, 25.5, and 15 MeV. For (^{3}He,d), the incident energies are 130, 110, 90, and 70 MeV, while for (^{3}He,p) they are 90 and 70 MeV.

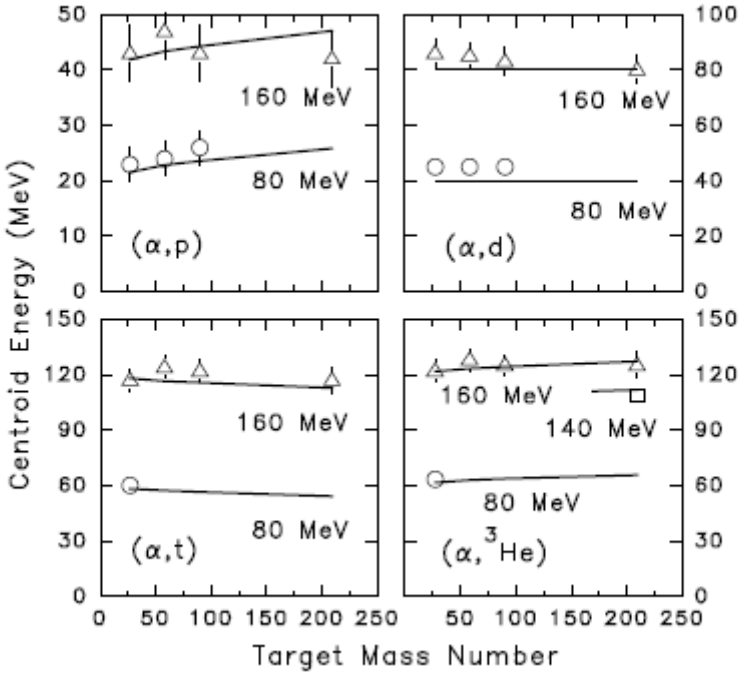

FIG. 3. Experimental peak energies for (α,p), (α,d), (α,t), and (α,^{3}He) breakup at the indicated incident energies. The points show the values extracted from the data, while the lines represent the systematic values obtained from Eq. (1).

2.4 PEAK SHAPES AND WIDTHS

2.4.1 Basic systematics

The breakup peaks are assumed to have a Gaussian shape so that the normalized energy distribution is

$$P_E(E) = \frac{1}{\sqrt{2\pi}\omega} \exp\left[-\frac{(E-E_0)^2}{2\omega^2}\right] T_E(E) \quad (5)$$

where ω is the peak width, E is the energy of the observed breakup fragment, and $P_E(E)$ integrates to unity.

The full width at half maximum (FWHM) of the breakup peaks is denoted as $F = 2.35\omega$. Values for F were estimated from spectra in the database. They appear to be largely independent of emission angle and only weakly dependent on target mass number. A workable empirical formula for this width, given in MeV, is

$$F = 62\left[1 - \frac{1}{\exp(E_{inc}/173)}\right]\left[1 - \frac{A}{155(S_{a,b})^2}\right] - 3\Theta(A_a - A_b - 1.5) \qquad (6)$$

where $S_{a,b}$ is the energy required to separate the projectile into the observed fragment b and its complement, and Θ is the Heaviside step function, which is zero for a negative argument and one for a positive argument. Both E_{inc} and $S_{a,b}$ are given in MeV. The last term in Eq. (6) lowers the FWHM for (^{3}He,p), (α,p) and (α,d) breakup relative to the channels where only a single nucleon is absorbed by the target. This difference between channels with $A_b = A_a - 1$ and those with $A_b < A_a - 1$ was unexpected but appears again in the angular distribution systematics discussed below. A comparison of widths obtained from Eq. (6) with the experimental values for (d,p), (^{3}He,d), and (^{3}He,p) breakup reactions is shown in Fig. 4. Similar results for α-particle breakup are shown in Fig. 5. Agreement is generally good except for (α,^{3}He). The discrepancies between experiment and the base systematics in the (α,^{3}He) case are due to the effect of the kinematic limit on the fragment energy, which needs to be taken into account.

In fact, the peak shapes, widths, and, in extreme cases, even their positions can all be modified by either the Coulomb barrier or the maximum-energy cutoff in the spectrum due to energy conservation. These effects have not been observed in deuteron breakup, but the maximum-energy-cut off effect plays a role in (α,t) as well as (α,^{3}He) breakup, as can be seen in the smaller empirical widths in Fig. 5. Both effects have been included in the model, as discussed in the next section.

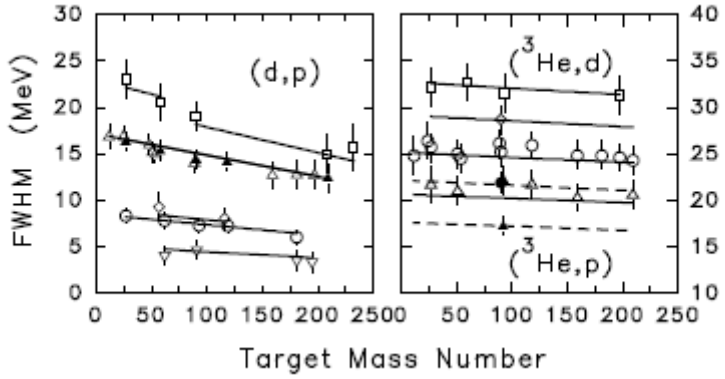

FIG. 4. FWHM for (d,p) and (^{3}He,d) breakup peaks. The points show the experimental values extracted from data in the literature, while the lines are obtained from Eq. (6). The incident energies for the (d,p) curves are (from top to bottom) 80, 70, 56, 27.5, 25.5, and 14.8 MeV. At 56 MeV, the solid points are those for the targets where data are available at a number of different detection angles. The open points show the results at 30 degrees. The incident energies for the (^{3}He,d) curves are 130, 110, 90, and 70 MeV. There are also empirical values for (^{3}He,p) breakup on ^{90}Zr at 90 and 70 MeV. These are given by the solid data points and the dashed calculated curves.

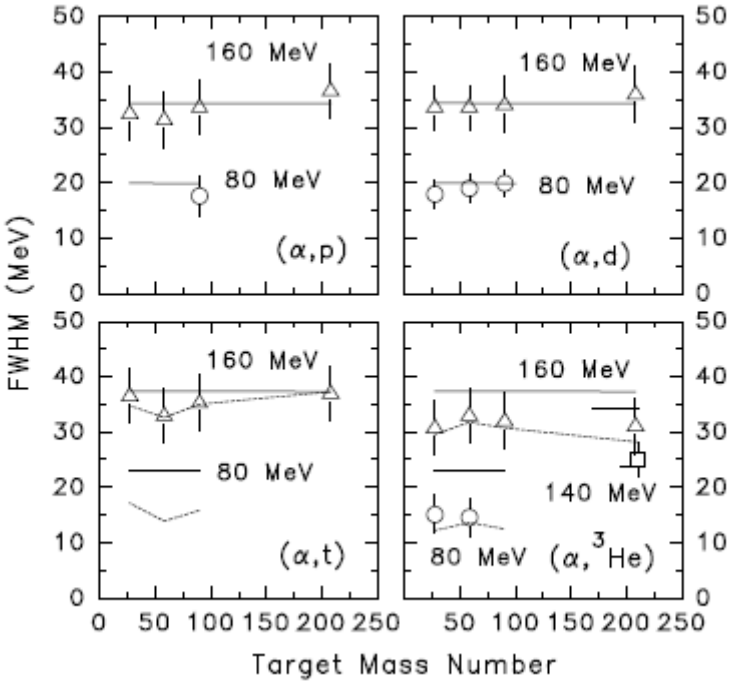

FIG. 5. FWHM for α-particle breakup peaks. The points show the experimental values extracted from data in the literature, the solid lines are obtained from the base systematics of Eq. (6), and the dotted lines include the effects of the kinematic limit on the maximum fragment energy according to Eq. (7). The calculated widths are shown for (α,t) breakup at 80 MeV even though there are no experimental values.

2.4.2 Modifications from the Maximum-Energy Cut-off and the Coulomb Barrier

Some of the (α,*t*) and (α,^{3}He) breakup peaks appear to be asymmetric, with the higher emission energy side being narrower. This is due to restrictions placed on the peak width by the kinematic limit on the energy of the observed fragment. This effect can be included in the model by leaving the peak in its normal position and using different widths for the two halves of the Gaussian distribution. If E_{max} is the maximum energy kinematically allowed and $H = F/2$ is the half width at half maximum from the base systematics, then the full width at half maximum becomes

$$F_{eff} = H + \min[H, 0.6(E_{max} - E_0)] \tag{7}$$

where the factor of 0.6 is an empirical estimate. The resulting FWHM values for the current data set are different from the base systematics only for (α,*t*) and (α,^{3}He) breakup, and the reduced values from Eq. (7) are shown as dashed curves in Fig. 5.

In more extreme cases than those observed in the current database, it is possible to have $E_{max} < E_0$, so that E_{max} becomes the new peak energy. The results for the observed asymmetric peaks have been extended to these cases in the interest of arriving at a global model. Two additional ranges of E_{max} are needed. In general, the peak shape for each range of E_{max} is characterized by the half widths at half maximum, H_- and H_+, for the half Gaussians lying below and above the peak energy E_{pk}, respectively, so that the effective FWHM becomes

$$F_{eff} = H_- + H_+ \tag{8}$$

The full prescription is summarized in Table II, where the results for the peak energy can be summarized as $E_{pk} = \min(E_0, E_{max})$.

TABLE II: EQUATIONS FOR THE HALF WIDTHS AT HALF MAXIMUM FOR THE LOWER AND UPPER HALF GAUSSIANS OF THE BREAKUP FRAGMENT ENERGY DISTRIBUTION.

Range	$\boldsymbol{H_-}$	$\boldsymbol{H_+}$	$\boldsymbol{E_{pk}}$
$E_0 + 1.67H \leq E_{max}$	H	H	E_0
$E_0 \leq E_{max} < E_0 + 1.67H$	H	$0.6(E_{max} - E_0)$	E_0
$E_0 - 1.67H \leq E_{max} < E_0$	$H - 0.6(E_0 - E_{max})$	0	E_{max}
$E_{max} < E_0 - 1.67H$	0	0	

Finally, there is the question of the exit-channel Coulomb barrier. If it is high enough relative to the energy of the breakup peak, then it could distort the peak shape, so that the equation for the Gaussian should be multiplied by a barrier penetrability factor:

$$T_E(E) = \left[1 + \exp\left(\frac{(C_b - E)}{C_b/3}\right)\right]^{-1} \tag{9}$$

where E is the energy of the observed fragment. The penetrability factor was not included in the analysis of the data to determine the systematics of the breakup peaks (position, shape or magnitude), nor did it seem to be needed, but it is tentatively included in the model.

The resulting equation for the peak shape is then

$$P_E(E) = \frac{1}{\sqrt{2\pi}\omega} \exp\left[-\frac{(E - E_{pk})^2}{2(2\omega_i)^2}\right] T_E(E) \tag{10}$$

where

$$\omega = \omega_+ + \omega_- = \frac{F_{eff}}{2.35} \tag{11}$$

$$\omega_+ = \frac{H_+}{2.35} = \frac{1}{2.35}\max\{0, \min[H, 0.6(E_{max} - E_0)]\} \tag{12}$$

$$\omega_- = \frac{H_-}{2.35} = \frac{1}{2.35}\max(0, \{H - \max[0, 0.6(E_0 - E_{max})]\}) \tag{13}$$

$$\omega_i = \begin{cases} \omega_- \text{for } E \leq E_{pk} \\ \omega_+ \text{for } E > E_{pk} \end{cases} \tag{14}$$

In the base case, in which neither the kinematic limit nor the Coulomb barrier distorts the peak shape, the energy integral over the peak shape is clearly unity, from the normalization of the plain Gaussian. When the kinematic limit on the maximum energy of the detected fragment comes into play, the use of $\omega = \omega_+ + \omega_-$ in the pre-exponential of Eq. (10) preserves the normalization to unity for peaks with a finite width. However, the Coulomb penetrability, if it is truly applicable, clearly lowers the breakup cross section.

2.5 BREAKUP ANGULAR DISTRIBUTIONS AND A-DEPENDENCE OF THE BREAKUP CROSS SECTION

Having established the emission-energy distribution of the breakup peaks, the next step is to describe the angular distribution of the detected fragments. Because this requires having data available at a significant number of angles for a given target as well as for a variety of breakup channels, incident energies and target masses, the database is more limited and the derived systematics are more tentative. Future revisions will surely be necessary.

2.5.1 Base systematics

For a given breakup channel and incident energy, the data from a variety of targets show that at each emission angle the breakup cross section is approximately proportional to $(D_0)^2$. Thus the data from different targets can be divided by $(D_0)^2$ and plotted as a function of emission angle in the laboratory system in order to study the average angular distribution systematics.

With the exception of the (*d*,*p*) breakup peaks for targets with A ≥ 90 at an incident energy of around 15 MeV, the remaining data show an angular distribution that is a negative exponential in the emission angle θ. This is shown for the 56 MeV (*d*,*p*) data in Fig. 6. Here the angle-differential cross section has been estimated from the empirical peak height and the systematic FWHM rather than by integrating the individual peaks.

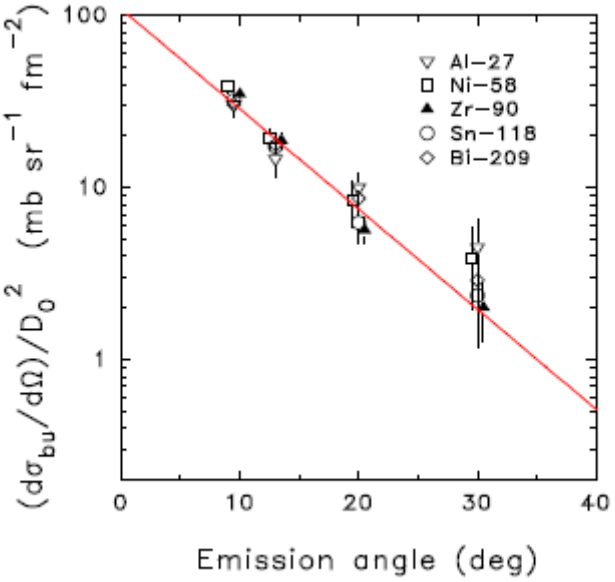

FIG. 6. Normalized angular distributions for (d,p) breakup at 56 MeV. The points show the experimental breakup cross sections divided by $(D_0)^2$ as a function of angle, while the line shows the best fit with an exponential in the emission angle.

The points in this and similar plots for different breakup channels and different incident energies were fitted with a dependence of the form

$$\frac{d\sigma_{bu}(\theta)}{d\Omega}\frac{1}{(D_0)^2} = Ke^{-a_{bu}\theta} \tag{15}$$

where K and a_{bu} were the fitting parameters. The results of this fitting are also shown in Fig. 6. The values of the angular distribution slope a_{bu} were then studied to look for systematics. Here again, as was the case for the peak widths, a difference seems to emerge between the breakup channels with $A_b = A_a - 1$ and those with $A_b < A_a - 1$. In the latter case, the angular distribution slope appears to be independent of incident and emission energy. On the other

hand, for $A_b = A_a - 1$, the results show a definite energy dependence which can be parameterized in terms of either the incident energy or the peak energy. The parameterization in terms of the peak energy, $E_{pk} = E_0$, gives a slightly better fit and is more consistent with the systematics for the underlying continuum angular distributions, which are likewise expressed as a function of the emission energy. The empirical average slope parameters a_{bu} are shown as a function of the average peak energy $\langle E_0 \rangle$ in Fig. 7. The error bars in the figure reflect only the uncertainty in the slope values assigned by the fitting program and do not include uncertainties due to background subtraction in extracting the peak heights from the experimental spectra or uncertainties in the values of $(D_0)^2$. A linear dependence of a_{bu} on the peak energy was tried first and was reported to the first FENDL-3 RCM, but data comparison with the full breakup model showed that it did not to give an accurate enough description of the data. The fitted slope parameters are given in rad^{-1} and now follow the relations

$$a_{bu} = \begin{cases} 4A_b + Z_b - 2 + 0.029E_0 + \frac{7.6}{A_a}[1 + \exp\{(12S_{ab} - E_0)/0.84S_{ab}\}]^{-1} & \text{for } A_b = A_a - 1 \\ 4.7 + A_b & \text{for } A_b < A_a - 1 \end{cases} \quad (16)$$

The results from these systematics are also shown in Fig. 7 and reproduce the general trends of the empirical values. Again, however, it must be emphasized that both the form and the parameter values were chosen to give a single, global mathematical description of current data and depend on physically reasonable reaction variables, but they must still be regarded as tentative and even somewhat arbitrary.

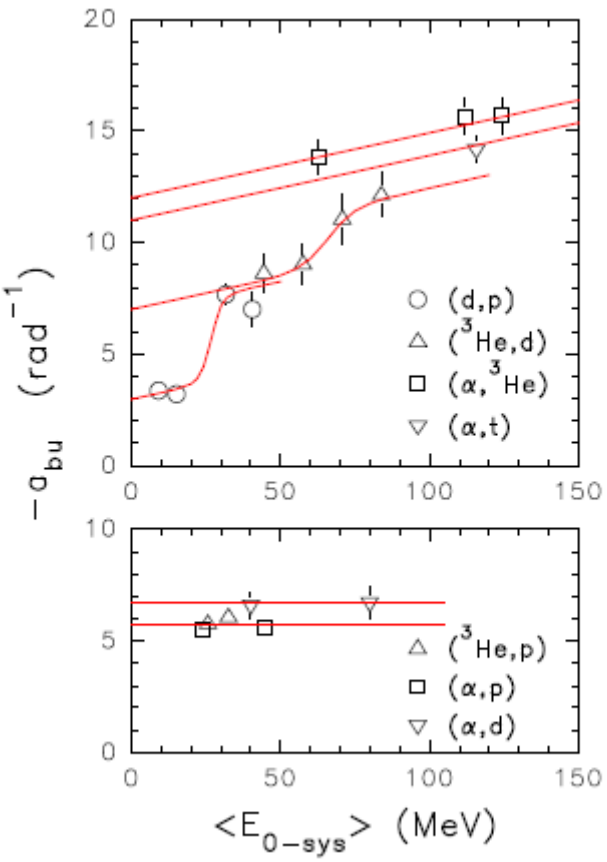

FIG. 7. Empirical values for the breakup-angular-distribution slope parameter a_{bu} as a function of the average centroid energy of the targets for which angular distributions were determined. The lines show the systematics given by Eq. (16).

2.5.2 Coulomb Dip at Forward Angles

For (*d*,*p*) breakup at around 15 MeV, the data for the heavier targets show that the angular distributions are low at forward angles, gradually increase, and then at higher angles begin to follow the normal exponential falloff with θ. The size of the dip at forward angles is correlated with the size of the Coulomb barrier relative to the incident energy. The dip has been parameterized as an angular penetrability factor multiplying the basic angular distribution of Eq. (15). The forward-angle dip does not seem to reduce the breakup cross section but simply to redistribute it to larger angles. Thus, in the presence of such a dip, the probability of emission at a particular angle θ becomes

$$P_\theta(\theta) = \frac{(a_{bu})^2+1}{2\pi}\, e^{-a_{bu}\theta} T_\theta(\theta) \tag{17}$$

$$T_\theta(\theta) = \frac{1}{I_{eff}}\left[1+\exp\left(\frac{\theta_0-\theta}{\omega_\theta}\right)\right]^{-1} \tag{18}$$

where the normalization $[(a_{bu})^2+1]/2\pi$ was included in the constant *K* in Eq. (15). Here θ_0 characterizes the angular "barrier" and ω_θ determines its width. Both are given in units of radians. The quantity I_{eff} keeps the angle integral of $P_\theta(\theta)$ normalized to unity. Values of θ_0 can be estimated for the heavier targets in (*d*,*p*) breakup at 14.8 and 15 MeV, and upper limits on θ_0 can be estimated for the lighter targets, where no dip is seen. For (*d*,*p*) breakup at higher energies and for other breakup channels, the systematics of θ_0 are not well determined, so the present results must be regarded as very tentative. For example, for (^{3}He,*d*) breakup at 70 and 90 MeV, angular distributions are available only for ^{90}Zr.

On the other hand, double-differential cross sections for these and other breakup channels are sometimes available for a series of targets at a single forward angle, and deviations for heavy targets from the usual $(D_0)^2$ dependence can provide evidence of a forward-angle dip. A rough estimate of θ_0 in such situations has been made by assuming that $\omega_\theta = \min(\theta_0/3, 0.1)$, as indicated by the (*d*,*p*) breakup trends at 15 MeV, and that the angle-integrated cross section is proportional to $(D_0)^2$. Calculations of the peak height at the experimental angle were carried out for different values of θ_0, and the factors required to normalize the calculated peak heights to the experimental values for a series of targets were estimated. For each breakup channel and incident energy, the required normalization factors were plotted as a function of θ_0 with the results for all of the targets on a single plot. The goal was to find a single normalization factor for each reaction channel and incident energy that corresponds to θ_0 values that vary smoothly in going from light to heavy targets and predicts at most a small dip for the lighter targets that show a peak cross section proportional to D_0 when no angular barrier is used in the calculations.

This kind of exercise was first carried out for (*d*,*p*) breakup at around 15 MeV, where angular distributions are available, to see how the method works. It was then applied to other reaction channels and incident energies where sufficient data were available. These are (*d*,*p*) at 56 MeV and (α,*d*) at 160 MeV, where only upper limits on θ_0 are obtained, and (^{3}He,*d*) at 70 and 90 MeV. The empirical values of θ_0 and the upper limits, given in radians, are shown in Fig. 8. They have been fitted with the relationship

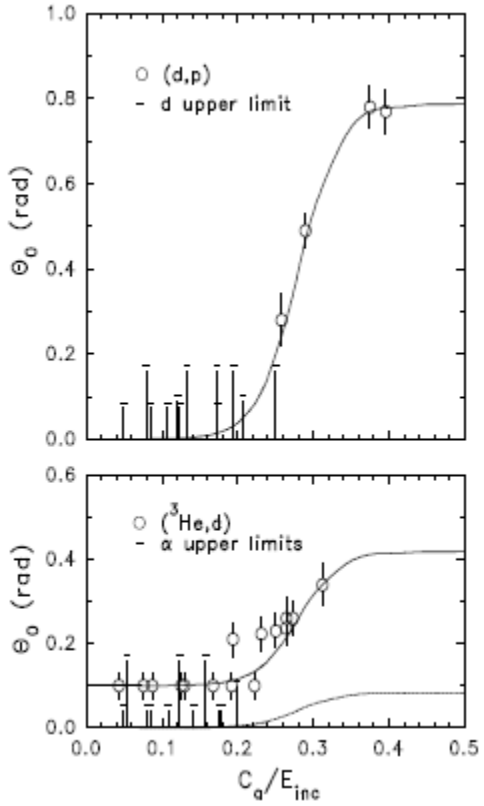

FIG. 8. Systematics of the critical angle θ_0 characterizing the forward-angle Coulomb dip in the angular distributions for the projectile-breakup cross section. The points show values extracted from the data, and the dashes with negative error bars indicate upper limits. The lines show the systematics given by Eq. (19)

$$\theta_0 \;=\; 0.1|Z_a - N_a| + \frac{1.75}{S_{ab}}\left[1 + \exp\left(\frac{0.28 - C_a/E_{inc}}{0.027}\right)\right]^{-1} \tag{19}$$

where the first term was determined largely from the low C_a/E_{inc} values for (^{3}He,*d*) breakup along with the upper limits for (*d*,*p*) breakup and α-particle breakup. The other numerical constants were the three fit parameters determined from (*d*,*p*) breakup. The $1/S_{ab}$ dependence is assumed in order to give a reasonable upper limit for (^{3}He,*d*) breakup. The values obtained from this equation are also shown in the figure. As previously noted, the width of the angular barrier has been estimated empirically from (*d*,*p*) breakup at 14.8 to 15 MeV and is given as

$$\omega_\theta = \min(0.1, \theta_0/3) \tag{20}$$

The normalization I_{eff} in Eq. (18) is defined approximately in terms of I_0, the factor for normalizing the integral when $\omega_\theta = 0$ (the sharp cutoff limit), and of the angle θ_{eff}, which, in the $\omega_\theta = 0$ limit would give the same integral as the real distribution with a finite ω_θ. These quantities are given by the relations

$$I_0 = e^{-a_{bu}\theta_0}(cos\theta_0 + a_{bu}sin\theta_0) \tag{21}$$

$$\theta_{eff} = \theta_0 + 2.35a_{bu}(\omega_\theta)^2(I_0 - 0.62) \tag{22}$$

$$I_{eff} = e^{-a_{bu}\theta_{eff}}(cos\theta_{eff} + a_{bu}sin\theta_{eff}) \tag{23}$$

The results obtained from Eqs. (17)-(23) for (*d*,*p*) breakup at 14.8 and 15 MeV are shown in Fig. 9 along with the corresponding data. The overall normalization was chosen to give a good fit to the nickel and copper data; it was not adjusted for the individual targets. If the

same equations are applied for (*d,p*) breakup at 25.5 MeV, the resulting forward angle dip occurs at angles smaller than those for which data are available, and the dip has no significant effect in reproducing the experimental angular distributions.

The results here for the Coulomb dip in the angular distributions must be regarded as very preliminary, since they have been derived and tested mainly for (*d,p*) breakup at around 15 MeV.

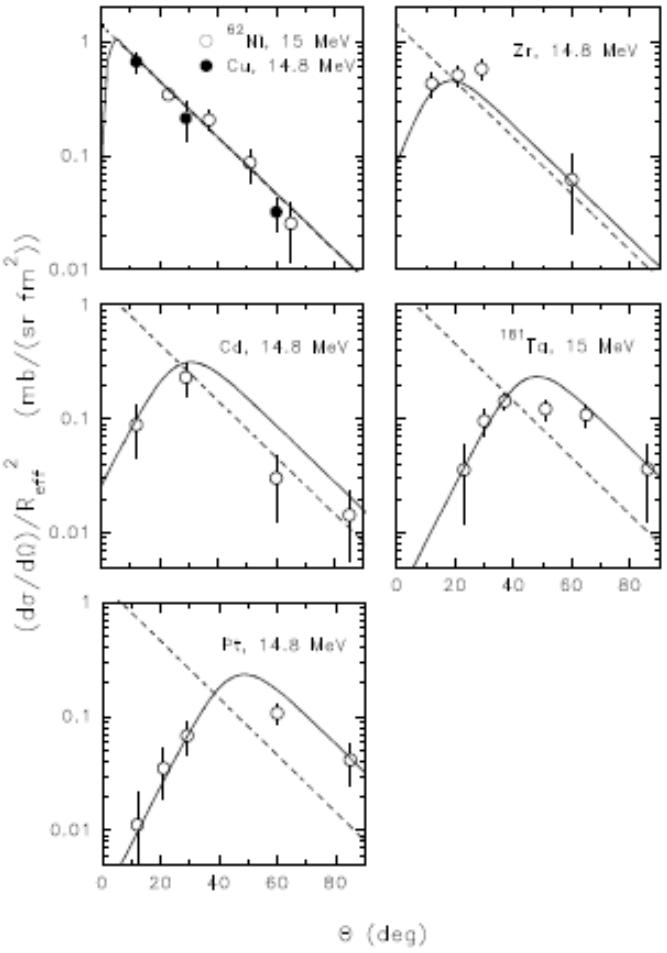

FIG. 9. Angular distributions for the (d,p) breakup peaks at incident energies of 14.8 and 15.0 MeV. The points show the results obtained from experimental spectra, the dashed curves show the results from Eq. (15), and the solid curves are obtained when the angular barriers are included using Eq. (17). All of the data at 14.8 MeV were measured on targets with natural isotopic abundance.

2.6 TOTAL BREAKUP CROSS SECTION

It has already been observed that the absolute cross section for projectile breakup at each emission energy and angle is proportional to $(D_0)^2$, the effective target-projectile separation distance at the interaction point, but the dependence on incident energy and on the specific breakup channel has yet to be determined. This can be obtained using the normalization constants from fitting the calculated angle-differential cross sections to the measured ones, using the measured peak heights and assuming the systematic values of the FWHM, as was done for the angular distributions. Dividing out the D_0 dependence, an average normalization constant for each breakup channel and incident energy can be obtained. These are shown in Fig. 10. Here the data from the database of Table I have been supplemented with three additional crude points estimated: ^{61}Ni(^{3}He,*p*) and (^{3}He,*n*) at 25.6 MeV [13] and from ^{nat}Al and ^{nat}Zr(α,n) at 140 MeV [14], which yield a single point in the figure. It should be noted,

however, that these normalization factors are strongly dependent on the angular distribution systematics, especially for those reactions in which the angular distribution falls off most rapidly with angle. Changing either the slope parameter or θ_0 can significantly change the normalization required.

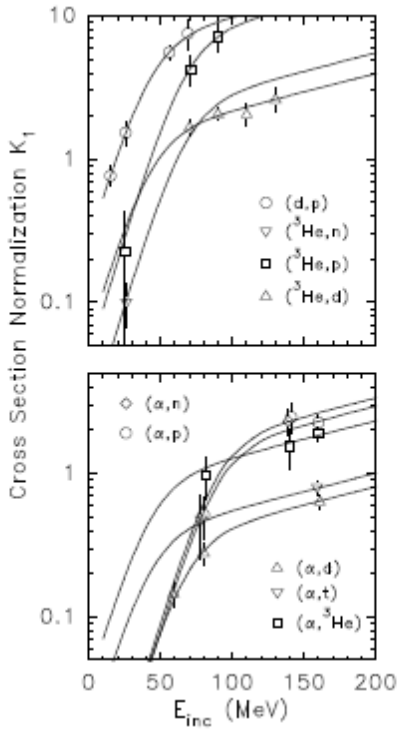

FIG. 10. Average normalization factors $\sigma_{ab}(E_{inc})/ (D_0)^2$ for the breakup peaks for the indicated breakup channels as a function of the incident projectile energy. The points show the results obtained from the experimental spectra, and the curves are obtained from Eq. (24).

Again, these results should be regarded as tentative. The most startling observation from Fig. 10 is that for each reaction channel where the data extend to high enough incident energies–(^{3}He,*d*), (α,t), and (α,^{3}He)–the breakup cross section at the higher energies seems to approach the same exponential dependence on the incident energy: This dependence has been fit using the data from these three channels. The results correspond to a dependence exp[E_{inc}/170 MeV]. At lower incident energies there is an initial barrier to be overcome. Thus the absolute breakup cross section can be written as

$$\sigma_{ab}(E_{inc}) = \mathcal{N}_{ab}(D_0)^2 \exp\left(\frac{E_{inc}}{170\ \text{MeV}}\right) T_{1/2}(E_{inc}) \qquad (24)$$

This leaves the absolute channel-specific normalization $\mathcal{N}_{ab}$ and the barrier-penetrability factor $T_{1/2}$ to be determined.

The barrier is characterized by the barrier height (the energy $E_{1/2}$ at which the penetrability $T_{1/2}$ reduces the cross section by a factor of two) and by the barrier width. A global form was sought for the function $T_{1/2}$, but the normalization factors $\mathcal{N}_{ab}$ were varied independently. Fits were performed to the (*d*,*p*), (^{3}He,*p*), (α,*p*), and (α,*d*) data assuming the asymptotic exponential dependence, while varying the parameters $\mathcal{N}_{ab}$, $T_{1/2}$, and ω_σ, the barrier width. Because the barrier is best determined for the (*d*,*p*) reactions and because the values of the width parameters were similar, the (*d*,*p*) value of ω_σ = 14 MeV was adopted, and the fits were then repeated using this fixed width in order to determine values of $T_{1/2}$. The resulting $T_{1/2}$ values were found to vary as (42 MeV)$(A_a - A_b)^{2/3}$. Fixing this value, fits to all of the breakup

channels in Fig. 10 were repeated to extract final values for the parameter $\mathcal{N}_{ab}$. The curves in Fig. 10 thus correspond to

$$T_{1/2}(E_{inc}) = \left[1 + \exp\left(\frac{E_{1/2} - E_{inc}}{14\ \text{MeV}}\right)\right]^{-1} \quad (25)$$

$$E_{1/2} = 42\ \text{MeV}\ (A_a - A_b)^{2/3} \quad (26)$$

with the $\mathcal{N}_{ab}$ values contained in Table III.

TABLE III: NORMALIZATION CONSTANTS $\mathcal{N}_{ab}$ FOR THE BREAKUP CROSS SECTION IN EQ. (24). (Values based on only one data point are given in parentheses. The indicated "sister channels" are ones for which no data were available for this analysis and whose normalization constants are assumed to be the same as those of the main channel in that row of the table.)

Breakup channel	$\mathcal{N}_{ab}$ (mb/fm^2)	Sister channel
(*d*,*p*)	5.4	(*d*,*n*)
(^{3}He,*n*)	(1.25)	(*t*,*p*)
(^{3}He,*p*)	5.0	(*t*,*n*)
(^{3}He,*d*)	1.22	(*t*,*d*)
(α,*n*)	(1.07)	
(α,*p*)	1.15	
(α,*d*)	0.32	
(α,*t*)	0.31	
(α,^{3}He)	0.73	

2.7 COMPARISONS WITH EXPERIMENT

The present model for projectile-breakup reactions was developed to describe average trends over an extended database. In addition, a Gaussian line shape was assumed and was taken to be independent of emission angle, just as the angular distribution is assumed to be independent of the energy of the detected projectile fragment. Therefore it is important to verify that the model's predictions are in reasonable agreement with measured breakup peaks for particular channels at specific incident energies and emission angles. To accomplish this, a short computer program was written to implement the model, calculating both single- and double-differential cross sections. The breakup peaks calculated in the program were compared with experimental spectra at specific angles for sample reactions. To make the comparisons, an estimate of the continuum cross section underlying the breakup peak was added to the calculated breakup cross section. Comparisons have so far been carried out only for (*d*,*p*) breakup at 15 and 56 MeV.

2.7.1 Deuteron breakup at around 15 MeV

For deuteron breakup at around 15 MeV, there are two data sets, both corresponding to the (*d*,*p*) channel, as indicated in Table I. The breakup cross section is quite low at this incident energy, making the comparisons difficult. In addition, the ^{181}Ta data from Ref. [2] were difficult to extract from the published figures because spectra for eight laboratory angles are shown, all as solid lines that cross each other in ambiguous ways above and below the main breakup peaks, thus introducing sizeable errors in estimating the continuum cross section underlying the breakup peak. The data analysis was also complicated by the presence of deuteron breakup on the detector collimator. A correction for this was made in Ref. [2] by

assuming that the 16 degree spectrum was all due to this collimator breakup and by subtracting that spectrum, scaled according to the elastic scattering intensity, from the spectra measured at other angles. However, the spectra at 120 and 170 degrees from deuteron breakup on tantalum are quite similar and show a peak at an energy close to the breakup peak. The intensity is much too high for the peaks to be due to breakup on tantalum, which should be negligible at these angles, and the peaks may represent collimator-breakup contamination. Therefore the 170 degree peak was treated as an extra background component. The data from Ref. [1] appears cleaner and the published graphs are easier to read.

Figs. 11-14 show comparisons between the calculation+background curves and the data. The agreement, while far from excellent, is reasonable given the low breakup cross section and the difficulties in estimating the underlying cross section. The most notable discrepancies are for aluminium, where the breakup cross section is particularly low; the 29 degree spectra from zirconium, where the calculations yield more intensity than the data; and the 51 degree results from tantalum, where the calculations yield less intensity. An interesting observation is that the spectra for the tantalum target, especially at 23 and 30 degrees, show signs of a second peak just slightly lower in energy than the breakup peak predicted by the general systematics. It is partly but not fully explained by the peak seen at backward angles, where breakup should be minimal, though it is possible that the contribution of this peak is greater at forward angles.

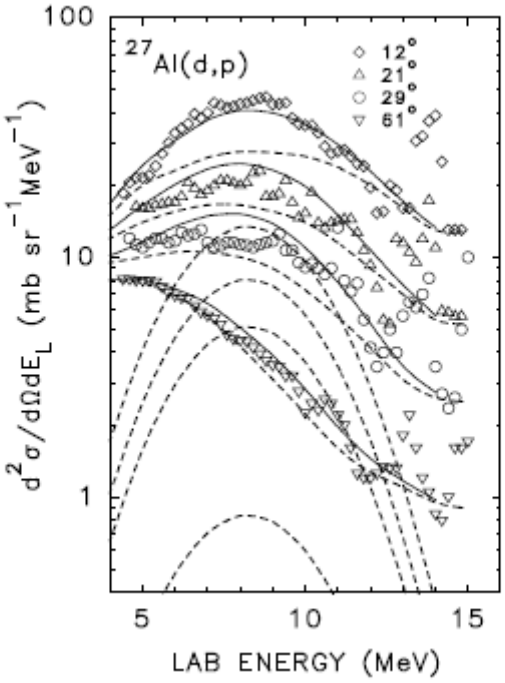

FIG. 11. Comparison of experimental and calculated double-differential breakup peaks for deuteron breakup on aluminium at 14.8 MeV. The points show the data from Ref. [1], the Gaussian-shaped dashed curves show the calculated breakup peaks, the other dashed lines show a reasonable estimate of the underlying cross section, and the solid curves show the total estimated spectra.

2.7.2 Deuteron breakup at 56 MeV

The data set at 56 MeV for (*d*,*p*) breakup [5] is particularly useful because it comprises a large number of targets, includes angles down to 9.5 degrees, and uses an incident energy in a range of interest for the FENDL-3 database. Comparisons between calculation and

experiment are shown in Figs. 15-19. The level of agreement here is, on average, significantly better than at 14.8 and 15 MeV, in part because the breakup cross section is higher, and in part because the dip at forward angles is not present as a complication. The results for the bismuth target show either a second peak at a slightly lower energy or a shoulder on the main breakup peak. This feature is not reproduced by the phenomenological model, and its origin is not understood.

2.8 REMAINING WORK

Work is continuing to complete the comparisons between the model breakup peaks and the experimental double-differential cross sections in the present database. If the results continue to be satisfactory, the new model will be incorporated into the TUNL pre-equilibrium reaction code PRECO [12], and the absorbed (or non-observed) fragment will be allowed to initiate an equilibration process as described by the exciton model. Once that coding has been completed, a larger body of full energy spectra will be analysed in order to complete the determination of the initial particle-hole configuration in the exciton model for complex-particle-induced reactions.

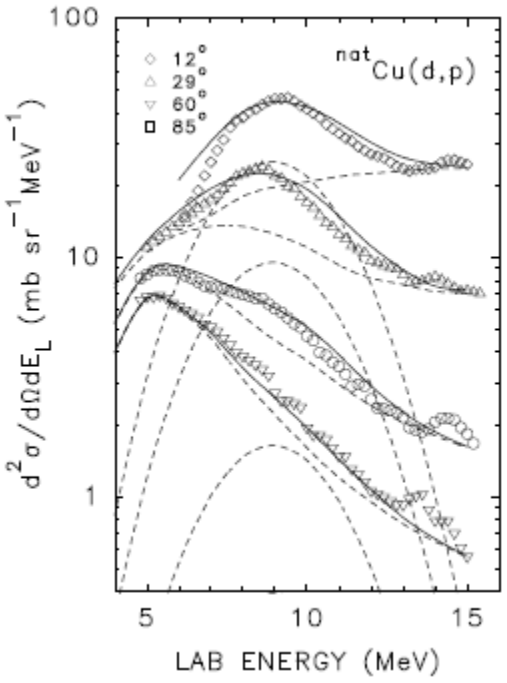

FIG. 12. Comparison of experimental and calculated double-differential breakup peaks for deuteron breakup on copper at 14.8 MeV. The points and curves have the same significance as in Fig. 11.

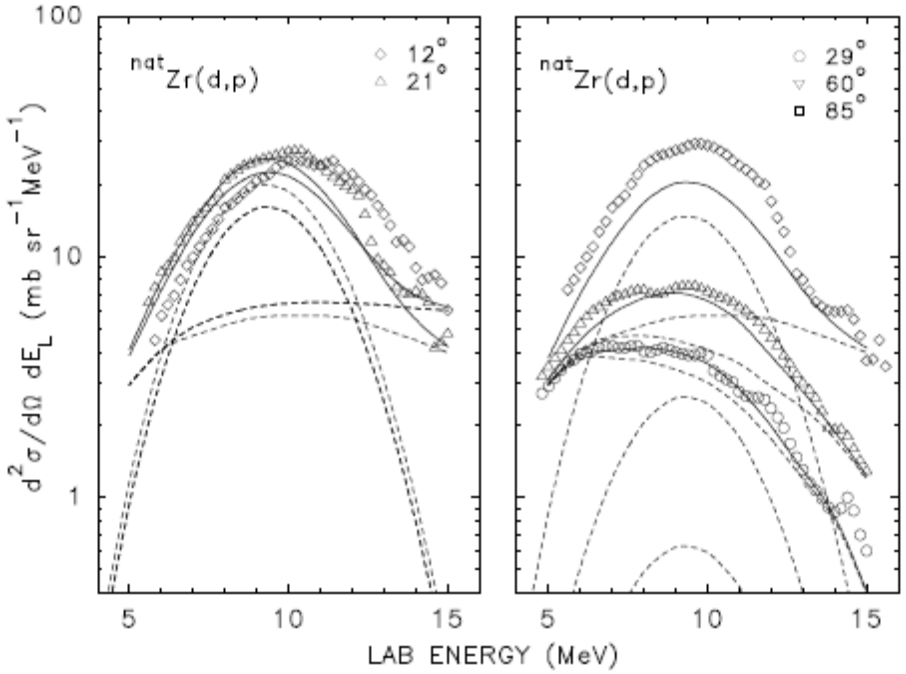

FIG. 13. Comparison of experimental and calculated double-differential breakup peaks for deuteron breakup on zirconium at 14.8 MeV. The points and curves have the same significance as in Fig. 11.

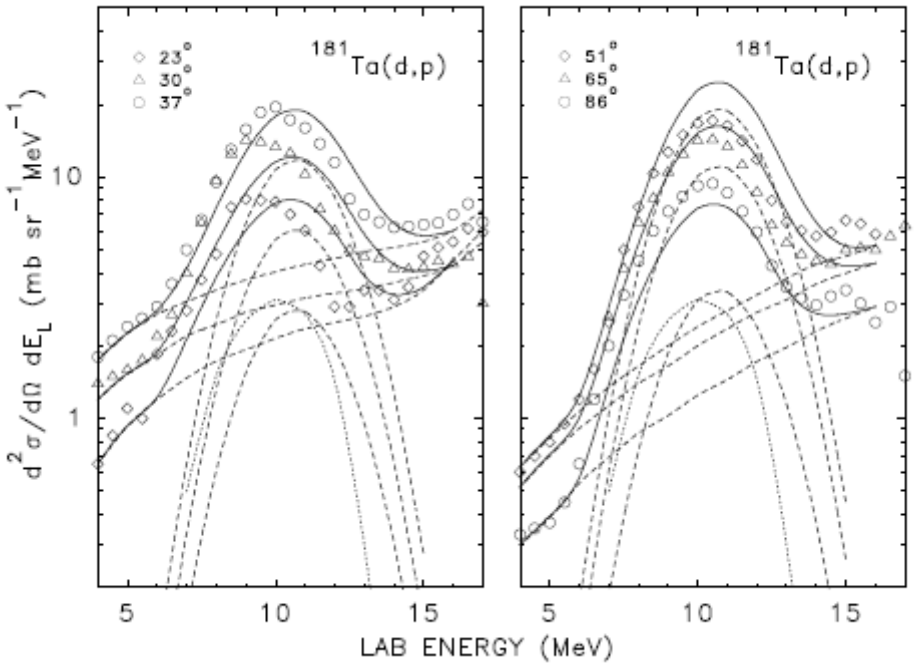

FIG. 14. Comparison of experimental and calculated double-differential breakup peaks for deuteron breakup on tantalum at 14.8 MeV. The points and curves have the same significance as in Fig. 11, except that the data are from Ref. [2], and the dotted curves show the background peak estimated from the 170 degree experimental spectrum, as discussed in the text. The data are actually in the centre-of-mass system, but for such a heavy target the differences between the laboratory and centre-of-mass systems are small.

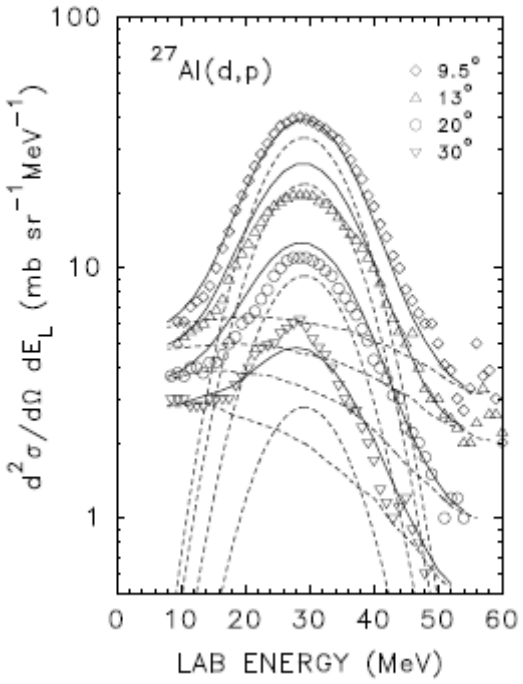

FIG. 15. Comparison of experimental and calculated double-differential breakup peaks for deuteron breakup on ^{27}Al at 56 MeV. The points show the data from Ref. [5], the Gaussian-shaped dashed curves show the calculated breakup peaks, the other dashed lines show a reasonable estimate of the underlying cross section, and the solid curves show the total estimated spectra.

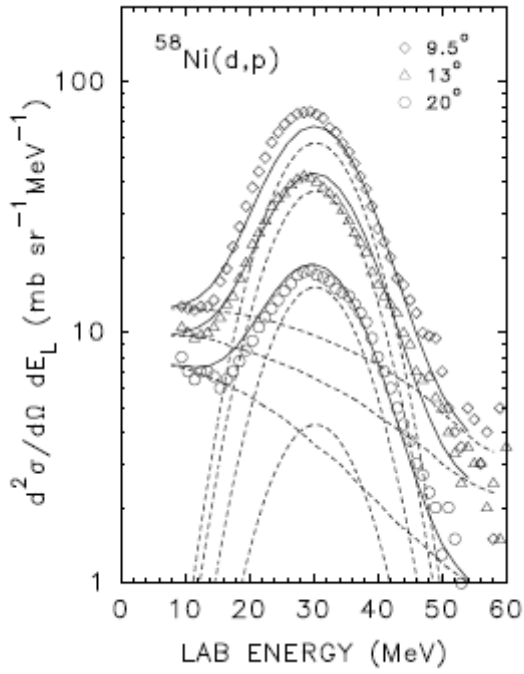

FIG. 16. Comparison of experimental and calculated double-differential breakup peaks for deuteron breakup on ^{58}Ni at 56 MeV. The points and curves have the same significance as in Fig. 15.

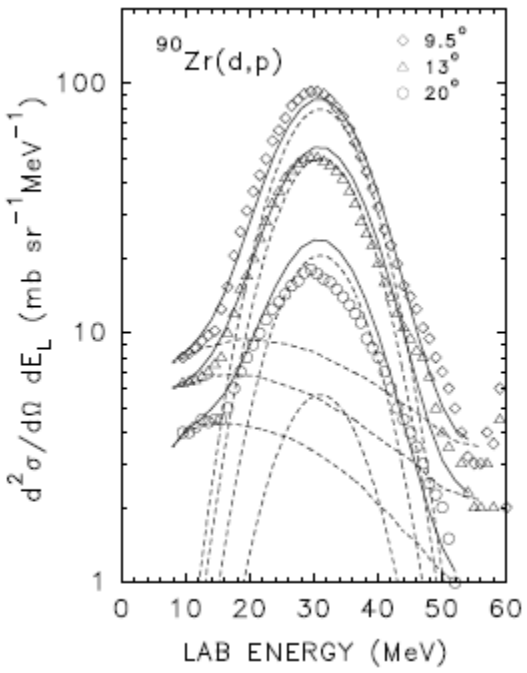

FIG. 17. Comparison of experimental and calculated double-differential breakup peaks for deuteron breakup on ^{90}Zr at 56 MeV. The points and curves have the same significance as in Fig. 15.

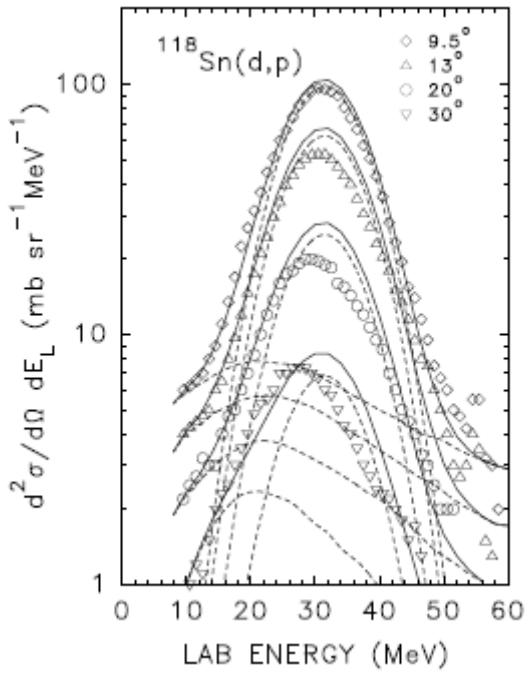

FIG. 18. Comparison of experimental and calculated double-differential breakup peaks for deuteron breakup on ^{118}Sn at 56 MeV. The points and curves have the same significance as in Fig. 15.

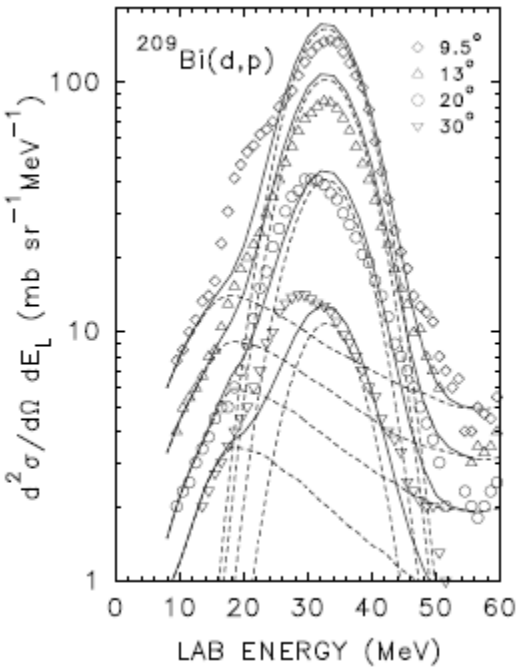

FIG. 19. Comparison of experimental and calculated double-differential breakup peaks for deuteron breakup on ^{209}Bi at 56 MeV. The points and curves have the same significance as in Fig. 15.

References for Section 2

[1] E.W. Hamburger, B.L. Cohen, R.E. Price, Phys. Rev. **121** (1961) 1143.

[2] J. Kleinfeller, J. Bisplinghoff, J. Ernst, T. Mayer-Kuckuk, G. Baur, B. Hoffmann, R. Shyam, F. Rösel, D. Trautman, Nucl. Phys. **A370** (1981) 205.

[3] J. Pampus, J. Bisplinghoff, J. Ernst, T. Mayer-Kuckuk, J. Rama Rao, G. Baur, F. Rösel, D. Trautman, Nucl. Phys. **A311** (1978) 141.

[4] A. Chavarier, N. Chevarier, A. Demeyer, A. Alevra, I.R. Lukas, M.T. Magda, M.E. Nistor, Nucl. Phys. **A237** (1975) 354.

[5] N. Matsuoka, M. Kondo, A. Shimizu, T. Saito, S. Nagamachi, Nucl. Phys. **A345** (1980) 1.

[6] J.R. Wu, C.C. Chang, and H.D. Holmgren, Phys. Rev. **C 19** (1979) 370.

[7] N. Matsuoka, A. Shimizu, K. Hosono, T. Saito, M. Kondo, H. Sakaguchi, Y. Toba, A. Goto, F. Ohtani, Nucl. Phys. **A311** (1978) 173.

[8] A. Djaloeis, J. Bojowald, S. Gopal, W. Oelert, N.G. Puttaswamy, P. Turek, and C. Mayer-Böricke, Phys. Rev. **C 27** (1983) 2389.

[9] J. R. Wu, C.C. Chang, H.D. Holmgren, R.W. Koontz, Phys. Rev. **C 20** (1979) 1284.

[10] J.R. Wu, C.C. Chang, H.D. Holmgren, Phys. Rev. Lett. **40** (1978) 1013.

[11] R.W. Koontz, C.C. Chang, H.D. Holmgren, J.R. Wu, Phys. Rev. Lett. **43** (1979) 1862.

[12] C. Kalbach Walker, "Users' Manual for PRECO-2006," unnumbered report, Triangle Universities Nuclear Laboratory, February 2007, available from the National Nuclear Data Center at Brookhaven National Laboratory, http://www.nndc.bnl.gov/nndcscr/model-codes/preco-2006/

[13] A. Chevarier, N. Chevarier, A. Demeyer, A. Alevra, R. Dumitrescu, I.R. Lukas, M.T. Magda, M.E. Nistor, Nucl. Phys. **A231** (1974) 64.

[14] A.M. Kalend, B.D. Anderson, A.R. Baldwin, R. Madey, J.W. Watson, C.C. Chang, H.D. Holmgren, R.W. Koontz, J.R. Wu, Phys. Rev. **C 28** (1983) 105.

3. Theoretical Modelling of Deuteron Elastic Scattering and Induced Activation on Light and Medium Nuclei for IFMIF EVEDA (M. Avrigeanu and V. Avrigeanu)

3.1 INTRODUCTION

Deuteron-induced reactions at low and medium energies have a great importance within several on-going strategic research programmes for international large-scale facilities such as ITER (International Thermonuclear Experimental Reactor), IFMIF (International Fusion Material Irradiation Facility), and SPIRAL-2 (System de Production d'Ions Radioactifs en Ligne - generation 2). Particularly, the Neutrons For Science (NFS) project at SPIRAL2, that involves deuteron beams, is focused on both academic research and applied physics related to neutron- as well as deuteron-induced reactions. Recent evaluations of deuteron-induced activation in the International Fusion Materials Irradiation Facility (IFMIF), e.g. [1], based on the preliminary deuteron part of the EAF library [2], show that the deuterons are more important than the neutrons by a factor of about 70 for the ratio of the deuteron– and neutron–induced activity [3]. An accurate knowledge of the deuteron activation cross sections is critical for selecting and validating the best structural materials for a number of key technologies. Thus, the IFMIF facility needs high accuracy deuteron nuclear data for estimation of the potential radiation hazards from the accelerating cavities and beam transport elements (Al, Fe, Cr, Cu, Nb) and metal and gaseous impurities of the Li loop (Be, C, O, N, Na, K, S, Ca, Fe, Cr, Ni), as well as for the assessment of induced radioactivity of the accelerator components, targets and beam stoppers in the energy range from the threshold up to 40 MeV.

Following the fact that the actual experimental and evaluated data for deuteron-induced reactions are less extensive and accurate than for neutrons, e.g. Refs. [3,4], there is now large attention paid to further measurements as well as to improved model calculations which should finally be able to describe the experimental data in order that the deuteron data libraries approach the standard of the established neutron ones.

The present IAEA Research Agreement has been devoted to theoretical modelling of deuteron elastic scattering and induced activation on light and medium nuclei, in order to provide high accuracy deuteron nuclear data for the IFMIF EVEDA by establishing the theoretical frame for deuteron activation cross sections calculations [5]. The description of deuteron-nucleus interaction represents an important test for both the appropriateness of reaction mechanism models and evaluation of nuclear data requested especially by the above mentioned research programmes. The weak binding energy of the deuteron, B = 2.224 MeV, is responsible for the high complexity of the interaction process that additionally involves a variety of reactions initiated by neutrons and protons following the deuteron breakup. This has been the reason hampering so far a comprehensive analysis involving large A-range of targets and incident-energy domain. Difficulties to interpret the deuteron-induced reaction data in terms of the usual reaction mechanism models have recently been re-investigated [6–15] searching for a consistent way to also include the breakup contribution within the activation cross section calculations.

A key ingredient of any deuteron activation cross section calculation is the deuteron optical model potential (OMP). In this respect, especially for low incident energies, e.g. below 20 MeV, there is no global optical model potential which describes the scattering data sufficiently well over a wide range of nuclei and energies [6–9,11,12,16,17]. Moreover, the very few measurements of deuteron elastic scattering angular distributions or total reaction

cross section corresponding to a target nucleus has made difficult the determination of high accuracy parameters for deuteron OMP. Consequently, a simultaneous analysis of the deuteron elastic–scattering and induced activation cross sections [6,7,11,12,17] should really involve a consistent input of nuclear model calculations [7–9], a prime interest for the optical model potential (OMP) parameters being motivated by their further use in calculations of all deuteron interaction cross sections.

Next, the usually neglected or very poorly taken into account (*d*,*p*) and (*d*,*n*) stripping as well as the (*d*,*t*) pick-up reaction contributions have been shown to be important at low incident energies [6–16], demanding an appropriate treatment within, e.g. the Coupled-Reaction Channels (CRC) formalism. Thus, the present work involves finding a deeper understanding of deuteron breakup, stripping and pick-up reactions, together and consistently with the better-known and described statistical emission.

3.2 OMP ANALYSIS

Increased accuracy of the OMP parameterization should be achieved by more elaborate analysis through a two-step approach [6,18–21]. In the first step, a semi-microscopic optical potential analysis provides the imaginary and spin-orbit parameterization, while within a second step a full phenomenological OMP can be obtained.

3.2.1 Semi-microscopic optical potential analysis

A semi-microscopic OMP may consist of the real Double Folding (DF) component, U_{DF}, phenomenological imaginary volume and surface derivative Woods-Saxon potentials, as well as a spin-orbit potential of the Thomas form [20]:

$$U(r) = V_C(r) + U_{DF}(r) + iW_V f(r, R_V, a_V) + iW_D g(r, R_D, a_D) + V_{SO}(r)\left(\frac{\hbar}{m_\pi c}\right)\mathbf{LS}\,\frac{1}{r}\frac{d}{dr}[f(r, R_{SO}, a_{VSO})] \quad (1)$$

where $V_C(r)$ is the Coulomb potential of a uniformly charged sphere of radius $R_C = r_C A^{1/3}$, and r_C=1.30 fm, $f(r, r_i, a_i) = (1 + exp[(r - r_i A^{1/3})/a_i])^{-1}$, $g(r, r_i, a_i) = -4a_i\, d/dr[f(r, r_i, a_i)]$, and $(\hbar/m_\pi)^2$ is the square of the pion Compton wavelength.

The basic formulas for calculations of the DF real component U_{DF} [22] as well as the basic model assumptions have been discussed elsewhere [18]. The direct and exchange components of the real microscopic optical potential U_{DF} are given in terms of the projectile and target nuclear densities, which are folded with the Paris M3Y effective NN interaction [23]. The knock-on exchange term of the folded potential has been calculated by using the approximation of Campi and Bouyssy [24], which preserves the first term of the expansion given by Negele and Vautherin [25] for the realistic density-matrix while the average relative momenta of nucleons are obtained from the modified Thomas-Fermi approximation of Krivine and Treiner [26] for the kinetic-energy density.

The deuteron density distribution has been obtained from the experimental charge form factors measured by Abbott *et al.* [27], and the nuclear density distribution of the target nuclei has been described by means of a two-parameter Fermi-type function with Negele's parameters [28] chosen to reproduce the electron scattering data.

Similarly to the previous studies [18,19] within our two-step OMP approach, the semi-microscopic analysis of the available experimental angular distributions of elastic–scattered deuterons provided the energy-dependent depths of the phenomenological imaginary surface W_D and volume W_V optical potential components. We have also made use in this aspect of the corresponding dispersive correction $\Delta U(r,E)$ [29] for the microscopic "parameter free" DF real potential. Concerning the spin-orbit potential, we found the parameterization of Ref. [30] quite suitable and have preserved it within the present analysis.

It should be emphasized that no adjustable parameter or normalization constant has been involved within this analysis for the real part of Eq. (1), in order to determine the phenomenological parameterization, so that the predictive power of this semi–microscopic potential is preserved. This can be seen from the comparison between the experimental [31] and semi-microscopical angular distributions for the ^{27}Al target nucleus at incident energies from 5 up to 15 MeV [31], shown in Fig. 1(a). Angular distributions calculated with Daehnick *et al.* [30] and Lohr-Haeberli [32] global OMPs are also shown. The average energy dependence of the local imaginary volume and surface potential depths of the semi-microscopic OMP are shown in Fig. 1(b), and the corresponding dispersive corrections to the real microscopic potential are shown in Fig. 1(c). The differential elastic scattering cross sections have been calculated by a modified version of the code SCAT2 [33] which includes the DF model potential as an option for the OMP real part.

3.2.2 Phenomenological OMP

In the second step of our OMP analysis [16,18,19] the microscopic real potential has been replaced by a phenomenological Woods-Saxon component. A full phenomenological OMP was then obtained by analysis of the same experimental data but keeping fixed the imaginary and spin-orbit potentials already determined. The advantage of having well settled already more than half of the usual OMP parameters obviously increases the accuracy of the data fit. The phenomenological elastic–scattering angular distributions for ^{27}Al target nucleus are shown in Fig. 1(d) and compared with the predictions of a recent global OMP [34]. The best agreement has been obtained using the energy–dependent phenomenological OMP parameter set given in Table II of Ref. [7].

Moreover, the measured total reaction cross sections [31] of deuterons have also been compared with the predictions of the present OMP, the global OMP [34], and the TALYS-1.4 code using the option of the OMP of Daehnick *et al.* [30] for deuterons. The results shown in Fig. 1(e) for ^{27}Al also support the present phenomenological OMP.

Unfortunately, such a complete deuteron potential analysis is not possible for each target nucleus of interest for deuteron activation cross sections calculations due to the still very scarce experimental data. This is the case for the ^{nat,63,65}Cu target element and nuclei [11]. In this case, due to only a few measurements of angular distributions of elastic scattered deuterons on ^{nat,63,65}Cu, the OMP analysis has been focused on the improvement of the already existing Daehnick *et al.* [30] potential. Therefore, some parameter adjustment, as shown in Table III of Ref. [11], led to a good description of the data (e.g., Fig. 2 of Ref. [11]).

3.3 DEUTERON BREAKUP EFFECTS ON ACTIVATION CROSS SECTIONS

The physical picture of the deuteron-breakup in the Coulomb and nuclear fields of the target nucleus considers two distinct processes, namely the elastic-breakup (EB) in which the target nucleus remains in its ground state and neither of the deuteron constituents interacts with it, and the inelastic-breakup or breakup fusion (BF), where one of these deuteron constituents

interacts with the target nucleus while the remaining one is detected. Under the assumption that the inelastic–breakup cross section for neutron emission σ^{n}_{BF} is the same as that for the proton emission σ^{p}_{BF}, the total breakup cross sections σ_{BU} is given by the sum (e.g., Ref. [35])

$$\sigma_{BU} = \sigma_{EB} + 2\sigma_{BF}^{n/p} \tag{2}$$

while the total neutron– and proton–emission breakup cross sections, σ^{n}_{BU} and respectively σ^{p}_{BU}, are given by

$$\sigma_{BU}^{n/p} = \sigma_{EB} + \sigma_{BF}^{n/p} \tag{3}$$

On the other hand, empirical parameterizations have been established [6] for the total nucleon–emission breakup fraction

$$f_{BU}^{(n/p)} = \sigma_{BU}^{n/p}/\sigma_R \tag{4}$$

and the elastic–breakup fraction

$$f_{EB} = \sigma_{EB}/\sigma_R \tag{5}$$

where σ_R is the deuteron total reaction cross section. These parameterizations have been obtained from an analysis of the experimental systematics [35–39] of the proton-emission spectra and angular distributions of deuteron-induced reactions on target nuclei from Al to Pb, at incident energies from 15 to 80 MeV. Their dependence on atomic Z and mass A numbers of the target nucleus, as well as deuteron incident energy E, is [6]:

$$f_{BU}^{(p)} = 0.087 - 0.0066Z + 0.00163ZA^{1/3} + 0.0017A^{1/3}E - 0.000002ZE^2 \tag{6}$$

$$f_{EB} = 0.031 - 0.0028Z + 0.00051ZA^{1/3} + 0.0005A^{1/3}E - 0.000001ZE^2 \tag{7}$$

Consequently, the inelastic breakup fraction f^{p}_{BF} is:

$$f_{BF}^{p} = f_{BU}^{p} - f_{EB} \tag{8}$$

and the corresponding nucleon inelastic–breakup cross sections, under the assumption that the inelastic–breakup cross section for neutron emission σ^{n}_{BF} is the same as that for the proton emission σ^{p}_{BF}, become

$$\sigma_{BF}^{n/p} = f_{BF}^{(n/p)}\,\sigma_R \tag{9}$$

A comparison with the total proton- and neutron-emission breakup cross-section parameterization of Kalbach [40],

$$\sigma_{BU}^{b} = K_{d,b}\frac{(A^{1/3}+0.8)^2}{1+\exp\frac{(13-E)}{6}}, K_{d,p} = 21, K_{d,n} = 18 \tag{10}$$

shows that the former parameterization [6] which considers equal breakup fractions for proton and neutron emission, additionally gives all breakup components, i.e. the total f^{p}_{BU}, elastic f_{EB}, and inelastic f^{p}_{BF} fractions.

The reaction cross sections, the total proton-emission breakup cross sections, as well as the corresponding elastic and inelastic breakup components are shown in Fig. 2 for the deuteron

interaction with ^{27}Al, ^{63,65}Cu, ^{59}Co, ^{93}Nb, and ^{231}Pa target nuclei. The importance of the breakup mechanism [6] for deuteron interaction with each nucleus is supported by the comparison of the total proton-emission breakup cross section with the corresponding deuteron reaction cross section.

The comparison of the total breakup cross sections predicted by either Avrigeanu *et al.* [6] or Kalbach [40], for deuteron interactions with target nuclei from Al to Pa, is shown in Fig. 3. Regardless of the differences between them, both parameterizations predict an increasing role of deuteron breakup with the increase of the mass/charge of target nuclei, pointing out the dominance of the breakup mechanism at deuteron incident energies below and around the Coulomb barrier of the ^{231}Pa target nucleus.

3.3.1 Phenomenological EB versus CDCC formalism

Concerning the energy dependence of the inelastic- and elastic-breakup components, the interest of the deuteron activation cross sections for incident energies up to 60 MeV has motivated an additional check [41] of the elastic-breakup parameterization extension beyond the energies considered formerly for the derivation of its actual form.

Actually, our parameterization [6] for the elastic-breakup was obtained from the analysis of the empirical systematics which cover an incident energy range from 15 to only 30 MeV. However, as it is shown in Fig. 4 for the ^{63}Cu and ^{93}Nb target nuclei, the elastic-breakup cross sections given by this empirical parameterization decrease for incident energies beyond the energy range within which it was established, while the total-breakup cross section has the opposite trend. Therefore, in the absence of available experimental deuteron elastic-breakup data at incident energies above 30 MeV, the correctness of an eventual extrapolation should be checked by comparison of the related predictions with results of a theoretical model, e.g., the Continuum-Discretized Coupled-Channels (CDCC) method [42–47].

The elastic-breakup component is treated within the CDCC formalism as an inelastic excitation of the projectile due to the nuclear and Coulomb interactions with the target nucleus. Therefore, the *d + target* scattering process is treated within a three-body model, comprising the two-body projectile and the inert target. Consideration of this inelastic excitation is performed through the coupling of the projectile unbound excited states in the solution of the scattering problem by means of the coupled channels approach. Since the deuteron has no bound excited states, any excitation in the *p-n* coordinate will break up it into a proton and a neutron. In order to deal with a finite set of coupled equations, an essential feature of the CDCC method is the introduction of a discretization procedure, in which the continuum spectrum is represented by a finite and discrete set of square-integrable functions. The most widely used method of continuum discretization is the so-called *binning* method [42,43], in which the continuum spectrum is truncated at a maximum excitation energy $E^*_{\max}$ and divided into a set of energy (or relative momentum) intervals. Each interval, or *bin*, is represented by a single square-integrable function, calculated by averaging the scattering states for the *p-n* relative motion within the bin width.

The neutron-proton bound and continuum states are modelled with a simple Gaussian interaction, fitted to the deuteron binding energy [42] and $^3S_1$ phase-shifts:

$$V_{np}(r) = -V_0 e^{-(r/r_0)^2} \tag{11}$$

where V_0 = 72.15 MeV and r_0 = 1.484 fm.

Moreover, the *p*-*n* relative angular momentum is also restricted by considering only a limited number of partial waves, in order to deal with a finite set of coupled equations. Finally, the three-body scattering wave function is expanded over the internal states of the deuteron as follows:

$$|\Psi(E)\rangle = \sum_{i=0}^{N} |\phi_i, \chi_i\rangle \tag{12}$$

where $|\phi_0\rangle$ is the ground-state wavefunction, and ϕ_i ($i \neq 0$) are the averaged (within each bin) continuum wave functions. The radial functions $\chi_i(\mathbf{R})$ describe the projectile-target relative motion for the elastic scattering ($i = 0$) and elastic breakup ($i \neq 0$) components.

The energy dependence of the elastic-breakup cross sections provided by the excitation of the continuum spectrum in the case of the deuteron interaction with ^{63}Cu and ^{93}Nb target nuclei is compared with the prediction of empirical systematics [6] in Fig. 4. The calculations were performed with the coupled-channels code FRESCO [48]. The elastic-breakup cross sections corresponding to the Kleinfeller *et al.* systematics (Table 3 of Ref. [38]) are also shown. The agreement of the CDCC elastic-breakup cross sections [41] and the latter systematics can be considered as a verification of the present advanced model approach. Moreover, the comparison shown in Fig. 4 points out that the CDCC calculations lead to elastic-breakup cross sections which follow the total-breakup cross section behaviour, and makes clear that the extrapolation of the empirical parameterization for the elastic-breakup cross sections, beyond the energies considered in this respect, should be done with caution [41].

A check of the reliability of CDCC parameters is given by a comparison between the experimental deuteron elastic-scattering angular distribution and the CDCC differential cross section corresponding to $|\phi_0\rangle$ state population [41]. The good agreement of the experimental elastic-scattering angular distributions for deuteron interaction with ^{63}Cu and ^{93}Nb target nuclei [49,50] with the CDCC calculations, shown in Fig. 5, supports the consistent CDCC parameterization.

Thus the CDCC method may help to improve the existing phenomenological approaches, and provide useful guidance for the assessment of their extrapolation accuracy. However, additional experimental deuteron data, like elastic-scattering angular distributions and inclusive neutron and proton spectra, are needed in order to validate the parameters involved in the CDCC as well as to complete the systematics of the elastic- and total-breakup cross sections over enlarged energy and target mass domains.

3.3.2 Inelastic-breakup enhancement of the deuteron activation cross sections

On the whole, the breakup process reduces the amount of the total reaction cross section that should be shared among different outgoing channels. On the other hand, the inelastic-breakup component, where one of deuteron constituents interacts with the target leading to a secondary composite nucleus, brings contributions to different reaction channels. The second–chance emission of particles from the original deuteron-target interaction is thus especially enhanced. Therefore, the absorbed proton or neutron following the breakup emission of a neutron or proton, respectively, contributes to the enhancement of the corresponding (*d,xn*) or (*d,xp*) reaction cross sections. In order to calculate this breakup enhancement for, e.g., the (*d,xn*) reaction cross sections, firstly the inelastic-breakup cross sections should be obtained by subtracting the elastic-breakup cross sections from the phenomenological total nucleon-breakup cross sections. Next, they should be multiplied by the ratios $\sigma_{(p,x)}/\sigma_R$ corresponding to the above-mentioned reactions of the absorbed proton with the target nucleus, where σ_R is the proton reaction cross section and *x* stands for various outgoing channels such as e.g. γ, *n*, *d*, or α [7–12]. These ratios have been expressed as

function of the deuteron incident energy using the Kalbach [51] formula for the peak energies of the deuteron-breakup emitted constituents in the centre-of-mass system:

$$\epsilon_{n(p)} = \frac{1}{2}(\epsilon_d - B_d \mp \frac{1.44Z}{1.5A^{1/3}+3.1}) \quad (13)$$

The inelastic-breakup contributions to the (*d,xp*) activation cross section due to the neutrons absorbed in further interactions with the target nucleus have been obtained in a similar way. The only difference was the replacement of the ratios $\sigma_{(p,x)}/\sigma_R$ by the ratios $\sigma_{(n,x)}/\sigma_{non}$, where the non-elastic cross section σ_{non} plays the same role for neutrons as σ_R for protons.

However, the assumed Gaussian line shape of the deuteron-breakup peak energies of the emitted constituents have quite large widths, showed in Fig. 6(a) for neutrons. Since the broad approximation of above method, adopted previously [7] for calculation of the breakup enhancement, a better estimation consists in a convolution of either the ratio $\sigma_{(n,x)}/\sigma_{non}$ or $\sigma_{(p,x)}/\sigma_R$ with the Gaussian line shape of the deuteron-breakup peak energies of the corresponding emitted constituent, for a given deuteron incident energy. The cases of deuterons with energies of 20, 30 and 40 MeV are shown in Fig. 6(b) together with the cross section ratio $\sigma_{(n,x)}/\sigma_{non}$. There are also shown the convolution results at each of these energies, while their area corresponds to the inelastic-breakup enhancement cross sections at every energy. Therefore, the resulting inelastic breakup enhancements due to (*n,2n*) but also of (*p,d*) interactions calculated with the convolution procedure are shown in Figs. 7a and 7b for the nuclear reaction mechanisms involved in the population of ^{58}Co and ^{92m}Nb residual nuclei through the ^{59}Co(*d,x*)^{58}Co and ^{93}Nb(*d,x*)^{92m}Nb processes respectively.

3.4 ONE-NUCLEON TRANSFER REACTIONS

Apart from the breakup contributions to deuteron interactions, an increased attention has to be paid to the direct reactions so far very poorly considered within deuteron activation analysis. For low and medium mass target nuclei and deuteron energies below and around the Coulomb barrier the interaction process proceeds largely through the direct reaction (DR) mechanism, while pre-equilibrium emission (PE) and evaporation from fully equilibrated compound nucleus (CN) also become important with the increase of the incident energy.

The appropriate calculations of the DR mechanism contributions, like stripping and pick-up, that are important at the low energy side of the (*d,p*), (*d,n*) and (*d,t*) excitation functions [6–8, 11,12,14], have been performed in the frame of the CRC formalism by using the code FRESCO [48]. The *n-p* interaction in the deuteron [42] as well as the *d-n* interaction in the triton [53] are assumed to have a Gaussian shape, while the transferred nucleon bound states were generated in a Woods–Saxon real potential [11].

Actually, the one-nucleon transfer reactions have been of critical importance for nuclear structure studies. Thus, the spectroscopic factors extracted from the analysis of experimental angular distributions of the corresponding emitted particles did contribute to the validation of the nuclear shell model. Consequently, the rich systematics of the achieved experimental spectroscopic factors makes possible the calculation of almost the total stripping and pick-up cross section contributions to the deuteron activation.

A particular note should concern the (*d,t*) pick-up mechanism contribution to the total (*d,t*) activation cross section also shown in Figs. 7a and 7b. Usually neglected in the deuteron activation cross sections calculations, the (*d,t*) pick-up process is responsible for the low-energy side of the excitation function, namely at energies between its threshold and the (*d,nd*)

and (*d,2np*) reaction thresholds that lead to the population of the same residual nucleus. In Figs. 7a and 7b these threshold energy values are given for a better understanding of the important role of the pick-up reaction in the deuteron interaction process at low incident energies. Finally, Fig. 7 may also be considered as a good example for illustrating the complexity of the deuteron interaction process involving breakup, pick-up, PE and CN reaction mechanisms.

3.5 STATISTICAL PARTICLE EMISSION

The PE and CN reaction mechanisms become important at incident energies above the Coulomb barrier. We have calculated the corresponding reaction cross sections by means of the codes STAPRE-H [54], and TALYS [55], taking into account also the breakup and DR results discussed above. Particularly, a consistent local parameter set was involved within the detailed analysis carried out using the code STAPRE-H.

The local analysis results have obviously a higher accuracy, the consistent set of statistical model parameters being validated using independent experimental data for, e.g., neutron total cross sections, proton reaction cross sections, resonance data, and gamma-ray strength functions based on neutron-capture data analysis [7,11,56]. On the other hand, no free parameters have been involved for the PE description within the generalized Geometry Dependent Hybrid model. However, a particular comment concerns the initial configuration of excited particles (*p*) and holes (*h*) for deuteron-induced reactions. Our previous analysis [7,8,11] pointed out 2*p*-1*h* initial configuration instead of the more usual 3*p*-1*h*. This point should be completely settled by further analysis of the measured and calculated cross sections obtained using various (*p,h*) configurations.

As an example of complete analysis of deuteron interactions with nuclei, the comparison of the measured and calculated activation cross sections of ^{nat,63,65}Cu + *d* [11] is shown in Fig. 8, all deuteron-induced reactions being properly described by the local consistent parameter set within the PE+CN code STAPRE-H and taking into account also the breakup and DR contributions. These results substantiate the correctness of nuclear mechanism descriptions that have been considered for the deuteron-nucleus interaction.

3.6 DIRECT INTERACTIONS IMPORTANCE

The importance of the breakup and one-nucleon transfer reaction mechanisms for the consistent analysis of the deuteron interactions with nuclei is revealed by the comparison of the experimental data and model calculations. Missing or inappropriate treatment of some reaction mechanism contributions leads to a less satisfactory description of the corresponding experimental data. We may note in this respect the underestimation of measured excitation functions of the reaction ^{nat}Cu(*d,x*)^{64}Cu by the most recent TENDL-2011 evaluated data [57], based on the TALYS code (Fig. 9). The comparison between Figs. 8(a) and 9 shows that the description of this excitation function cannot be obtained by consideration of only the PE and CN reaction mechanisms in TALYS. Its underestimation by the TENDEL-2011 evaluation points out the important role of the inelastic breakup enhancement through the ^{63}Cu(*n,γ*) capture reaction, the stripping ^{63}Cu(*d,p*), and pick-up ^{65}Cu(*d,t*) reactions.

3.6.1 Effects of neglecting stripping and pick-up

The spectroscopic studies performed by means of (*d,p*) reactions have pointed out a maximum of the stripping (*d,p*) excitation function around the deuteron incident energy of 8-

10 MeV. Therefore a consistent analysis of (*d*,*p*) processes at low incident energies has to include this mechanism on the basis of an appropriate theoretical framework e.g., the CRC method [48]. On the other hand, omission of the transfer reaction contributions to the deuteron activation cross sections can be hidden by inadequate values adopted for various model parameters. Unfortunately, this seems to be the case in a recent analysis of deuteron interactions concerning the excitation functions of the ^{45}Sc(*d*,*p*)^{46}Sc and ^{45}Sc(*d*,*t*)^{44}Sc reactions [58]. It considered the PE and CN processes by using the codes TALYS-1.2 [55] and EMPIRE [59], but ignored the stripping (*d*,*p*) and pick-up (*d*,*t*) contributions. The good description of the ^{45}Sc(*d*,*p*)^{46}Sc excitation function reported by Skobelev *et al.* [58] in such conditions has convinced us to reanalyse these reactions [60].

The results that we have obtained through a similar analysis of the ^{45}Sc(*d*,*p*)^{46}Sc reactions, involving only the PE and CN processes, are shown in Fig. 10(a). We have used in this work the whole TALYS-1.2 default input parameter set and, additionally, the adjusted value $r_{v,adj} = 1.12$ adopted in Ref. [58] for the reduced radius of the optical model (OM) volume potentials. The adjustment has been applied to both deuteron and proton OM potentials since no definite details have been given in Ref. [58] on which it should be applied. The corresponding effects led together to an increase of the (*d*,*p*) reaction cross section from ∼40% around the Coulomb barrier to less than 20% at 11.7 MeV. However, even these larger values underestimate the experimental data by a factor ranging from 2 to more than 4 at the same energies. Especially above the Coulomb barrier they are close to the content of the TENDL-2011 library [57], presented in Fig. 10(b). Conversely, these evaluated data as well as those we have calculated are smaller by a factor ∼2 with respect to the similar curve shown in Fig. 2 of Ref. [58]. As a result, the agreement with experimental data, e.g. the calculated ^{45}Sc(*d*,*p*)^{46}Sc excitation function reported in Ref. [58], cannot be replicated using input parameters reported by Skobelev *et al.*

As a matter of fact, the underestimation of the ^{45}Sc(*d*,*p*)^{46}Sc experimental data by PE and CN calculations, using the TALYS or EMPIRE codes, could be really expected due to the related absence of a suitable consideration of the direct stripping mechanism. This assumption is experimentally endorsed by population of more than 80 discrete levels up to ~4 MeV excitation energy in ^{46}Sc [63], by 7 MeV deuterons [61], as well as of ~200 discrete levels up to ~7 MeV excitation energy by 12 MeV deuterons [62]. Therefore a strong direct stripping contribution is maybe hidden by PE and CN parameters adjustment by Skobelev *et al.* in Ref. [58], but not reported in their paper.

Next, the underestimation of the (*d*,*t*) data by TALYS or EMPIRE calculations is clearly due to the omission of the direct processes contribution, this is proved by spectroscopic studies of the ^{44}Sc discrete levels strongly populated through (*d*,*t*) pick-up [64]. Actually, as has been already mentioned above, the low energy side of a (*d*,*t*) excitation function is described exclusively by the pick-up reaction mechanism as shown in Fig. 7. Nevertheless, the additional consideration of this reaction should be consistent with the unitary analysis of nuclear model predictions taking into account all available data for various reaction channels (e.g. Refs. [7,8,11–14,16,41]). Therefore the reported agreement between the experimental data and calculated results for the ^{45}Sc(*d*,*p*)^{46}Sc channel is questionable due to the apparent discrepancies for the ^{45}Sc(*d*,*t*)^{44}Sc channel shown in Fig. 2 from Ref. [58]. On the other hand, the related evaluated data shown in Fig. 10(b) as well as the present TALYS-1.2 results in Fig. 10(a) are twice larger than Skobelev *et al.* results.

3.6.2 Breakup dominance versus fission

A special point concerns the deuteron interactions with heavy nuclei, for which both breakup parameterizations of Refs. [6,40] point out the dominance of the breakup mechanism at the

incident energies below and around the Coulomb barrier, as shown in Fig. 3 for deuteron interaction with ^{231}Pa target nucleus. However, a definite dominance of the fission decay channel has been found by Morgenstern *et al.* [65] within the former ^{231}Pa(*d,3n*)^{230}U reaction cross section analysis around the Coulomb barrier. Thus, their fission cross section obtained within the EMPIRE-2 computer code assumptions [59] are quite close to the deuteron total reaction cross sections (Fig. 3 of Ref. [65]). On the other hand, they also noted that there is a significant decrease of the available compound-nucleus cross section due to the deuteron breakup, in spite of no quantitative assessment given in this respect. Nevertheless, since there are unfortunately no measured data, it is difficult to understand the quite large difference between EMPIRE and TALYS predicted (*d,f*) reaction cross sections [15].

Concerning the breakup mechanism dominance, it has been determined that future calculations of deuteron activation cross sections have to take into account both the huge leakage of initial flux toward the breakup process, as well as the inelastic breakup enhancement caused by the breakup nucleon interactions with the target nucleus. These opposite-effect contributions of the breakup mechanism are shown in Fig. 11(b) for the ^{231}Pa(*d,3n*)^{230}U reaction.

In order to emphasize the two distinct BU effects, we have not used the BU–inclusion option of TALYS by means of the Kalbach Walker parameterization [40] which give only the total proton- and neutron-emission breakup cross-sections, but not elastic and inelastic breakup components. Thus, we have obtained firstly the pre–equilibrium (PE) and CN contributions to the (*d,3n*) reaction cross sections, under the assumption of no breakup process (dash-dot-dotted curve in Fig. 11(b)). Then the BU reduction of these results was addressed by using a reduction factor $(1 - \sigma_{BU}/\sigma_R)$ of the deuteron total reaction cross section, shown in Fig. 11(b). The (*d,3n*) reaction cross sections obtained in this way are now in good agreement with the measured data just above the effective reaction threshold while formerly these data were also greatly overestimated. However, an underestimation by a factor up to 3 at E∼20 MeV becomes visible in Fig. 11(b). Nevertheless, the description of the reaction cross sections at the low energies may validate the PE and CN model parameters used in these calculations. Therefore, we used the RIPL-3 [67] recommendation for the deuteron optical potential of Ref. [34], the nucleon optical potentials for actinides [68] from the RIPL 2408 and RIPL 5408 potential segments [67] for neutrons and protons, respectively, the microscopic level densities of Hilaire *et al.* [69], and the WKB approximation for the fission path model [70].

Secondly, we aim to account for the inelastic breakup (BF) enhancement due to one of the deuteron constituents that interacts with the target nucleus and leads to a secondary CN, with further significant contributions to various deuteron-induced reaction channels. In the present case the absorbed proton, following the breakup neutron emission, contributes to the enhancement of the ^{230}U activation cross section through the ^{231}Pa(*p,2n*)^{230}U reaction.

In order to calculate this breakup enhancement of the ^{231}Pa(*d,3n*)^{230}U reaction, the nucleon BF cross section σ_{BF}^{n} [15] was multiplied by the convolution of the ratio $\sigma_{(p,2n)}/\sigma_{(p,R)}$ with the Gaussian distribution of the breakup–proton energies corresponding to a given incident deuteron energy, Eq. (11). The former as well as the latter quantities for three deuteron incident energies are shown in Fig. 11(a). The areas of the related convolution results correspond to the BF enhancement of the (*d,3n*) reaction cross sections at the given deuteron energies. The energy dependence of this BF enhancement of the ^{231}Pa(*d,3n*)^{230}U activation cross section is shown by the dot-dashed curve in Fig. 11(b), while the corresponding total activation of ^{230}U is finally compared with the experimental data [65]. The realistic treatment of the BF enhancement by taking into account the quite large widths Γ of the breakup–proton

energy distributions (see the upper insertion in Fig. 11(a)), has led to a rather accurate description of data. Further improvements of the breakup analysis may provide a better account of the related energy dependence.

3.7 CONCLUSIONS

The main goal of the present work, the subject of the IAEA Research Agreement No. 14996/RO on "Theoretical Modelling of Deuteron Elastic Scattering and Induced Activation on Light and Medium Nuclei for IFMIF EVEDA", has been to establish a theoretical framework for a unitary analysis of the nuclear reaction mechanisms responsible for the deuteron interactions with nuclei: elastic scattering, breakup, stripping, pick-up, pre-equilibrium and statistical emissions. Such an analysis is required by the complexity of the deuteron interaction with nuclei which has triggered various weak approximations widely used so far. Thus, there are still notable deuteron-induced reaction studies that took into account only the statistical emission and eventually a 'reduction factor' of the compound nucleus cross section due to direct processes. However, this reduction factor does not allow the distinction between processes such as the breakup and stripping mechanisms that lead to quite different energy ranges of the consequently emitted particles, the inelastic breakup enhancement to various reaction channels also being totally ignored. Therefore, only the appropriate consideration of the DR makes possible the description of the low incident energies side of the excitation functions corresponding to channels which include stripping or pick-up mechanisms in addition to PE+CN mechanisms. On the other hand, consideration of the deuteron breakup plays a key role for the reaction channels with a second and third emitted particle added to the first one. Thus, in order to obtain a complete description of the (*d,xp*) or (*d,xn*) reaction cross sections, it should also take into account the neutrons/protons which, following the breakup protons/neutrons emission, are absorbed in further interactions with the target nucleus.

As a consequence there is a need for a detailed theoretical treatment of each reaction mechanism contribution in order to obtain a reliable understanding of the interaction process as well as accurate values for the calculated deuteron activation cross sections. Moreover, the comparison of the experimental deuteron activation cross sections with our nuclear model calculations as well as with the corresponding TENDL-2011 evaluations motivates a detailed theoretical treatment of the deuteron interaction process. Firstly, the overall agreement between the measured data and model calculations verifies the theoretical framework associated to deuteron interaction process but also to each reaction mechanism involved in the deuteron-target nucleus interaction. On the other hand, there are shown in Figs. 12, 13, and 14 obvious discrepancies between the experimental data and corresponding TENDL-2011 evaluations. These discrepancies are the result of overlooking the inelastic breakup enhancement, as well as of an inappropriate treatment of the stripping and pick-up processes.

However, the associated theoretical frames for stripping, pick-up, PE and CN are already settled, while increased attention should be paid to the breakup mechanism concerning its theoretical description including the inelastic component. Moreover, the improvement of the deuteron breakup description requires also complementary experimental studies of, e.g., the (*d,xn*) and (*p*,(*x* − 1)*n*), or (*d,xp*) and (*n*,(*x* − 1)*p*) reaction cross sections for the same target nucleus and within correlated incident–energy ranges [65,66]. Furthermore, the associated inclusive neutron and proton spectra measurements that allow the distinction among various contributing mechanisms are also highly requested, as well as (*d,pf*) angular correlations,

when the deuteron induced fission process is analysed. Of course the suitability of the breakup empirical parameterizations could thus be checked and updated.

Given the increased interest for deuteron interaction process not only for applied purposes but also for fundamental research as surrogate reaction studies, e.g. Ref. [71], the usefulness of detailed theoretical and experimental investigations of the breakup of weakly bound projectiles including deuterons is obvious.

Acknowledgments

This work was partly supported by a grant of the Romanian National Authority for Scientific Research, CNCS UEFISCDI, project number PN-II-ID-PCE-2011-3-0450.

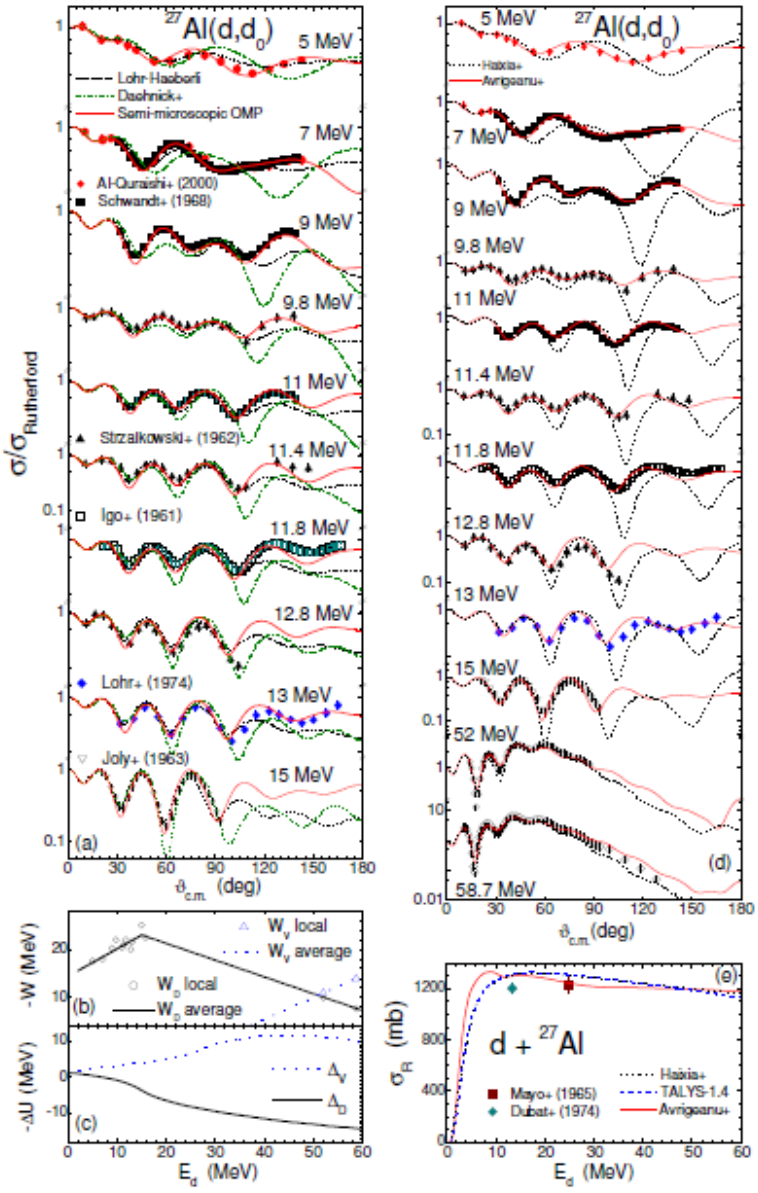

FIG. 1. Optical model potential analysis of the deuteron interaction with ^{27}Al [6] (see text for more details).

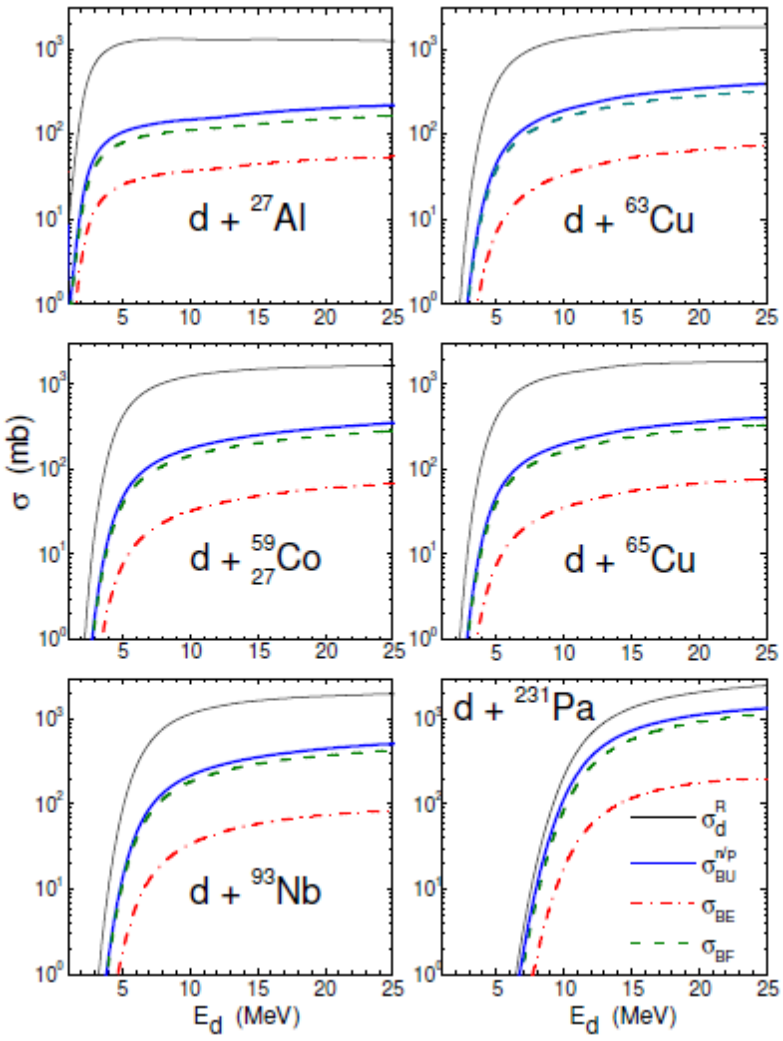

FIG. 2. The energy dependence of the total (thick solid curves), elastic (dot-dashed curves), and inelastic (dashed curves) proton-emission breakup cross sections [6] for deuteron interaction with ^{27}Al, ^{63,65}Cu, ^{59}Co, ^{93}Nb, and ^{231}Pa target nuclei, while the deuteron total reaction cross section σ_R is shown by thin solid curves.

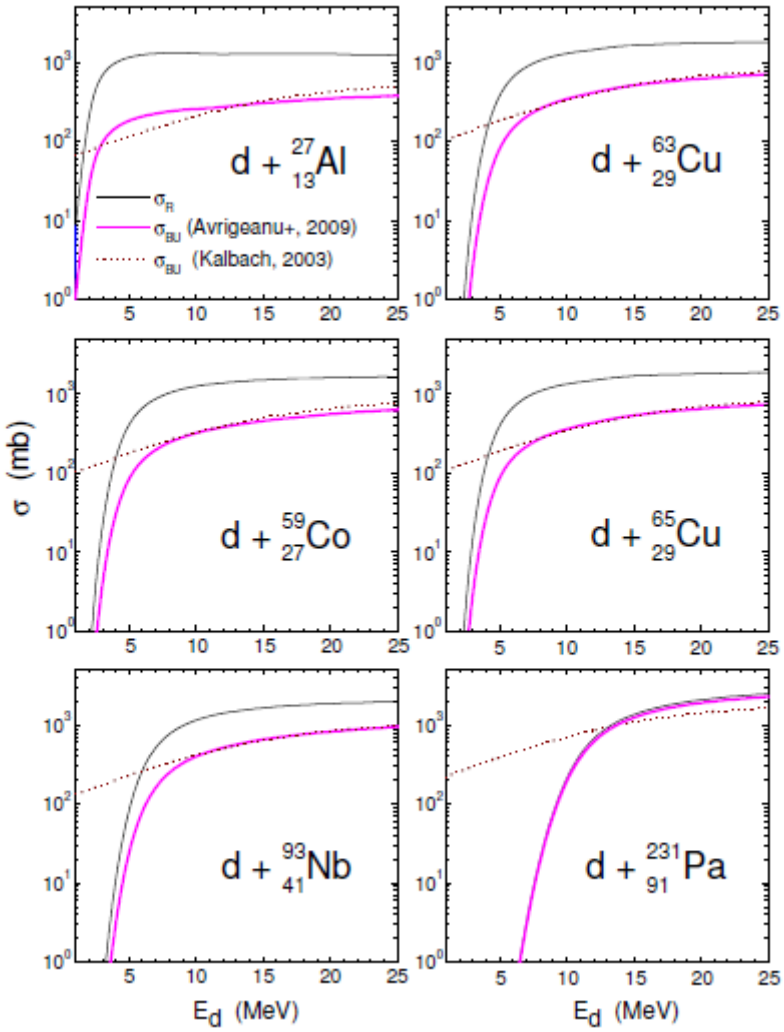

FIG. 3. The energy dependence of the total breakup cross sections given by Avrigeanu et al. [6] (solid thick curves) and Kalbach [40] (dotted curves) parameterizations for deuteron interactions with ^{27}Al, ^{63,65}Cu, ^{59}Co, ^{93}Nb, and ^{231}Pa target nuclei, while the deuteron total reaction cross section σ_R is shown by thin solid curves.

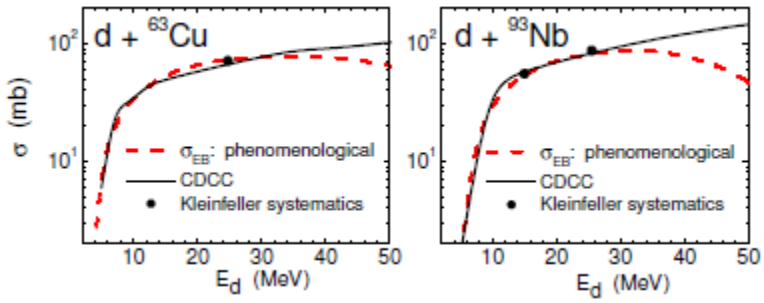

FIG. 4. Energy dependence of the empirical [6] (dashed curves) and CDCC [41] (solid curves) elastic breakup cross sections for deuteron scattering on ^{63}Cu and ^{93}Nb target nuclei. The solid circle is the value from Kleinfeller systematics [38].

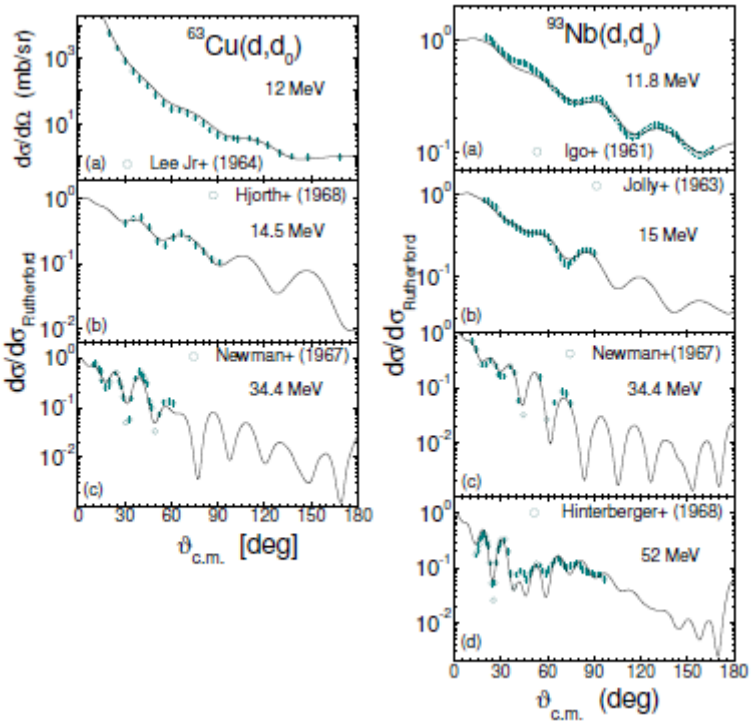

FIG. 5. Comparison of measured and calculated (CDCC) angular distributions of deuteron elastic scattering on (a) ^{63}Cu at E_d = 12, 14.5, and 34.4 MeV [49], and (b) ^{93}Nb at E_d = 11.8, 15, 34.4, and 52 MeV [50].

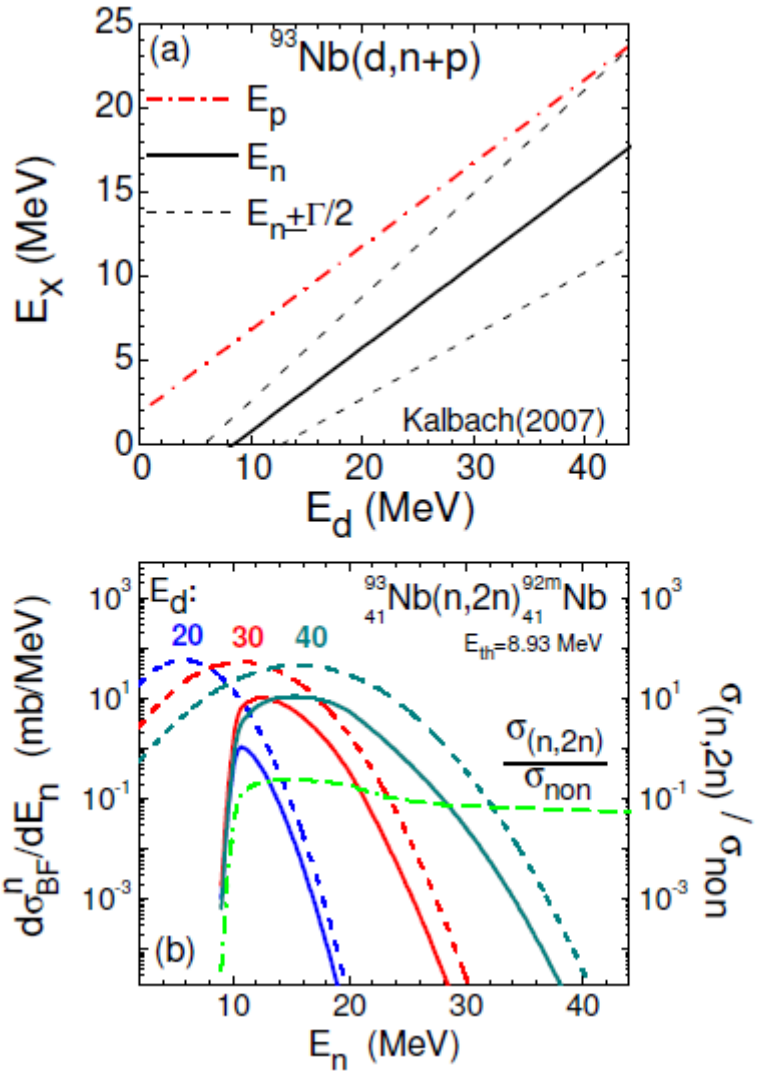

FIG. 6. (a) The centroid E_x of assumed Gaussian line shape [51] for deuteron–breakup peak energies of emitted neutrons (solid curve) and protons (dash-dotted curve), and the corresponding $E_n \pm \Gamma/2$ values (dashed curves) calculated for deuterons interacting with ^{93}Nb nucleus. (b) The convolution of the cross section ratio $\sigma_{(n,2n)}/\sigma_{non}$ for the target nucleus ^{93}Nb (dash-dotted curve) with the Gaussian line shape of the deuteron-breakup peak energies of the corresponding emitted neutrons, for deuterons with energies of 20, 30 and 40 MeV, as noted on their top, (solid curves), and the convolution results at each deuteron energy (dashed curves).

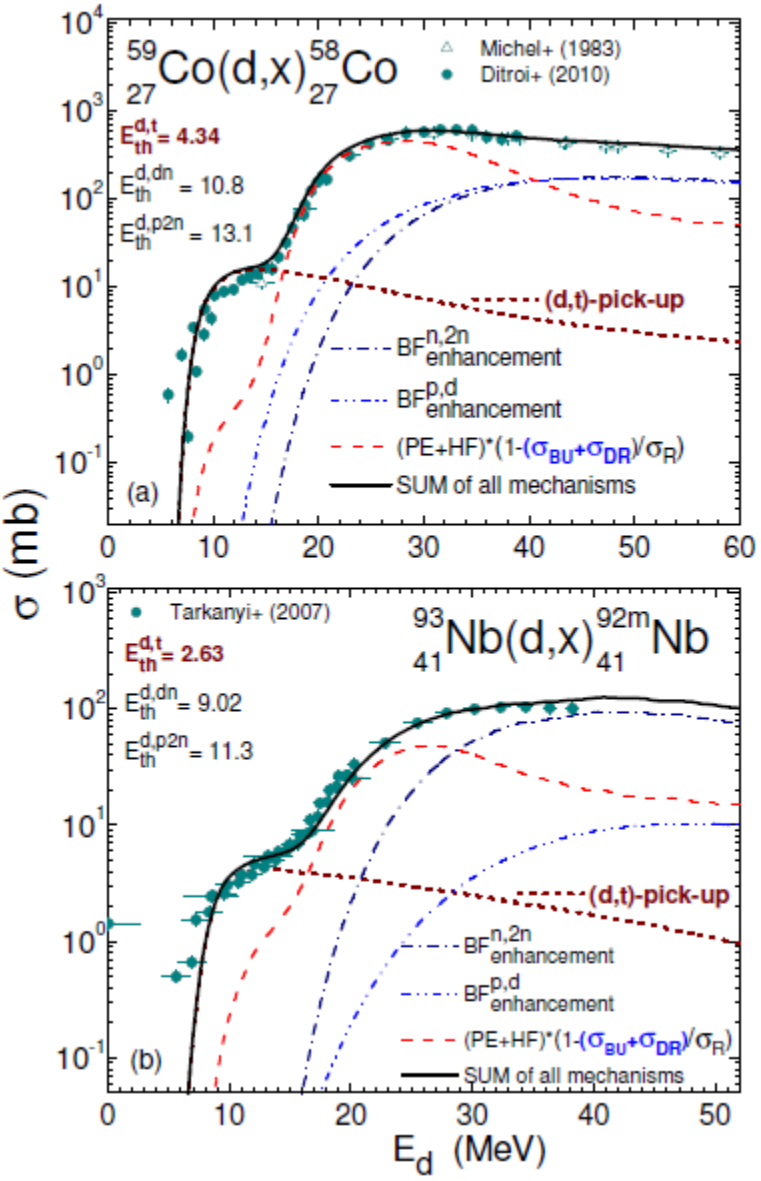

FIG. 7. Comparison of measured data [52] for deuteron interactions with the ^{59}Co (a) and ^{93}Nb (b) target nuclei, and complete analysis results (solid curves) [14] taking into account the deuteron inelastic breakup enhancement through (n,2n) (dot-dashed curves) and (p,d) (dot-dot-dashed curves) reactions, the (d,t) pick-up reaction (dotted), and the PE+CN (dashed curves) contributions to the activation of ^{58}Co and ^{92m}Nb residual nuclei. Various reaction threshold energies (E_{th})) are given in MeV.

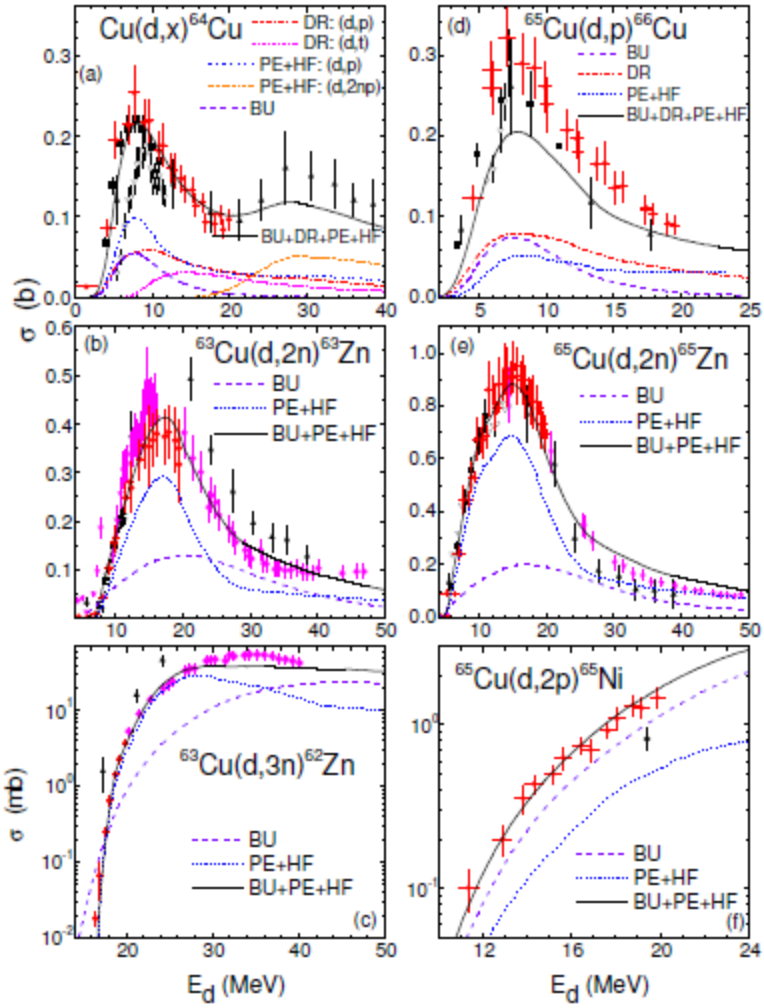

FIG. 8. Comparison of measured data (see [11] and references therein) and complete analysis results (solid curves) taking into account the deuteron inelastic breakup (dashed curves), DR for the (d,p) reactions (dash-dotted curves) and (d,t) reaction (short dash-dotted curve), and PE+CN corrected for initial deuteron flux leakage through breakup and DR processes (dotted and short-dotted curves for (d,2np) reaction) mechanism contributions to the deuteron interactions with ^{nat,63,65}Cu target nuclei [11].

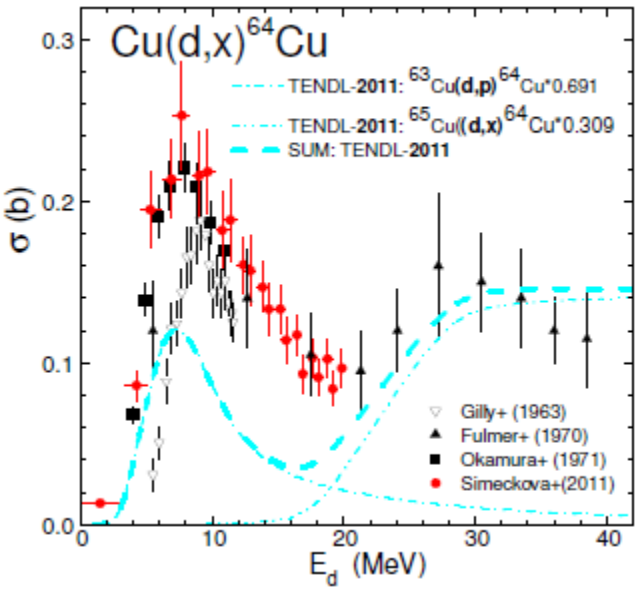

FIG. 9. Comparison of measured excitation function of the reaction ^{nat}Cu(d,x)^{64}Cu (see [11] and references therein) and the TENDL-2011 evaluated data [57] (dashed curve) taking into account the contributions from both ^{63}Cu (dot-dashed curve) and ^{65}Cu (dot-dot-dashed curve) target nuclei to the ^{64}Cu residual nucleus activation.

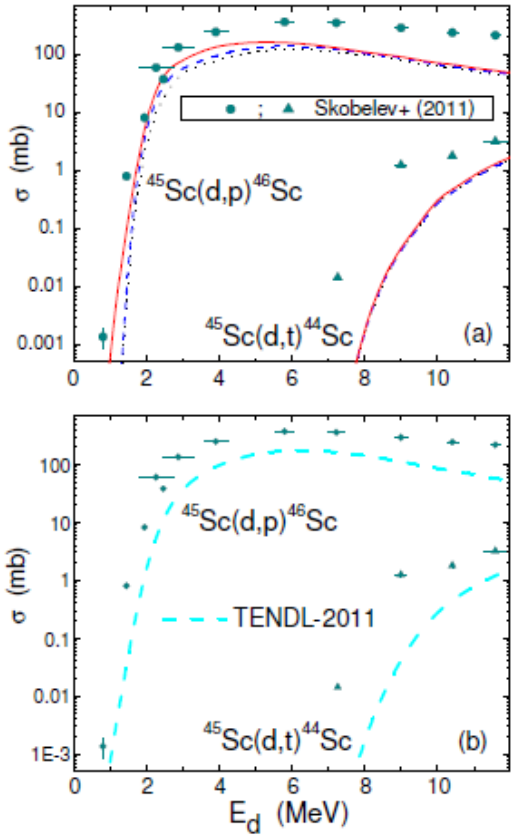

FIG. 10. Comparison of measured excitation functions for the reactions ^{45}Sc(d,p)^{46}Sc (dots) and ^{45}Sc(d,t)^{44}Sc (triangles) [58], and either (a) the calculated results obtained by using the code TALYS-1.2 [55] with default input parameters (dotted curves) as well as adjusted [58] OMP for deuterons (dashed curves) as well as for deuterons and protons (solid curves), or (b) the corresponding TENDL-2011 evaluated data [57] (dashed curves).

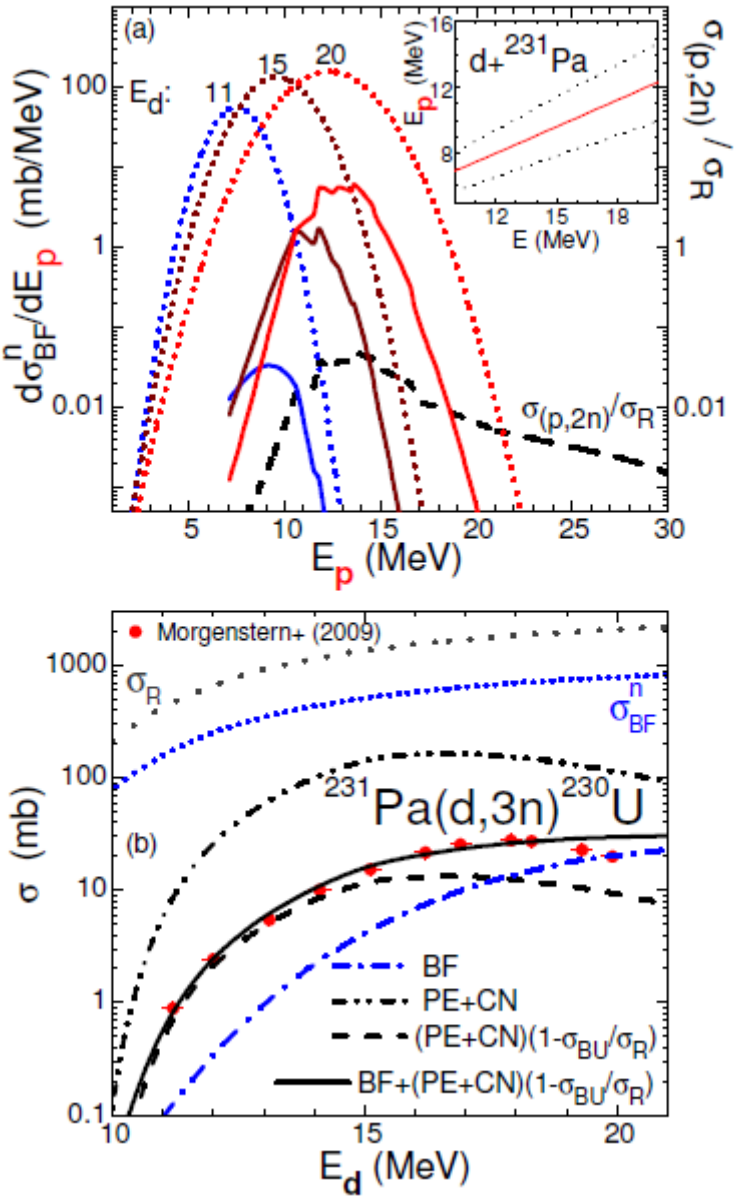

FIG. 11. (a) Results (solid curves) of the convolution of the cross section ratio $\sigma_{(p,2n)}/\sigma_{(p,R)}$ for the target nucleus ^{231}Pa (dashed) with the Gaussian distribution (dotted) of breakup–protons energies for deuterons on ^{231}Pa at incident energies of 10, 15 and 20 MeV noted on their top; in the insert: centroid of the Gaussian distribution of breakup–protons energies [51] versus the deuteron incident energy (solid curve) on ^{231}Pa, and the related $E_p \pm \Gamma/2$ values (dashed). (b) Detailed analysis of ^{231}Pa(d,3n)^{230}U reaction: the deuteron total reaction cross sections (dotted), nucleon inelastic–breakup cross section (short dotted), BF enhancement (dash-dotted), and the (d,3n) reaction cross sections calculated without (dash-dot-dotted) and with (dashed) inclusion of the BU effect on σ_R, as well as of the BF enhancement (solid).

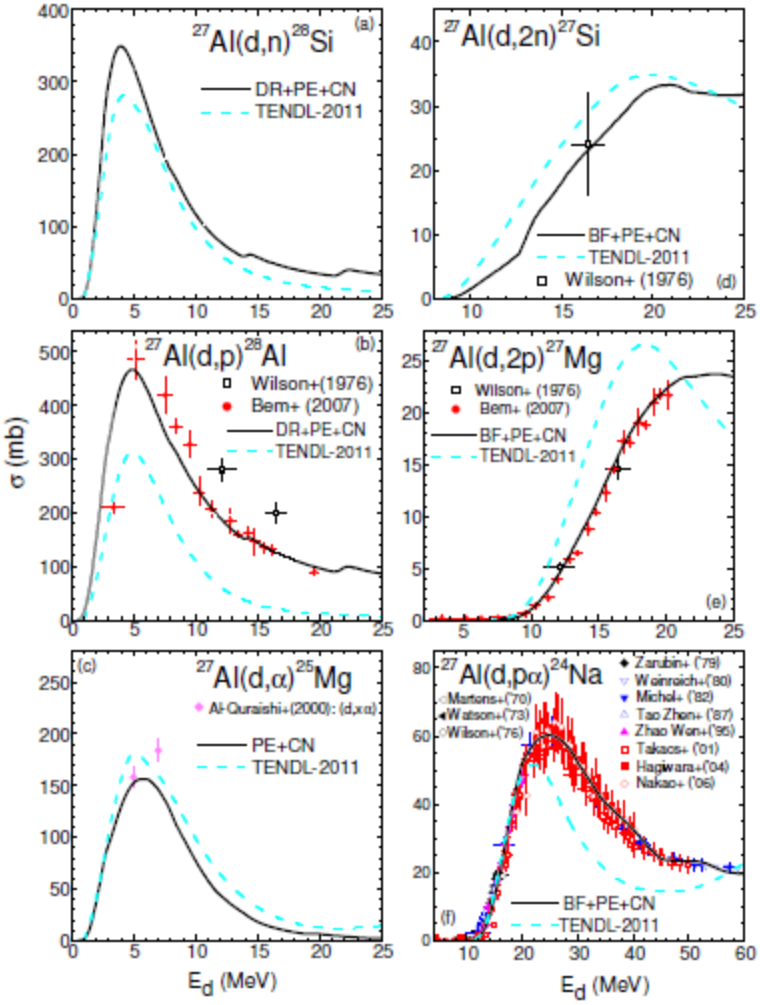

FIG. 12. Comparison of measured data (see [7] and references therein) with the complete theoretical analysis results taking into account BF, DR, and PE+CN reaction mechanism contributions to the deuteron interactions with ^{27}Al target nucleus [7] (solid curves), and with the TENDL-2011 evaluations [57] (dashed curves).

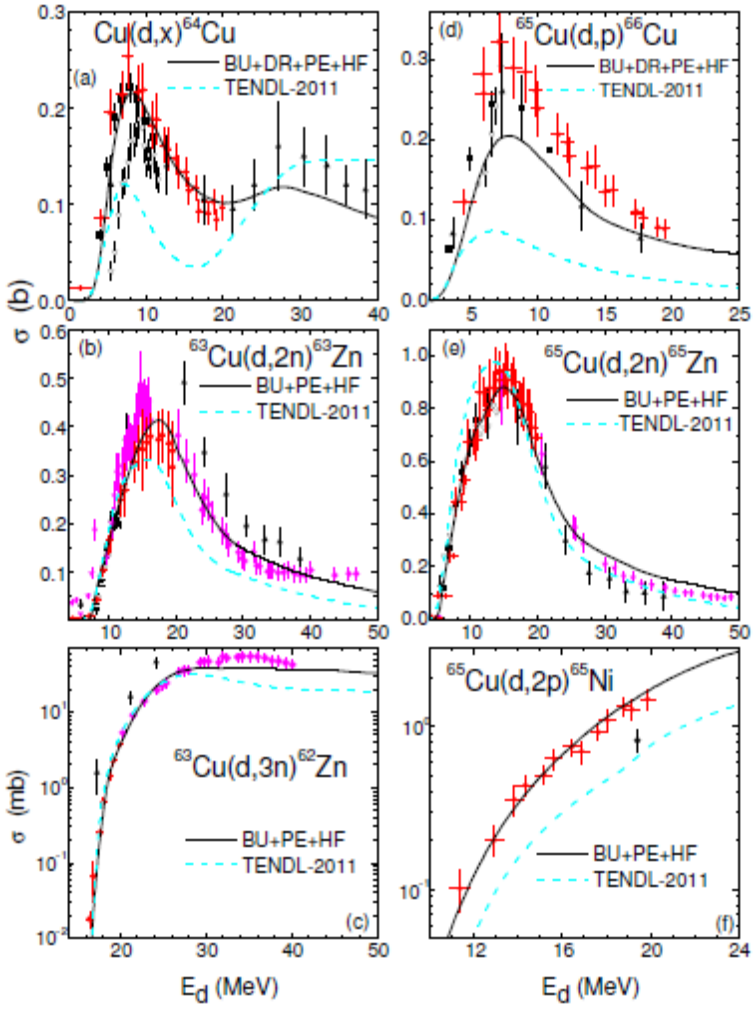

FIG. 13. Same as in Fig. 12, but for deuterons interactions with $^{nat,63,65}Cu$.

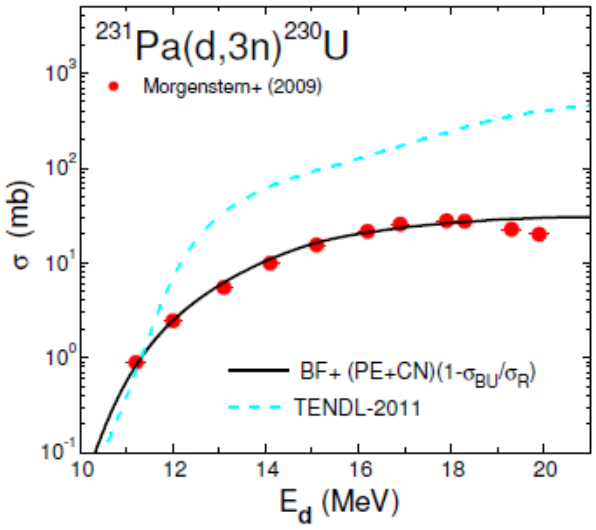

FIG. 14. Comparison of the measured [65], calculated (solid curve), and most recently evaluated [57] (dashed) excitation function of the reaction $^{231}Pa(d,3n)^{230}U$.

References for Section 3

[1] A. Ibarra, A. Möslang, R. Lässer, R. Ferdinand, R. Andreani, E. Surrey, B. Riccardi, V. Heinzel, H. Klein, U. Fischer, R. Forrest, M. Gasparotto, Fusion Eng. Design **82** (2007) 2422.

[2] R.A. Forrest, J. Kopecky, J.-Ch. Sublet, The European Activation File: EAF-2005 cross section library, UKAEA FUS 515 (2004).

[3] R.A. Forrest, I. Cook, Fusion Eng. Design **82** (2007) 2478.

[4] S.P. Simakov, P. Bém, V. Burjan, U. Fischer, R.A. Forrest, M. Götz, M. Honusek, H. Klein, V. Kroha, J. Novák, A. Sauer, E. Šimečková, R. Tiede, Fusion Eng. Design **83** (2008) 1543.

[5] R. Forrest, A. Mengoni, Summary Report of the IAEA Technical Meeting on Nuclear Data Library for Advanced Systems-Fusion Devices, INDC(NDS)-0525, April 2008.

[6] M. Avrigeanu, W. von Oertzen, R.A. Forrest, A.C. Obreja, F.L. Roman, V. Avrigeanu, Fusion Eng. Design **84** (2009) 418.

[7] P. Bém, E. Šimečková, M. Honusek, U. Fischer, S.P. Simakov, R.A. Forrest, M. Avrigeanu, A.C. Obreja, F.L. Roman, V. Avrigeanu, Phys. Rev. **C 79** (2009) 044610.

[8] M. Avrigeanu, V. Avrigeanu, EPJ Web of Conferences 2 (2010) 01004.

[9] M. Avrigeanu, V. Avrigeanu, J. Phys: Conf. Ser. 205 (2010) 012014.

[10] E. Šimečková, P. Bém, M. Götz, M. Honusek, J. Mrázek, J. Novák, M. Štefánik, L. Závorka, M. Avrigeanu, V. Avrigeanu, EPJ Web of Conferences 8 (2010) 07002.

[11] E. Šimečková, P. Bém, M. Honusek, M. Štefánik, U. Fischer, S.P. Simakov, R.A. Forrest, A.J. Koning, J.-C. Sublet, M. Avrigeanu, F.L. Roman, V. Avrigeanu, Phys. Rev. **C 84** (2011) 014605.

[12] M. Avrigeanu, V. Avrigeanu, J. Korean Phys.Soc. **59** (2011) 903.

[13] E. Šimečková, P. Bém, M. Honusek, L. Závorka, U. Fischer, S.P. Simakov, R.A. Forrest, M. Avrigeanu, V. Avrigeanu, F.L. Roman, J. Korean Phys. Soc. **59** (2011) 1928.

[14] M. Avrigeanu, V. Avrigeanu, EPJ Web of Conferences 21 (2012) 07003.

[15] M. Avrigeanu, V. Avrigeanu, A.J. Koning, Phys. Rev. **C 85** (2012) 034603.

[16] M. Avrigeanu, W. von Oertzen, U. Fischer, V. Avrigeanu, Nucl. Phys. **A759** (2005) 327.

[17] M. Avrigeanu, H. Leeb, W. von Oertzen, F.L. Roman, V. Avrigeanu, O. Bersillon, *et al.* (Eds.), Proc. Int. Conf. on Nuclear Data for Science and Technology, Nice, 2007, EDP Sciences, Paris (2008) pp. 219.

[18] M. Avrigeanu, W. von Oertzen, A.J.M. Plompen, V. Avrigeanu, Nucl. Phys. **A723** 104 (2003). M. Avrigeanu V. Avrigeanu, Phys. Rev. **C 73** (2006) 038801.

[19] M. Avrigeanu, A.C. Obreja, F.L. Roman, V. Avrigeanu, W. von Oertzen, At. Data Nucl. Data Tables **95** (2009) 501.

[20] M. Avrigeanu, H. Leeb, W. von Oertzen, F.L. Roman, V. Avrigeanu, in: E. Gadioli (Ed.), Proc. 11th Int. Conf. on Nuclear Reaction Mechanisms, Varenna, Ricercha Sci. Ed. Perm., Supplemento 126, Milano (2006) pp. 193.

[21] M. Avrigeanu, W. von Oertzen, A.C. Obreja, F.L. Roman, V. Avrigeanu, in Proc. 12th Int. Conf. on Nuclear Reaction Mechanisms, 15-19 June 2009, Villa Monastero, Varenna, Italy, F. Cerutti and A. Ferrari (Eds.) CERNProceedings-2010-001-V-1 (CERN, Geneva, 2010); http://cdsweb.cern.ch/record/1237907/files/p159.pdf.

[22] Dao T. Khoa, W. von Oertzen, Phys. Lett. **B304** (1993) 8; **B342** (1995) 6; Dao T. Khoa, W. von Oertzen, H.G. Bohlen, Phys. Rev. **C 49** (1994) 1652; Dao T. Khoa, W. von Oertzen, A.A. Ogloblin 1996 Nucl. Phys. **A602** (1996) 98.

[23] N. Anantaraman, H. Toki, G. Bertsch, Nucl. Phys. **A 398** (1983) 279.

[24] X. Campi, A. Bouyssy, Phys. Lett. **B 73** (1978) 263.

[25] J.W. Negele, D. Vautherin, Phys. Rev. **C 5** (1972) 1472.

[26] H. Krivine, J. Treiner, Phys. Lett. **B 88** (1979) 212.
[27] D. Abbott, A. Ahmidouch, H. Anklin, J. Arvieux, *et al*., Phys. Rev. Lett. **84** (2000) 5053.
[28] J.W. Negele, Phys. Rev. **C 1** (1970) 1260.
[29] C. Mahaux, H. Ngo, G.R. Satchler, Nucl. Phys. **A449** (1986) 354.
[30] W.W. Daehnick, J.D. Childs, Z. Vrcelj, Phys. Rev. **C 21** (1980) 2253.
[31] Experimental Nuclear Reaction Data (EXFOR); www-nds.iaea.or.at/exfor.
[32] J.M. Lohr, W. Haeberli, Nucl. Phys. **A 232** (1974) 381.
[33] O. Bersillon, Code SCAT2, Note CEA-N-2227 (1972).
[34] Haixia An, Chonghai Cai., Phys. Rev. **C 73** (2006) 054605.
[35] M.G. Mustafa, T. Tamura, T. Udagawa, Phys. Rev. **C35** (1987) 2077.
[36] J. Pampus, J. Bisplinghoff, J. Ernst, T. Mayer-Kuckuk, J. Rama Rao, G. Baur, F. Rosel, D. Trautmann, Nucl. Phys. **A 311** (1978) 141.
[37] J.R. Wu, C.C. Chang, H.D. Holmgren, Phys. Rev. **C19** (1979) 370.
[38] J. Kleinfeller, J. Bisplinghoff, J. Ernst, T. Mayer-Kuckuk, G. Baur, B. Hoffmann, R. Shyam, F. Rosel, D. Trautmann, Nucl. Phys. **A 370** (1981) 205.
[39] N. Matsuoka, M. Kondo, A. Shimizu, T. Saito, S. Nagamachi, H. Sakaguchi, A. Goto, F. Ohtani, Nucl. Phys. **A345** (1980) 1.
[40] C. Kalbach Walker, TUNL Progress Report XLII (2002-2003) p. 82-83, Triangle University Nuclear Laboratory; www.tunl.duke.edu/publications/tunlprogress/2003/.
[41] M. Avrigeanu, A.M. Moro, Phys. Rev. **C 82** (2010) 037601.
[42] M. Kawai, M. Kamimura, K. Takesako, Prog. Theor. Phys. Suppl. **184** (1969) 118.
[43] N. Austern, Y. Iseri, M. Kamimura, M. Kawai, G. Rawitscher, M. Yahiro, Phys. Rep. **154** (1987) 125.
[44] R.A.D. Piyadasa, M. Kawai, M. Kamimura, M. Yahiro, Phys. Rev. **C 60** (1999) 044611.
[45] A.M. Moro, F. M. Nunes, Nucl. Phys. **A 767** (2006) 138.
[46] A.M. Moro, J.M. Arias, J. Gómez-Camacho, F. Pérez-Bernal, Phys. Rev. **C 80** (2009) 054605.
[47] A.M. Moro, F.M. Nunes, R.C. Johnson, Phys. Rev. **C 80** (2009) 064606.
[48] I.J. Thompson, Comput. Phys. Rep. **7** (1988) 167; v.FRES 2.3 (2007).
[49] L.L. Lee Jr., J.P. Schiffer, Phys. Rev. **134** (1964) B765, EXFOR C1024 entry; S.A. Hjorth, E.K. Lin, Nucl. Phys. **A116** (1968) 1, EXFOR C1075 entry; E. Newman, L.C. Becker, B.M. Freedom, Nucl. Phys. **A100** (1967) 225, EXFOR C1067 entry.
[50] R.K. Jolly, E.K. Lin, B.L. Cohen, Phys. Rev. **130** (1963) 2391, EXFOR C1023 entry; F. Hinterberger, G. Mairle, U. Schmidt-Rohr, G.J. Wagner, P. Turek, Nucl. Phys. **A111** (1968) 265, EXFOR D0225 entry; G. Igo, W. Lorenz, U. Schmidt-Rohr, Phys. Rev. **124** (1961) 8332, EXFOR D0239 entry.
[51] C. Kalbach Walker, in: TUNL Progress Report, vol. XLVI (2007), p. 78. www.tunl.duke.edu/publications/tunlprogress/2007/tunlxlvi.pdf ; C. Kalbach Walker, 1st Research Co-ordination Meeting of the Fusion Evaluated Nuclear Data Library FENDL 3.0, 2-5 December 2008, IAEA, Vienna, http://www-nds.iaea.org/fendl3/RCM1 documents.html.
[52] Experimental Nuclear Reaction Data (EXFOR), www-nds.iaea.or.at/exfor; R. Michel, M. Galas, Appl. Rad. Isotopes **34** (1983) 1325, EXFOR A0209 entry; F. Ditroi, F. Tarkanyi, S. Takacs, A. Hermanne, M. Baba, A.V. Ignatyuk, Nucl. Instr. Meth. **B 268** (2010) 2571, EXFOR D4232 entry; F. Tarkanyi, A. Hermanne, F. Ditroi, S. Takacs, Nucl. Instr. Meth. **B 255** (2007) 297, EXFOR D4156 entry.
[53] P. Guazzoni, L. Zetta, A. Covello, A. Gargano, B.F. Bayman, T. Faestermann, G. Graw, R. Hertenberger, H.-F. Wirth, M. Jaskola, Phys. Rev. **C 83** (2011) 044614.
[54] M. Avrigeanu, V. Avrigeanu, IPNE Report NP-86-1995, Bucharest, 1995, Refs. therein; News NEA Data Bank 17, 22 (1995).

[55] A.J. Koning, S. Hilaire, M.C. Duijvestijn, TALYS-1.0, in Proc. Int. Conf. on Nuclear Data for Science Technology, Nice, 2007 (EDP Sciences, Paris, 2008); version TALYS-1.2, December 2009; version TALYS-1.4, December 2011; http://www.talys.eu/home/.
[56] M. Avrigeanu, S. Chuvaev, A.A. Filatenkov, R.A. Forrest, M.W. Herman, A.J. Koning, A.J.M. Plompen, F.L. Roman, V. Avrigeanu, Nucl. Phys. **A806** (2008) 15.
[57] A.J Koning, D. Rochman, TENDL-2011: TALYS-Based Evaluated Nuclear Data Library (December 29, 2011), http://www.talys.eu/tendl-2011/
[58] N.K. Skobelev, A.A. Kulko, V. Kroha, V. Burjan, Z. Hons, A.V. Daniel, N.A. Demeskhina, R. Kalpakchieva, A. Kugler, J. Mrazek, Yu.E. Penoinzhkevich, S. Piskor, E. Simeckova, E.I. Voskoboynik, J. Phys. G: Nucl. Part. Phys. **38** (2011) 035106.
[59] M. Herman, R. Capote, B.V. Carlson, P. Oblozinsky, M. Sin, A. Trkov, H. Wiencke, V. Zerkin, Nucl. Data Sheets **108** (2007) 2655.
[60] M. Avrigeanu, V. Avrigeanu, http://arxiv.org/abs/1105.1881v1.
[61] R. Rapaport, A. Sperduto, W.W. Bruechner, Phys. Rev. **151** (1966) 939.
[62] J.N. Roy, A.R. Majunder, H.M. Sen Gupta, Phys. Rev. **C 46** (1992) 144.
[63] S.-C. Wu, Nucl. Data Sheets **91** (2000) 1.
[64] J.A. Cameron, S. Balraj, Nucl. Data Sheets **88** (1999) 299.
[65] A. Morgenstern, O. Lebeda, J. Stursa, R. Capote, M. Sin, F. Bruchertseifer, B. Zielinska, C. Apostolidis, Phys. Rev. **C 80** (2009) 054612.
[66] A. Morgenstern, O. Lebeda, J. Stursa, F. Bruchertseifer, R. Capote, J. McGinley, G. Rasmussen, M. Sin, B. Zielinska, C. Apostolidis, Anal. Chem. **80** (2008) 8763; Experimental Nuclear Reaction Data (EXFOR); www-nds.iaea.or.at/exfor; A. Morgenstern, *et al*., EXFOR D0562 entry.
[67] R. Capote, M. Herman, P. Oblozinsky, P.G. Young, S. Goriely, T. Belgya, A.V. Ignatyuk, A.J. Koning, S. Hilaire, V.A. Plujko, M. Avrigeanu, O. Bersillon, M.B. Chadwick, T. Fukahori, Zhigang Ge, Yinlu Han, S. Kailas, J. Kopecky, V.M. Maslov, G. Reffo, M. Sin, E.Sh. Soukhovitskii, P. Talou, Nucl. Data Sheets **110** (2009) 3107; http://www-nds.iaea.org/RIPL-3/.
[68] R. Capote, S. Chiba, E. Soukhovitskii, J.M. Quesada, E. Bauge, J. Nucl Sci. Technol. **45** (2008) 333.
[69] S. Goriely, S. Hilaire, A.J. Koning, Phys. Rev. **C 78** (2008) 064307.
[70] M. Sin, R. Capote, A. Ventura, M. Herman, P. Obložinský, Phys. Rev. **C 74** (2006) 014608.
[71] B. Jurado *et al*., Determination of neutron-induced cross sections via the surrogate reaction method, Workshop on Nuclear Data Measurements, Nov. 28–29, 2011, Issy-les-Moulineaux; http://www.gedeon.prd.fr/ .

4. Evaluations of (d,p) cross sections (A.V. Ignatyuk)

4.1 INTRODUCTION

In accordance with the recommendations of the last CRP Meetings [1,2] new versions of the proton and deuteron data libraries FENDL-3P and FENDL-3D, based mainly on the recent TENDL-2011 evaluations, has been compiled. For the proton-induced reactions a reasonable agreement between these evaluations and the available experimental data was obtained in most cases. However, for the deuteron-induced reactions the TENDL-2011 evaluations essentially underestimate the (*d,p*) reaction cross sections. In the present report the main shortcomings of the previous evaluations are analysed and a new phenomenological approach is proposed for a systematic description of the (*d,p*) cross sections. The revised version of the FENDL-3D library has been prepared that includes the corrected (*d,p*) data for all nuclides with the mass number above 20.

4.2 STATISTICAL CODES AND THEIR MODIFICATIONS

A variety of codes based on the statistical theory of nuclear reactions are used nowadays for the calculation and evaluation of nuclear reaction cross-sections. Most of these codes include rather similar approximations for the description of nuclear processes and properties of excited nuclei, but the codes differ essentially in their input parameters and required computing time. One of the simplest is the ALICE code [3] based on the geometry-dependent hybrid (GDH) or the hybrid multi-step (HMS) pre-equilibrium models and the Weisskopf-Ewing evaporation description of equilibrium processes. The modified code ALICE-IPPE [4] was developed to include the pre-equilibrium cluster emission and the advanced systematics of the nuclear level densities.

Some shortcomings of the ALICE-family codes relate to a disregard of the angular momentum and parity conservation laws. More sophisticated codes taking into account these conservation rules require not only a longer computation time, but also much more input information on the nuclear level structure. The GNASH [5], EMPIRE [6] and TALYS [7] codes are widely used currently for practical evaluations of both the neutron and charged particle reaction cross sections. Main input parameters of these codes are usually estimated on the basis of the RIPL libraries [8] and that makes the obtained results quite similar. Essential discrepancies between calculations relate to the pre-equilibrium processes for which many various approaches are proposed. To reduce the dispersion of results, adjustment to experimental data could play a crucial role for an accurate evaluation of the corresponding cross sections.

During the last decade systematic measurements of the deuteron induced reactions have been performed for about 20 metal targets having mostly natural isotopic composition [9]. We will discuss only a part of the obtained data related to the (*d,p*) reaction.

The experimental data for the ^{181}Ta(*d,p*)^{182}Ta reaction are compared in Fig. 1 with the TENDL-2007 and TENDL-2011 evaluations, as well as with the calculations performed with the statistical codes [10]. The disagreement of the TENDL-2007 evaluation with the experiments is about a factor 20-100 for the whole energy region. It should be noted that the calculations with the previous versions of the ALICE-IPPE and EMPIRE-II codes demonstrated similar disagreements of the (*d,p*) cross sections for many nuclei [11-15].

It is well known that for the (*d,p*) reactions at low energies the direct stripping processes play a dominant role and such processes are not considered by the standard statistical models. To

achieve a reasonable description of the available data the consistent direct reaction approaches should be used. The corresponding calculations are voluminous and very time-consuming. A more simple phenomenological approach was chosen to update the statistical codes. The general relations for direct transfer reactions in the continuum [16] were taken to simulate the (*d*,*p*) transitions and the energy dependent enhancement factor in these relations was adjusted empirically to describe the whole set of the observed (*d*,*p*) cross sections for medium and heavy nuclei [13]. The codes including such modifications were named ALICE-D and EMPIRE-D and their results for the ^{181}Ta(*d*,*p*)^{182}Ta reaction are compared with the experimental data in Fig. 1. Both codes were applied to describe the observed (*d*,*p*) cross sections for many other nuclei [13,14], for which the disagreements with the TENDL-2007 evaluations were always similar to the shown one above.

The similar simulation of the (*d*,*p*) reaction was also included in the last version of the TALYS code used for the TENDL-2011 evaluations. The obtained cross section at the near-threshold energies is much higher than in the TENDL-2007 library, but it is still essentially lower than the experimental data (Fig. 1). The systematic underestimation of the (*d*,*p*) cross sections is observed in the TENDL-2011 files for all cases where the experimental data are available. Some additional examples will be considered below together with a phenomenological description shown in Fig. 1 by a red curve.

4.3 PHENOMENOLOGICAL SYSTEMATICS OF THE (*d*,*p*) CROSS SECTIONS

Taking into account uncertainties of theoretical models it was decided to construct a rather simple phenomenological description of the available experimental data. The analytical function used for this purpose should to have a shape similar to the results of theoretical models, but its parameters could be estimated from a fit to experimental data. The following function was selected

$$\sigma(E) = \frac{a_1}{1+\exp(\frac{b-E}{c})}[a_2\exp(-E/d_1) + (1-a_2)\exp(-E/d_2)] \qquad (1)$$

where the factor before the square brackets defines the low-energy increasing part of the (*d*,*p*) cross section and the terms in the square brackets characterize the decreasing part. A need for two decreasing components corresponds to two different mechanisms of nuclear reaction: the direct processes connected with the low-energy excitation of single-particle degrees of freedom and the pre-equilibrium processes responsible for more complex excitations of nuclei.

To estimate all parameters of Eq. (1) we need the experimental data up to high enough energies. The available data for the ^{59}Co(*d*,*p*) reaction are compared in Fig. 2 with various model calculations and the phenomenological description (1) with the parameters fitted to the data. Similar results for the ^{197}Au(*d*,*p*) reaction are shown in Fig. 3. To better see the differences between the model descriptions of data the logarithmic ordinate scale is used for the last figure.

The obtained parameters of Eq. (1) for both targets are presented in Table I. Because a rather small number of the experimental points are below the cross section maximum the parameter *c* was excluded from the fitting and its value *c* = 0.75 MeV was fixed for the ^{59}Co target. Owing to the limited high-energy part of the ^{197}Au data the parameter d_2 was fixed to the value 35 MeV under the fitting.

TABLE I. PARAMETERS OF THE (*d,p*) CROSS SECTION DESCRIPTION ESTIMATED FROM THE EXPERIMENTAL DATA FITTING

Parameter	**^{59}Co(*d,p*)**	**^{197}Au(*d,p*)**
a_1	751±87 mb	904±121 mb
b	5.13±0.22 MeV	9.86±0.11 MeV
c	0.75 MeV was fixed	0.716±.035 MeV
a_2	0.891±0.011	0.876±.015
d_1	7.21±0.61 MeV	7.05±0.84 MeV
d_2	37.34±2.76 MeV	35.0 MeV was fixed

Unfortunately, the amount of experimental data on the (*d,p*) reaction for other targets is even smaller than for the two above nuclei. So, it is difficult to estimate all the required parameters from an analysis of the available data. In the case of ^{181}Ta we were forced to fix beside the parameters c and d_2 also the parameter d_1 or a_2. The resulting description of experimental data with the fixed d_1 = 7.1 and d_2 = 35 MeV is shown for this nucleus in Fig. 1. The remaining fitted parameters are the following: a_1 = 832±68 mb, b = 9.31±0.12 MeV, a_2 = 0.861±0.015.

Similar scattered experimental data are available for the target of ^{141}Pr. They are shown in Fig. 4 together with various calculations. Again one can note a strong underestimation of the (*d,p*) cross section in the TENDL-2007 and TENDL-2011 evaluations. The phenomenological description is obtained in this case with the fixed parameters of c, d_1 and d_2 as above and the fitted parameters: a_1 = 742±70 mb, b = 8.06±0.13 MeV, a_2 = 0.848±0.026.

The parameter b determines the effective threshold of the (*d,p*) reaction and it should be close to the height of the Coulomb barrier for the corresponding target. Using the relation for the barrier

$$b = \frac{e^2 Z}{r_{eff} A^{1/3}} \tag{2}$$

where e^2 = 1.44 MeV fm, Z is the charge and A is the mass numbers of the target, we can estimate the effective radius parameter r_{eff} corresponding to the obtained parameter b. The parameters a_1 and r_{eff} estimated from the performed analysis are shown in Fig. 5. The mean value of the radius parameter is r_{eff} = 1.985±0.045 fm, while the dependence of the parameter a_1 on the mass number can be approximated as

$$a_1 = 672 + 0.871A \text{ mb} \tag{3}$$

An uncertainty of this estimation is about 10-15 %. A limited amount of experimental data on the (*d,p*) cross sections does not allow to suppose any structural effects in the mass dependence of this parameter.

Equations (1-3) can be considered as the unified systematic of the (*d,p*) cross sections for the whole mass region with the remaining parameters taken as the fixed ones: c = 0.75 MeV, a_2= 0.848, d_1 = 7.1 and d_2 = 35 MeV. Uncertainties of such systematic are mainly determined by the uncertainties of the two parameters: a_1 and a_2. If we suppose that uncertainties of a_2

are about 7-10%, the uncertainty of the systematic with the recommended parameters should be about 25-30%.

Recently rather accurate experimental data on the (*d,p*) reaction were obtained for ^{45}Sc [15,17]. These data are compared in Fig. 6 with the phenomenological description (1) for the fitted parameters and for the unified ones. The TENDL-2011 estimations are shown too. Of course, the description with the fitted parameters is always better than with the unified ones. The difference between two approaches is about 17% at the cross-section maximum and it decreases with a growth of the deuteron energy.

From the comparison with the experimental data considered above we can conclude that the proposed systematics is certainly much better than the available TENDL-2011 evaluations. For energies above 20 MeV it is even better than ALICE-D and EMPIRE-D calculations. The shortcomings of the latter calculations result from the selection of the pre-equilibrium model parameter. To improve the predictive power of the available statistical codes their parameters should be estimated more consistently for the channels with a significant contribution to the direct processes.

4.4 UPDATED FENDL-3D LIBRARY

In accordance with results of the performed analysis it was decided to adopt the above systematics in the FENDL-3D library for the (*d,p*) cross sections conserving the TENDL-2011 evaluations for other reaction channels [2].

For the residual nuclides with long-lived isomer states we need in such an approach beside the integral cross sections also the branching coefficients determining the relative probability for production of the ground and isomer states. Such coefficients depend strongly on the schemes of gamma-transitions between the low-lying levels and they are much less depending on the reaction channels. Most of the statistical models describe quite reasonably the available experimental data on the branching coefficients for nuclides with well-established schemes of gamma-transitions [5-7]. So, we have supposed that the branching coefficients estimated in TENDL-2011 are reasonable enough to combine them with the above systematics for evaluations of the isomer state yields.

An example of the evaluated isomer-production cross sections for the ^{59}Co(*d,p*) reaction is shown in Fig. 7. The integral cross section is calculated in this case for the unified parameters and differs a little from the cross section presented before for the fitted parameter (Fig. 2). The ground state production can be obtained as a difference between the integral and isomeric cross sections. Unfortunately, the available experimental data are scanty to test the systematic predictions for the isomer production.

The preliminary version of FENDL-3D included the evaluated activation cross sections for 803 nuclides adopted from TENDL-2011. For 787 nuclides with the mass number of $A \geq 20$ the (*d,p*) sections of the corresponding files have been changed on the cross sections of the above systematics. For the residual long-lived isomers the cross sections are given for both the ground and isomeric states. For 16 lightest nuclides with $A < 20$ a difference between the systematics and TENDL-2011 results is not great, and without additional experimental data it is difficultly to prefer one evaluation over another. So, the TENDL-2011 files for these nuclides have been conserved in the updated library without changes.

4.5 CONCLUSION

TENDL-2011 libraries for protons and deuterons were tested against the available experimental data for the most important materials related to the IFMIF project. The main results of the test are discussed in detail in the previous report of the present contract. Additional calculations with the ALICE-D and EMPIRE-D codes were performed to study effects of input model parameters on the analyzed data. For the proton-induced reactions a reasonable agreement between the evaluations and the available experimental data was obtained in most cases.

For the deuteron-induced reactions the TENDL-2011 evaluations essentially underestimate the (*d,p*) reaction cross sections for most of the nuclei. The phenomenological systematics of the (*d,p*) cross sections, developed under the current CRP project, have been recommended as an alternative version of the corresponding data [2]. The updated version of the FENDL-3D library have been prepared and transmitted to the IAEA Nuclear Data Section.

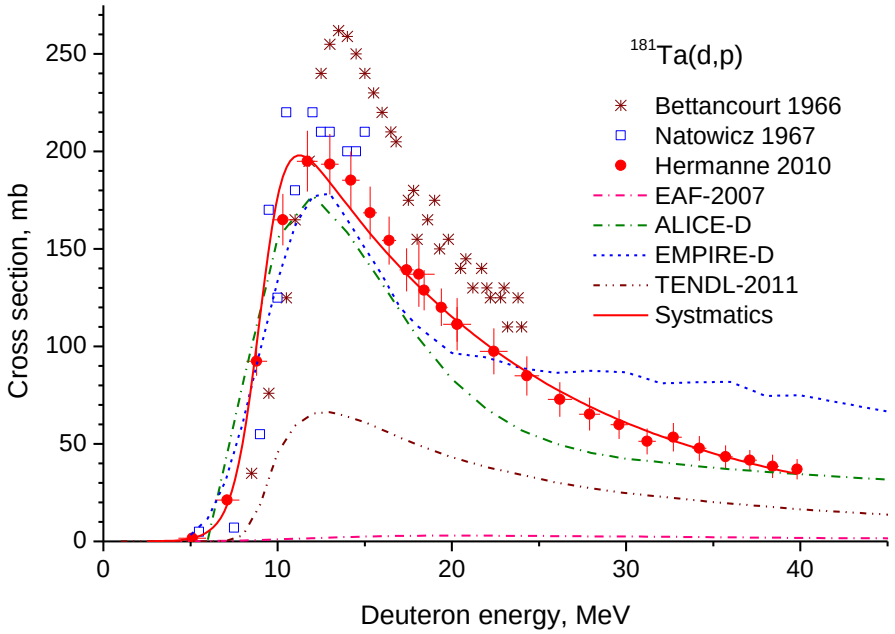

FIG. 1. Experimental data for the ^{181}Ta(d,p)^{182}Ta reaction cross section are compared with various calculations

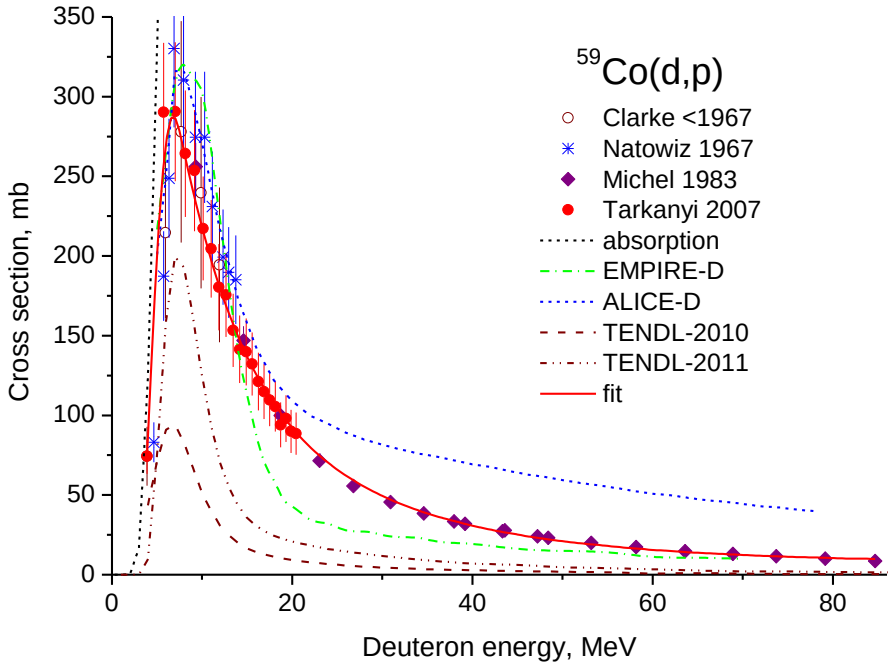

FIG. 2. The same as Fig. 1 for the ^{59}Co(d,p) reaction

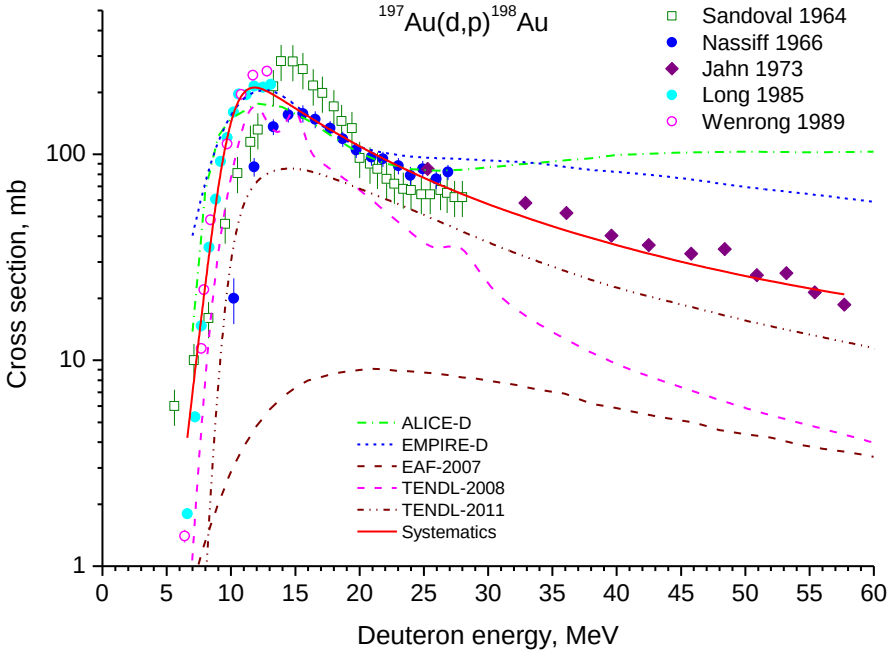

FIG. 3. The same as Fig. 1 for the ^{197}Au(d,p) reaction

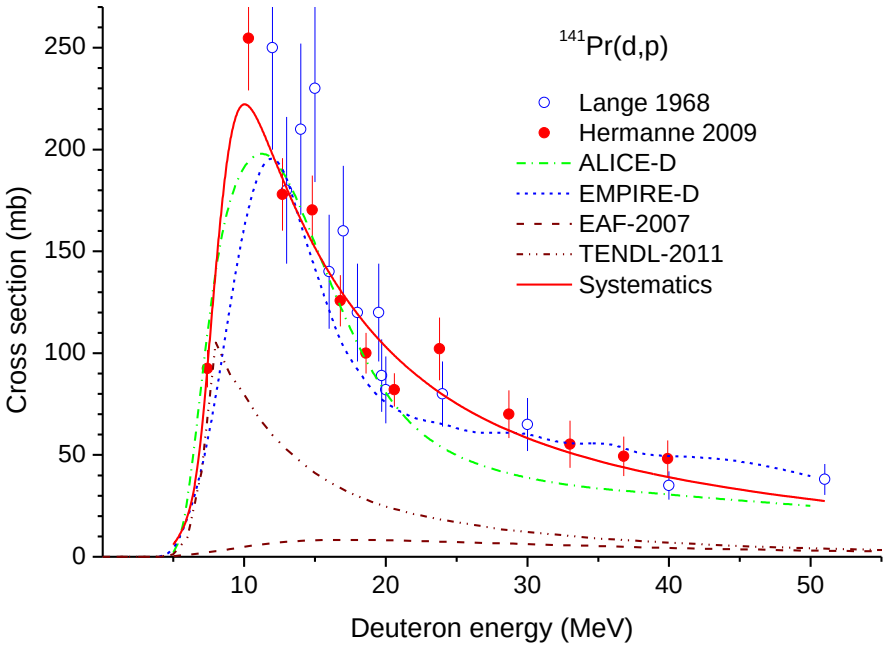

FIG. 4. The same as Fig. 1 for the ^{141}Pr(d,p) reaction

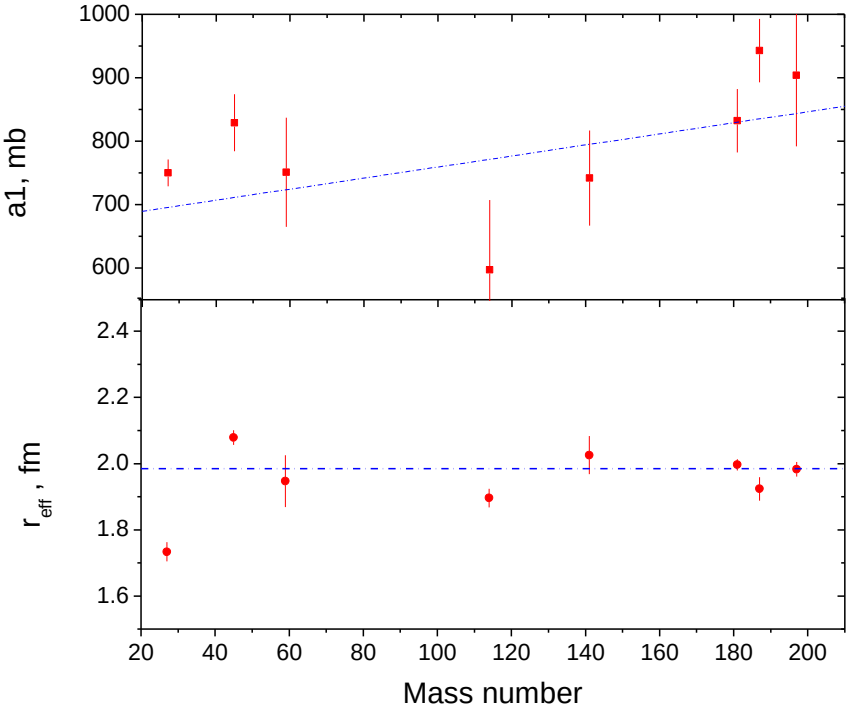

FIG. 5. Parameters of Eq. (1) and (2) estimated from the analysis of experimental data. Dash-dotted lines show the recommended parameters.

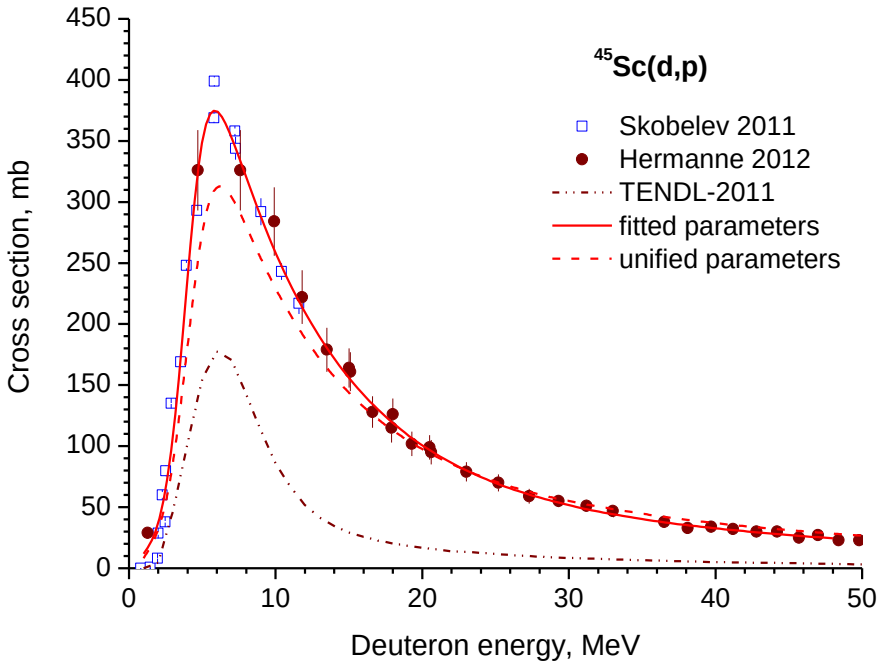

FIG. 6. The same as Fig. 1 for the ^{45}Sc(d,p) reaction

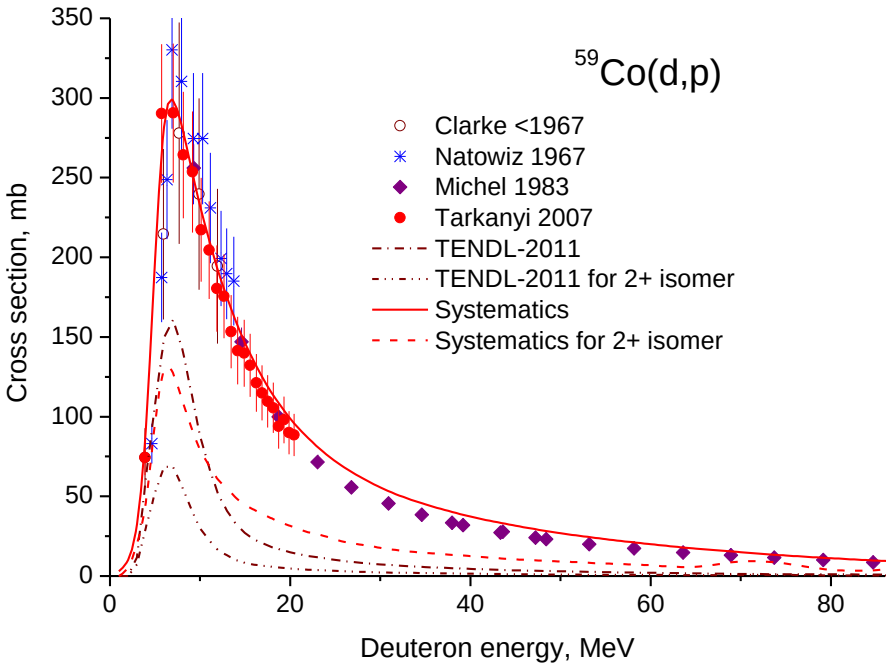

FIG. 7. Evaluated integral and 2^+-isomer production cross sections for the ^{59}Co(d,p) reaction are compared with experimental data

References for Section 4

[1] Summary Report from the Second Research Coordination Meeting on Nuclear Data Libraries for Advanced Systems – Fusion Devices, INDC(NDS)-0567, IAEA, Vienna, 2010.

[2] Summary Report from the Third Research Coordination Meeting on Nuclear Data Libraries for Advanced Systems – Fusion Devices, INDC(NDS)-0602, IAEA, Vienna, 2012.

[3] M. Blann. Ann. Rev. Nucl. Sci. **25** (1975) 123.

[4] A.I. Dityuk, A.Yu. Konobeyev, V.P. Lunev, Yu.N. Shubin. New Version of the Advanced Computer Code ALICE-IPPE, Report INDC (CCP)-410, IAEA, Vienna, 1998.

[5] P.G. Young, E.D. Arthur, M.B. Chadwick. Theory and Use of the GNASH Code. In: Nuclear Reaction Data and Nuclear Reactors. Eds. A. Gandini, G. Reffo, World Sci., Singapore, 1998, **v.1**, pp. 227-404.

[6] M. Herman, R. Capote, B.V. Carlson, P. Oblozinsky, M. Sin, A. Trkov, H. Wiencke, V. Zerkin, Nucl. Data Sheets. **108** (2007) 2655-2715.

[7] A.J. Koning, S. Hilaire, M. Duijvestijn, TALYS-1.0, in: Proc. Int. Conf. Nuclear Data for Science and Technology, 22-27 April 2007, Nice, France, O. Bersillon, F. Gunsing, E. Bauge, R. Jacqmin, S. Leray (Eds.), EDP Sciences, 2008, Vol. 1, pp. 211-214. See also "TALYS-1.0: A nuclear reaction program", User Manual, NRG/CEA, December 2007.

[8] R. Capote, M. Herman, P. Oblozinsky, P.G. Young, S. Goriely, T. Belgya, A.V. Ignatyuk, A.J. Koning, S. Hilaire, V.A. Plujko, M. Avrigeanu, O. Bersillon, M.B. Chadwick, T. Fukahori, Zhigang Ge, Yinlu Han, S. Kailas, J. Kopecky, V.M. Maslov, G. Reffo, M. Sin, E.Sh. Soukhovitskii, P. Talou, Reference Input Parameter Library (RIPL-3), Nuclear Data Sheets, 110 (12), 2009, pp 3107-3214. (see *http://www-nds.iaea.org/RIPL-3/*).

[9] F. Tarkanyi, A. Hermanne, F. Ditroi, S. Takacs, F. Szelecsenyi, B. Kiraly, J. Csikai, M. Sonck, M.S. Uddin, M. Hagiwara, M. Baba, T. Ido, T. Ohtsuki, Yu.N. Shubin, S.F. Kovalev, A.I. Dityuk, A.V. Ignatyuk. Cross sections of deuteron induced nuclear reactions on metal targets. In: Proc. Int. Conf. Nuclear Data for Science and Technology (Nice-2007), O. Bersillon, F. Gunsing, E. Bauge, R. Jacqmin, S. Leray (Eds.), EDP Sciences, 2008, vol. 2, 1027-1030.

[10] A. Hermanne, L. Daraban, F. Tarkanyi, F. Ditroi, A.V. Ignatyuk, R. Adam Rebeles, M. Baba, Nucl. Instr. Meth. **B267** (2009) 3293-3301.

[11] F. Tárkányi, A. Hermanne, S. Takács, K. Hilgers, S.F. Kovalev, A.V. Ignatyuk, S.V. Qaim, Appl. Radiat. Isotopes **65** (2007) 1215–1220.

[12] F. Tárkányi, A. Hermanne, S. Takács, F. Ditrói, B. Király, S.F. Kovalev, A.V. Ignatyuk, Nucl. Instr. Meth. **B266** (2008) 3529-3534.

[13] A. Hermanne, F. Tárkányi, S. Takács, F. Ditrói, M. Baba, T. Ohtshuki, I. Spahn, A.V. Ignatyuk, Nucl. Instr. Meth. **B266** (2009) 3346-3352.

[14] F. Ditrói, F. Tárkányi, S. Takács, A. Hermanne, M. Baba, A.V. Ignatyuk, Nucl. Instr. Meth. **B268** (2010) 2571-2577.

[15] A. Hermanne, R. Adam Rebeles, F. Tarkanyi, S. Takacs, M.P. Takacs, J. Csikai, A. Ignatyuk, Nucl. Instr. Meth. **B270** (2012) 106-115.

[16] C.K. Kalbach. Exciton Model Pre-equilibrium Code with Direct Reactions, PRECO-2000 Manual. TUNL, Duke University, Durham, USA, 2001.

[17] N.K. Skobelev, A.A. Kulko, V. Kroha, *et al*., J. Phys. **G38** (2011) 035106.

5. Charged particle activation cross section data for FENDL-3 [2008-2009] (F. Tárkányi, B. Király)

5.1 INTRODUCTION

In the present status report we summarize the results of experimental and compilation work of ATOMKI Group, performed with the aim to prepare evaluated data for FENDL-3.

In the experimental works, collaborating partners from Belgium and Japan have participated who are not mentioned here individually. Co-authors from the collaborating institutes can be found in the related new publications (see References).

5.2 EXPERIMENTAL RESULTS

To complete the experimental database for the important nuclear reactions, new experiments have been made. The data evaluations are in progress. The summary of the experiments is collected in Table I.

The main partners in the measurements of charged particle induced nuclear data for FENDL-3 are: ATOMKI (Hungary), VUB Brussels (Belgium) and CYRIC, Tohoku University (Japan).

The results were published in scientific journals (Nuclear Instruments and Methods B, Applied Radiation and Isotopes, see References).

5.3 COMPILATION AND EVALUATION

The compilation and critical analysis of the literature data for all reaction assigned to the ATOMKI Group have been started and - due to the large number of reactions - partly completed.

Deuteron and proton activation cross sections were compiled up to 50 MeV and 100 MeV, respectively. In addition to the EXFOR database, some other important reference sources should be checked (e.g. Nuclear Science References, NNDC, Brookhaven National Laboratory and Landolt-Bornstein books).

The list of the compiled reactions on the targets proposed by U. Fischer is given in Table II and Table 3.

The preparation of the list of the missing, duplicated and wrong EXFOR entries is in progress.

5.4 COMPARISON WITH THE THEORETICAL RESULTS

The theoretical analysis of the very contradictory experimental results is in progress. The TALYS curves, available in TENDL-2009 and PADF, are added to the graphs. However, presently we can handle other theoretical libraries only in complicated way due to the well-known MT problems. In the future, in this work, we count on the collaboration with A.V. Ignatyuk (IPPE, Obninsk, Russia).

5.5 EXAMPLES

To represent the present status of our work collected and plotted experimental and theoretical data on Co and Ta targets, bombarded with deuteron beam are shown at the end of this report. At this early stage the quality of the figures is not the best.

According to the figures, the predictivity of the model codes is not very good, as it is expected in case of deuteron induced reactions.

5.6 SOME CONCLUSION FROM THE WORK ALREADY DONE

- The number of the reactions is so large (~300 deuteron and ~400 proton) that the critical evaluation of the experimental data (reading all original papers) will have some limitations.
- There are many very disturbing mistakes in the compiled EXFOR entries.
- The use of the theoretical libraries for simple users is complicated due to the ENDF coding. (This problem arose earlier, when we wanted to make comparison with our experimental results.)
- The list of the reactions included in the presently available theoretical libraries is limited. Some reactions needed for our work are missing.
- The prediction capability of the theoretical codes for deuteron induced reactions is poor.

5.7 FUTURE PLANS

- Extension of the compilation with the experimental data found using the secondary reference sources (e.g. Nuclear Science References, NNDC, Brookhaven National Laboratory and Landolt-Bornstein books).
- De-selection of the contradictory data taking into account the experimental circumstances.
- Finishing the comparison of the experimental data with the results of TENDL-2009.
- Comparison of the experimental data also with the available ALICE-IPPE and EMPIRE-II calculations for reactions measured by the ATOMKI Group.

5.8 CRP RELATED PUBLICATIONS (2008-2009)

1. F. Ditrói, F. Tárkányi, S. Takács, M.S. Uddin, M. Hagiwara, M. Baba, A. Ignatyuk, S.F. Kovalev, *Investigation of excitation functions of deuteron induced nuclear reactions on lead*, J. Radioanal. Nucl. Chem. **276** (2008) 835.
2. F. Ditrói, S. Takács, F. Tárkányi, M. Baba, E. Corniani, Yu.N. Shubin, *Study of proton induced reactions on niobium targets up to 70 MeV*, Nucl. Instrum. Methods Phys. Res. **266** (2008) 5087.
3. R. Adam-Rebeles, P. Van den Winkel, A. Hermanne, F. Tárkányi, *New measurement and evaluation of the excitation function of ^{64}Ni(p,n) reaction for the production of ^{64}Cu*, Nucl. Instrum. Methods Phys. Res. **267** (2009) 457.
4. F. Ditrói, A. Hermanne, E. Corniani, S. Takács, F. Tárkányi, Gy. Csikai, Yu.N. Shubin, *Investigation of proton induced reactions on niobium at low and medium energies*, Nucl. Instrum. Methods Phys. Res. **267** (2009) 3364.
5. A. Hermanne, L. Daraban, F. Tárkányi, S. Takács, F. Ditrói, A. Ignatyuk, R. Adam-Rebeles, M. Baba, *Excitation functions for some W, Ta and Hf radionuclides obtained by*

deuteron irradiation of ^{181}Ta up to 40MeV, Nucl. Instrum. Methods Phys. Res. **267** (2009) 19:3293.
6. B. Király, S. Takács, F. Ditrói, F. Tárkányi, A. Hermanne, *Evaluated activation cross sections of longer-lived radionuclides produced by deuteron induced reactions on natural iron up to 10 MeV*, Nucl. Instrum. Methods Phys. Res. **267** (2009) 15.
7. M. Haji-Saeid, M.R.A. Pilai, T.J. Ruth, D.J. Schlyer, P. Van den Winkel, M.M. Vora, R. Capote Noy, L. Carroll, J.C. Clark, J. Comor, M. Dehnel, R. Ferrieri, R.D. Finn, J.S. Fowler, M.J. Schueller, F. Tárkányi, *Cyclotron produced radionuclides: Physical characteristics and production methods*, IAEA Technical Reports Series 468 (2009) 266.
8. F. Ditrói, S. Takács, F. Tárkányi, M. Baba, R.W. Smith, *Investigation of proton and deuteron induced reactions on Cobalt*, Submitted abstract, ND2010 Conference, Korea.
9. F. Tárkányi, A. Hermanne, B. Király, S. Takács, F. Ditrói, M. Baba, A.V. Ignatyuk, *Investigation of activation cross sections of deuteron induced reactions on indium up to 40 MeV for production of a $^{113}Sn(^{113m}In)$ generator*, Submitted abstract, ND2010 Conference, Korea.
10. F. Tarkanyi, S. Takacs, F Ditroi, A. Hermanne, M. Sonck, M. Baba., H. Yamazaki, M.S. Uddin, A.V. Ignatyuk, *Study of production of the ^{99m}Tc radioisotope via charged particle induced reactions up to 100 MeV: new data and review*, Submitted abstract, ENC 2010 (European Nuclear Conference), Barcelona, Spain.

TABLE I. CROSS SECTION DATA MEASUREMENTS FOR FENDL-3.

Material	**Target**	**Primary proton beam**	**Material**	**Target**	**Primary deuteron beam**
Molybdenum	^{nat}**Mo**Re foils Mo foils	70 MeV p 36 MeV p	Molybdenum	^{nat}**Mo**Re Mo foils	40 MeV d 21 MeV d
Tantalum	^{nat}Ta foils	36 MeV p	Gold	Au foils	21 MeV d
Vanadium	^{nat}V foils	70 MeV p	Vanadium	^{nat}V foils	40 MeV d 21 MeV d
Cobalt	^{nat}Co foils	70 MeV p	Cobalt	^{nat}Co foils	40 MeV d 21 MeV d
Tungsten	^{nat}W foils	36 MeV p	Tungsten	^{nat}W foils	21 MeV d
Lead	^{nat}Pb foils	36 MeV p	Lead	^{nat}Pb foils	21 MeVn d
Manganese	^{nat}**Mn**CuNi foils	70 MeV p 36 MeV p	Manganese	^{nat}**Mn**CuNi foils	40 MeV d 21 MeV d
Copper	^{nat}Mn**Cu**Ni foils	70 MeV p 36 MeV p	Copper	^{nat}Mn**Cu**Ni foils	40 MeV d 21 MeV d
Nickel	^{nat}MnCu**Ni** foils	70 MeV p 36 MeV p	Nickel	^{nat}MnCu**Ni** foils	40 MeV d 21 MeV d
Indium	^{nat}In foils	70 MeV p	Indium	^{nat}In foils	40 MeV d 21 MeV d
			Titan	^{nat}Ti foils	21 MeV d 10 MeV d
			Iron	^{nat}Fe foils	10 MeV d

TABLE II. SUMMARY OF THE ACTIVATION CROSS SECTIONS OF CRP RELATED DEUTERON INDUCED REACTIONS UP TO 50 MEV.

Target	Product
Ag	^{3}H ^{105}Ag, ^{106m}Ag, ^{106g}Ag, ^{108m}Ag, ^{110m}Ag, ^{110g}Ag ^{107}Cd, ^{109}Cd ^{109g}Pd
Al	^{1}H, ^{2}H, ^{3}H ^{3}He, ^{4}He ^{7}Be ^{27}Mg ^{22}Na, ^{24}Na ^{28}Al ^{27}Si
C	^{1}H ^{13}N, ^{14}N ^{11}C, ^{14}C ^{10}B ^{8}Li ^{7}Be
Co	^{56}Ni, ^{57}Ni ^{55}Co, ^{56}Co, ^{57}Co, ^{58}Co, ^{60}Co, ^{60m}Co ^{52}Fe, ^{59}Fe ^{52}Mn, ^{54}Mn, ^{56}Mn ^{51}Cr ^{48}V ^{46}Sc, ^{47}Sc
Cr	^{50m}Mn, ^{51}Mn, ^{52}Mn, ^{52m}Mn, ^{53}Mn, ^{54}Mn, ^{56}Mn ^{49}Cr, ^{51}Cr, ^{55}Cr ^{48}V, ^{52}V
Cu	^{3}H ^{4}He ^{52}Mn, ^{56}Mn ^{52}Fe, ^{59}Fe ^{57}Co, ^{58}Co, ^{60}Co ^{57}Ni, ^{65}Ni ^{61}Cu, ^{62}Cu, ^{64}Cu, ^{66}Cu ^{62}Zn, ^{63}Zn, ^{65}Zn
Fe	^{4}He ^{51}Cr ^{52m}Mn, ^{52g}Mn, ^{54}Mn, ^{56}Mn ^{53}Fe, ^{59}Fe ^{55}Co, ^{56}Co, ^{57}Co, ^{58}Co
H	^{1}H, ^{2}H, ^{3}H ^{3}He, ^{4}He
Li	Neutron ^{1}H, ^{3}H ^{3}He, ^{4}He ^{7}Be, ^{8}Be, ^{9}Be ^{5}Li, ^{6}Li, ^{7}Li, ^{8}Li
Mn	^{55}Fe ^{51}Cr ^{54}Mn, ^{56}Mn
Mo	^{88}Zr ^{90}Nb, ^{92m}Nb, ^{95m}Nb, ^{95g}Nb, ^{96}Nb ^{99}Mo, ^{101}Mo ^{93m}Tc, ^{93g}Tc, ^{94m}Tc, ^{94g}Tc, ^{95m}Tc, ^{95g}Tc, ^{96}Tc, ^{97}mTc, ^{99m}Tc, ^{101}Tc

N	^{11}C ^{13}N, ^{16}N ^{15}O ^{8}Li
Nb	^{1}H, ^{3}H ^{93m}Mo ^{90}Nb, ^{91m}Nb, ^{92m}Nb, ^{95}Nb ^{90}Y ^{88}Zr, ^{89}Zr
Ni	^{1}H, ^{2}H, ^{3}H ^{3}He, ^{4}He ^{51}Cr ^{52g}Mn, ^{54}Mn, ^{56}Mn ^{55}Co, ^{56}Co, ^{57}Co, ^{58}Co, ^{60}Co, ^{61}Co ^{56}Ni, ^{57}Ni, ^{65}Ni ^{55}Fe, ^{59}Fe ^{59}Cu, ^{60}Cu, ^{61}Cu, ^{62}Cu, ^{64}Cu
O	^{13}N, ^{14}N, ^{16}N ^{18}F, ^{17}F ^{19}O
P	No data in EXFOR, other sources should be checked
S	^{34m}Cl ^{30}P, ^{32}P
Sb	^{116}Te, ^{118}Te, ^{119}Te, ^{121m}Te, ^{121g}Te, ^{123m}Te ^{118m}Sb, ^{119}Sb, ^{122}Sb, ^{124}Sb ^{108}Sn, ^{113}Sn, ^{117m}Sn, ^{121}Sn ^{111}In, ^{114m}In
Si	^{7}Be ^{22}Na, ^{24}Na ^{28}Al, ^{29}Al ^{29}P, ^{32}P
Sn	^{3}H ^{111g}In, ^{114m}In ^{110}Sn, ^{113g}Sn, ^{117m}Sn, ^{123m}Sn, ^{123g}Sn ^{115}Sb, ^{116m}Sb, ^{117}Sb, ^{118m}Sb, ^{120m}Sb, ^{122}Sb, ^{124}Sb, ^{125}Sb
Ta	^{1}H ^{175}Ta, ^{178}Ta, ^{180g}Ta, ^{182m}Ta, ^{182g}Ta ^{176}W, ^{177}W, ^{178}W, ^{181}W ^{173}Hf, ^{175}Hf, ^{179m}Hf, ^{180m}Hf, ^{181}Hf ^{126}Xe, ^{127}Xe, ^{128}Xe
Ti	^{4}He ^{43}Sc, ^{44m}Sc, ^{44g}Sc, ^{46}Sc, ^{47}Sc, ^{48}Sc ^{47}V, ^{48}V, ^{49}V
V	^{3}H ^{4}He ^{47}Ca ^{48}Cr, ^{49}Cr, ^{51}Cr ^{44m}Sc, ^{44g}Sc, ^{46}Sc, ^{47}Sc, ^{48}Sc ^{48}V, ^{49}V ^{41}Ar ^{42}K, ^{43}K
W	^{185}W, ^{187}W ^{181}Re, ^{182m}Re, ^{182g}Re, ^{183}Re, ^{184m}Re, ^{184g}Re, ^{186g}Re ^{182}Ta, ^{183}Ta, ^{184}Ta

TABLE III. SUMMARY OF THE ACTIVATION CROSS SECTIONS OF CRP RELATED PROTON INDUCED REACTIONS UP TO 100 MEV.

Ag	^{3}H ^{7}Be ^{94m}Tc, ^{94g}Tc ^{97}Ru ^{99g}Rh, ^{100g}Rh, ^{101m}Rh, ^{102g}Rh, ^{105g}Rh ^{100}Pd, ^{101}Pd, ^{103}Pd, ^{104}Pd ^{103}Ag, ^{104}Ag, ^{105}Ag, ^{106m}Ag, ^{106g}Ag ^{104}Cd, ^{105}Cd, ^{107}Cd, ^{109}Cd
Al	^{3}H ^{7}Be, ^{9}Be, ^{10}Be ^{14}C ^{18}F ^{22}Na, ^{24}Na ^{23}Mg, ^{28}Mg ^{26}Al ^{26}Si, ^{27}Si
C	^{3}H ^{7}Be, ^{10}Be ^{10}C, ^{11}C, ^{14}C ^{13}N
Co	^{7}Be ^{44m}Sc, ^{46g}Sc, ^{47}Sc ^{48}V, ^{53}V ^{48}Cr, ^{51}Cr ^{51}Mn, ^{52m}Mn, ^{52g}Mn, ^{54}Mn, ^{56}Mn ^{52}Fe, ^{53m}Fe, ^{53g}Fe, ^{55}Fe, ^{59}Fe ^{55}Co, ^{56}Co, ^{57}Co, ^{58m}Co, ^{58g}Co ^{56}Ni, ^{57}Ni, ^{59}Ni, ^{60}Ni
Cr	^{45}Ti ^{48}V ^{48}Cr, ^{49}Cr, ^{51}Cr ^{50m}Mn, ^{50g}Mn, ^{51}Mn, ^{52m}Mn, ^{52g}Mn, ^{53}Mn, ^{54}Mn, ^{56}Mn
Cu	^{7}Be ^{44m}Sc, ^{44g}Sc, ^{46g}Sc ^{48}V ^{48}Cr, ^{49}Cr, ^{51}Cr, ^{52}Mn, ^{54}Mn ^{56}Mn, ^{52}Fe, ^{55}Fe, ^{59}Fe ^{55}Co, ^{56}Co, ^{57}Co, ^{58m}Co, ^{58g}Co, ^{60}Co, ^{61}Co ^{56}Ni, ^{57}Ni ^{60}Cu, ^{61}Cu, ^{62}Cu, ^{64}Cu ^{60}Zn, ^{62}Zn, ^{63}Zn, ^{65}Zn, ^{66}Zn
Fe	^{3}H ^{7}Be, ^{10}Be ^{36}Cl ^{44m}Sc, ^{44g}Sc, ^{46g}Sc, ^{47}Sc, ^{48}Sc ^{44}Ti ^{48}V ^{48}Cr, ^{51}Cr ^{51}Mn, ^{52m}Mn, ^{52g}Mn, ^{53}Mn, ^{54}Mn ^{52}gFe, ^{53m}Fe, ^{53g}Fe, ^{55}Fe ^{55}Co, ^{56}Co, ^{57}Co, ^{58m}Co, ^{58g}Co, ^{59}Co
Li	^{3}H, ^{7}Be
Mn	^{10}Be ^{43}K ^{44m}Sc, ^{46}Sc, ^{47}Sc, ^{48}Sc ^{48}V ^{48}Cr, ^{51}Cr ^{52g}Mn, ^{54}Mn ^{52}Fe, ^{53m}Fe, ^{53g}Fe, ^{55}Fe

Mo	^{86}Y, ^{87m}Y, ^{87g}Y, ^{88}Y ^{86}Zr, ^{88}Zr, ^{89m}Zr, ^{89g}Zr ^{88m}Nb, ^{88g}Nb ^{89g}Nb, ^{90}Nb, ^{92m}Nb, ^{95m}Nb, ^{96}Nb, ^{97}Nb ^{90}Mo, ^{93m}Mo, ^{99}Mo ^{93m}Tc, ^{93g}Tc, ^{94m}Tc, ^{94g}Tc, ^{95m}Tc, ^{95g}Tc, ^{96m}Tc, ^{96g}Tc, ^{99m}Tc, ^{99g}Tc
N	^{3}H ^{7}Be, ^{10}Be ^{11}C ^{13}N ^{14}O, ^{15}O
Nb	^{94}Mo, ^{93m}Mo, ^{93g}Mo ^{90}Mo ^{92m}Nb, ^{91m}Nb, ^{90}Nb, ^{89m}Nb ^{89g}Zr, ^{88}Zr ^{88}Y, ^{87m}Y, ^{87g}Y, ^{86g}Y
Ni	^{3}H ^{7}Be, ^{10}Be ^{26}Al ^{41}Ca ^{44m}Sc, ^{46g}Sc, ^{47}Sc ^{47}V, ^{48}V, ^{49}V, ^{50}V ^{48}Cr, ^{51}Cr ^{52}Mn, ^{53}Mn, ^{54}Mn ^{52}Fe, ^{53m}Fe, ^{55}Fe, ^{59}Fe, ^{60}Fe ^{55}Co, ^{56}Co, ^{57}Co, ^{58m}Co, ^{58g}Co, ^{60}Co, ^{61}Co ^{56}Ni, ^{57}Ni, ^{59}Ni ^{59}Cu, ^{60}Cu, ^{61}Cu, ^{62}Cu, ^{64}Cu
O	^{7}Be,^{10}Be ^{11}C, ^{14}C ^{13}N ^{15}O ^{17}F, ^{18}F
P	^{22}Na,^{24}Na ^{29}Al ^{28}Mg ^{30}P
S	^{22}Na, ^{24}Na ^{28}Mg ^{34m}Cl
Sb	^{117}Te, ^{118}Te, ^{119m}Te, ^{119g}Te ^{121m}Te, ^{121g}Te, ^{123m}Te, ^{123g}Te ^{120m}Sb, ^{122}Sb ^{117m}Sn
Si	^{3}H ^{7}Be,^{10}Be ^{14}C ^{18}F ^{22}Na, ^{24}Na ^{27}Mg, ^{28}Mg ^{25}Al, ^{26}Al, ^{28}Al, ^{29}Al ^{27}Si ^{28}P, ^{29}P

Sn	^{109g}In, ^{110g}In, ^{111}In, ^{114m}In, ^{117m}In ^{113g}Sn, ^{117m}Sn ^{115}Sb, ^{116m}Sb, ^{116g}Sb, ^{117}Sb, ^{118m}Sb, ^{118g}Sb, ^{119}Sb, ^{120m}Sb, ^{120g}Sb, ^{122m}Sb, ^{122g}Sb, ^{124m1}Sb, ^{124m2}Sb, ^{124g}Sb
Ta	^{167}Tm ^{169}Yb ^{169}Lu, ^{170}Lu, ^{171}Lu, ^{172}Lu, ^{173}Lu, ^{174g}Lu, ^{179}Lu ^{170}Hf, ^{172}Hf, ^{173}Hf, ^{175}Hf, ^{179m2}Hf ^{175}Ta, ^{176}Ta, ^{177}Ta, ^{178m}Ta, ^{178g}Ta, ^{180g}Ta ^{178}W, ^{179}W, ^{180}W, ^{181}W
Ti	^{7}Be, ^{10}Be ^{24}Na ^{34m}Cl, ^{36}Cl, ^{38}Cl, ^{39}Cl ^{42}K, ^{43}K ^{47}Ca ^{43}Sc, ^{44m}Sc, ^{44g}Sc, ^{46g}Sc, ^{47}Sc, ^{48}Sc ^{44}Ti, ^{45}Ti ^{47}V, ^{48}V, ^{49}V
V	^{7}Be ^{24}Na ^{38}Cl, ^{39}Cl ^{42}K, ^{43}K ^{45}Ca, ^{47}Ca ^{43}Sc, ^{44m}Sc, ^{44g}Sc, ^{46g}Sc, ^{47}Sc, ^{48}Sc ^{44}Ti, ^{45}Ti ^{48}V, ^{49}V ^{48}Cr, ^{49}Cr, ^{51}Cr
W	^{83}Rb ^{85g}Sr ^{87g}Y, ^{88}Y ^{88}Zr ^{169}Yb ^{171}Lu, ^{173}Lu, ^{177}Lu ^{173}Hf, ^{175}Hf, ^{179m2}Hf, ^{181}Hf ^{176}Ta, ^{177}Ta, ^{182}Ta, ^{183}Ta, ^{184}Ta ^{178}W ^{180}Re, ^{181}Re, ^{183}Re, ^{184m}Re, ^{184g}Re, ^{186m}Re, ^{186}Re

Example: Co+d

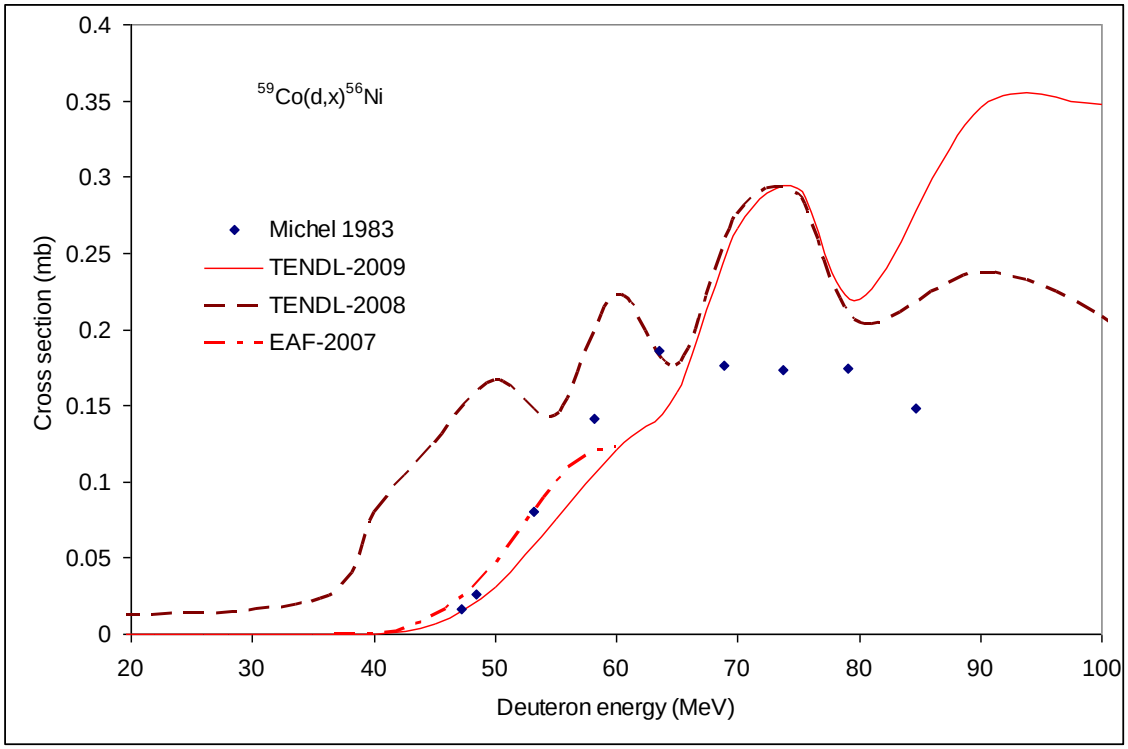
^{59}Co(d,x)^{56}Ni
Michel 1983
TENDL-2009
TENDL-2008
EAF-2007
Cross section (mb)
Deuteron energy (MeV)
0.4
0.35
0.3
0.25
0.2
0.15
0.1
0.05
0
20
30
40
50
60
70
80
90
100

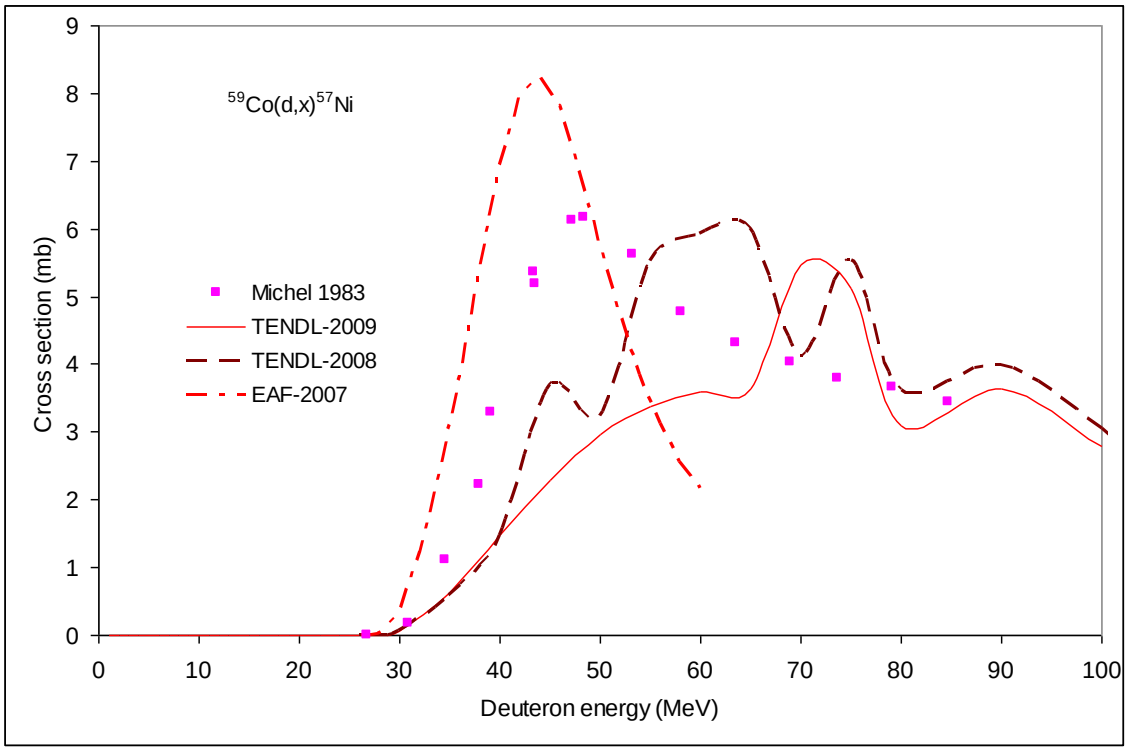
^{59}Co(d,x)^{57}Ni
Michel 1983
TENDL-2009
TENDL-2008
EAF-2007
Cross section (mb)
Deuteron energy (MeV)
9
8
7
6
5
4
3
2
1
0
0
10
20
30
40
50
60
70
80
90
100

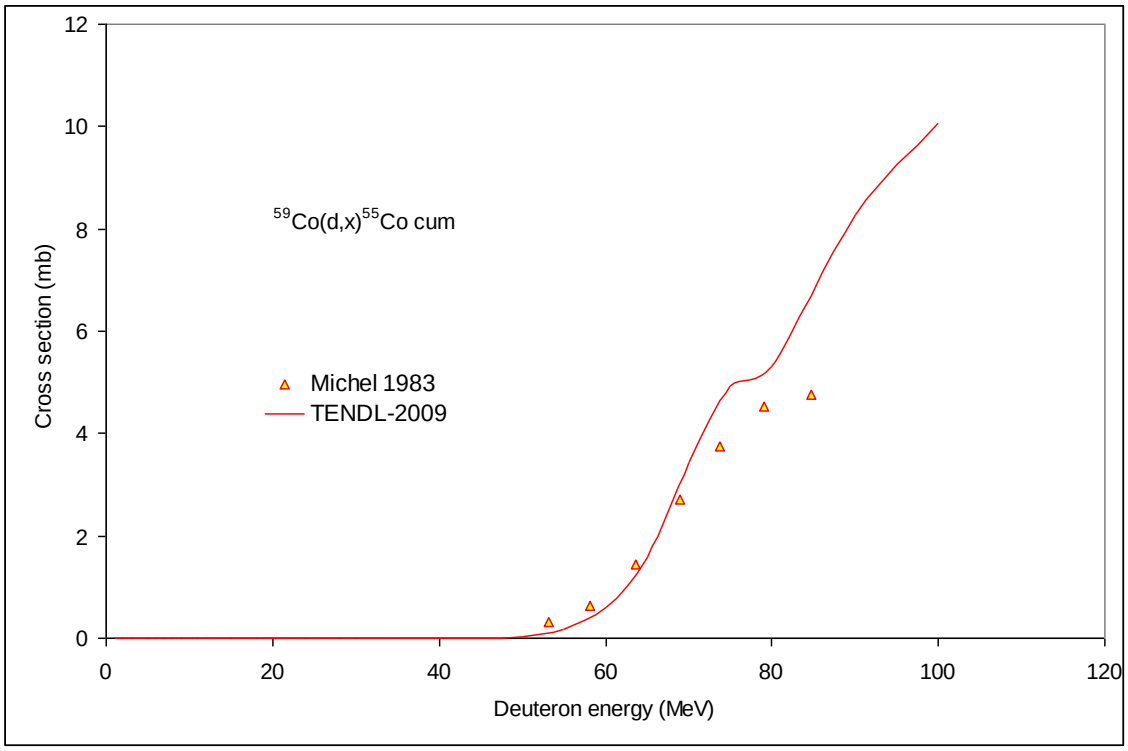
12
10
8
6
4
2
0
0
20
40
60
80
100
120
Cross section (mb)
Deuteron energy (MeV)
59Co(d,x)55Co cum
Michel 1983
TENDL-2009

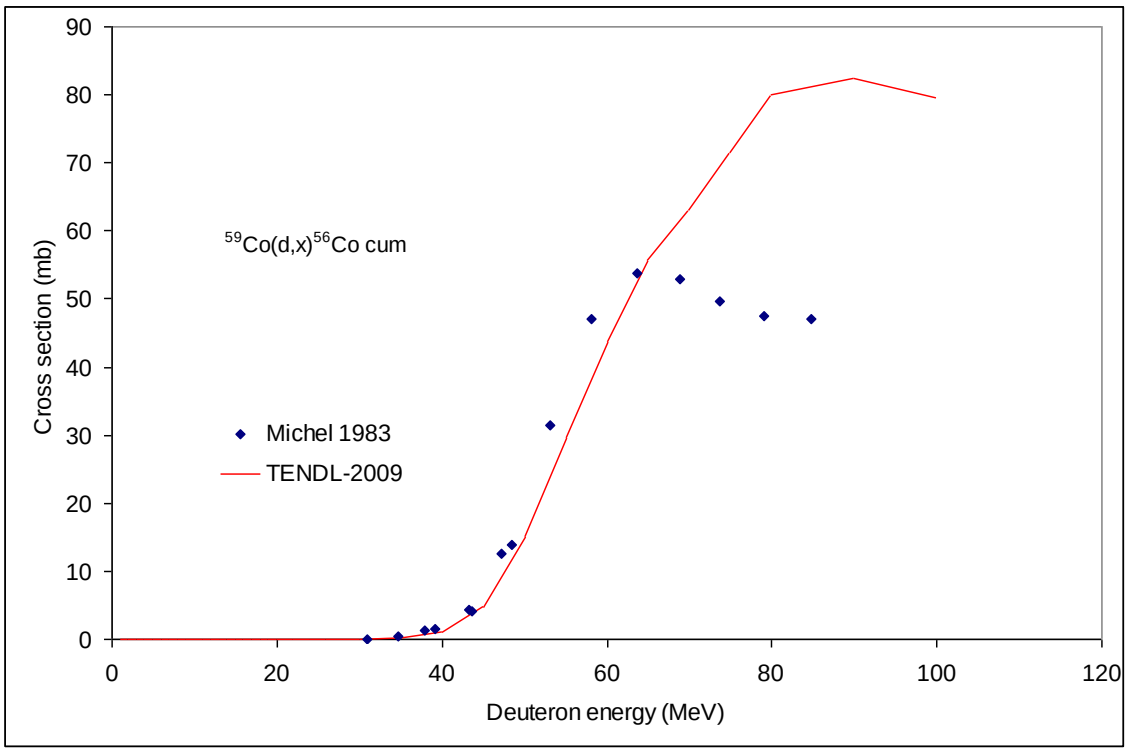
90
80
70
60
50
40
30
20
10
0
0
20
40
60
80
100
120
Cross section (mb)
Deuteron energy (MeV)
59Co(d,x)56Co cum
Michel 1983
TENDL-2009

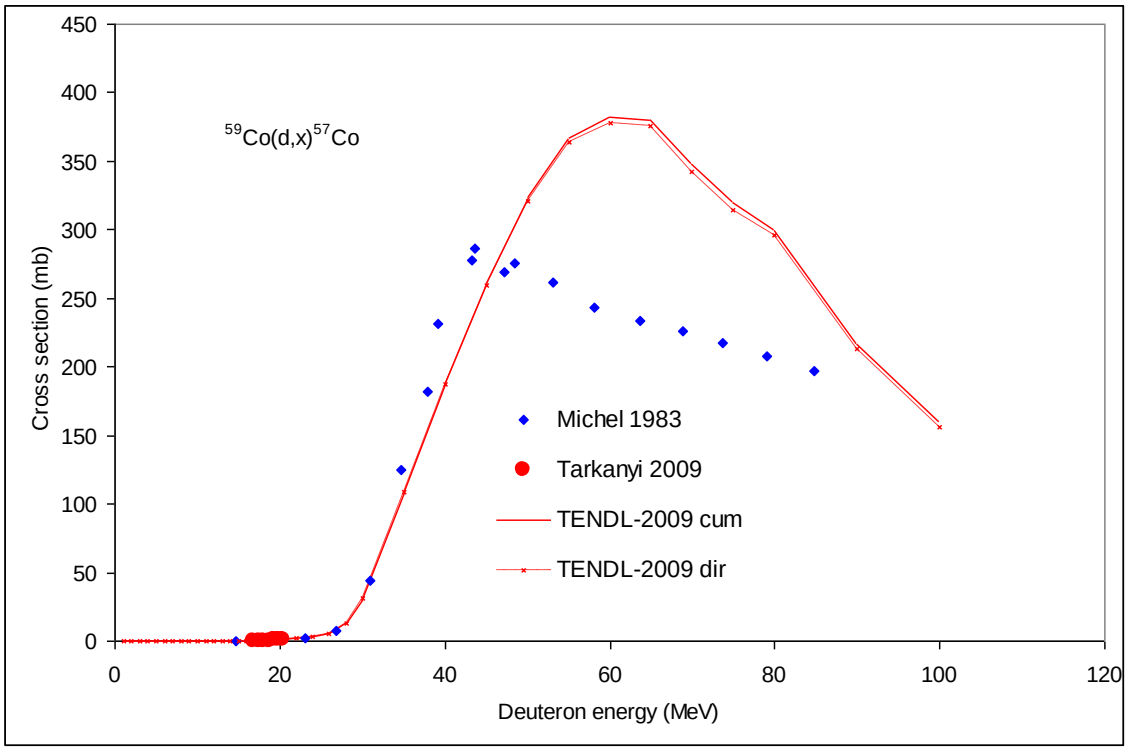
^{59}Co(d,x)^{57}Co
Cross section (mb)
Deuteron energy (MeV)
Michel 1983
Tarkanyi 2009
TENDL-2009 cum
TENDL-2009 dir
0
50
100
150
200
250
300
350
400
450
0
20
40
60
80
100
120

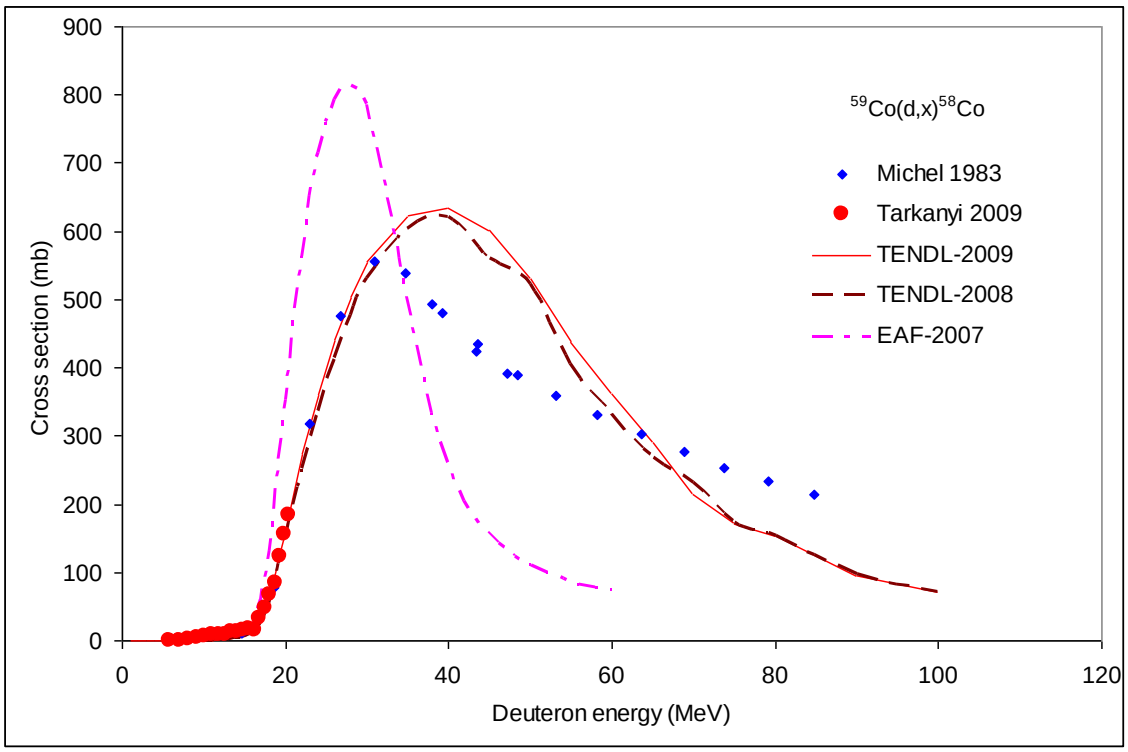
^{59}Co(d,x)^{58}Co
Cross section (mb)
Deuteron energy (MeV)
Michel 1983
Tarkanyi 2009
TENDL-2009
TENDL-2008
EAF-2007
0
100
200
300
400
500
600
700
800
900
0
20
40
60
80
100
120

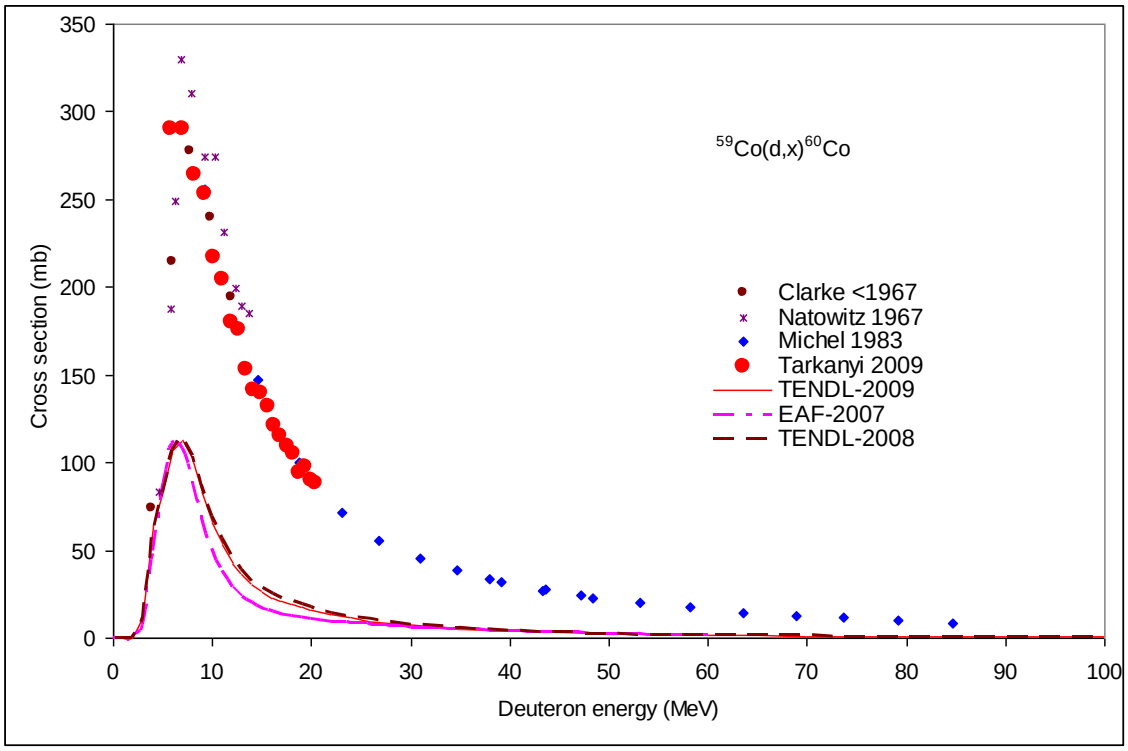
^{59}Co(d,x)^{60}Co
Clarke <1967
Natowitz 1967
Michel 1983
Tarkanyi 2009
TENDL-2009
EAF-2007
TENDL-2008
Cross section (mb)
Deuteron energy (MeV)
0
50
100
150
200
250
300
350
0
10
20
30
40
50
60
70
80
90
100

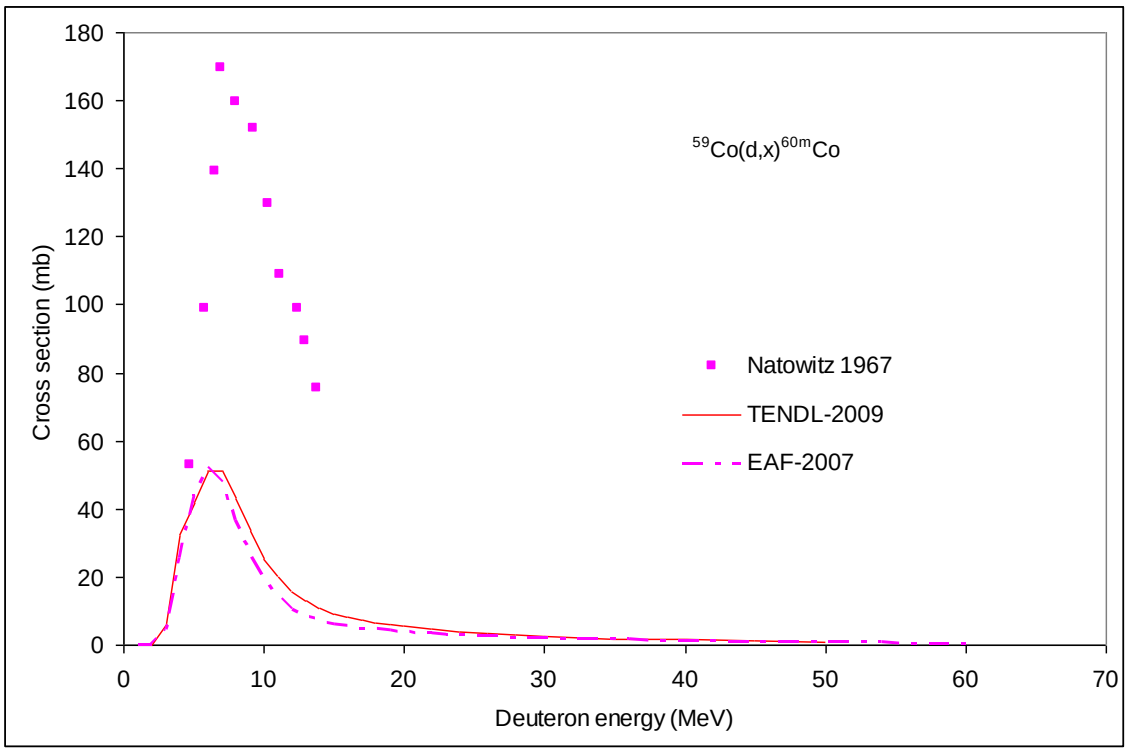
^{59}Co(d,x)^{60m}Co
Natowitz 1967
TENDL-2009
EAF-2007
Cross section (mb)
Deuteron energy (MeV)
0
20
40
60
80
100
120
140
160
180
0
10
20
30
40
50
60
70

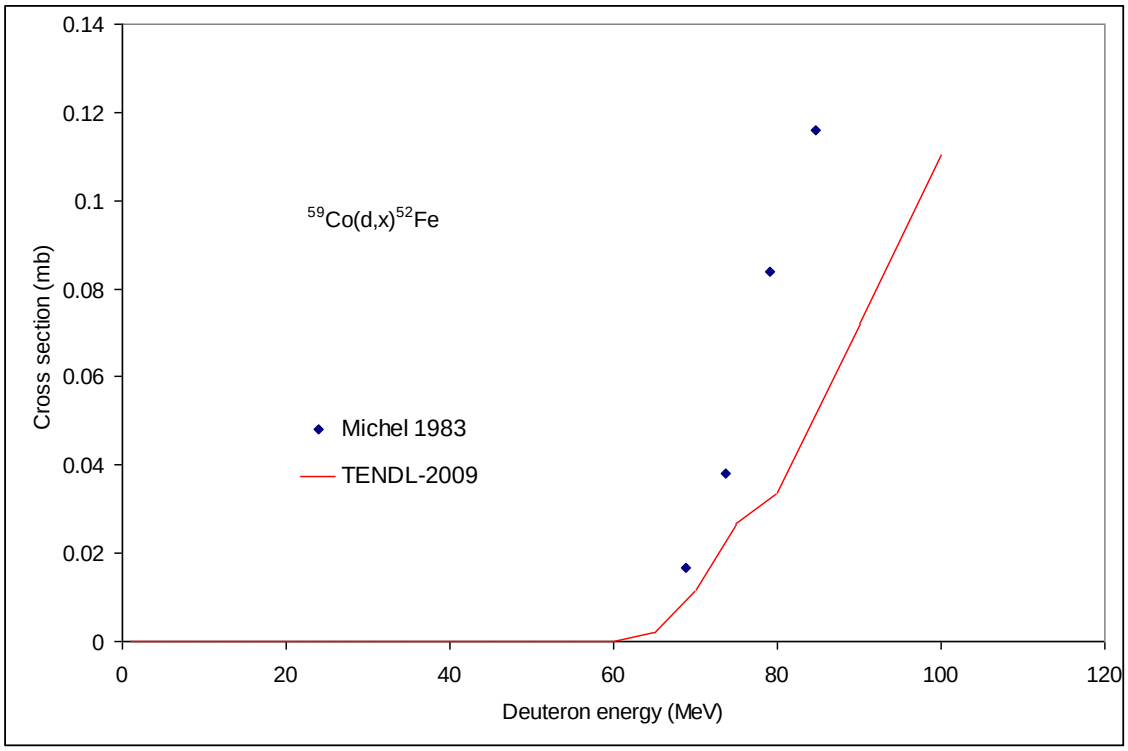
0.14
0.12
0.1
0.08
0.06
0.04
0.02
0
Cross section (mb)
59Co(d,x)52Fe
Michel 1983
TENDL-2009
0
20
40
60
80
100
120
Deuteron energy (MeV)

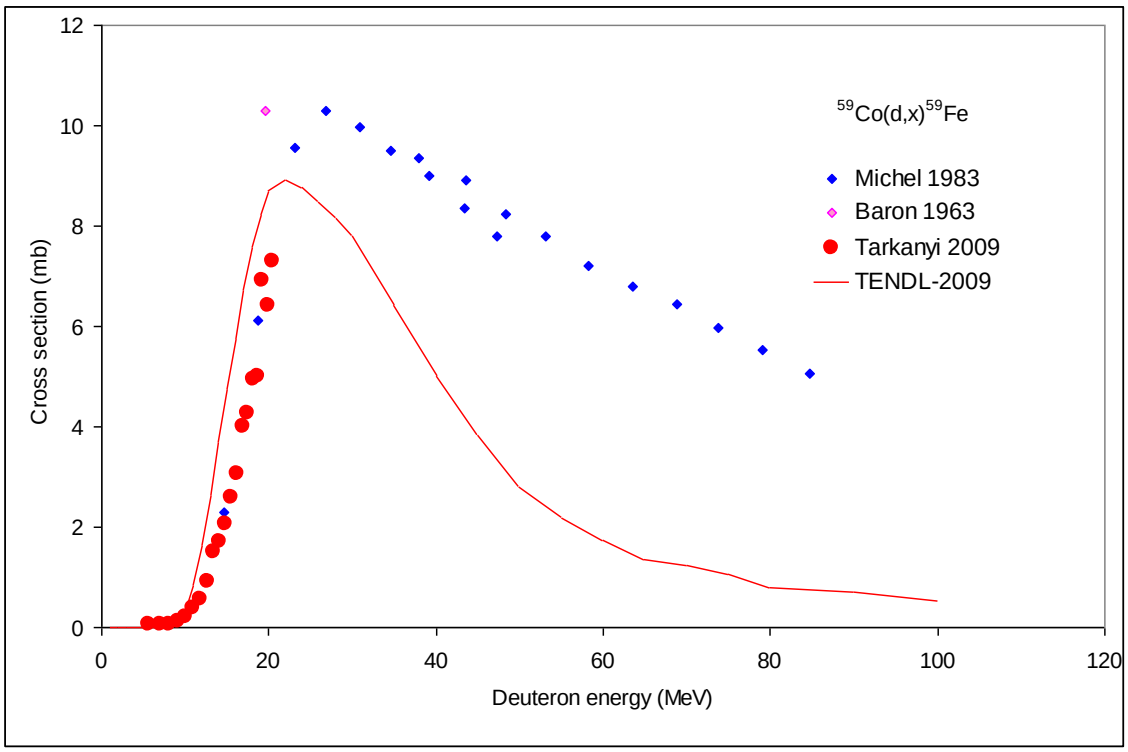
12
10
8
6
4
2
0
Cross section (mb)
59Co(d,x)59Fe
Michel 1983
Baron 1963
Tarkanyi 2009
TENDL-2009
0
20
40
60
80
100
120
Deuteron energy (MeV)

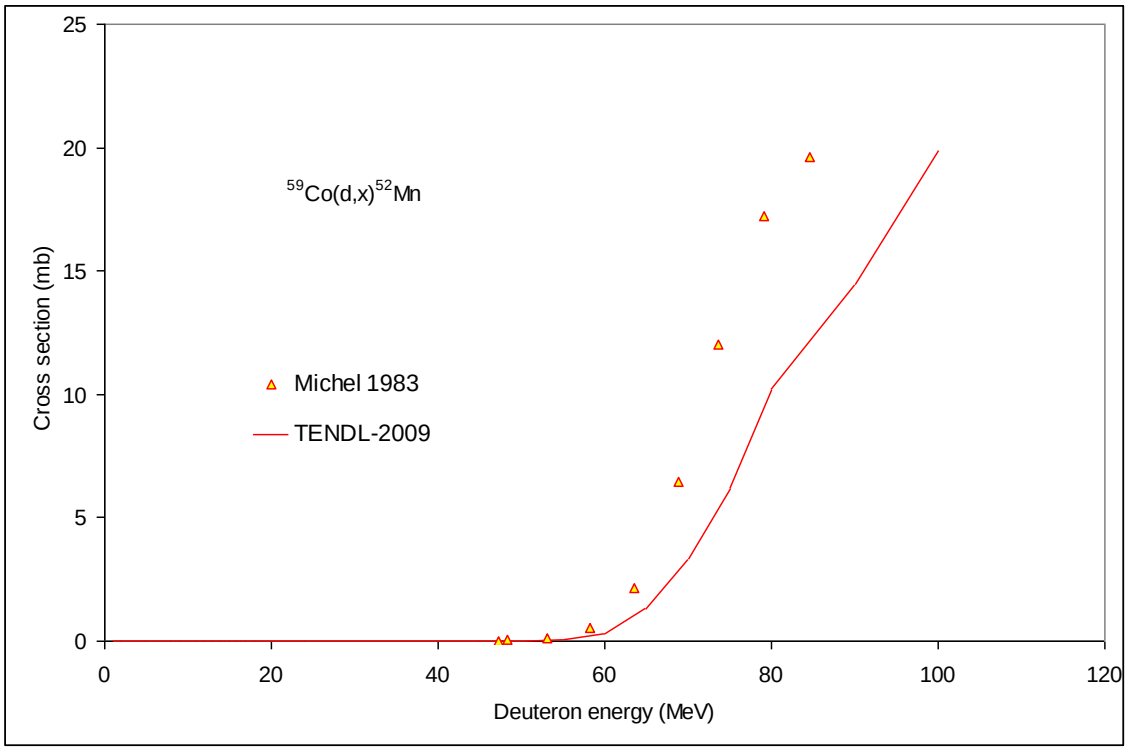
25
20
15
10
5
0
0
20
40
60
80
100
120
Cross section (mb)
Deuteron energy (MeV)
59Co(d,x)52Mn
Michel 1983
TENDL-2009

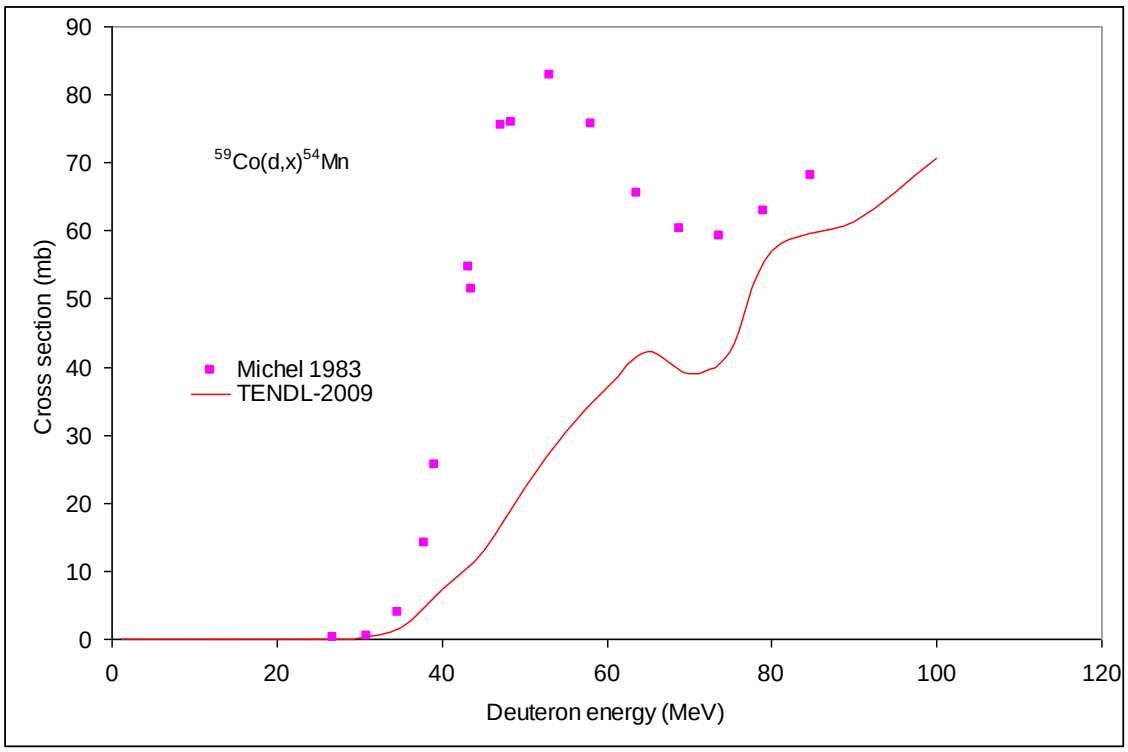
90
80
70
60
50
40
30
20
10
0
0
20
40
60
80
100
120
Cross section (mb)
Deuteron energy (MeV)
59Co(d,x)54Mn
Michel 1983
TENDL-2009

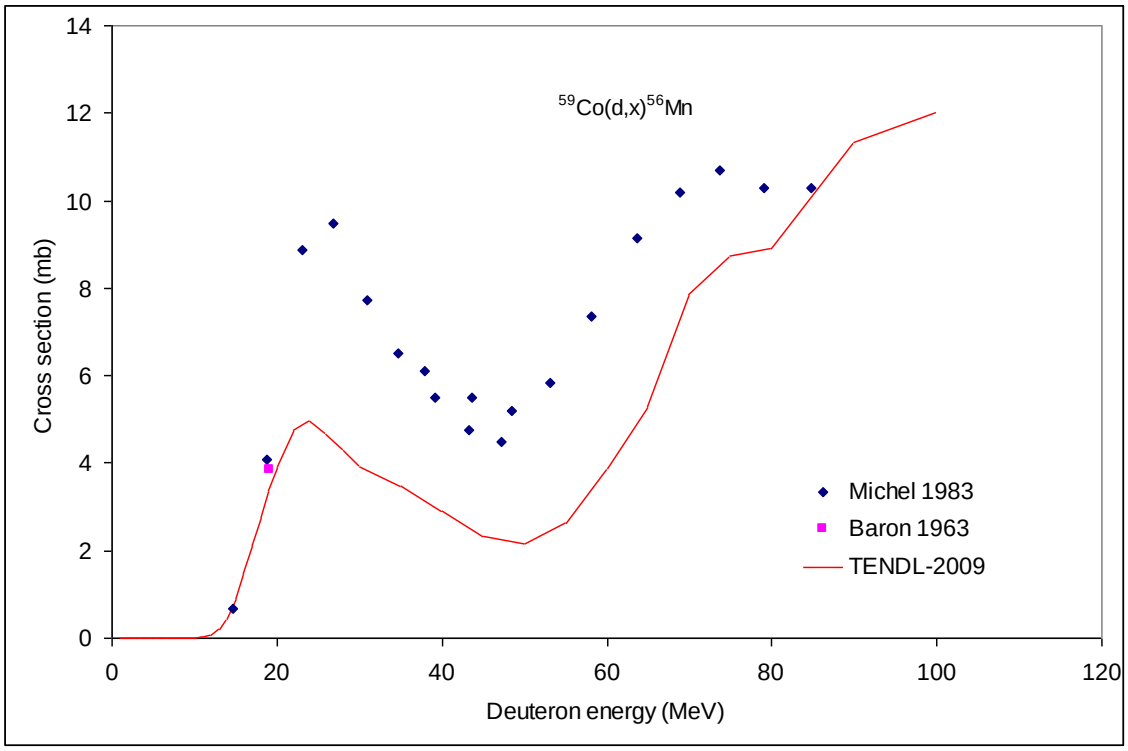
^{59}Co(d,x)^{56}Mn
Cross section (mb)
Deuteron energy (MeV)
Michel 1983
Baron 1963
TENDL-2009
0
2
4
6
8
10
12
14
0
20
40
60
80
100
120

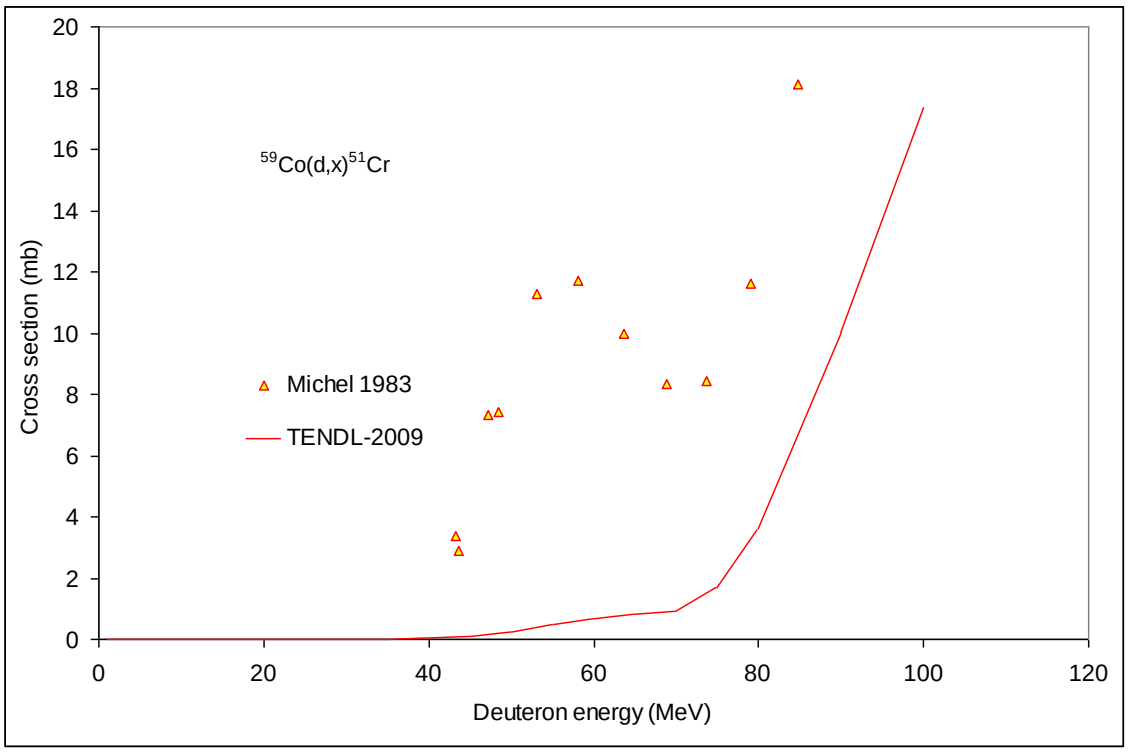
^{59}Co(d,x)^{51}Cr
Cross section (mb)
Deuteron energy (MeV)
Michel 1983
TENDL-2009
0
2
4
6
8
10
12
14
16
18
20
0
20
40
60
80
100
120

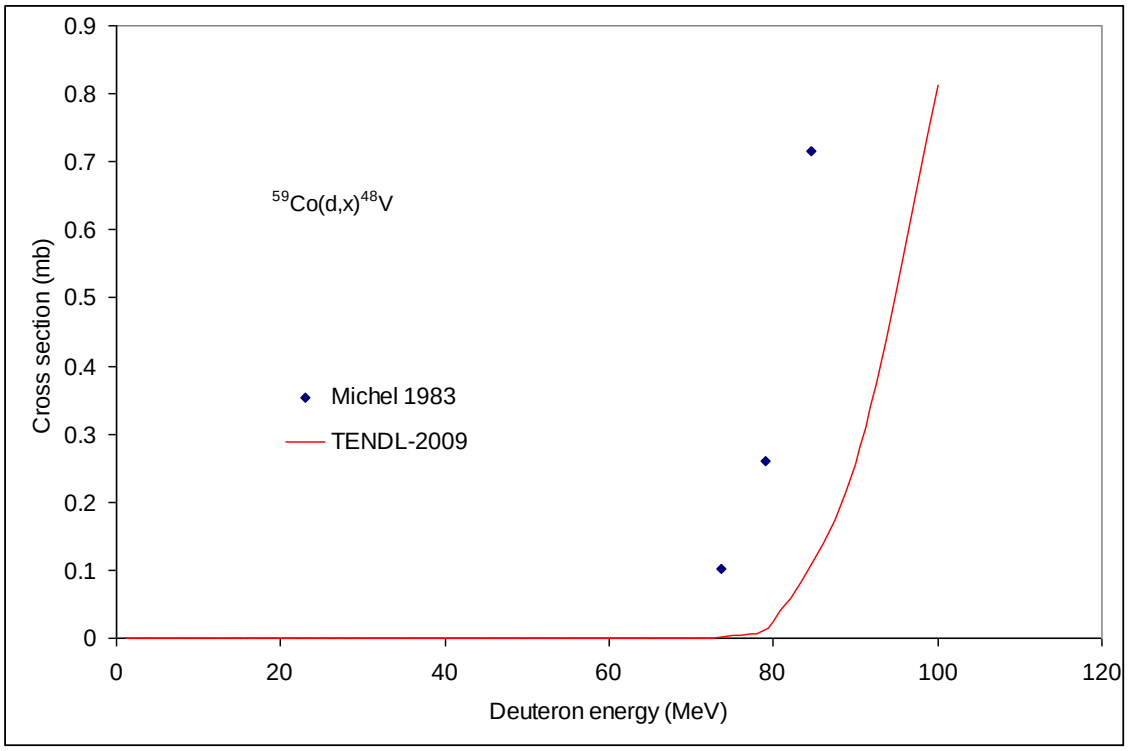
0.9
0.8
0.7
0.6
0.5
0.4
0.3
0.2
0.1
0
Cross section (mb)
59Co(d,x)48V
Michel 1983
TENDL-2009
0
20
40
60
80
100
120
Deuteron energy (MeV)

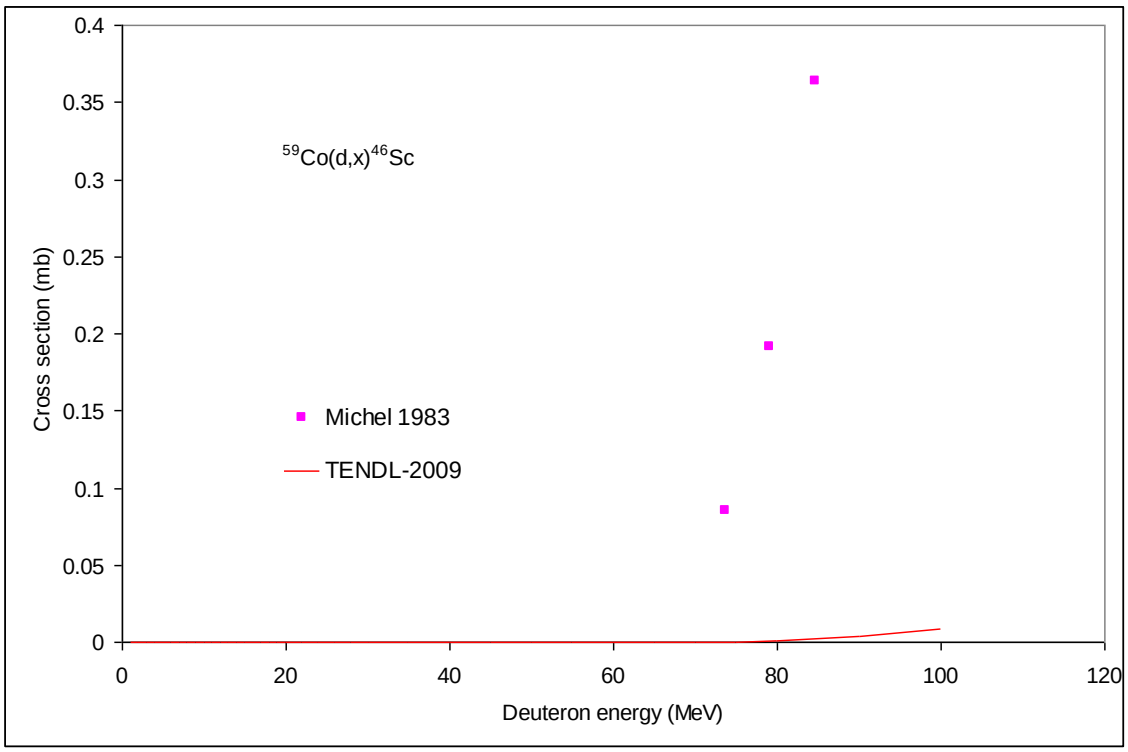
0.4
0.35
0.3
0.25
0.2
0.15
0.1
0.05
0
Cross section (mb)
59Co(d,x)46Sc
Michel 1983
TENDL-2009
0
20
40
60
80
100
120
Deuteron energy (MeV)

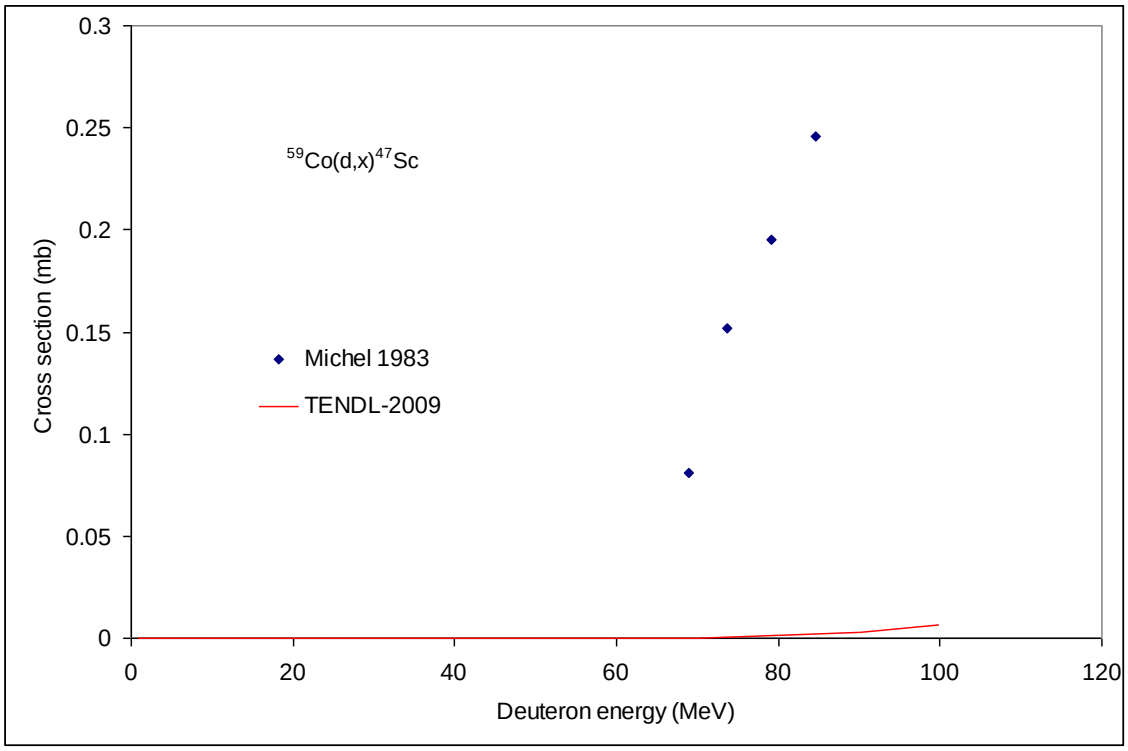
0.3
0.25
0.2
0.15
0.1
0.05
0
Cross section (mb)
59Co(d,x)47Sc
Michel 1983
TENDL-2009
0
20
40
60
80
100
120
Deuteron energy (MeV)

Example: Ta+d

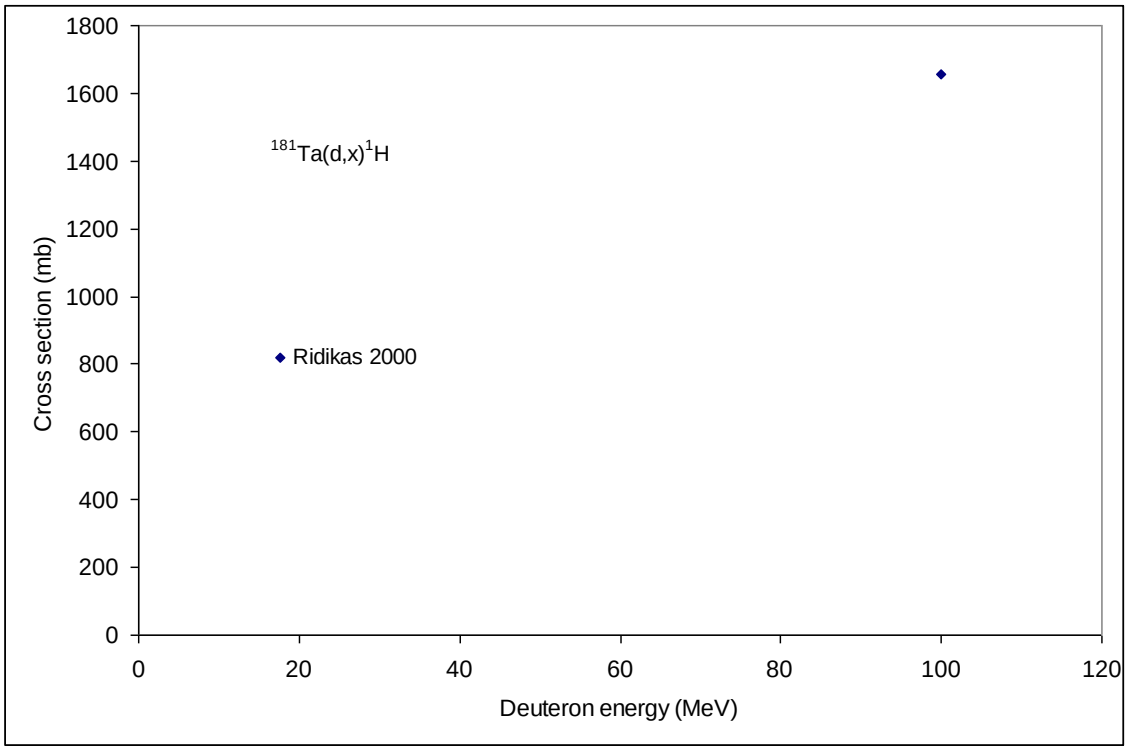
181Ta(d,x)1H
Ridikas 2000
Cross section (mb)
Deuteron energy (MeV)
0
200
400
600
800
1000
1200
1400
1600
1800
0
20
40
60
80
100
120

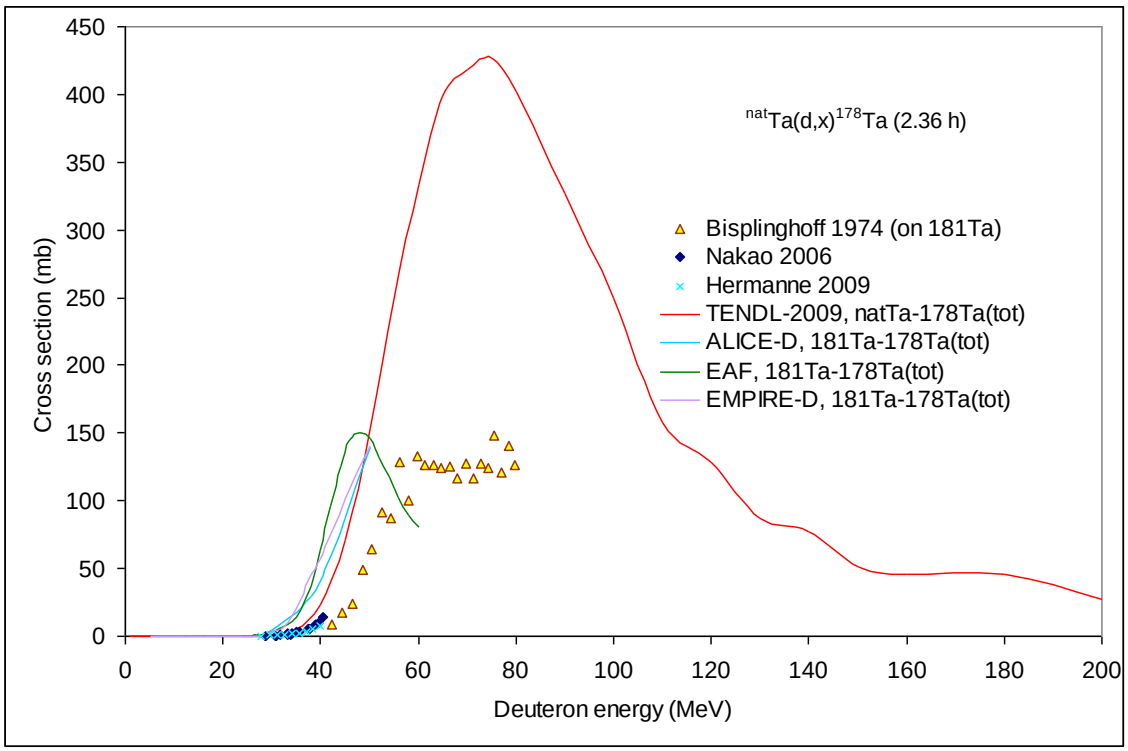
natTa(d,x)178Ta (2.36 h)
Bisplinghoff 1974 (on 181Ta)
Nakao 2006
Hermanne 2009
TENDL-2009, natTa-178Ta(tot)
ALICE-D, 181Ta-178Ta(tot)
EAF, 181Ta-178Ta(tot)
EMPIRE-D, 181Ta-178Ta(tot)
Cross section (mb)
Deuteron energy (MeV)
0
50
100
150
200
250
300
350
400
450
0
20
40
60
80
100
120
140
160
180
200

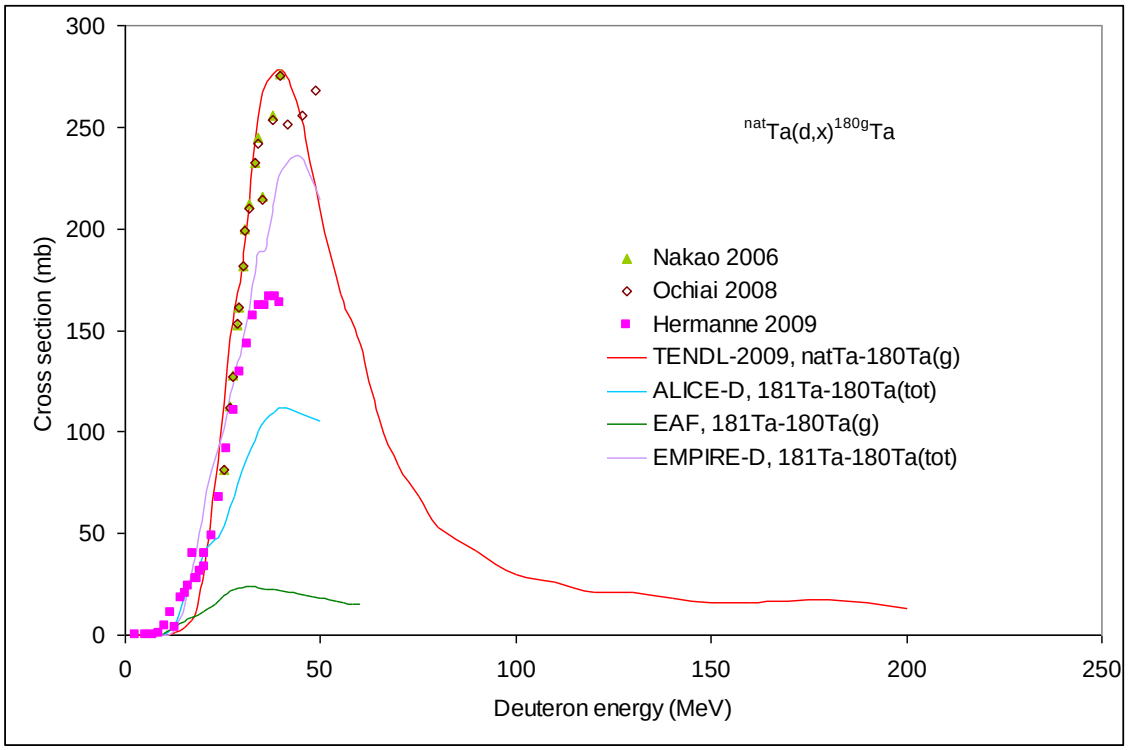
300
250
200
150
100
50
0
Cross section (mb)
0
50
100
150
200
250
Deuteron energy (MeV)
natTa(d,x)180gTa
Nakao 2006
Ochiai 2008
Hermanne 2009
TENDL-2009, natTa-180Ta(g)
ALICE-D, 181Ta-180Ta(tot)
EAF, 181Ta-180Ta(g)
EMPIRE-D, 181Ta-180Ta(tot)

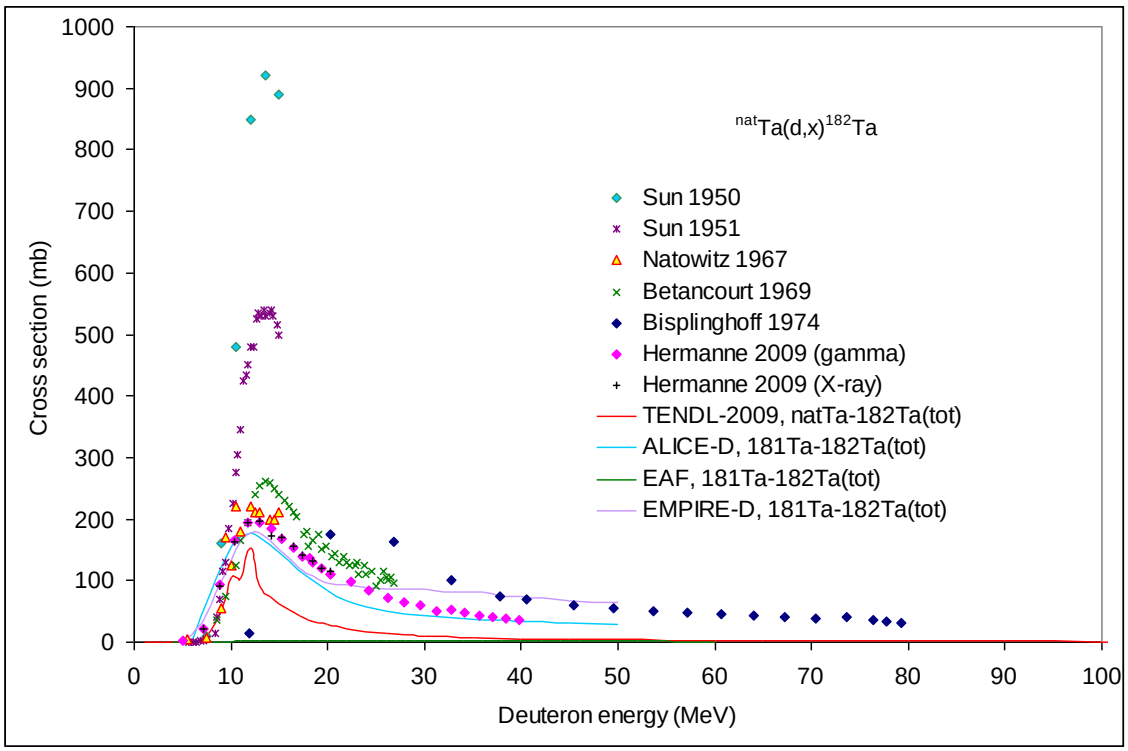
1000
900
800
700
600
500
400
300
200
100
0
Cross section (mb)
0
10
20
30
40
50
60
70
80
90
100
Deuteron energy (MeV)
natTa(d,x)182Ta
Sun 1950
Sun 1951
Natowitz 1967
Betancourt 1969
Bisplinghoff 1974
Hermanne 2009 (gamma)
Hermanne 2009 (X-ray)
TENDL-2009, natTa-182Ta(tot)
ALICE-D, 181Ta-182Ta(tot)
EAF, 181Ta-182Ta(tot)
EMPIRE-D, 181Ta-182Ta(tot)

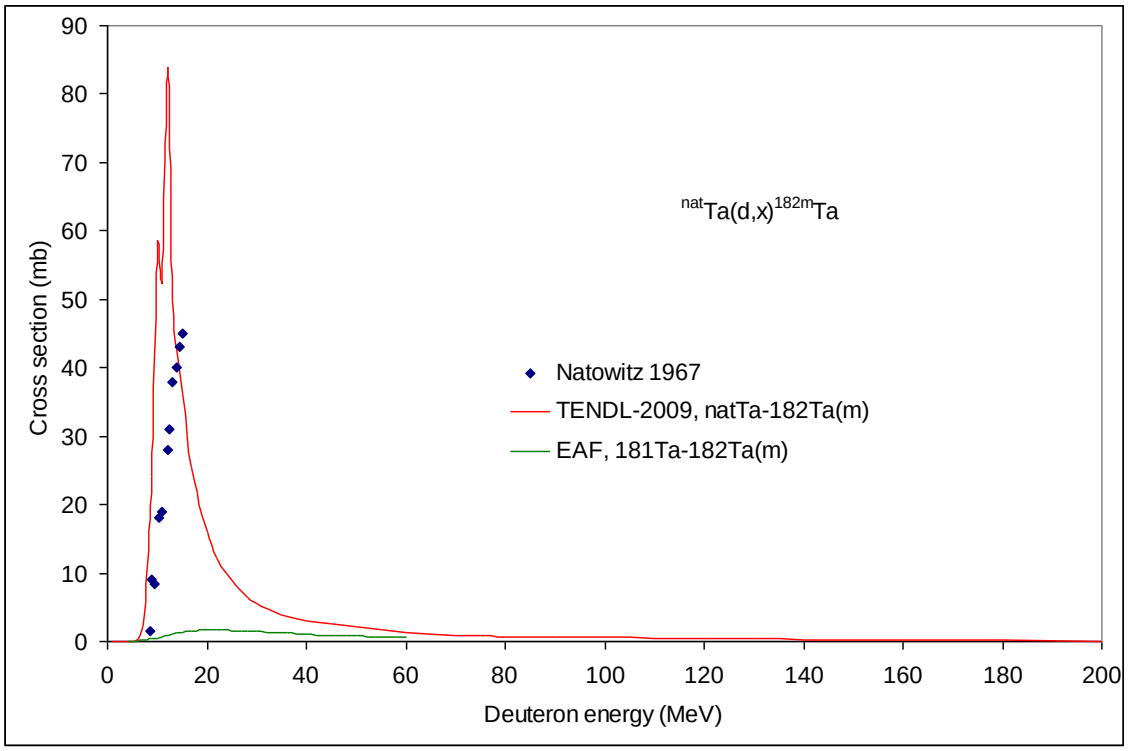
90
80
70
60
50
40
30
20
10
0
Cross section (mb)
0
20
40
60
80
100
120
140
160
180
200
Deuteron energy (MeV)
natTa(d,x)182mTa
Natowitz 1967
TENDL-2009, natTa-182Ta(m)
EAF, 181Ta-182Ta(m)

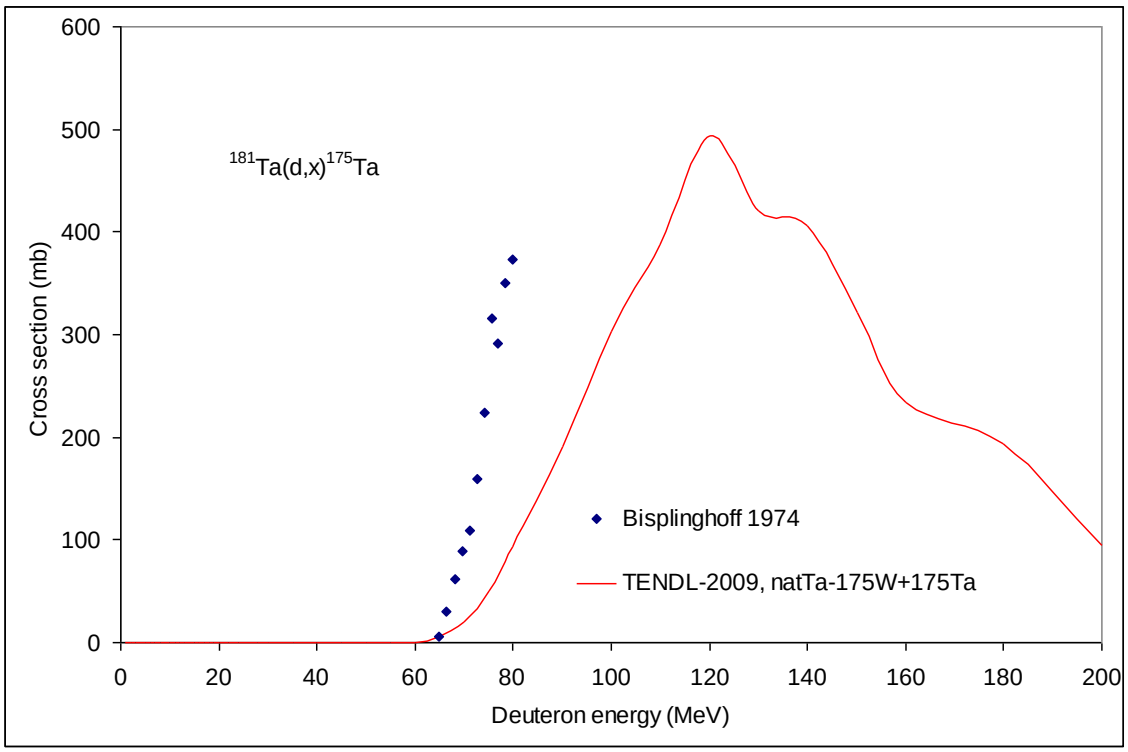
600
500
400
300
200
100
0
Cross section (mb)
0
20
40
60
80
100
120
140
160
180
200
Deuteron energy (MeV)
181Ta(d,x)175Ta
Bisplinghoff 1974
TENDL-2009, natTa-175W+175Ta

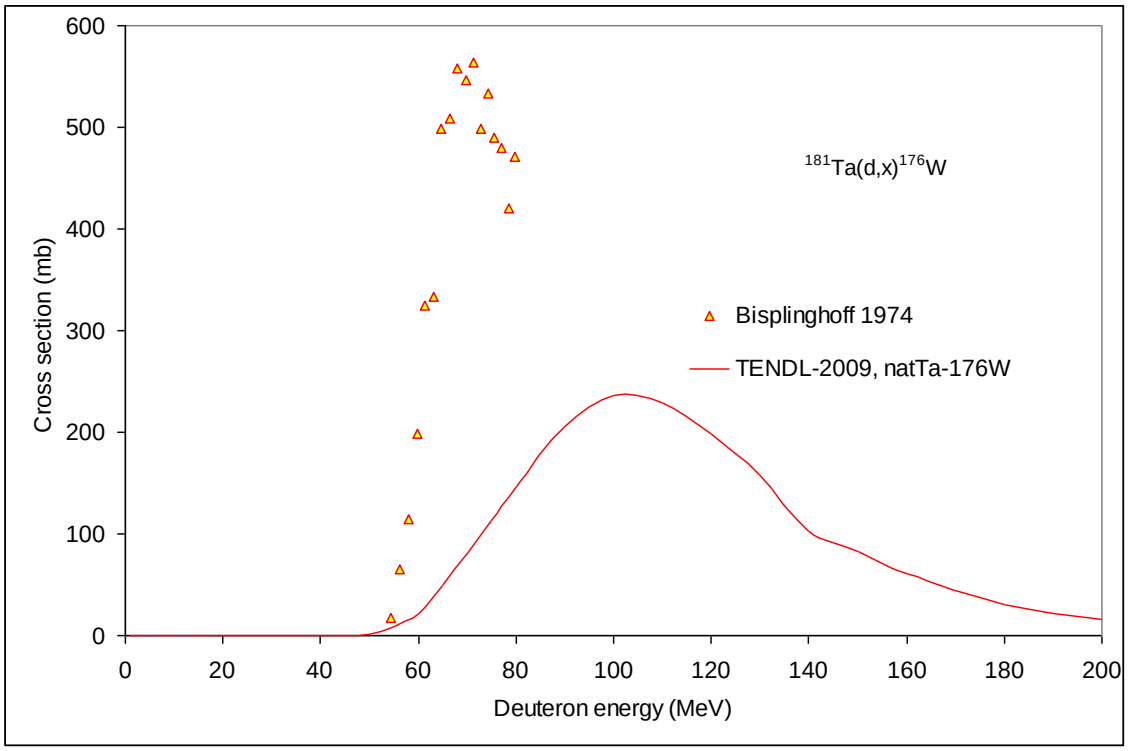
600
500
400
300
200
100
0
Cross section (mb)
0
20
40
60
80
100
120
140
160
180
200
Deuteron energy (MeV)
^{181}Ta(d,x)^{176}W
Bisplinghoff 1974
TENDL-2009, natTa-176W

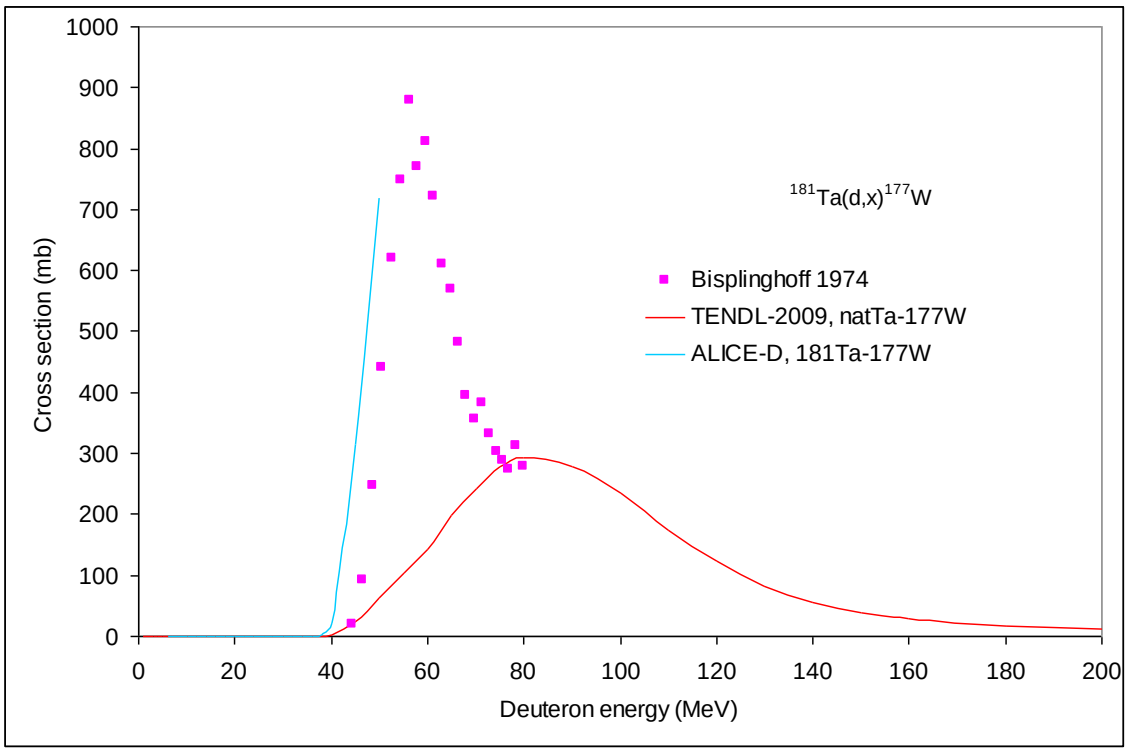
1000
900
800
700
600
500
400
300
200
100
0
Cross section (mb)
0
20
40
60
80
100
120
140
160
180
200
Deuteron energy (MeV)
^{181}Ta(d,x)^{177}W
Bisplinghoff 1974
TENDL-2009, natTa-177W
ALICE-D, 181Ta-177W

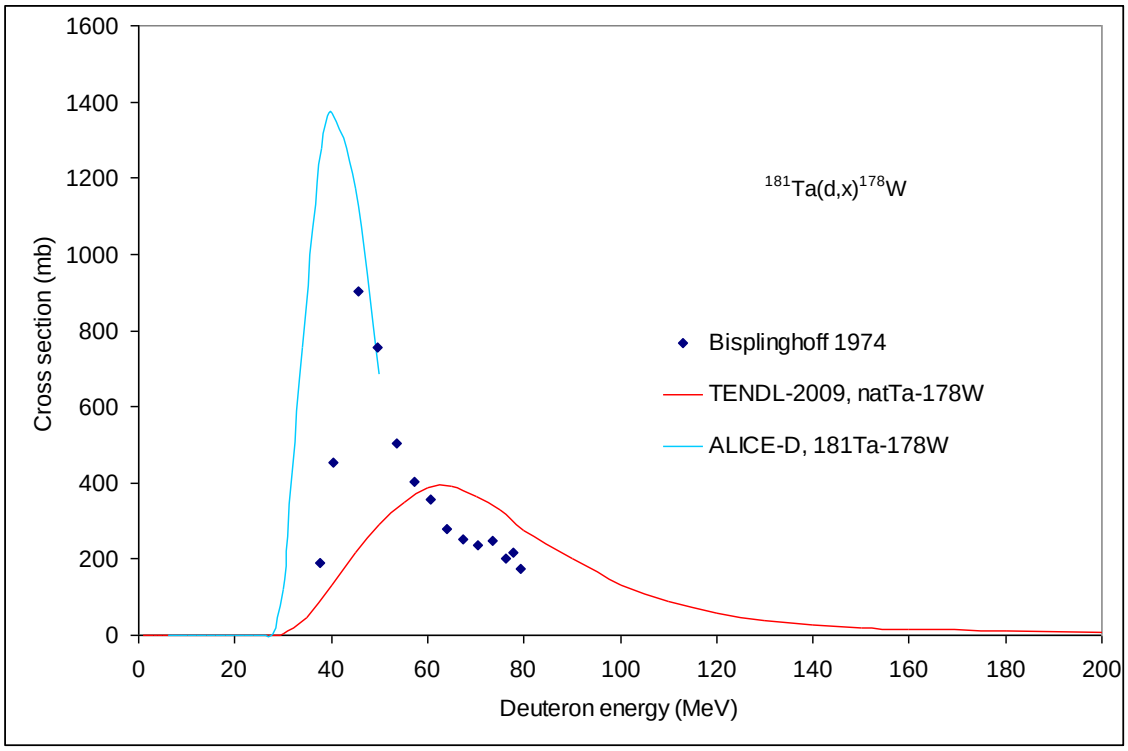
1600
1400
1200
1000
800
600
400
200
0
Cross section (mb)
0
20
40
60
80
100
120
140
160
180
200
Deuteron energy (MeV)
181Ta(d,x)178W
Bisplinghoff 1974
TENDL-2009, natTa-178W
ALICE-D, 181Ta-178W

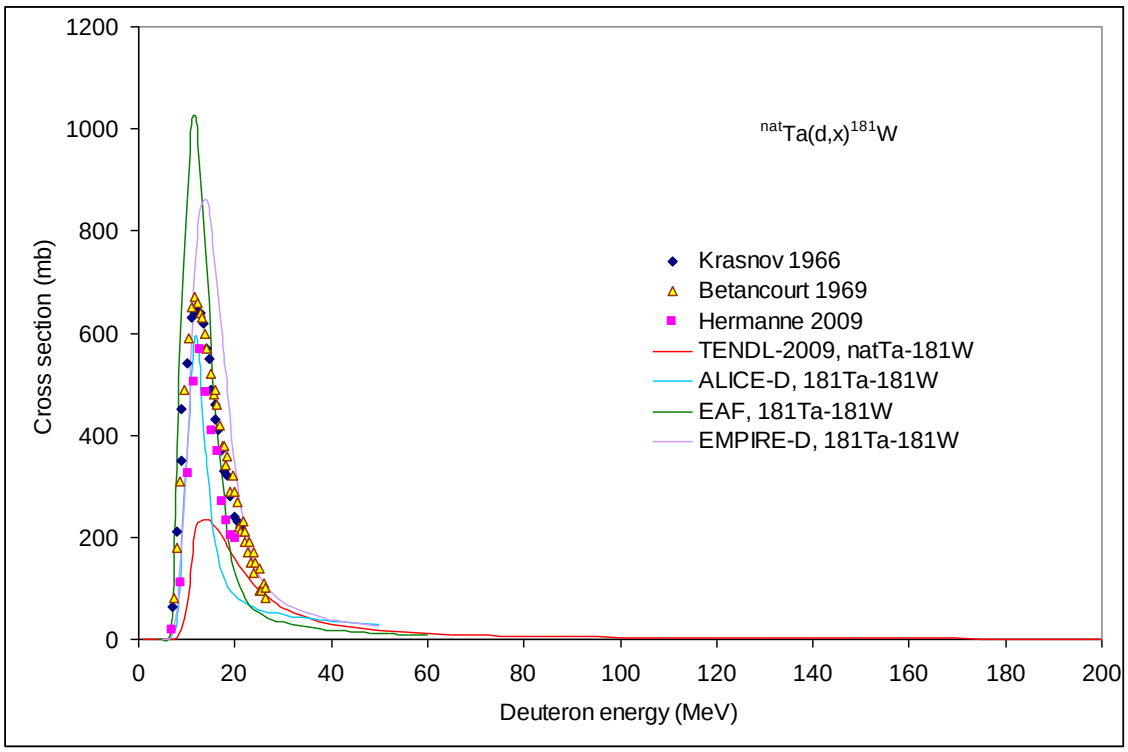
1200
1000
800
600
400
200
0
Cross section (mb)
0
20
40
60
80
100
120
140
160
180
200
Deuteron energy (MeV)
natTa(d,x)181W
Krasnov 1966
Betancourt 1969
Hermanne 2009
TENDL-2009, natTa-181W
ALICE-D, 181Ta-181W
EAF, 181Ta-181W
EMPIRE-D, 181Ta-181W

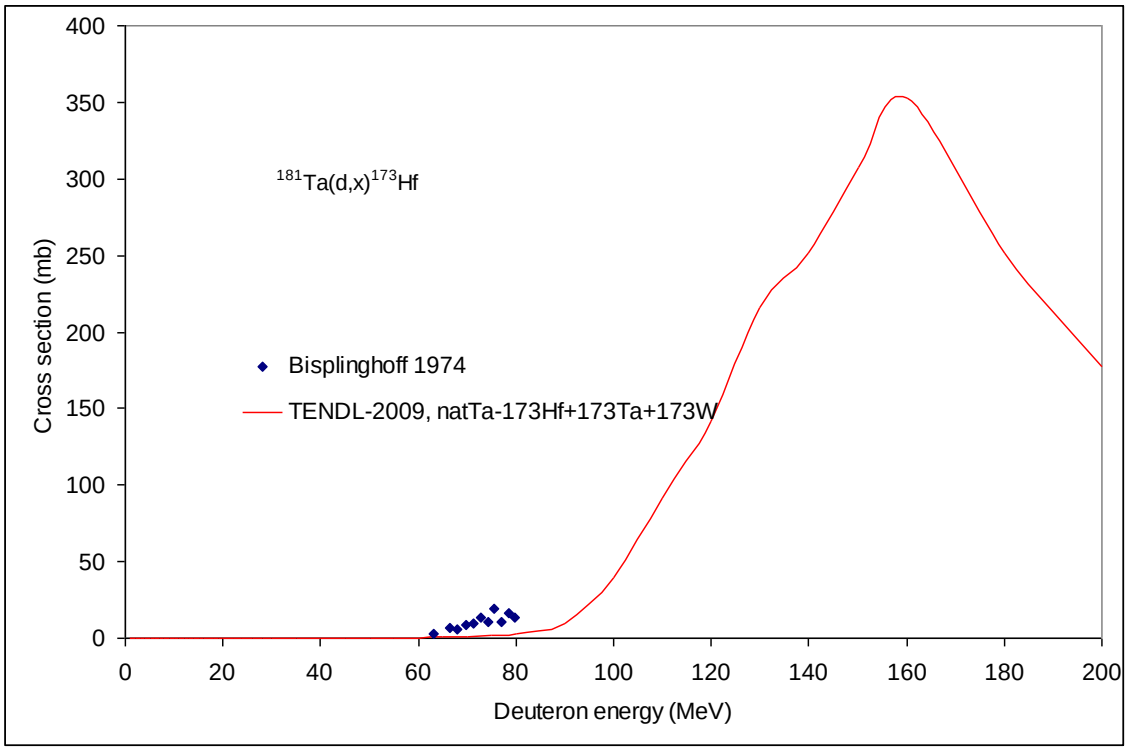
400
350
300
250
200
150
100
50
0
Cross section (mb)
^{181}Ta(d,x)^{173}Hf
Bisplinghoff 1974
TENDL-2009, natTa-173Hf+173Ta+173W
0
20
40
60
80
100
120
140
160
180
200
Deuteron energy (MeV)

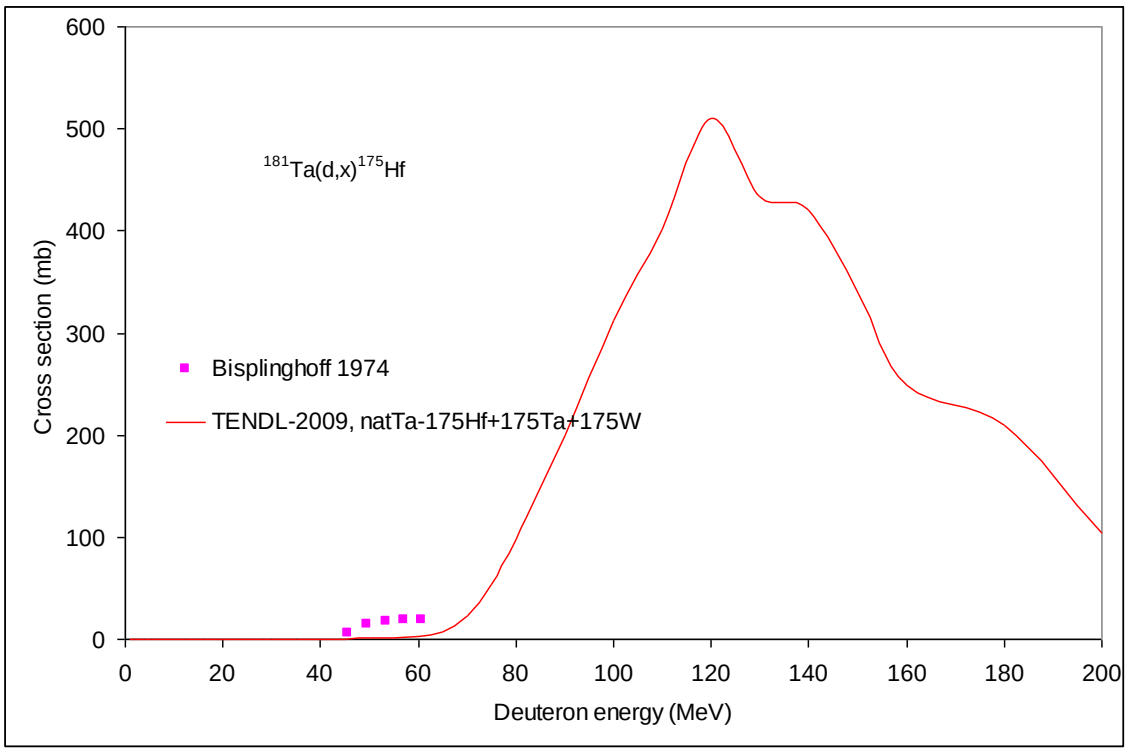
600
500
400
300
200
100
0
Cross section (mb)
^{181}Ta(d,x)^{175}Hf
Bisplinghoff 1974
TENDL-2009, natTa-175Hf+175Ta+175W
0
20
40
60
80
100
120
140
160
180
200
Deuteron energy (MeV)

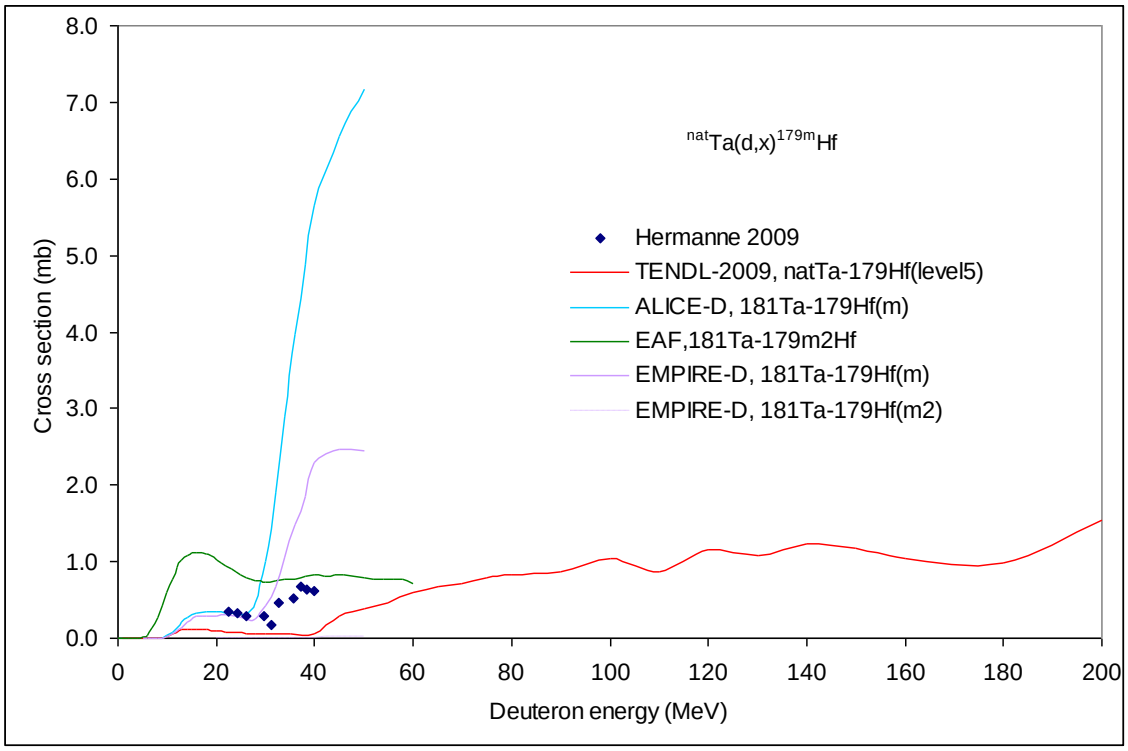
^{nat}Ta(d,x)^{179m}Hf
Hermanne 2009
TENDL-2009, natTa-179Hf(level5)
ALICE-D, 181Ta-179Hf(m)
EAF,181Ta-179m2Hf
EMPIRE-D, 181Ta-179Hf(m)
EMPIRE-D, 181Ta-179Hf(m2)
Cross section (mb)
Deuteron energy (MeV)
0.0
1.0
2.0
3.0
4.0
5.0
6.0
7.0
8.0
0
20
40
60
80
100
120
140
160
180
200

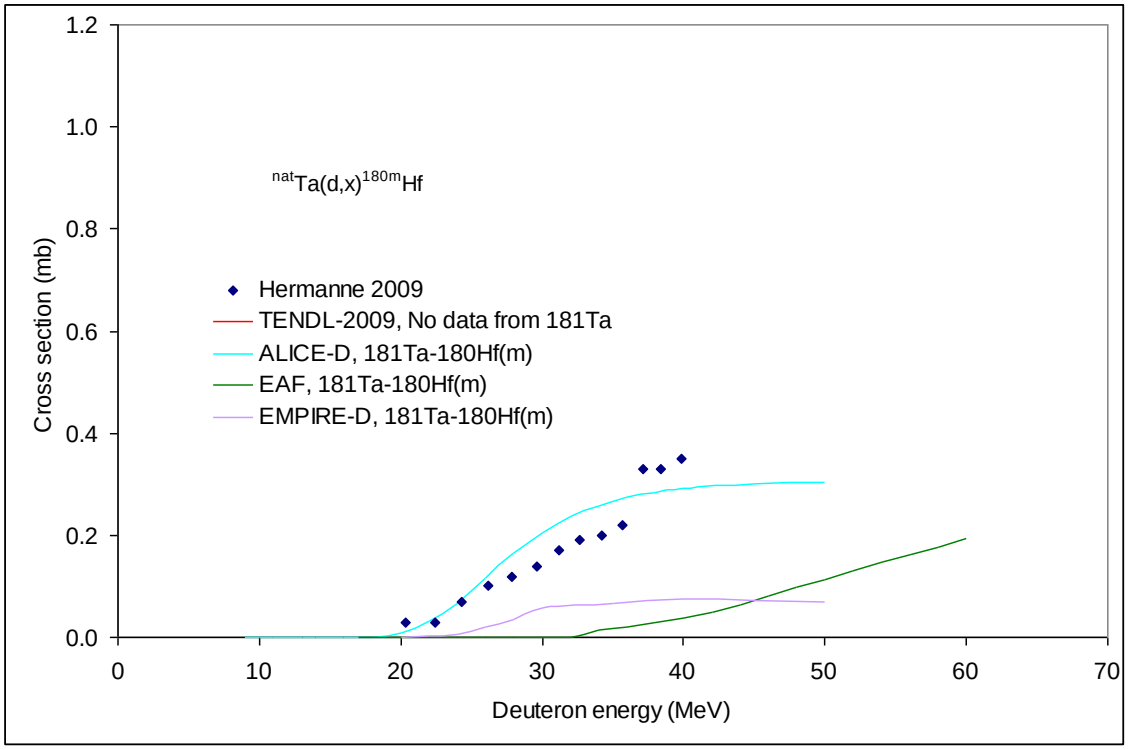
^{nat}Ta(d,x)^{180m}Hf
Hermanne 2009
TENDL-2009, No data from 181Ta
ALICE-D, 181Ta-180Hf(m)
EAF, 181Ta-180Hf(m)
EMPIRE-D, 181Ta-180Hf(m)
Cross section (mb)
Deuteron energy (MeV)
0.0
0.2
0.4
0.6
0.8
1.0
1.2
0
10
20
30
40
50
60
70

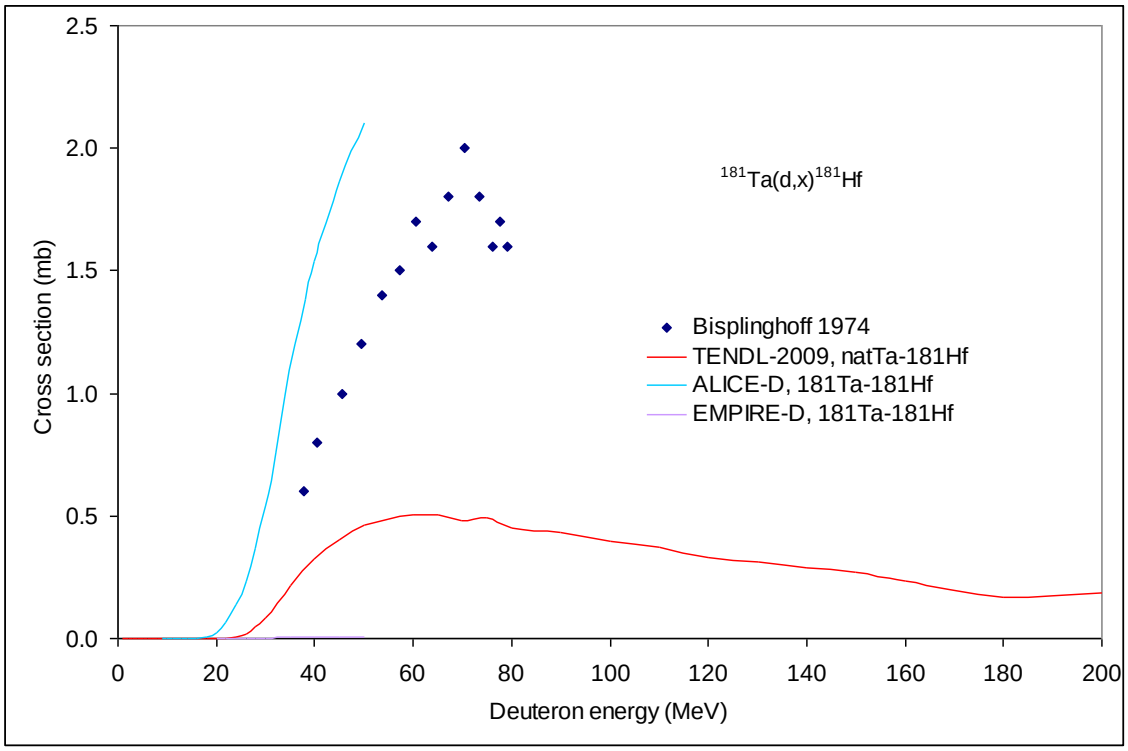
2.5
2.0
1.5
1.0
0.5
0.0
Cross section (mb)
0
20
40
60
80
100
120
140
160
180
200
Deuteron energy (MeV)
^{181}Ta(d,x)^{181}Hf
Bisplinghoff 1974
TENDL-2009, natTa-181Hf
ALICE-D, 181Ta-181Hf
EMPIRE-D, 181Ta-181Hf

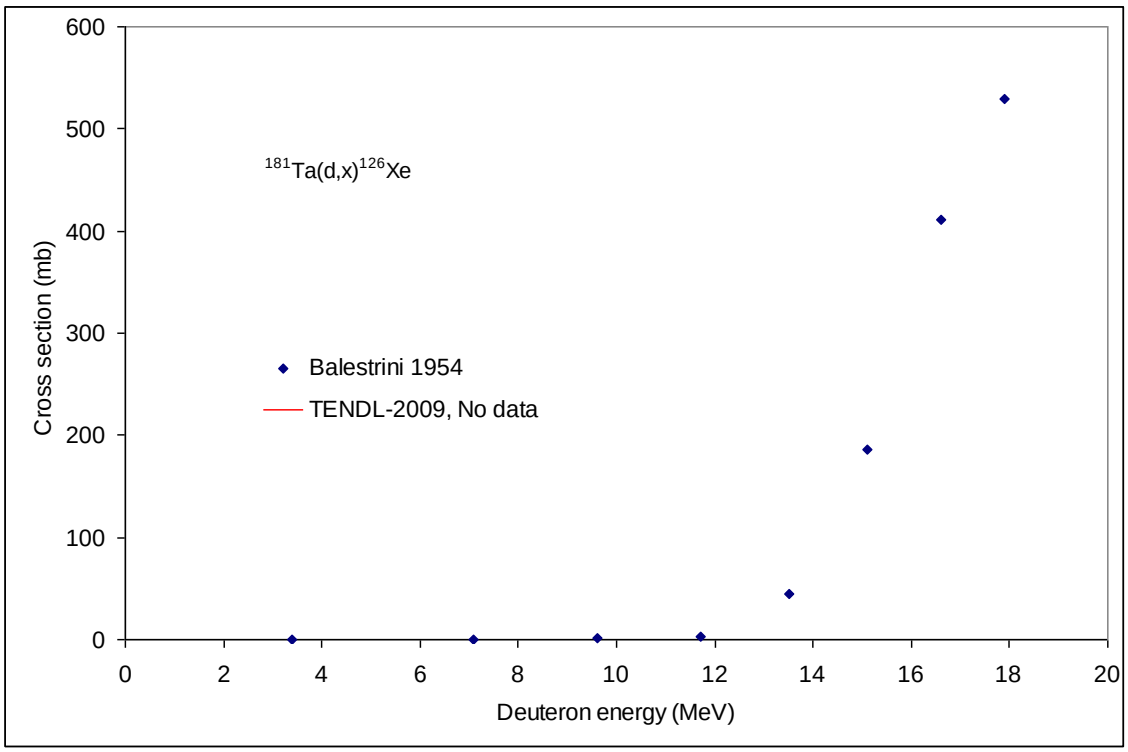
600
500
400
300
200
100
0
Cross section (mb)
0
2
4
6
8
10
12
14
16
18
20
Deuteron energy (MeV)
^{181}Ta(d,x)^{126}Xe
Balestrini 1954
TENDL-2009, No data

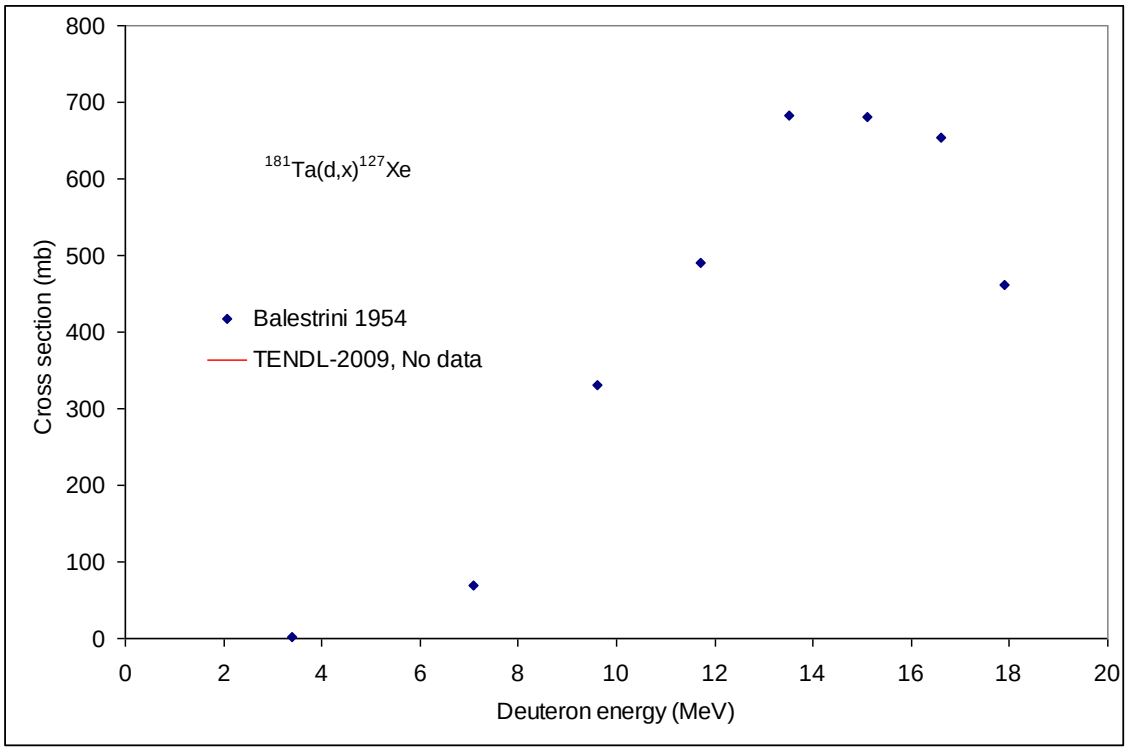
^{181}Ta(d,x)^{127}Xe
Balestrini 1954
TENDL-2009, No data
Cross section (mb)
Deuteron energy (MeV)
0
100
200
300
400
500
600
700
800
0
2
4
6
8
10
12
14
16
18
20

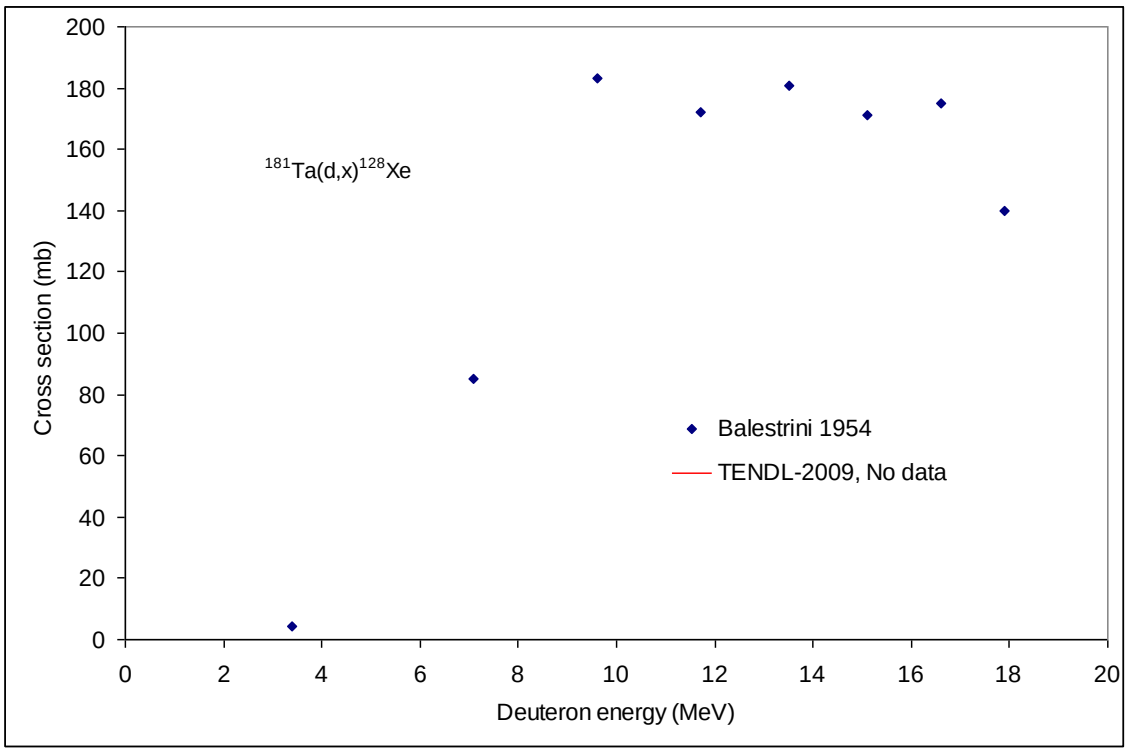
^{181}Ta(d,x)^{128}Xe
Balestrini 1954
TENDL-2009, No data
Cross section (mb)
Deuteron energy (MeV)
0
20
40
60
80
100
120
140
160
180
200
0
2
4
6
8
10
12
14
16
18
20

6. Charged particle activation cross section data for FENDL-3 [2010] (F. Tárkányi, B. Király)

6.1 INTRODUCTION

In the present status report we summarize the results of experimental and compilation work of ATOMKI Group, performed in 2010 with the aim to prepare evaluated data for FENDL-3.

In the experimental works, collaborating partners from Belgium and Japan have participated who are not mentioned here individually. Co-authors from the collaborating institutes can be found in the related new publications (see References).

6.2 NEW EXPERIMENTAL RESULTS

Some years ago, to meet requirements of practical applications, we started to establish an experimental activation database by performing new experiments and a systematic survey of existing data of deuteron induced cross sections up to 50 MeV. Today, this study involves around five hundred reactions taking place on the following 50 target elements: B, N, Ne, Al, Si, Sc, Ti, V, Cr, Mn, Fe, Co, Ni, Cu, Zn, Kr, Y, Zr, Nb, Mo, Rh, Pd, Ag, Cd, In, Sn, Te, Xe, Cs, La, Ce, Pr, Nd, Gd, Tb, Ho, Er, Tm, Yb, Lu, Hf, Ta, W, Re, Os, Ir, Pt, Au, Tl, Pb. To complete the experimental database for the important nuclear reactions, new experiments have been made in 2010 on B, Si, Sc, Cr, Mn, Ni, Cu, Cs, La, Ce, Nd, Gd, Tb, Lu, Hf, Os, Tl. The data evaluations are in progress. Additionally we have unpublished partly evaluated data for V, Kr, Rh, Pd, Ho, Yb and Pb.

The main partners in the measurements of charged particle induced nuclear data for FENDL-3 are: ATOMKI (Hungary), VUB Brussels (Belgium) and CYRIC, Tohoku University (Japan).

The results were published in scientific journals (Nuclear Instruments and Methods B, Applied Radiation and Isotopes, ND 2010, NEMEA-6, ENC-2010 conferences, etc.).

6.3 COMPILATION AND EVALUATION

The compilation and critical analysis of the literature data for all reaction assigned to the ATOMKI Group have been completed for deuteron induced reactions.

Deuteron activation cross sections were compiled up to 50 MeV. The list of the compiled reactions is given in Table I. It includes 35 targets and 393 reactions, many more than proposed in the CRP.

The supplied Excel files contain:

- experimental data found in the EXFOR database,
- experimental data found elsewhere and not included in the EXFOR database,
- experimental data measured by our research group (ATOMKI) either published or not published yet,
- theoretical results calculated by means of the TALYS code available in the TENDL-2009, TENDL-2010 and EAF-2007 databases,
- theoretical results calculated by means of the ALICE-D and EMPIRE-D codes if they were available due to our previous collaboration with A.V. Ignatyuk (IPPE, Russia),
- figures showing plotted these experimental data and theoretical curves.

6.4 COMPARISON WITH THE THEORETICAL RESULTS

The compiled experimental data are compared with the TALYS calculated (and fitted) data available in the TENDL-2009, TENDL-2010 and EAF-2007 libraries and with the ALICE-D and EMPIRE-D curves in some cases.

6.5 CONCLUSIONS

- The status of the experimental database is still poor, especially above 20 MeV.
- The use of the theoretical libraries is complicated for simple users due to the ENDF format (EAF-2007).
- Some reactions for isomeric states in the presently available theoretical libraries are missing, which makes the comparison impossible.
- The prediction capability of the theoretical codes for deuteron induced reactions is poor; therefore a statistical analysis of the disagreement is required to estimate the average uncertainties of data in the activation data libraries.

6.6 FUTURE PLANS

- Finishing the compilation of experimental data of the proton induced reactions and comparison of the experimental data with the results of TENDL-2009, TENDL-2010, EAF-2007 and PADF-2007 libraries.
- Completing the evaluation of the new experimental data measured by our group (ATOMKI) in collaboration with the Belgian and Japanese groups.
- Completing the deuteron activation data library with other targets important and useful in this project.

6.7 OTHER REMARKS AND COMMENTS

We would like to propose:
1. To establish a complete activation database of deuteron induced reactions for various applications (similarly to PADF file) like

- accelerator based neutron sources (IFMIF, Spiral),
- target and accelerator technology in medical isotope production,
- thin layer activation technique (TLA) and
- development of theoretical codes.

Advantages of deuteron induced reactions comparing to other charged particles:

- easy and cheap to accelerate,
- stopping power for deuterons is the second best after protons,
- deuteron break-up produce high intensity neutrons,
- production of radionuclides with (d,n) reaction is not possible with protons,
- (d,2n) reaction is more productive than (p,n) reaction on target of medium mass number.

2. To estimate the average predictivity of the generally used TALYS code, to make numerical comparison between the theory and the experimental data.
3. To add the final recommended data to the EXFOR database.

6.8 RELATED PUBLICATIONS ON ACTIVATION CROSS SECTIONS OF CHARGED PARTICLE INDUCED REACTIONS (2010)

1. F. Ditrói, F. Tárkányi, S. Takács, A. Hermanne, M. Baba, A.V. Ignatyuk, *Investigation deuteron-induced reactions on cobalt*, Nucl. Instrum. Methods Phys. Res. **B 268** (2010) 17-18:2571-2577.
2. A. Hermanne, F. Tárkányi, S. Takács, P. Van den Winkel, R. Adam-Rebeles, A. Ignatyuk, S.F. Kovalev, *Production of the therapeutic radioisotope ^{114m}In through the ^{116}Cd(p,3n)^{114m}In reaction*, Appl. Radiat. Isot. **68** (2010) 1:14-17.
3. A. Hermanne, F. Tárkányi, S. Takács, R. Adam-Rebeles, S. Spellerberg, A. Ignatyuk, H. Schweickert, *Optimisation of the long lived ^{121}Te contaminant in production of ^{123}I through the ^{124}Xe(p,x) route*, Chemické Listy **104** (2010) 14:S198-S199.
4. S. Takács, A. Hermanne, F. Tárkányi, A. Ignatyuk, *Cross-sections for alpha particle produced radionuclides on natural silver*, Nucl. Instrum. Methods Phys. Res. **B 268** (2010) 1:2-12.
5. S. Takács, F. Tárkányi, A. Hermanne, R. Adam-Rebeles, *Activation cross sections of deuteron-induced nuclear reactions on hafnium*, Nucl. Instrum. Methods Phys. Res. **B 268** (2010) 22:3443-3451.
6. F. Tárkányi, A. Hermanne, S. Takács, F. Ditrói, B. Király, H. Yamazaki, M. Baba, A. Mohammadi, A.V. Ignatyuk, *New measurements and evaluation of excitation functions for (p,xn), (p,pxn) and (p,2pxn) reactions on ^{133}Cs up to 70MeV proton energy*, Appl. Radiat. Isot. **68** (2010) 1:47-58.
7. F. Tárkányi, A. Hermanne, S. Takács, B. Király, I. Spahn, A.V. Ignatyuk, *Experimental study of the excitation functions of proton induced nuclear reactions on ^{167}Er for production of medically relevant ^{167}Tm*, Appl. Radiat. Isot. **68** (2010) 2:250-255.
8. F. Tárkányi, A. Hermanne, B. Király, S. Takács, A.V. Ignatyuk, *Study of excitation functions of alpha-particle induced nuclear reactions on holmium for ^{167}Tm production*. Appl. Radiat. Isot. **68** (2010) 3:404-411.
9. F. Tárkányi, F. Ditrói, B. Király, S. Takács, A. Hermanne, H. Yamazaki, M. Baba, A. Mohammadi, A.V. Ignatyuk, *Study of activation cross sections of proton induced reactions on barium: Production of ^{131}Ba → ^{131}Cs*, Appl. Radiat. Isot. **68** (2010) 1869-1877.
10. F. Tárkányi, S. Takács, F. Ditrói, B. Király, A. Hermanne, M. Sonck, M. Baba, H. Yamazaki, M.S. Uddin, A.V. Ignatyuk, *Study of production of ^{99m}Tc radioisotope via charged particle induced reactions up to 100 MeV: New data and review*, European Nuclear Conference, ENC 2010, Barcelona, Spain, 30 May-2 June 2010, Proc. http://euronuclear.org/events/enc/enc2010/transactions.htm (2010) 5.
11. F. Tárkányi, A. Hermanne, S. Takács, M. Sonck, Z. Szûcs, B. Király, A.V. Ignatyuk, *Investigation of alternative production routes of ^{99m}Tc: Deuteron induced reactions on ^{100}Mo*, Appl. Radiat. Isot. **69** (2011) 1:18-25.
12. F. Tárkányi, A. Hermanne, B. Király, S. Takács, F. Ditrói, M. Baba, A.V. Ignatyuk, *Investigation of activation cross sections of deuteron induced reactions on indium up to 40 MeV for production of ^{113}Sn/^{113m}In generator*, Appl. Radiat. Isot. **69** (2011) 1:26-36.
13. F. Ditrói, S. Takács, F. Tárkányi, *et al.*, *Investigation of proton and deuteron induced reactions on cobalt*. Proc. Int. Conf. Nucl. Data Sci. Techn., Jeju Island, Korea, 26-30 April, 2010 (2010).
14. R. Adam-Rebeles, F. Tárkányi, S. Takács, et al. *Activation cross section of deuteron induced reaction on natural thallium for the production of ^{203}Pb*. Proc. Int. Conf. Nucl. Data Sci. Techn. Jeju Island, Korea, 26-30 April, 2010 (2010).
15. F. Tárkányi, F. Ditrói, S. Takács, B. Király, Gy. Csikai, *et al.*, *Systematic study of activation cross sections of deuteron induced reactions used in accelerator applications*

Proc. Workshop on Nuclear Measurements, Evaluations and Applications. NEMEA 6. Krakow, Poland, 25-29 Oct., 2010 (2010)

16. A. Hermanne, R. Adam Rebeles, F. Tárkányi, S. Takács, I. Spahn, A.V. Ignatyuk *High yield production of the medical radioisotope ^{167}Tm by the ^{167}Er(d,2n) reaction*, Appl. Radiat. Isot., In Press, Corrected Proof, Available online 13 October 2010
17. A. Hermanne, F. Tarkanyi, S. Takacs, R. Adam Rebeles, A. Ignatyuk, S. Spellerberg, R. Schweikert *Limitation of the long-lived 121Te contaminant in production of 123I through the 124Xe(p,x) route*, Appl. Radiat. Isot., In Press, Corrected Proof, Available online 18 November 2010
18. F. Tárkányi, A.Hermanne, S. Takács, F. Ditrói, M.Baba, A.V. Ignatyuk. *Experimental study of the excitation functions of deuteron induced reactions on ^{nat}Sn up to 40 MeV*, Nucl. Instrum. Methods Phys. Res. B
19. A. Hermanne, R. Adam Rebeles, F. Tarkanyi, S. Takacs, I. Shahn, A.V. Ignatyuk *High yield production of the medical radioisotope ^{167}Tm by the ^{167}Er(d,2n) reaction* Appl. Radiat. Isot.
20. A. Hermanne, R. Adam Rebeles, F. Tarkanyi, S. Takacs, B. Kiraly, A. Ignatyuk, Cross sections of deuteron induced reactions on natCr up to 50MeV: experiments and *comparison with theoretical codes*, Nucl. Instrum. Methods B (submitted)
21. F. Tárkányi, F. Ditrói, A. Hermanne, S. Takács, B. Király, H. Yamazaki, M. Baba, A. Mohammadi, A.V. Ignatyuk, *Activation cross-sections of deuteron induced nuclear reactions on gold up to 40 MeV*, Nucl. Instrum. Methods B (submitted)
22. R. Adam-Rebeles, F. Tárkányi, S. Takács, *et al*., *Activation cross section of deuteron induced reaction on natural thallium for the production of ^{203}Pb* (Abstr.: p. 74). Int. Conf. Nucl. Data for Sci. Techn. Jeju Island, Korea, 26-30 April, 2010 (2010)
23. F. Ditrói, S. Takács, F. Tárkányi, *et al*., *Investigation of proton and deuteron induced reactions on cobalt*, Int. Conf. Nucl. Data for Sci. Techn. Jeju Island, Korea, 26-30 April, 2010 (2010)
24. A. Hermanne A., F. F. Tárkányi, S. Takács, et al. 3 : Optimization of the long lived ^{121}Te contaminant in production of ^{123}I trough the ^{124}Xe(p,x) route. 16th Radiochemical Conference. RadChem 2010. Marianské Lazné, Czech Republic, 18-23 April, 2010 (2010)
25. A. Hermanne, F. Tárkányi, S. Takács, *et al*., *High Yield production of the medical radioisotope ^{167}Tm by the ^{167}Er(d,2n) reaction* (Abstr.: p. 191), Int. Conf. Nucl. Data for Sci. Techn. Jeju Island, Korea, 26-30 April, 2010 (2010)
26. B. Király, F. Tárkányi, S. Takács, F. Ditrói, *et al*., *Investigation of production of the medical radioisotope ^{167}Tm at accelerators* (Abstr.: p. 181), 10th European Conference on Accelerators in Applied Research and Technology. Athens, Greece, 13-17 Sept., 2010 (2010)
27. S. Takács, F. Tárkányi, *et al*., *Activation cross sections of proton-induced nuclear reactions on hafnium* (Abstr.: p. 91), 10th European Conference on Accelerators in Applied Research and Technology. Athens, Greece, 13-17 Sept., 2010 (2010)
28. S. Takács, F. Tárkányi, *et al*., *Activation cross section of deuteron induced nuclear reactions on hafnium* (Abstr.: p. 211). Int. Conf. Nucl. Data for Sci. Techn. Jeju Island, Korea, 26-30 April, 2010 (2010).
29. F. Tárkányi , B. Király, S. Takács, F. Ditrói, *et al*., *Investigation of activation cross sections of deuteron induced reactions on indium up to 40 MeV for production of ^{113}Sn/^{113m}In generator*. 10th European Conference on Accelerators in Applied Research and Technology. Athens, Greece, 13-17 Sept., 2010 0 (2010)0-X./ 0.000 0 ATOMKI ref. code: P22883. 0 citations.
30. F. Tárkányi, S. Takács, F. Ditrói, B. Király , *et al*., *Investigation of activation cross sections of deuteron-induced reactions on vanadium, molybdenum, tin and gold for accelerator technology*. 10th European Conference on Accelerators in Applied Research and Technology. Athens, Greece, 13-17 Sept., 2010 (2010)

31. F. Tárkányi, S. Takács, F. Ditrói, B. Király, *et al*., *Study of production of ^{99m}Tc radioisotope via charged particle induced reactions up to 100 MeV: New data and review*. European Nuclear Conference ENC 2010. Barcelona, Spain, 30 May - 2 June, 2010 (2010).
32. F. Tárkányi, F. Ditrói, S. Takács, B. Király, Gy. Csikai, *et al*., *Systematic study of activation cross sections of deuteron induced reactions used in accelerator applications* (Abstr.: p. 34). Workshop on Nuclear Measurements, Evaluations and Applications. NEMEA 6. Krakow, Poland, 25-29 Oct., 2010 (2010)

TABLE I. SUMMARY OF THE COMPILED ACTIVATION CROSS SECTIONS OF DEUTERON INDUCED REACTIONS UP TO 50 MEV.

Target (product number)	**Product**	**Unpubl. data**
Ag (7)	^{3}H,^{105}Ag,^{106m}Ag,^{106g}Ag,^{107}Cd,^{109}Cd,^{109g}Pd	
Al (12)	^{1}H,^{2}H, ^{3}H,^{3}He,^{4}He^{7},Be,^{18}F,^{27}Mg,^{22}Na,^{24}Na,^{28}Al,^{27}Si	
Au (13)	^{3}H,^{195m,195g,196,197m,197g,199m}Hg,^{192,194,195g,196m,196g,198g}Au	X
C (8)	^{1}H,^{13}N,^{14}N,^{11}C,^{14}C,^{10}B,^{8}Li,^{7}Be	
Cd (22)	^{3}H,^{108m,108g,109mg,110m,110g,111,112m,113m,114m,115m,116m,117m}In,^{111m,115m,115g,117m,117g}Cd, ^{105g,106m,110m,111}Ag	
Co (17)	^{56}Ni,^{57}Ni,^{55}Co,^{56}Co,^{57}Co,^{58}Co,^{60}Co,^{60m}Co,^{52}Fe,^{59}Fe,^{52}Mn,^{54}Mn,^{56}Mn,^{51}Cr,^{48}V,^{46}Sc,^{47}Sc	
Cr (14)	^{50m}Mn,^{51}Mn,^{52}Mn,^{52m}Mn,^{53}Mn,^{54}Mn,^{56}Mn,^{49}Cr,^{51}Cr,^{55}Cr,^{48}V,^{52}V,^{46}Sc,^{47}Sc	X
Cu (18)	^{3}H,^{4}He,^{52}Mn,^{56}Mn,^{52}Fe,^{59}Fe,^{57}Co,^{58}Co,^{60}Co,^{57}Ni,^{65}Ni,^{61}Cu,^{62}Cu,^{64}Cu,^{66}Cu,^{62}Zn,^{63}Zn, ^{65}Zn	X
Fe (13)	^{4}He,^{51}Cr,^{52m}Mn,^{52g}Mn,^{54}Mn,^{56}Mn,^{53}Fe,^{59}Fe,^{55}Co,^{56}Co,^{57}Co,^{58m}Co,^{58g}Co	
H (4)	^{1}H,^{3}H,^{3}He,^{4}He	
In (9)	^{113mg}Sn,^{116m}In,^{ind115m}In,^{114m}In,^{ind113m}In,^{cum111}In,^{115g}Cd,^{111m}Cd,^{112g}Ag	
Ir (9)	^{188,189,191,193m}Pt,^{189,190g,192g,194m,194g}Ir	
Li (11)	Neutron,^{1}H,^{3}H,^{4}He,^{7}Be,^{8}Be,^{9}Be,^{5}Li,^{6}Li,^{7}Li,^{8}Li	
Mn (4)	^{51}Cr,^{52g}Mn,^{54}Mn,^{56}Mn	X
Mo (22)	^{88}Zr,^{89}Zr,^{90}Nb,^{91m}Nb,^{92m}Nb,^{95m}Nb,^{95g}Nb,^{96}Nb,^{90}Mo,^{93m}Mo,^{99}Mo,^{101}Mo,^{93m}Tc,^{93g}Tc, ^{94m}Tc,^{94g}Tc,^{95m}Tc,^{95g}Tc,^{96}Tc,^{97m}Tc,^{99m}Tc,^{101}Tc	X
N (5)	^{8}Li,^{11}C,^{13}N,^{16}N,^{15}O	
Nb (9)	^{1}H,^{3}H,^{93m}Mo,^{90}Nb,^{91m}Nb,^{92m}Nb,^{90}Y,^{88}Zr,^{89}Zr	
Ni (26)	^{1}H,^{2}H,^{3}H,^{3}He,^{4}He,^{51}Cr,^{52g}Mn,^{54}Mn,^{56}Mn,^{55}Co,^{56}Co,^{57}Co,^{58}Co,^{60}Co,^{61}Co,^{56}Ni,^{57}Ni,^{65}Ni, ^{55}Fe,^{59}Fe,^{58}Cu,^{59}Cu,^{60}Cu,^{61}Cu ^{62}Cu,^{64}Cu	X
O (4)	^{14}N,^{16}N,^{18}F,^{17}F,	
P	No data in EXFOR, other sources should be checked	
Pb (7)	^{202,203,204,205,206,207}Bi,^{209}Pb	X
Pd (4)	^{103,104g,110m,111}Ag	X
Pt (14)	^{191,192,193,194,195,196,196m2,198m,198g,199}Au,^{191,195m,197}Pt,^{192}Ir	
Rh (5)	^{103}Pd,^{101m,101g,102m,102g}Rh	X
S (3)	^{34m}Cl,^{30}P,^{32}P	
Sb (24)	^{116}Te,^{118}Te,^{119m}Te,^{121m}Te,^{121g}Te,^{123m}Te,^{118m}Sb,^{119}Sb,^{120m}Sb^{122}Sb,^{124}Sb,^{108}Sn,^{113g}Sn,^{117m}S n, ^{121}Sn,^{111}In,^{114m}In,^{110m}Ag,^{111}Ag,^{112}Ag,^{107}Cd,^{109}Cd,^{115m}Cd,^{115}Cd	
Si (7)	^{7}Be,^{22}Na, ^{24}Na,^{28}Al,^{29}Al,^{29}P,^{32}P	X
Sn (15)	^{3}H,^{111}In,^{114m}In,^{110}Sn,^{113g}Sn,^{117m}Sn,^{125}Sn,^{115}Sb,^{116m}Sb,^{117}Sb,^{118m}Sb,^{120m}Sb,^{122}Sb,^{124}Sb,^{125}S b	X
Ta (18)	^{1}H,^{175}Ta,^{178}Ta,^{180g}Ta,^{182m}Ta,^{182g}Ta,^{176}W,^{177}W,^{178}W,^{181}W,^{173}Hf,^{175}Hf,^{179m}Hf,^{180m}Hf,^{181}Hf, ^{126}Xe,^{127}Xe,^{128}Xe	
Ti (9)	^{4}He,^{43}Sc,^{44m}Sc,^{44g}Sc,^{46}Sc,^{47}Sc,^{48}Sc,^{47}V,^{48}V	
V (16)	^{3}H,^{4}He,^{47}Ca,^{48}Cr,^{49}Cr,^{51}Cr,^{44m}Sc,^{44g}Sc,^{46}Sc,^{47}Sc,^{48}Sc,^{48}V,^{49}V,^{41}Ar,^{42}K,^{43}K	X
W (12)	^{185}W,^{187}W,^{181}Re,^{182m}Re,^{182g}Re,^{183}Re,^{184m}Re,^{184g}Re,^{186g}Re,^{182}Ta,^{183}Ta,^{184}Ta	
Y (12)	^{87,88,89m,89g}Zr,^{87m,87g,88,90m,90g}Y,^{85g,87m,89}Sr	
Zn (19)	^{61,62,63,64,65,66,67,68}Ga,^{61,62,63,65,69m,69g,71}Zn^{61,64,67}Cu,^{58}Co	
Zr (22)	^{89m,89g,90,91m,92m,95m,95g,96,97}Nb,^{88,89,95,97}Zr,^{86,87m,87g,88,90m,90g,92}Y,^{85}Sr,^{83}Rb	

7. Charged particle activation cross section data for FENDL-3 (F. Tárkányi)

7.1 INTRODUCTION

In the present status report we summarize the results of experimental and compilation work of ATOMKI Group, performed in 2011 with the aim to prepare evaluated data for FENDL-3.

In the experimental works, collaborating partners from Belgium and Japan have participated who are not mentioned here individually. Co-authors from the collaborating institutes can be found in the related new publications (see References).

7.2 EXPERIMENTAL RESULTS

Some years ago, to meet requirements of practical applications, we started to establish an experimental activation database by performing new experiments and a systematic survey of existing data of deuteron induced cross sections up to 50 MeV and for protons up to 100 MeV. The experimental results for the deuteron induced reactions were summarized in our previous report. Here we present on our experimental activation data of proton induced reactions. Today, this study involves around four hundred reactions taking place on the following around 50 target elements: B, N, Ne, Al, Ar, Sc, Ti, V, Mn, Fe, Co, Ni, Cu, Zn, Kr, Rb, Y, Zr, Nb, Mo, Pd, Ag, Cd, In, Sn, Te, Xe, Cs, Ba, Nd, Ho, Er, Tm, Yb, Hf, Ta, W, Re, Ir, Pt, Au, Pb.

The summary of the experimental results on protons are collected in Table I. We have numerous unpublished partly evaluated data. The main partners in the measurements of charged particle induced nuclear data for FENDL-3 are: ATOMKI (Hungary), VUB Brussels (Belgium) and CYRIC, Tohoku University (Japan). The results were published in scientific journals and presented at conferences (see references).

TABLE I. SUMMARY OF THE EXPERIMENTAL ACTIVATION CROSS SECTION DATA OF THE ATOMKI COLLABORATION.

Target	**Investigated reaction products**	**E_{max} (MeV)**
^{nat}B	^{nat}B(p,x)^{7}Be	**17.5**
^{nat}N	^{14}N(p,x)^{13}N, ^{11}C	**17**
^{nat}Ne	^{22}Ne(p,n)^{22}Na	**17.3**
^{27}Al	^{27}Al(p,x)^{22,24}Na	**67**
^{38}Ar	^{38}Ar(p, n)^{38}K	**18**
^{45}Sc	^{45}Sc(p,x)^{43}K, ^{43}Sc, ^{44m,44g}Sc, ^{44}Ti	**37**
^{nat}Ti	^{nat}Ti(p,x)^{48}V, ^{47,44m,44g,43}Sc	**32,18,30,17**
^{nat}V*	^{51,48}Cr, ^{48}V, ^{48,47,46,44}Sc	**67**
^{55}Mn*	^{52}Fe, ^{51,52,54}Mn, ^{48,49,51}Cr, ^{48}V	**67**
^{nat}Fe	^{nat}Fe(p,xn)^{56}Co	**18**
^{59}Co*	^{59}Co(p,x)^{55,56,57,58,}Co, ^{54}Mn, ^{52}Mn, ^{52}Fe, ^{57,56}Ni	70
^{64}Ni, ^{nat}Ni	^{64}Ni(p,n)^{64}Cu, ^{nat}Ni(p,x)^{57}Ni, ^{57,56}Co, ^{55}Co	25,32,18,44,30
^{nat}Cu	^{nat}Cu(p,x)^{62,63,65}Zn	**32, 18**
^{66}Zn, ^{67}Zn, ^{68}Zn, ^{nat}Zn	^{66}Zn(p,x)^{66,65}Ga, ^{67}Zn(p,x)^{66,67}Ga, ^{68}Zn(p,x)^{66,67,68}Ga, ^{nat}Zn(p,x)^{66,67}Ga, ^{62,65,69m}Zn, ^{64}Cu, ^{57}Ni, ^{55,56,57,58}Co, ^{52,54}Mn	**21, 26, 67**
^{78}Kr, ^{82}Kr , ^{83}Kr, ^{nat}Kr	^{78}Kr(p,pn)^{77}Kr, ^{78}Kr(p,x)^{77}Br and ^{78}Kr(p,α)^{75}Br, ^{82}Kr(p,2n)^{81}Rb, ^{83}Kr(p,3n)^{81}Rb, ^{82}Kr(p,n)^{82m}Rb, ^{83}Kr(p,2n)^{82m}Rb, ^{84}Kr(p,3n)^{82m}Rb,	**20,30**
^{nat}Rb	^{nat}Rb(p,xn)^{82,83mg,85mg,87m}Sr, ^{81,82m,83,84mg,86mg}Rb	**70**
^{89}Y	^{89}Y(p,x)^{89,88,86}Zr, ^{88,87,87m,86}Y, ^{85,83,82}Sr, ^{84,83}Rb	**79**

^{nat}Zr	^{90,92m,95m,95g,96}Nb, ^{88}Y	**17,37**
^{93}Nb	^{93}Nb(p,x)^{90,93m}Mo, ^{92m,91m,90}Nb, ^{86,88,89}Zr, ^{86,88,89}Zr, ^{86,87mg,88}Y, ^{85}Sr	**40,67**
^{nat}Mo	^{99,93m}Mo, ^{99m,96,95,95m,94}Tc, ^{96,95,92m,90}Nb, ^{89,88,86}Zr, ^{88,87,86}Y	**67,38**
^{nat}Pd	^{nat}Pd(p,x)^{97}Ru, ^{101m}Rh, ^{109}Pd, ^{103,104,105,106m,110m}Ag	**68,37**
^{nat}Ag	^{nat}Ag(p,x)^{106m,105}Ag, ^{103,101,100}Pd, ^{105,102,101m,100,99}Rh, ^{97}Ru	**78**
^{111}Cd, ^{112}Cd, ^{116}Cd, ^{nat}Cd	^{nat}Cd(p,xn), ^{107g,108m,108g,109g,110m,110g,111g,112m,113m,114m,115m,116m}In, ^{107,109,111m,115g}Cd, ^{103,104g,105g,106m,110m,111g,113g}Ag, ^{111}Cd(p,xn)^{111m,g,110m,109m1,m2,g}In In, ^{112}Cd(p,xn)^{111m,g,110m,110g}In,	36,66,75,30,30
^{nat}In *	^{113mg,110}Sn, ^{ind115m,114m,cum111,110,109}In,	70
^{nat}Sn	^{109}In, ^{110}In, ^{111}In, ^{114m}In, ^{113}Sn, ^{117m}Sn, ^{115}Sb, ^{120m}Sb., ^{116m}Sb, ^{117}Sb, ^{118m}Sb, ^{122}Sb, ^{124}Sb	67
^{124}Te, ^{nat}Te	^{124}Te(px)^{123,124}I, ^{nat}Te(p,x)^{121g}Te, ^{121,123,124,126,128,130g}I	31,18
^{124}Xe, ^{131}Xe, ^{nat}Xe*	^{124}Xe(p,x)^{121}I, ^{123}Cs, ^{123}Xe, ^{131}Xe(p,n)^{131,122m}Cs, ^{122}, ^{121}Xe, ^{121}I , ^{nat}Xe(p,x)$^{127,129,130g,132,134m.134g,135m,136}$Cs, ^{125,127,129m,131m,133m,135}Xe	**35,44,37**
^{133}Cs	^{133}Cs(p,x)^{133m,133mg,131mg,129g,129m,128Ba,} ^{132,129cum,127cum}Cs, $^{129m(ind),127cum,125cum}$Xe	**70**
^{nat}Ba	^{nat}Ba(p,x)^{135,132mg}La, ^{ind135m,cum133m,cum133mg,cum131mg}Ba, ^{136mg,134mg,132,cum129}Cs	**70**
^{nat}Nd*	^{nat}Nd(p,x)^{143,144,146,148m,148g,149,150}Pm, ^{138,139m,141,147,149}Nd, ^{142}Pr, ^{139}Ce	**67**
^{165}Ho*	^{165}Ho(p,x)^{165}Er	**35**
^{167}Er, ^{nat}Er	^{167}Er(p,xn)^{167,166}Tm, ^{168}Er(p,n)^{168}Tm, ^{166}Er(p,2n)^{165}Tm, ^{nat}Er(p,x)^{163,165,166,167,168,170}Tm, ^{cum161}Er	**16.70**
^{169}Tm	^{169}Tm(p,x)^{169,167,166}Yb, ^{168,167,166}Tm	**36.45**
^{nat}Yb	^{nat}Yb(p,xn)^{173,172mg,171mg,170,167}Lu, ^{175cum,166cum}Yb, ^{173ind,172ind,168,167cum,165cum}Tm, ^{169}Lu	**70**
^{nat}Hf	^{nat}Hf(p,x)^{173,174,175,176,177,178m,180g}Ta	**36**
^{nat}Ta	^{173,174,175,176,177,178m}Ta, ^{173,175,179m2,180m}Hf, ^{173,177g}Lu	**36**
^{nat}W	^{nat}W(p,x)^{181,182m,182g,183,184g,186}Re	**32**
^{nat}Re*	^{nat}Re(p,x)^{181,182,183m,185}Os, ^{181,182m,182g,183,184m,184g,186}Re, ^{185}W	**67**
^{nat}Ir	^{nat}Ir(p, xn)^{188,189,191}Pt, ^{185,186g,188,189,190g,192g}Ir, ^{185}Os	**67**
^{nat}Pt	^{nat}Pt(p,x)^{191,192,193,194,195,196m,g,196m2,198g}Au, ^{188,189,191,195}Pt, ^{88,189,190,192,194m}Ir	**70**
^{197}Au	^{197}Au(p,x)^{197m}Hg, ^{196}Au	**18**
^{nat}Pb*	^{nat}Pb(p,x)^{202,203,204,205,207}Bi, ^{201,202m,203}Pb, ^{199,200,201,202}Tl	**36**

To complete the experimental data base new experiments were done on deuteron activation cross section data on 15 targets up to 50 MeV deuterons (Table. II.).

TABLE II. NEW MEASUREMENTS FOR DEUTERON INDUCED REACTIONS (2011)

Target	**Particle**	**Accelerator**	**Laboratory**	**E_{in}**
Mg,Ni	d	Cyclone90	LLN(Louvain la Neuve)	50
Nd,Yb,Cr,Cu,Ti	d	Cyclone90	LLN(Louvain la Neuve)	50
Tb,Dy	d	Cyclone90	LLN(Louvain la Neuve)	50
Pb,Sb	d	Cyclone90	LLN(Louvain la Neuve)	50
C,Ti	d	Cyclone90	LLN(Louvain la Neuve)	50
Si,Ni	d	Cyclone90	LLN(Louvain la Neuve)	50

7.3 COMPILATION AND EVALUATION

The compilation of the literature data for all reaction assigned to the ATOMKI Group have been completed for proton induced reactions. The activation cross sections were compiled up to 200-300 MeV The list of the compiled reactions is given in Table III. EXFOR database, literature data and results of own measurements were used. The number of reactions is over 400 for the following targets: Ag, Al, C, Co, Cr, Cu, Fe, Li, Mn, Mo, N, Nb, Ni, O, P, S, Sb, Si, Sn, Ta, Ti, V, W. New measurements were started in cases of unreliable literature data. The preparation of the list of the missing, duplicated and wrong EXFOR entries is still in progress. The experimental data are compared with results in TENDL-2010.

TABLE III. THE COMPILED PROTON INDUCED REACTIONS

Target	A(p,x)Product	No.
Ag	^{3}H ^{7}Be ^{94m}Tc, ^{94g}Tc ^{97}Ru ^{99g}Rh, ^{100g}Rh, ^{101m}Rh, ^{102g}Rh, ^{105g}Rh ^{100}Pd, ^{101}Pd, ^{103}Pd, ^{104}Pd ^{103}Ag, ^{104}Ag, ^{105}Ag, ^{106m}Ag, ^{106g}Ag ^{104}Cd, ^{105}Cd, ^{107}Cd, ^{109}Cd	23
Al	^{2}H, ^{3}H ^{3}He, ^{4}He ^{7}Be, ^{9}Be, ^{10}Be ^{14}C ^{18}F ^{21}Ne, ^{22}Ne ^{22}Na, ^{24}Na ^{23}Mg, ^{28}Mg ^{26}Al ^{26}Si, ^{27}Si	18
C	^{3}H ^{8}Li ^{7}Be, ^{10}Be ^{10}C, ^{11}C, ^{14}C ^{13}N	8
Co	^{7}Be ^{22}Na,^{24}Na ^{42}K, ^{43}K ^{44m}Sc, ^{46g}Sc, ^{47}Sc ^{48}V, ^{53}V ^{48}Cr, ^{51}Cr ^{51}Mn, ^{52m}Mn, ^{52g}Mn, ^{54}Mn, ^{56}Mn ^{52}Fe, ^{53m}Fe, ^{53g}Fe, ^{55}Fe ^{55}Co, ^{56}Co, ^{57}Co, ^{58m}Co, ^{58g}Co ^{56}Ni, ^{57}Ni, ^{59}Ni, ^{60}Ni	30
Cr	^{45}Ti ^{48}V ^{48}Cr, ^{49}Cr, ^{51}Cr ^{50m}Mn, ^{50g}Mn, ^{51}Mn, ^{52m}Mn, ^{52g}Mn, ^{53}Mn, ^{54}Mn	12
Cu	^{7}Be ^{22}Na, ^{24}Na ^{38}Cl, ^{42}K, ^{43}K ^{44m}Sc, ^{44g}Sc, ^{46g}Sc ^{48}V ^{48}Cr, ^{49}Cr, ^{51}Cr, ^{52}Mn, ^{54}Mn,^{56}Mn ^{52}Fe, ^{55}Fe, ^{59}Fe ^{55}Co, ^{56}Co, ^{57}Co, ^{58g}Co, ^{60}Co, ^{61}Co ^{56}Ni, ^{57}Ni ^{60}Cu, ^{61}Cu, ^{62}Cu, ^{64}Cu ^{60}Zn,^{61}Zn, ^{62}Zn, ^{63}Zn, ^{65}Zn, ^{66}Zn	37
Fe	^{3}H ^{3}He ^{7}Be, ^{10}Be ^{22}Na, ^{24}Na ^{32}P ^{36}Cl ^{42}K, ^{43}K ^{44m}Sc, ^{46g}Sc, ^{47}Sc, ^{48}Sc ^{44}Ti ^{48}V ^{48}Cr, ^{51}Cr	32

	^{51}Mn, ^{52g}Mn, ^{53}Mn, ^{54}Mn ^{52g}Fe, ^{53m}Fe, ^{53g}Fe, ^{55}Fe ^{55}Co, ^{56}Co, ^{57}Co, ^{58m}Co, ^{58g}Co, ^{59}Co	
Li	^{3}H, ^{7}Be	2
Mn	^{10}Be ^{22}Na, ^{24}Na ^{43}K ^{44m}Sc, ^{46}Sc, ^{47}Sc, ^{48}Sc ^{48}V ^{48}Cr, ^{51}Cr ^{52g}Mn, ^{54}Mn ^{52}Fe, ^{53m}Fe, ^{53g}Fe, ^{55}Fe	17
Mo	^{86}Y, ^{87g}Y, ^{88}Y ^{86}Zr, ^{88}Zr, ^{89m}Zr, ^{89g}Zr ^{88m}Nb, ^{88g}Nb, ^{89g}Nb, ^{90}Nb, ^{91m}Nb, ^{92m}Nb, ^{95m}Nb, ^{95g}Nb, ^{96}Nb, ^{97}Nb ^{89g}Zr ^{90}Mo, ^{93m}Mo, ^{99}Mo ^{93m}Tc, ^{93g}Tc, ^{94m}Tc, ^{94g}Tc, ^{95m}Tc, ^{95g}Tc, ^{96m}Tc, ^{96g}Tc, ^{99m}Tc, ^{99g}Tc	31
N	^{3}H ^{7}Be, ^{10}Be ^{11}C ^{13}N ^{14}O, ^{15}O	7
Nb	^{94}Mo, ^{93m}Mo, ^{93g}Mo, ^{90}Mo ^{92m}Nb, ^{91m}Nb, ^{90}Nb, ^{89m}Nb ^{89g}Zr, ^{88}Zr ^{88}Y, ^{87m}Y, ^{87g}Y, ^{86g}Y ^{7}Be	15
Ni	^{3}H ^{7}Be, ^{10}Be ^{41}Ca ^{44m}Sc, ^{46g}Sc, ^{47}Sc ^{47}V, ^{48}V, ^{49}V, ^{50}V ^{48}Cr, ^{51}Cr ^{52}Mn, ^{53}Mn, ^{54}Mn ^{52}Fe, ^{53m}Fe, ^{55}Fe, ^{59}Fe, ^{60}Fe ^{55}Co, ^{56}Co, ^{57}Co, ^{58g}Co, ^{60}Co, ^{61}Co ^{56}Ni, ^{57}Ni, ^{59}Ni ^{59}Cu, ^{60}Cu, ^{61}Cu, ^{62}Cu, ^{64}Cu	35
O	^{3}H ^{7}Be, ^{10}Be ^{11}C, ^{14}C ^{13}N ^{15}O ^{17}F, ^{18}F	9
P	^{22}Na, ^{24}Na ^{29}Al ^{28}Mg ^{30}P	5
S	^{22}Na, ^{24}Na ^{28}Mg ^{34m}Cl	4
Sb	^{117}Te, ^{118}Te, ^{119m}Te, ^{119g}Te ^{121m}Te, ^{121g}Te, ^{123m}Te, ^{123g}Te ^{120m}Sb, ^{122}Sb ^{117m}Sn	11
Si	^{3}He ^{7}Be, ^{10}Be ^{14}C ^{18}F ^{22}Na, ^{24}Na	16

	^{27}Mg, ^{28}Mg ^{25}Al, ^{26}Al, ^{28}Al, ^{29}Al ^{27}Si ^{28}P, ^{29}P	
Sn	^{109g}In, ^{110g}In, ^{111}In, ^{114m}In, ^{117m}In ^{113g}Sn, ^{117m}Sn ^{115}Sb, ^{116m}Sb, ^{116g}Sb, ^{117}Sb, ^{118m}Sb, ^{118g}Sb, ^{119}Sb, ^{120m}Sb, ^{120g}Sb, ^{122m}Sb, ^{122g}Sb, ^{124m1}Sb, ^{124m2}Sb, ^{124g}Sb	21
Ta	^{167}Tm ^{169}Yb ^{169}Lu, ^{170}Lu, ^{171}Lu, ^{172}Lu, ^{173}Lu, ^{174g}Lu, ^{179}Lu ^{170}Hf, ^{172}Hf, ^{173}Hf, ^{175}Hf, ^{179m2}Hf ^{175}Ta, ^{176}Ta, ^{177}Ta, ^{178m}Ta, ^{178g}Ta, ^{180g}Ta ^{178}W, ^{179}W, ^{180}W, ^{181}W	24
Ti	^{7}Be, ^{10}Be ^{22}Na, ^{24}Na ^{34m}Cl, ^{36}Cl, ^{38}Cl, ^{39}Cl ^{42}K, ^{43}K ^{47}Ca ^{43}Sc, ^{44m}Sc, ^{44g}Sc, ^{46g}Sc, ^{47}Sc, ^{48}Sc ^{44}Ti, ^{45}Ti ^{47}V, ^{48}V, ^{49}V, ^{50}V	23
V	^{7}Be ^{22}Na, ^{24}Na ^{27}Si, ^{31}Si ^{32}P, ^{33}P ^{35}S, ^{34}Cl, ^{38}Cl, ^{39}Cl ^{42}K, ^{43}K ^{45}Ca, ^{47}Ca ^{43}Sc, ^{44m}Sc, ^{44g}Sc, ^{46g}Sc, ^{47}Sc, ^{48}Sc ^{44}Ti, ^{45}Ti ^{47}V, ^{48}V, ^{49}V ^{48}Cr, ^{49}Cr, ^{51}Cr, ^{52}Cr	30
W	^{83}Rb ^{85g}Sr ^{87g}Y, ^{88}Y ^{88}Zr ^{169}Yb ^{171}Lu, ^{173}Lu, ^{177}Lu ^{173}Hf, ^{175}Hf, ^{179m2}Hf, ^{181}Hf, ^{184}Hf ^{176}Ta, ^{177}Ta, ^{182}Ta, ^{183}Ta, ^{184}Ta ^{178}W ^{181}Re, ^{183}Re, ^{184m}Re, ^{184g}Re, ^{186}Re	25
Total		435

7.4 SHORT OVERVIEW ON THE EARLIER INVESTIGATIONS OF THE PROTON INDUCED ACTIVATION DATA

The available data were gathered in different types of experiments:

- In the low energy nuclear physics era measurements were mainly done with the aim of investigation of basic nuclear reaction mechanisms (isotopic cross sections).
- A more systematic study of thick (and thin) target yields for many targets was done up to/at 22 MeV in IPPE Obninsk for practical applications.
- Systematic study of excitation functions for many targets was done up GeV by a Hannover group (Michel, *et al*) for practical applications by using targets with natural isotopic composition.
- Activation cross sections for production of diagnostic and therapeutic reactions and the by-products was investigated by many groups (FZ Julich, Milano, iThemba, BNL, ATOMKI, UJV Rez, VUB, etc.)
- Valuable systematic study of excitation functions for many enriched targets (A< 100) up 35 MeV was done by Levkovskii.
- By recognizing the importance of activation data for broad range of new data measurements are in progress, etc.

7.5 COMPARISON WITH THE THEORETICAL RESULTS

The compiled experimental data are compared with the TALYS calculated (and fitted) data available in the TENDL-2009, TENDL-2010 libraries.

7.6 FORMAT

MS EXCEL is used to collect experimental and theoretical data, to make the necessary corrections or normalizations and to create graphs. Annex 1 shows an example for Cu targets.

7.7 COMPILATION RESULTS

The activation files are sent simultaneously to IAEA NDS and to the participating theoretical group participating in the FENDL-3 CRP. The data are available on the IAEA/NDS web site (https://www-nds.iaea.org/fendl30/about/document.html).

7.8 CONCLUSIONS ON COMPILATION AND EVALUATION

Due to the large scale applications and the energy range, the number of reactions is very large, and requires significant amount of work.
Some relevant EXFOR compilations are missing. Therefore, systematic transfer of missing data for all reactions from the LB is proposed.
Methodology for CP evaluation activation cross sections and for preparation recommended data is missing.

7.9 CONCLUSIONS ON THE THEORETICAL PREDICTIONS

The predictivity of *a'priori* theoretical results is moderate. Moderate success was obtained also in precise evaluation. Presently the model results are very useful in evaluation of measurements, and in extrapolation. The disagreement with the theory is very significant in many cases. Problems with the theories remain unresolved or are only partially solved by introducing new phenomenological models and parameters. Even more problems are predicted by using microscopic models.

The comparison shows the basic importance of experimental data for proper selection of input parameters and for normalisation of theoretical results. In case of charged particle activation data even the success of the normalised theoretical results are far from the requirements.

7.10 SOME CONCLUSIONS ON THE PERFORMED EXPERIMENTS

The measurements produce very useful information for many applications and for development of the theory.
It is very important to continue the experiments to obtain more reliable "broad field activation data file" which can be used in many applications. Especially important (and rear) the systematic experimental studies (well established experimental technique, expertise in measurements and data evaluation, ..). Very few reliable integral experimental data were obtained for validation of evaluated data. Considering new applications it is very important to extend the energy range of proton induced reaction up to 200-250 MeV.
The experimental practice, the compilation and the data evaluation show the importance of decay data to get reliable cross section data (especially the nonlinear "non-correctable" parameters like half-life). The compilations show that in many cases there are problems with the basic knowledge on definitions and proper use of experimental techniques. Manual for activation cross section measurements are required including precise definition and determination of the contributing parameters, like:

- number of target nuclei (thickness, uniformity, composition, etc.)
- number of incident particles (primary beam, beam broadening, time dependence…..)
- energy of the incident particle (primary beam energy, medium energy,…)
- effect of secondary neutrons
- proper application of decay data
- proper selection of the irradiation time, the measurement of spectra as a function of time
- proper measurement of cumulative cross sections
- energy averaged cross sections – thick targets
- definitions of cross section, cumulative cross sections, integral yields (physical, etc.)
- etc.

7.11 RELATED PUBLICATIONS ON ACTIVATION CROSS SECTIONS OF PROTON AND DEUTERON INDUCED REACTIONS (ATOMKI PARTICIPANT, 2011-12)

Publications, proceedings

[1] R. Adam-Rebeles, A. Hermanne, P. Van den Winkel, F. Tárkányi, S. Takács, J. Korean Phys. Soc. **59** (2011) 23:1975-1978

[2] F. Ditrói, S. Takács, F. Tárkányi, R.W. Smith, M. Baba, J. Korean Phys. Soc. **59** (2011) 23:1697-1700

[3] F. Ditrói, F. Tárkányi, S. Takács, A. Hermanne, H. Yamazaki, M. Baba, A. Mohammadi, A.V. Ignatyuk, Nucl. Instrum. Methods Phys. Res. B **269** (2011) 1878-1883.

[4] F. Ditrói, F. Tárkányi, S. Takács, A. Hermanne, H. Yamazaki, M. Baba, A. Mohammadi, A.V. Ignatyuk, Nucl. Instrum. Methods Phys. Res. B **269** (2011) 18:1963-1972.

[5] A. Hermanne, F. Tárkányi, S. Takács, R. Adam-Rebeles, A.V. Ignatyuk, S. Spellerberg, R. Schweikert, Appl. Radiat. Isot. **69** (2011) 2:358-368.

[6] A. Hermanne, R. Adam-Rebeles, F. Tárkányi, S. Takács, I. Spahn, A.V. Ignatyuk, Appl. Radiat. Isot. **69** (2011) 2:475-481.
[7] A. Hermanne, R. Adam-Rebeles, F. Tárkányi, S. Takács, B. Király, A.V. Ignatyuk, Nucl. Instrum. Methods Phys. Res. B **269** (2011) 7:695-699.
[8] A. Hermanne, R. Adam-Rebeles, F. Tárkányi, S. Takács, M. Takács, A.V. Ignatyuk, Nucl. Instrum. Methods Phys. Res. B **269** (2011) 21:2563-2571.
[9] S. Takács, F. Tárkányi, A. Hermanne, R. Adam-Rebeles, Nucl. Instrum. Methods Phys. Res. B **269** (2011) 2824-2834.
[10] F. Tárkányi, A. Hermanne, S. Takács, M. Sonck, Z. Szûcs, B. Király, A.V. Ignatyuk, Appl. Radiat. Isot. **69** (2011) 1:18-25.
[11] F. Tárkányi, A. Hermanne, B. Király, S. Takács, F. Ditrói, M. Baba, A.V. Ignatyuk, Appl. Radiat. Isot. **69** (2011) 1:26-36.
[12] F. Tárkányi, F. Ditrói, A. Hermanne, S. Takács, B. Király, M. Baba, A.V. Ignatyuk, Nucl. Instrum. Methods Phys. Res. B **269** (2011) 4:405-416.
[13] F. Tárkányi, F. Ditrói, A. Hermanne, S. Takács, B. Király, H. Yamazaki, M. Baba, A. Mohammadi, A.V. Ignatyuk, Nucl. Instrum. Methods Phys. Res. B **269** (2011) 12:1389-1400.
[14] F. Tárkányi, F. Ditrói, S. Takács,A. Hermanne, M. Baba, A.V. Ignatyuk, Nucl. Instrum. Methods Phys. Res. B **269** (2011) 1792-1800.
[15] F. Tárkányi, A. Hermanne, F. Ditrói, S. Takács, B. Király, Gy. Csikai, M. Baba, H. Yamazaki, M.S. Uddin, A.V. Ignatyuk, S.M. Qaim, *Systematic study of activation cross-sections of deuteron induced reactions used in accelerator applications.* Workshop on Nuclear Measurements, Evaluations and Applications. NEMEA 6. Krakow, Poland, 25-28 Oct., 2010. Proceedings. Eds: OECD Nuclear Energy Agency, Nuclear Science. Paris, OECD Publ. (NEA/NSC/DOC(2011)4) **0** (2011) 1:203-214.
[16] M. Al-Abyad, A.S. Abdel-Hamid, F. Tárkányi, F. Ditrói, S. Takács, U. Seddik, I. Bashter, Appl. Radiat. Isot. **70** (2012) 257-X.
[17] F. Ditrói, F. Tárkányi, S. Takács, A. Hermanne, A.V. Ignatyuk, M. Baba, Nucl. Instrum. Methods Phys. Res. B **270** (2012) 61-X.
[18] F. Tárkányi, A. Hermanne, S. Takács, F. Ditrói, I. Spahn, A.V. Ignatyuk, Appl. Radiat. Isot. **70** (2012) 309.
[19] A. Hermanne, R. Adam-Rebeles, F. Tárkányi, S. Takács, M. Takács, Gy. Csikai, A.V. Ignatyuk, Nucl. Instrum. Methods Phys. Res. B **270** (2012) 1:106-115.
[20] F. Tárkányi, F. Ditrói, S. Takács, B. Király, A. Hermanne, M. Sonck, M. Baba, A.V. Ignatyuk, Nucl. Instrum. Methods Phys. Res. B **274** (2012)1:1-25.
[21] F. Ditrói, F. Tárkányi, S. Takács, R. Dóczi, A. Hermanne, A.V. Ignatyuk, Appl. Radiat. Isot. **70** (2012) 574-582.

Submitted

[22] F. Tárkányi, A. Hermanne, S. Takács, F. Ditrói, A.V. Ignatyuk, Nucl. Instrum. Methods Phys. Res. B (accepted).
[23] S. Takács, M.P. Takács, A. Hermanne, F. Tárkányi, R. Adam Rebeles, Nucl. Instrum. Methods Phys. Res. B, In Press, Accepted Manuscript, Available online 20 February 2012, (in print).
[24] Hermanne, S. Takács, F. Tárkányi, R. Adam-Rebeles, A. Ignatyuk, Appl. Radiat. Isot., In Press, Accepted Manuscript, Available online 18 February 2012 (in print).
[25] A. Hermanne, F. Tarkanyi, S. Takacs, R. Adam-Rebeles, A.V. Ignatyuk, Nucl. Instrum. Methods Phys. Res. B.

Abstract, poster, talk

[26] F. Ditrói, S. Takács, F. Tárkányi, *et al*., *Development of thin layer activation technique towards radioactive isotpe application under the free handling limit,* 11th International Conference on Applications of Nuclear Techniques, Crete, Greece, 12-18 June, 2011 **0** (2011).

[27] A. Hermanne, F. Tárkányi, S. Takács, B. Király, *et al*., *Cross sections of deuteron induced reactions on 45Sc up to 50 MeV: Experiments and comparison with theoretical codes*, 11th International Conference on Applications of Nuclear Techniques. Crete, Greece, 12-18 June, 2011 **0** (2011).

[28] A. Hermanne, F. Tárkányi, S. Takács, R. Adam-Rebeles, Gy. Csikai, *Experimental cross sections of Be-7 production in Al, Si, Mg and C by deuteron irradiation up to 50 MeV (Abstr.: p. 37),* 3rd International Nuclear Chemistry Congress. Palermo, Sicily, Italy, 18-23 Sept., 2011 **0** (2011).

[29] S. Takács, F. Ditrói, F. Tárkányi, M. Takács, *et al*., *Proposal of reactions on nickel for monitoring deuteron beam in the 10-50 MeV energy*, 11th International Conference on Applications of Nuclear Techniques. Crete, Greece, 12-18 June, 2011 **0** (2011).

[30] F. Tárkányi, S. Takács, F. Ditrói, *et al*., *Study of activation cross sections of deuteron induced nuclear reactions on manganese, rhodium and palladium for nuclear applications.*
11th International Conference on Applications of Nuclear Techniques. Crete, Greece, 12-18 June, 2011 **0** (2011).

[31] F. Tárkányi, F. F. Ditrói, *Cyclotrons in medicine: Production routes of therapeutic radioisotopes,* 7th Annual CYCLEUR Workshop on Cyclotron Research and Radio-labelled Nanoparticles, Ispra, Varese, Italy, 28-29 Nov., 2011 **0** (2011).

[32] F. Tárkányi, *Applied nuclear research and applications in MTA Atomki,* Nuclear Physics European Collaboration Committee 72 Meeting. Budapest, Hungary, 7-8 Oct., 2011 **0** (2011).

ANEX 1 Figures and table for illustrations of the comparison of experimental and theoretical data

Experimental and theoretical excitation functions for the natCu(p,x) reaction

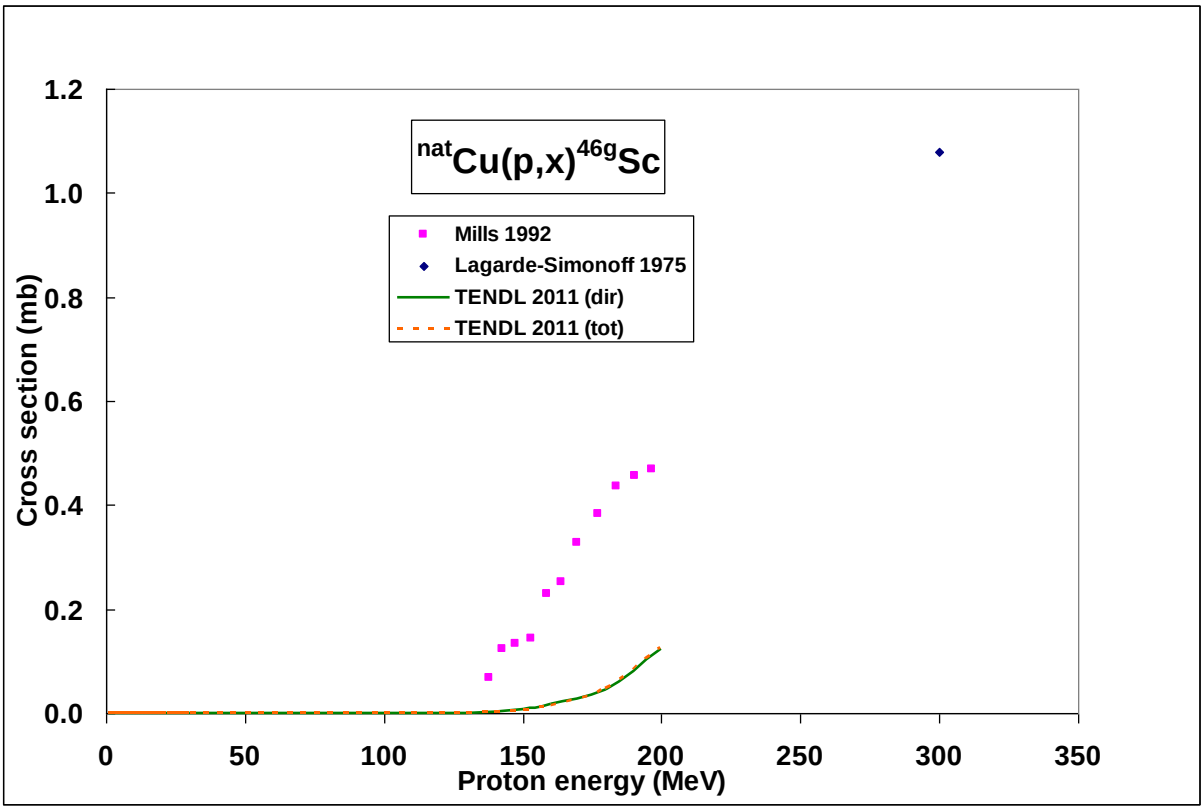

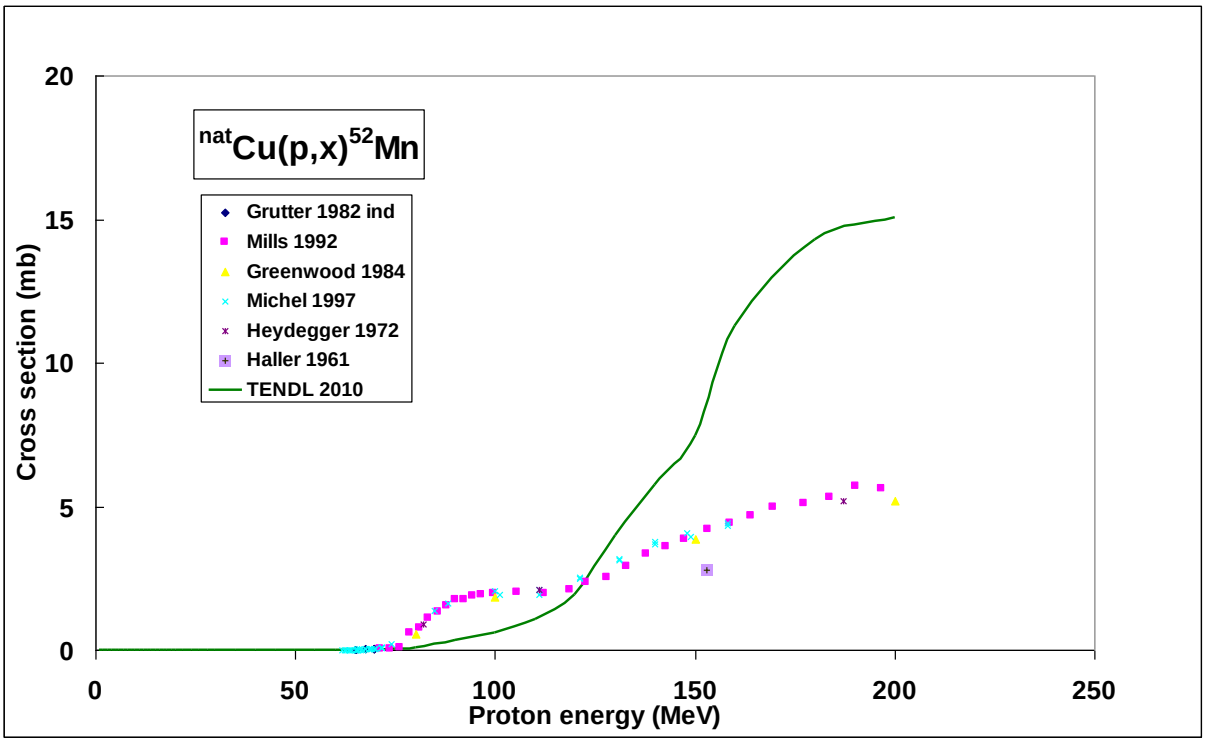

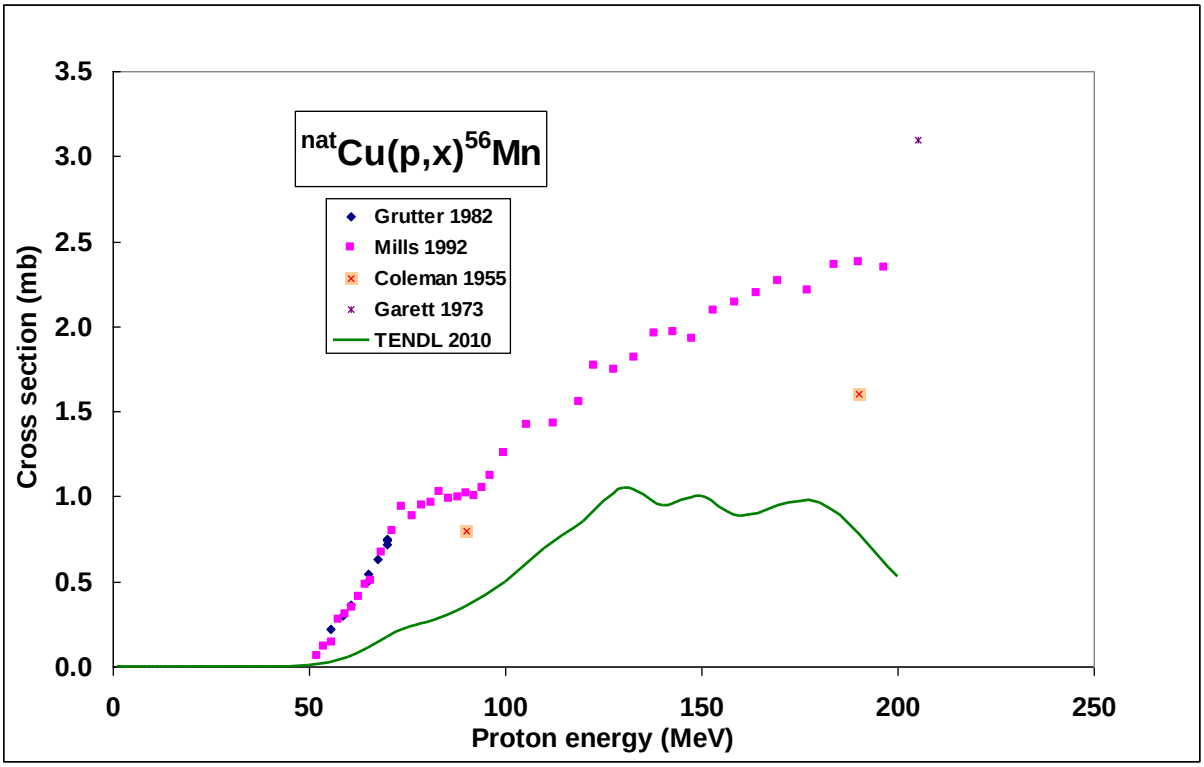
natCu(p,x)56Mn
Grutter 1982
Mills 1992
Coleman 1955
Garett 1973
TENDL 2010
Cross section (mb)
Proton energy (MeV)
0.0
0.5
1.0
1.5
2.0
2.5
3.0
3.5
0
50
100
150
200
250

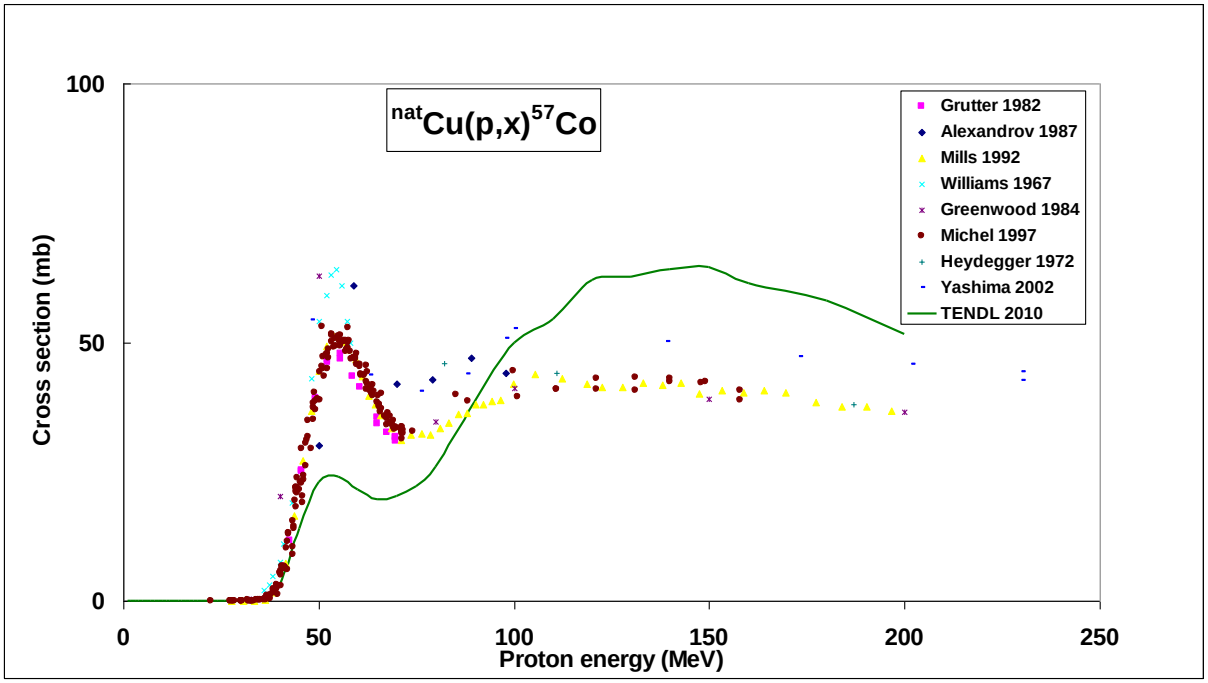
natCu(p,x)57Co
Grutter 1982
Alexandrov 1987
Mills 1992
Williams 1967
Greenwood 1984
Michel 1997
Heydegger 1972
Yashima 2002
TENDL 2010
Cross section (mb)
Proton energy (MeV)
0
50
100
0
50
100
150
200
250

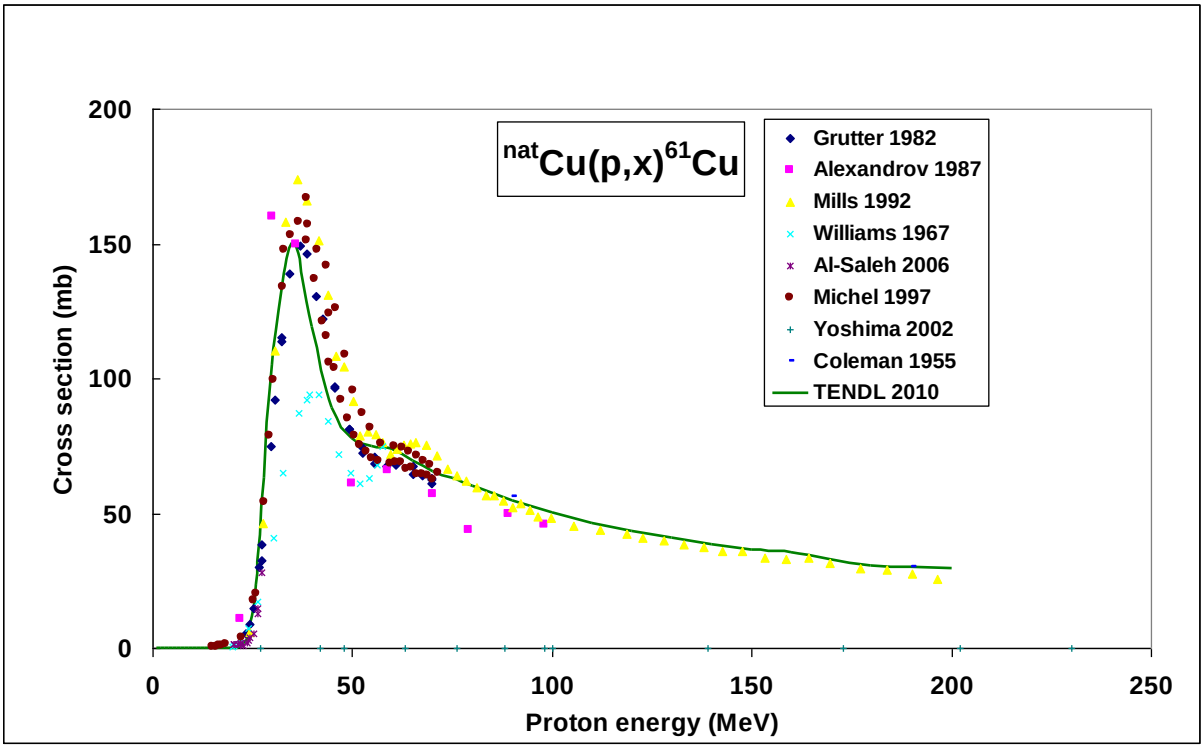
natCu(p,x)61Cu
Grutter 1982
Alexandrov 1987
Mills 1992
Williams 1967
Al-Saleh 2006
Michel 1997
Yoshima 2002
Coleman 1955
TENDL 2010
Cross section (mb)
Proton energy (MeV)
0
50
100
150
200
250

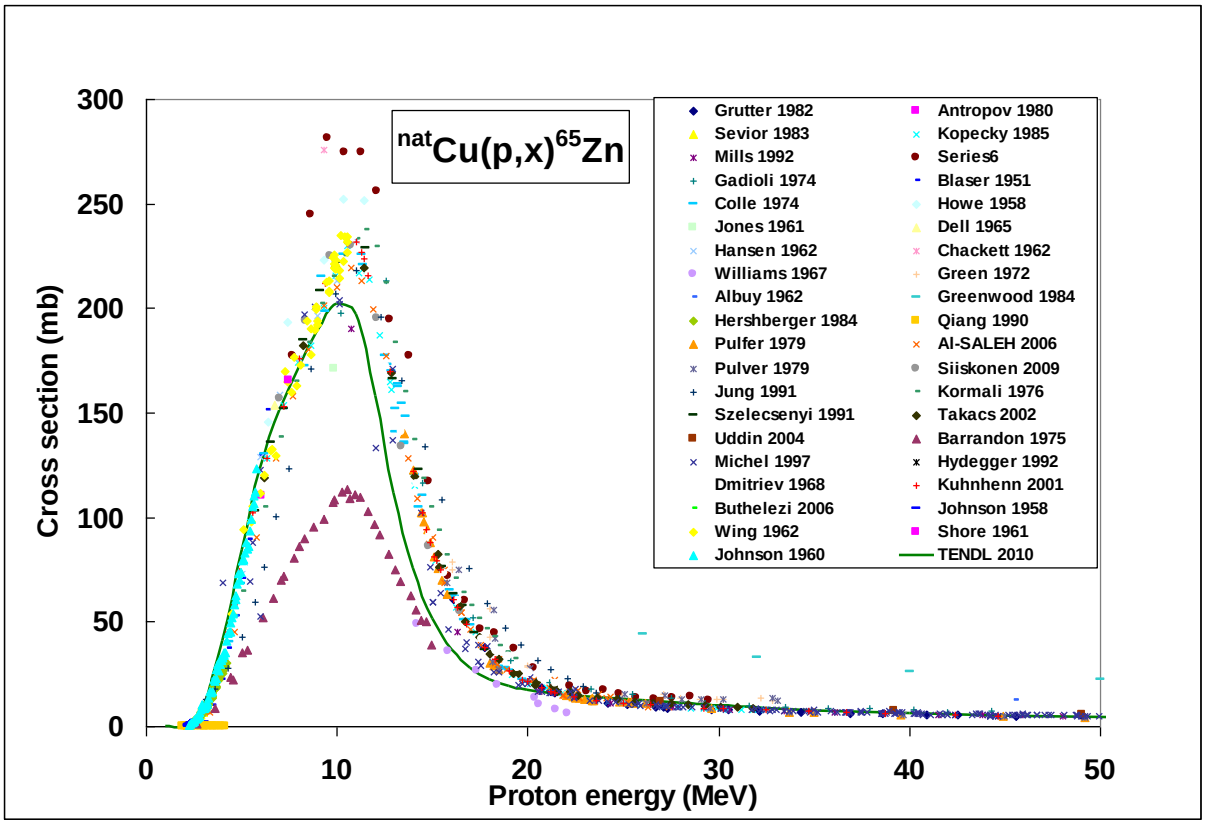
natCu(p,x)65Zn
Grutter 1982
Sevior 1983
Mills 1992
Gadioli 1974
Colle 1974
Jones 1961
Hansen 1962
Williams 1967
Albuy 1962
Hershberger 1984
Pulfer 1979
Pulver 1979
Jung 1991
Szelecsenyi 1991
Uddin 2004
Michel 1997
Dmitriev 1968
Buthelezi 2006
Wing 1962
Johnson 1960
Antropov 1980
Kopecky 1985
Series6
Blaser 1951
Howe 1958
Dell 1965
Chackett 1962
Green 1972
Greenwood 1984
Qiang 1990
Al-SALEH 2006
Siiskonen 2009
Kormali 1976
Takacs 2002
Barrandon 1975
Hydegger 1992
Kuhnhenn 2001
Johnson 1958
Shore 1961
TENDL 2010
Cross section (mb)
Proton energy (MeV)
0
50
100
150
200
250
300
10
20
30
40
50

Target	Product	Comparison	Product
Cu	7Be	no TENDL	7Be
	22Na	no TENDL	22Na
	24Na	no TENDL	24Na
	38Cl	no TENDL	38Cl
	42K	underestimation in the whole energy range	42K
	43K	underestimation in the whole energy range	43K
	44mSc	underestimation in the whole energy range	44mSc
	46gSc	underestimation in the whole energy range	46gSc
	47Sc	underestimation in the whole energy range	47Sc
	48Sc	underestimation in the whole energy range	48Sc
	48V	overestimation at high energies (above 150 MeV)	48V
	48Cr	overestimation in the whole energy range	48Cr
	49Cr	overestimation at high energies	49Cr
	51Cr	underestimation at low energy, overestimation at high energies	51Cr
	52Mn	underestimation at low energy, overestimation at high energies	52Mn
	54Mn	underestimation in all energy range	54Mn
	56Mn	underestimation in all energy range	56Mn
	52Fe	No TENDL for (g)	52gFe
	55Fe	overestimation at high energy, scarce exp. data	55Fe
	59Fe	underestimation at high energies	59Fe
	55Co	underestimation at low energy, overestimation at high energies	55Co
	56Co	underestimation at low energy, overestimation at high energies	56Co
	57Co	underestimation at low energy, overestimation at high energies	57Co
	58gCo	underestimation in all energy range	58gCo
	60Co	underestimation practically in all energy range	60Co
	61Co	problem with exp. data	61Co

	56Ni	underestimation at low energy	56Ni
	57Ni	underestimation at low energy, overestimation at high energies	57Ni
	60Cu	underestimation at low energy	60Cu
	61Cu	OK	61Cu
	62Cu	OK	62Cu
	64Cu	OK	64Cu
	60Zn	scarce exp., underestimation	60Zn
	61Zn	underestimation at low energy	61Zn
	62Zn	underestimation at low energy	62Zn
	63Zn	underestimation at low energy	63Zn
	65Zn	OK	65Zn
	66Zn	scarce exp., only at threshold	66Zn

8. Improvement of Evaluated Nuclear Data Files with Emphasis on Activation and Dosimetry Reactions (A. Trkov)

8.1 INTRODUCTION

Researchers from the Jožef Stefan Institute are actively involved in the development of the fusion technology through the Slovenian Fusion Association. Neutronics calculations are one of the key areas of expertise and FENDL library is the reference library for the ITER device. The quality of the nuclear data library is therefore of great concern, which drives the motivation for participation in the CRP. Specific contributions to the CRP are briefly described below.

8.2 EVALUATED NUCLEAR DATA FILES OF THE TUNGSTEN ISOTOPES

Tungsten is an important material for fusion technology because it is the primary candidate for the first wall material because of its nuclear and mechanical properties. Benchmarking of existing evaluations revealed severe deficiencies. In addition, there is the need to extend the energy range to at least 60 MeV for tentative computational simulations in the IFMIF facility, designed to test the material properties under severe irradiation conditions.

A consortium of evaluators under the coordination of the IAEA started the development work to produce entirely new evaluated nuclear data files for the tungsten isotopes based on calculations with the EMPIRE-II nuclear model code, covariance matrix prior using the Monte Carlo technique and the final covariances based on available experimental data from EXFOR through the GANDR system by the generalised least squares method. Extensive validation of the data was done using the FNG-W benchmark from the SINBAD compilation and a series of fast criticality safety benchmarks from the ICSBEP compilation. The results with the new data greatly improve the agreement between the calculated and the integral parameters measured in the benchmark experiments. Some details were presented at the Port Jefferson conference (TRKOV, Andrej, CAPOTE, Roberto, KODELI, Ivan Aleksander, LEAL, Luiz C. Evaluation of Tungsten nuclear reaction data with covariances. Nucl. data sheets (N.Y. N.Y.), 2008, issue 12, vol. 109, p.p. 2905-2909). Since then, small refinements were made to eliminate formatting inconsistencies. The evaluations were adopted for the ENDF/B-VII.1 evaluated nuclear data library, which is available from any one of the Nuclear Data Centres. Independent validation for ENDF/B-VII.1 confirmed the improved performance of the tungsten evaluations. Full intercomparison plots comparing competing evaluations with experimental data from EXFOR and a commented summary, including a brief discussion of the benchmark results is available the IAEA web site http://www-nds.iaea.org/wolfram/final.htmlx.

8.3 ACE LIBRARY FOR THE MCNP-FAMILY OF CODES FROM THE FENDL-3 FILES

The most widely used codes for data testing belong to the MCNP-family of Monte Carlo transport codes, which read the cross section data in the so-called ACE format. At the first RCM it was agreed that a starter library would be assembled and that the corresponding ACE files would be prepared. The ACE files and the corresponding directory files were set up and delivered to the IAEA. The scripts, data processing inputs and auxiliary codes were also prepared and installed on the IAEA computers so that the final library could be generated in-house, including any subsequent corrections and additions, if needed. Patches for the NJOY

code system were developed to enable processing of covariances of the cross sections for the excitation of metastable targets.

8.4 EVALUATED NUCLEAR DATA FILE FOR MANGANESE

Manganese is one of the constituents of alloys for structural components and a dosimetry material. Its nuclear data evaluation is indispensable for the design of nuclear devices. Existing ^{55}Mn evaluations extended only up to 20 MeV and showed deficiencies in the resonance region. A consortium of evaluators under the coordination of the IAEA started the development work to produce entirely new evaluated nuclear data file based on calculations with the EMPIRE-II nuclear model code and the covariance matrix prior using the Monte Carlo technique. Some nuclear model parametric studies, covariance evaluation, file assembly and validation were carried out at JSI. The ORNL resonance parameters evaluation by Derrien *et al.*, was included in the file. The new evaluation solves the long-standing discrepancy between the resonance integral calculated from the resonance parameters and the one measured by the activation technique. The broad-resolution shape of the capture cross sections is confirmed by simulating the Grenoble lead-slowing-down experiment. The evaluation was accepted also for ENDF/B-VII.1 library. The evaluation reflects the current state of the knowledge. Possible improvements above the resonance range and in the covariance data might be needed in the future.

8.5 OTHER EVALUATIONS

The evaluations for the Cd isotopes were reviewed. A new set of resonance parameters for all isotopes was evaluated at IRMM, based on the new measurements that were performed there. They were incorporated into the ENDF/B-VII.1 evaluated nuclear data library, except ^{113}Cd for which the evaluation by Mughabghab from BNL was adopted. Although Mughabghab's parameters differ slightly from the IRMM evaluation, the differences in the shape of the cross sections are negligible and are not expected to influence the integral performance of the evaluations. The status of the evaluations for the Cr isotopes in the currently proposed FENDL-3 library was checked and corrections were proposed. The MAT number of ^{15}N was changed to 728.

8.6 VALIDATION

Methods and procedures were developed to simplify integral testing of the data against experimentally measured integral cross sections such as the thermal value, the resonance integral and the ^{252}Cf spontaneous fission spectrum averaged cross sections.

8.7 EXTENSION OF EVALUATIONS FOR ^{3}H, ^{3}HE AND ^{4}HE TO 60 MEV

The ^{3}H evaluation from ENDF/B-VII.1b4 was taken as a starter file. The extension of the total cross section was based on the data by Phillips, Battat, Katsurov. For the elastic angular distributions flat extrapolation to 60 MeV was done. The (n,2n) cross sections were taken from the ENDF/B-VI.8 library. The (n,3n) cross sections were taken from the EAF-2010 file.

The ^{3}He evaluation from the JENDL-4 library was taken as starter file. The total cross section extension was based on the data by Haesner, Goulding, Battat. Elastic angular distributions were extrapolated flat to 60 MeV. The capture data in ENDF/B-VII.1b4 are newer and were adopted. For the (n,p) Haesner data were used, extrapolated to 60 MeV. The data from the same author were used to determine the (n,d) cross sections, extrapolated flat to 60 MeV.

The ^{4}He evaluation from ENDF/B-VII.1b4 was taken as a starter file. The extension of the total cross section was based on the data by Haesner, Shamu, Battat. To describe the elastic

angular distributions the Arnold data at 60 MeV were fitted and interpolated linearly to existing data below 20 MeV because no other measurements are available. The cross sections for the (n,2n) reaction were taken form EAF-2010. The cross sections for the (n,d) reaction follow the Shamu data (which are not in EAF-2010).

Further details with cross section plots were provided in the three sections that follow.

9. Extension of the H-3 Evaluation to 60 MeV for FENDL-3(A. Trkov)

9.1 INTRODUCTION

One of the objectives of the IAEA CRP on the FENDL-3 library is to provide evaluated nuclear reaction data for all materials relevant for fusion-related neutronics calculations up to incident neutron energies of 60 MeV. Starter evaluations were selected and in case they did not extend up to the desired incident neutron energies, the Japanese colleagues extended the range to at least 60 MeV using data from the TENDL-2010 library. Unfortunately this was not possible for the light nuclides because TENDL-2010 is based on nuclear model calculations, which are not applicable for the lightest nuclides. The evaluations in the new ENDF/B-VII.1b4 library for ^{1}H and ^{2}H cover the desired energy range, but no evaluation extends beyond 20 MeV for ^{3}H, ^{3}He and ^{4}He. In the present work the extension of the ^{3}H evaluation to 60 MeV is described.

9.2 PROCEDURES

The FENDL-3 starter library contains the ENDF/B-VII.0 evaluation. In this library the (n,2n) reaction cross sections are grossly underestimated, compared to a single measurement by Mather [1] (see the discussion below) so the cross sections for this reaction were replaced by those from ENDF/B-VI.8 in the candidate evaluation for ENDF/B-VII.1. This modified evaluation was taken as a starting point for FENDL-3. The evaluation was checked against the experimental data in the EXFOR database. Extension to each reaction was made as described below. In the plots the updated evaluation (extended to 60 MeV, labelled “fendl3”) is compared with the ENDF/B-VII.0 evaluation (labelled “e70”) and the experimental data.

9.3 TOTAL CROSS SECTION

The data of Phillips [2], Battat [3] and Katsurov [4] were considered. The total cross section is the sum of the partials. The constituent reaction cross sections (mainly the elastic), were adjusted such that the total cross section matched the bulk of the experimental points. The total cross section plot is shown on Figure 1.

9.4 ELASTIC CROSS SECTION

Measurements of the competing reactions (n,2n) and (n,3n) exist only at 14 MeV and are negligible in comparison with the elastic cross section. At energies above 20 MeV the measurements of Seagrave indicate a distinct drop in the elastic cross sections. Considering the constraint on the measured total cross section, this could indicate that the competing reactions are becoming significant. However, there are no measurements of the competing reactions at these energies that could support such an increase, so the elastic cross section was extrapolated linearly in log-log scale with the gradient adjusted to match the measured total cross sections. The elastic cross section plot is shown on Figure 2.

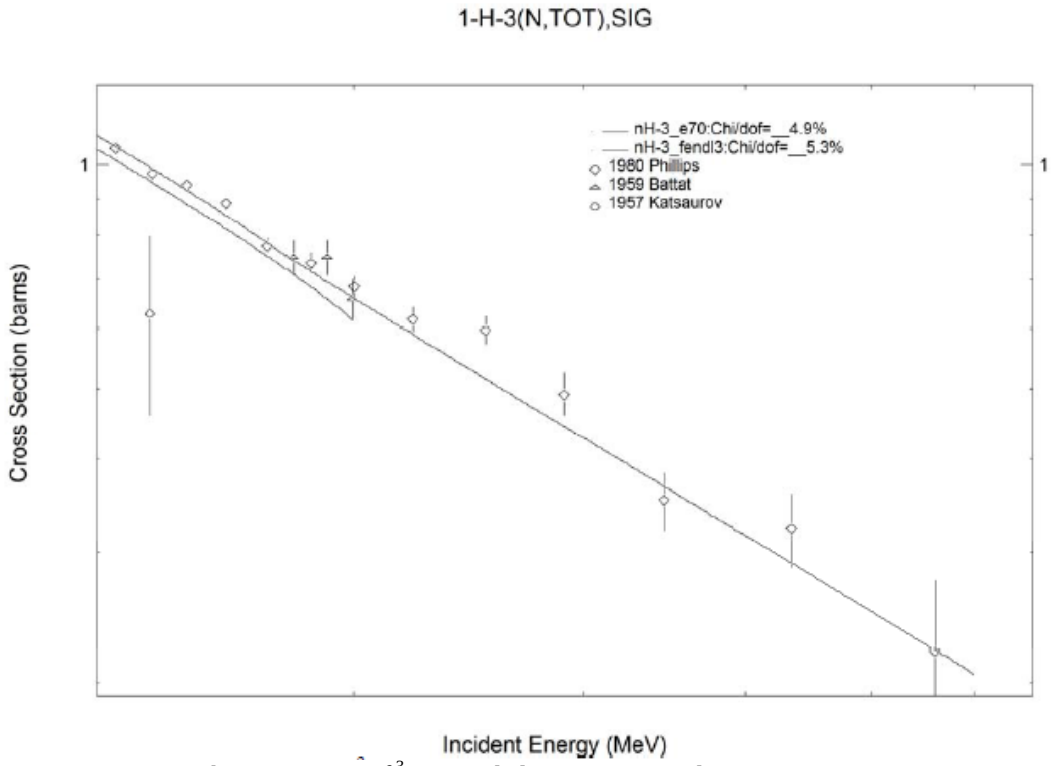

FIG. 1. Total cross section of ^{3}H extended to neutron incident energies up to 60 MeV.

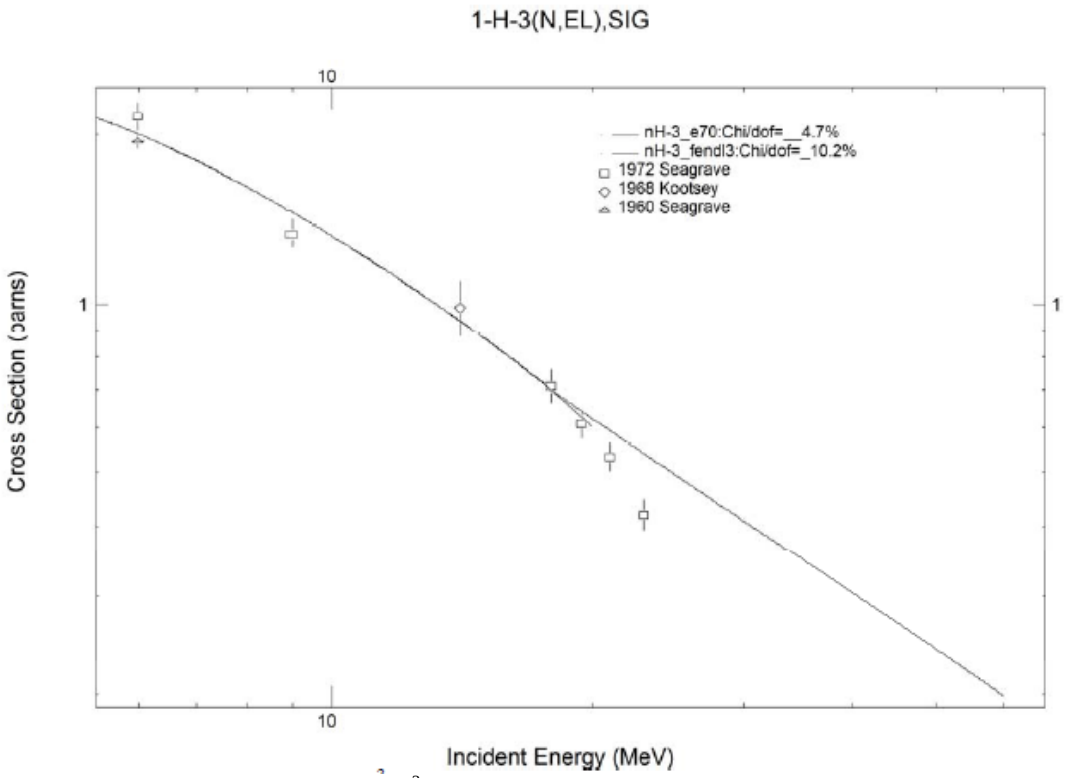

FIG. 2. Elastic cross section of ^{3}H extended to neutron incident energies up to 60 MeV.

9.5 ELASTIC ANGULAR DISTRIBUTIONS

Above 20 MeV measurements of the elastic angular differential cross sections by Seagrave [1] are available and they extend up to 23 MeV. The plots of the cross sections are shown on Figures 3 and 4. The angular distributions are in good agreement with the measurements. A flat extrapolation to 60 MeV was performed.

9.6 NON-ELASTIC CROSS SECTION

The non-elastic reaction cross sections are redundant and can be reconstructed from the cross sections of the constituting (n,2n) and (n,3n) reactions. Some measurements declared to be the non-elastic cross section exist in EXFOR by Seagrave, which suggest a strong increase of the (n,2n) and (n,3n) cross sections above 20 MeV, but since the same author also reported the declining elastic cross sections in this energy range, an error in the assignment of the contributions to the reaction cannot be excluded. The experimental data were ignored. The plot of the cross sections is shown on Figure 5.

9.7 TWO-NEUTRON EMISSION CROSS SECTION

The two-neutron emission cross section has a threshold at 8.35 MeV. A single measurement by Mather [1] is available. This measurement was strongly under predicted in ENDF/B-VII.0 library. The cross sections were replaced by those from the ENDF/B-VI.8 evaluation, which are in good agreement with the measurement. For this reason the ENDF/B-VII.1b4 evaluation for this material was taken as a starting point. The data were extrapolated linearly in log-log scale to approximately preserve the gradient of the cross sections at 20 MeV. The plot of the cross sections is shown on Figure 6. The angular distributions and the emission spectra were extrapolated flat to 60 MeV.

9.8 THREE-NEUTRON EMISSION CROSS SECTION

The three-neutron emission cross section has a threshold at 11.32 MeV. A single measurement by Mather [1] is available. The cross sections are not present in the ENDF/B-VII.0 evaluation, but they appear in JEFF-3.2 and originate from the CENDL-2 evaluation and were normalised to the measured cross section at 14 MeV. The cross sections for this reaction are also present in the EAF-2010 library and tend to be somewhat higher, but they are given up to 60 MeV. The cross sections from the EAF-2010 library were adopted for the FENDL-3 library for this reaction. The plot of the cross sections is shown on Figure 7. Since no double-differential data exist in any of the evaluated data files, the neutron emission is assumed isotropic in the laboratory system and the emission spectrum is represented by the evaporation spectrum with an effective temperature of 600 keV, independent of incident neutron energy.

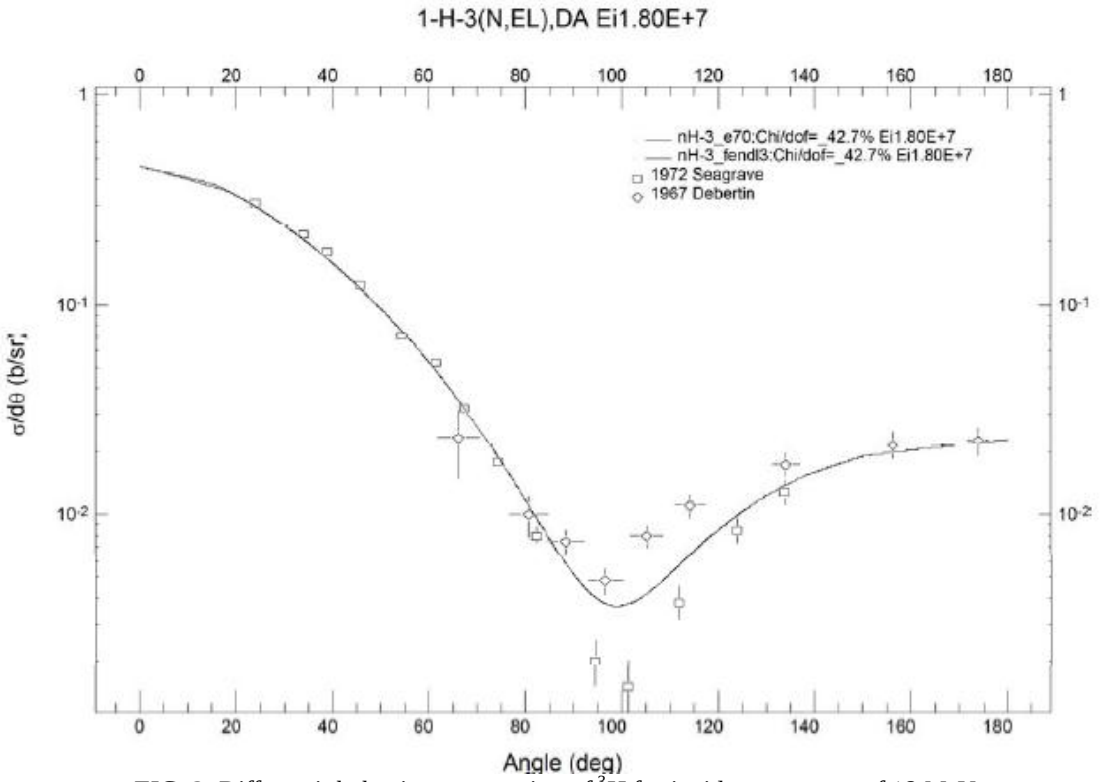

FIG. 3. Differential elastic cross section of ^{3}H for incident neutrons of 18 MeV.

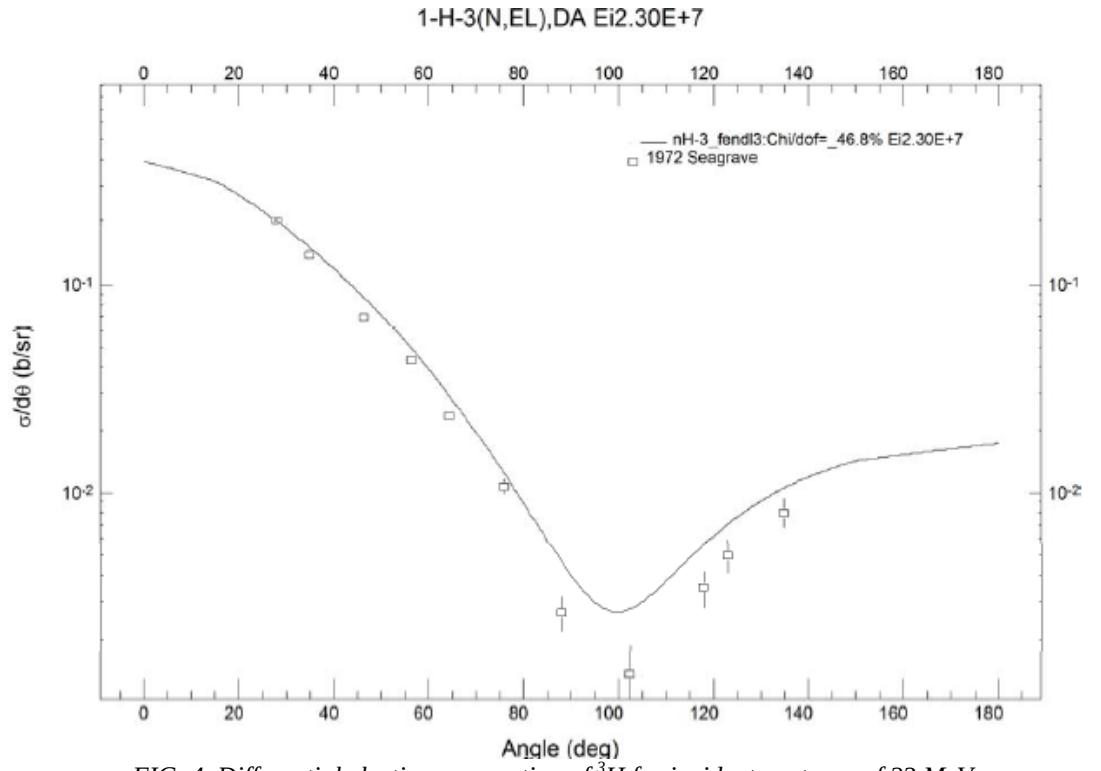

FIG. 4. Differential elastic cross section of ^{3}H for incident neutrons of 23 MeV.

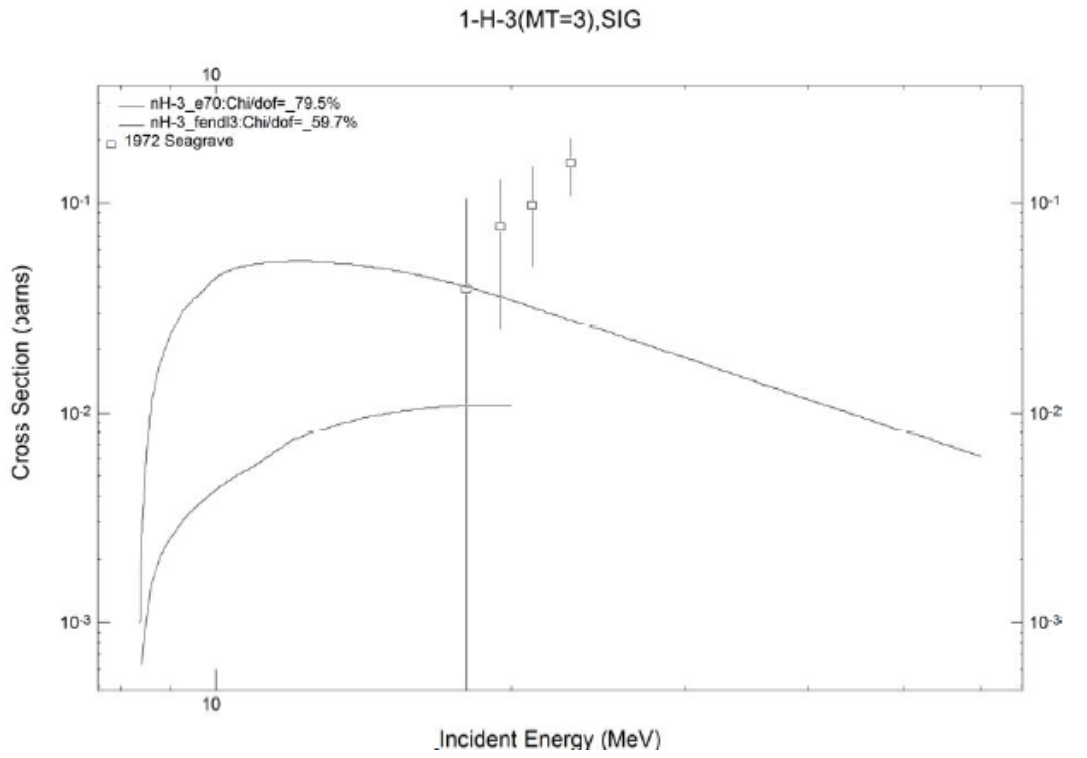

FIG. 5. Non-elastic cross section of ^{3}H.

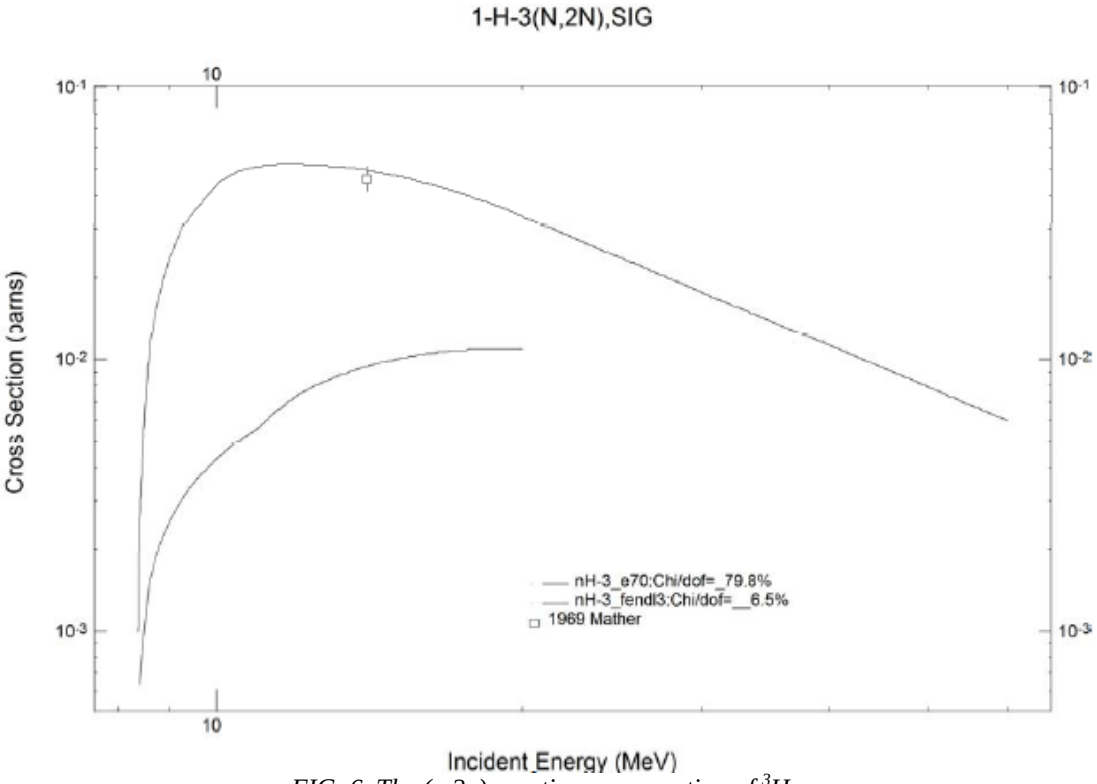

FIG. 6. The (n,2n) reaction cross section of ^{3}H.

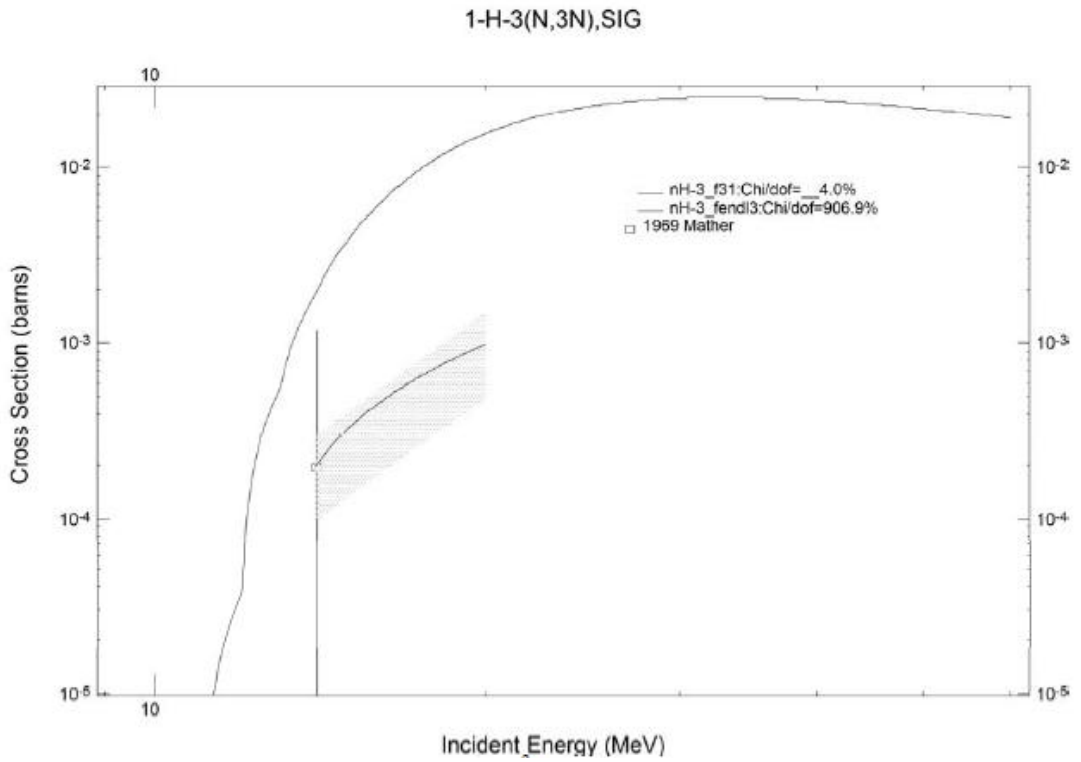

FIG. 7. The (n,3n) reaction cross section of ^{3}H.

9.9 VERIFICATION

The CHECKR code reported no problems. Fizcon reports that for MT=16 in MF=5 the value of U is not consistent. It seems likely that this is a false message because FIZCON compares (Q+U)/Q to a tolerance of 10^{-3}, but U is given in the laboratory system while the Q-value is defined in the centre-of-mass system. The PSYCHE code reports that the scattering radius of 0.364 is not in the range between 0.1011 and 0.2456, but this is the evaluator's choice. PSYCHE also reports that the total secondary energy exceeds the available energy for the (n,2n) reaction, but this problem is inherited from the original evaluation.

Processability of the file is checked by running the codes of the PrePro-2010 series including LINEAR, RECENT, SIGMA1 and FIXUP. Further testing is done by running NJOY to generate an ACE library for Monte Carlo codes like MCNP and a MATXS library for deterministic codes. The heating curve generated by the HEATR module is useful for checking potential energy-balance problems and is shown in Figure 8. The figure did not reveal any problems. The plots produced by the ACER module also showed nothing suspicious and are not presented.

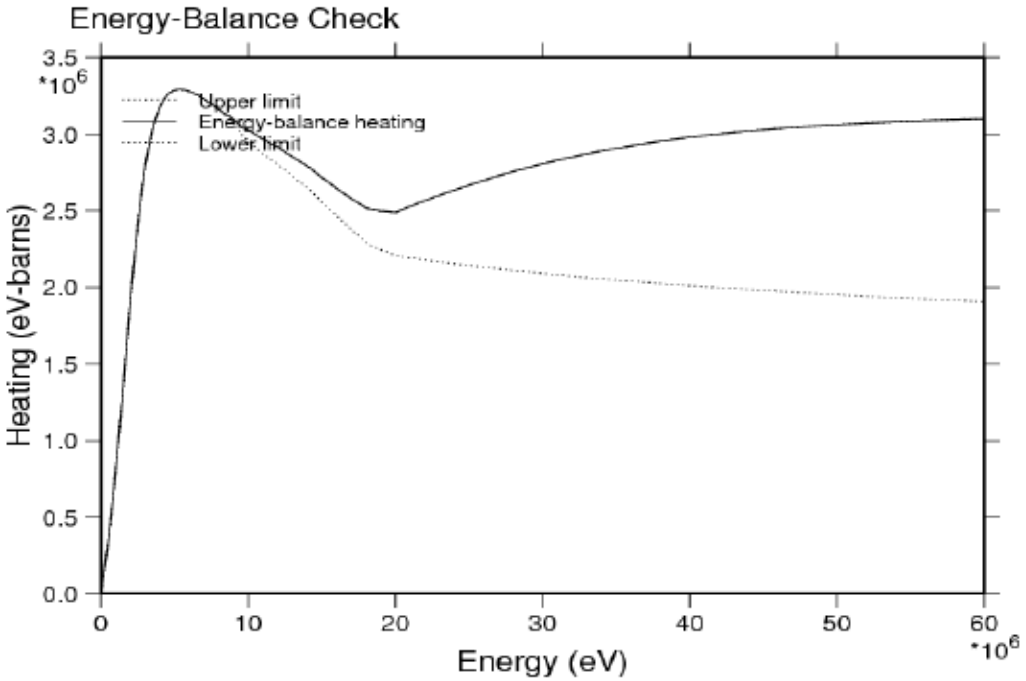

FIG. 8. Plot of the heating in ^{3}H calculated by the HEATR module of NJOY.

9.10 CONCLUSIONS

An ad-hoc evaluated nuclear data file for ^{3}H for incident neutrons with energies up to 60 MeV was produced for inclusion in the FENDL-3 library by extending the ENDF/B-VII.1b4 evaluation. It incorporates the information contained in other evaluated data files and the experimental EXFOR database. The trends in the total cross section are consistent with the measured data. The experimental information on the other reaction channels is poor and there are no theoretical model calculations to support the data included in the evaluation. The evaluation is complete in the sense that it allows the preparation of application libraries, but should not be relied upon for detailed calculations that are sensitive to the non-elastic reactions on tritium.

References for Section 9

[1] D.S. Mather, L.F. Pain, Measurement of (n,2n) and (n,3n) cross sections at 14 MeV incident energy, A.W.R.E. Aldermaston Reports; No.47/69 (1969), EXFOR: 20794.

[2] T.W. Phillips, B.L. Berman, Phys. Rev. **C 22** (1980) 384, EXFOR 10945.

[3] M.E. Battat, R.O. Bondelid, J.H. Coon, L. Cranberg, R.B. Day, F. Edeskuty, A.H. Frentrop, R.L. Henkel, R.L. Mills, R.A. Nobles, J.E. Perry, D.D. Phillips, T.R. Roberts, S.G. Sydoriak, Nucl. Phys. **12** (1959) 291, EXFOR 11021.

[4] L.N. Katsaurov, R.M. Musaeljan, V.I. Popov, At. Ehnerg. Suppl. **5**, (1957) 71, EXFOR 40773.

10. Extension of the He-3 Evaluation to 60 MeV for FENDL-3 (A. Trkov)

10.1 INTRODUCTION

One of the objectives of the IAEA CRP on the FENDL-3 library is to provide evaluated nuclear reaction data for all materials relevant for fusion-related neutronics calculations up to incident neutron energies of 60 MeV. Starter evaluations were selected and in case they did not extend up to the desired incident neutron energies, the Japanese colleagues extended the range to at least 60 MeV using data from the TENDL-2010 library. Unfortunately this was not possible for the light nuclides because TENDL-2010 is based on nuclear model calculations, which are not applicable for the lightest nuclides. The evaluations in the new ENDF/B-VII.1b4 library for ^{1}H and ^{2}H cover the desired energy range, but no evaluation extends beyond 20 MeV for ^{3}H, ^{3}He and ^{4}He. In the present work the extension of the ^{3}He evaluation to 60 MeV is described.

10.2 PROCEDURES

The JENDL-4 evaluation is taken as a starting point. The evaluation was checked against the experimental data in the EXFOR database. Extension to each reaction was made as described below. In the plots the JENDL-4 evaluation (extended to 60 MeV, labelled "fendl3") is compared with the ENDF/B-VII.1b4 evaluation (labelled "e71") and the experimental data.

10.3 TOTAL CROSS SECTION

The data of Haesner [1], Goulding [2] and Battat [3] were considered. The total cross section is the sum of the partials. The constituent reaction cross sections (mainly the elastic), were adjusted such that the total cross section matched the bulk of the experimental points. The total cross section plot is shown on Fig. 1.

10.4 ELASTIC CROSS SECTION

The competing reactions (n,p) and (n,d) are small. The elastic cross sections were extrapolated linearly on log-log scale with a gradient adjusted to match the measured total cross sections. Experimental data for the elastic cross sections above 20 MeV by Haesner [1] are available in EXFOR, but they seem to be strongly underestimated and are inconsistent with the measured total cross sections, so they are ignored. The elastic cross section plot is shown on Fig. 2.

10.5 ELASTIC ANGULAR DISTRIBUTIONS

Above 20 MeV measurements of the elastic angular differential cross section by Haesner [1] are available and they extend up to 30 MeV. The plots of the cross sections are shown on Figures 3 to 5. The angular distributions in the JENDL-4 evaluation are in good agreement with the measurements. Some systematic discrepancy is due to the underestimation of the elastic cross section as evident from Fig. 2. A flat extrapolation to 60 MeV was performed.

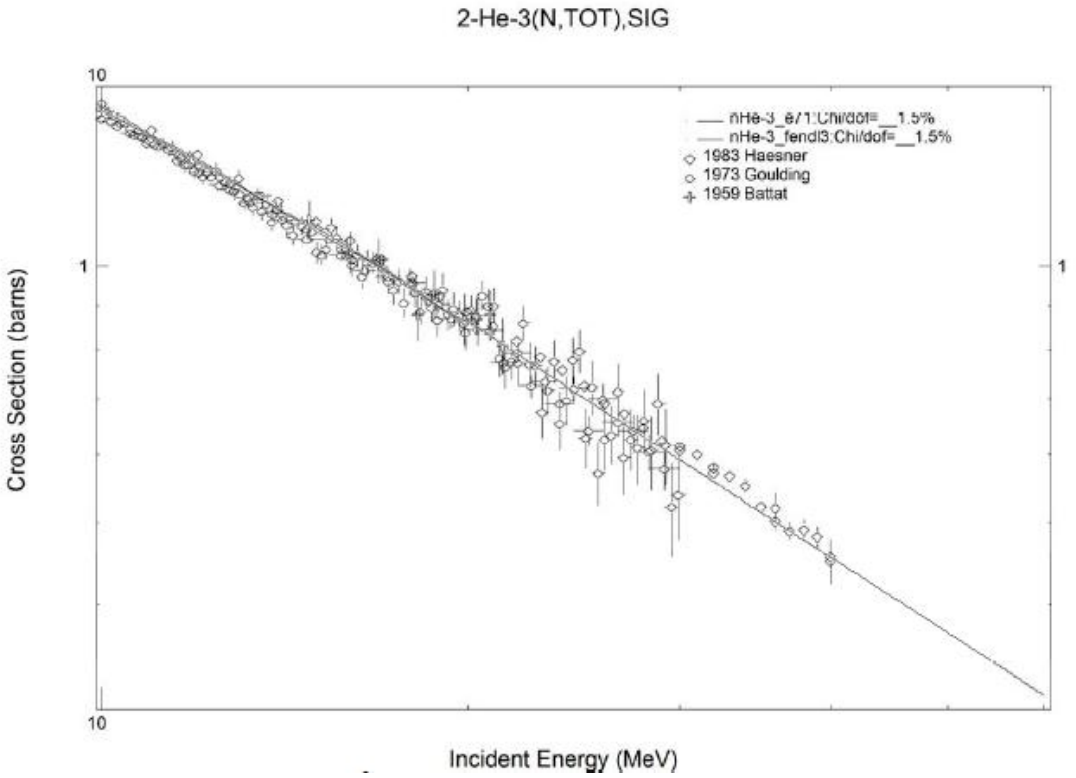

FIG. 1. Total cross section of ^{3}He extended to neutron incident energies up to 60 MeV.

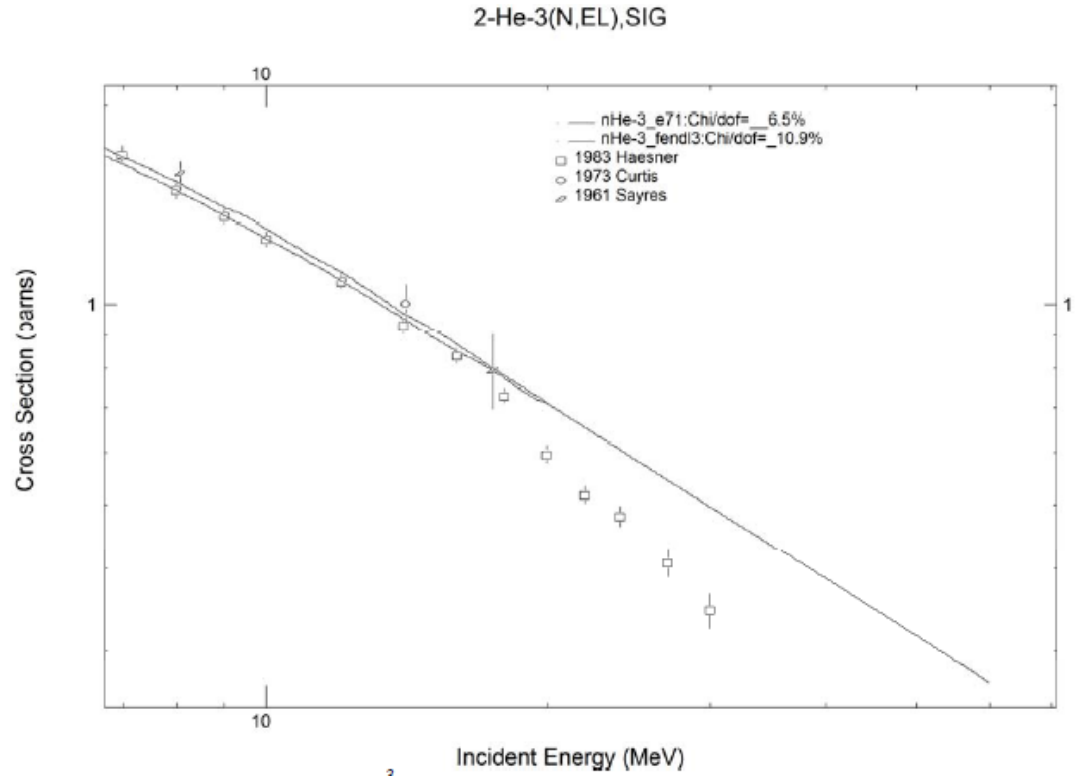

FIG. 2. Elastic cross section of ^{3}He extended to neutron incident energies up to 60 MeV.

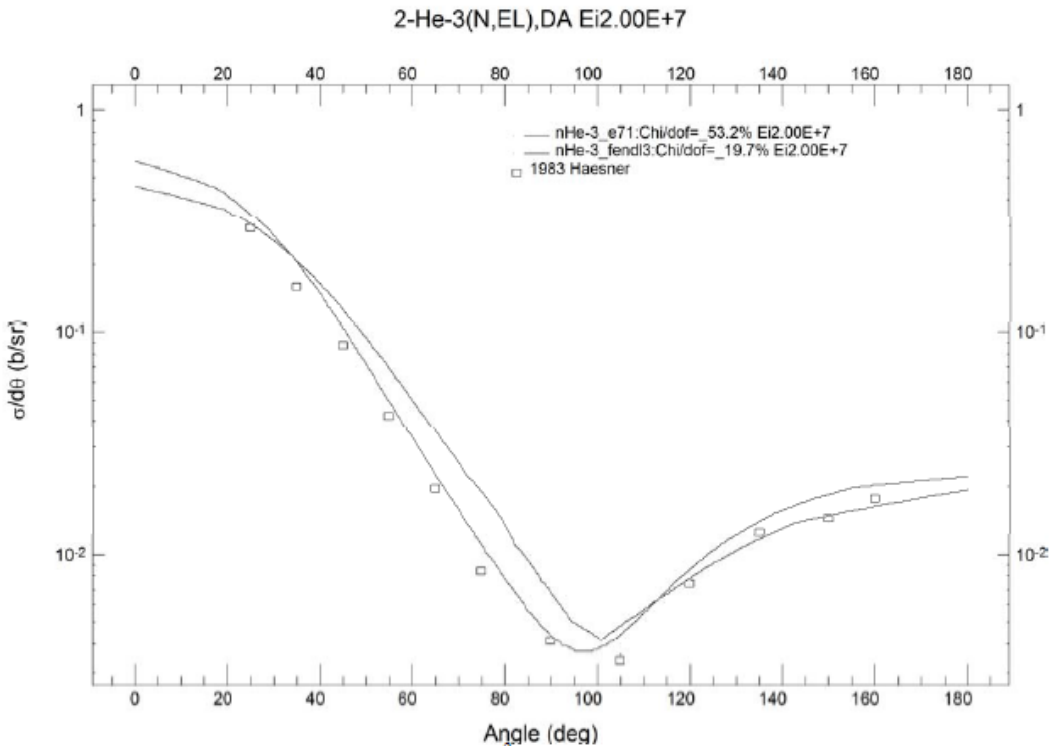

FIG. 3. Differential elastic cross section of ^{3}He for incident neutrons of 20 MeV.

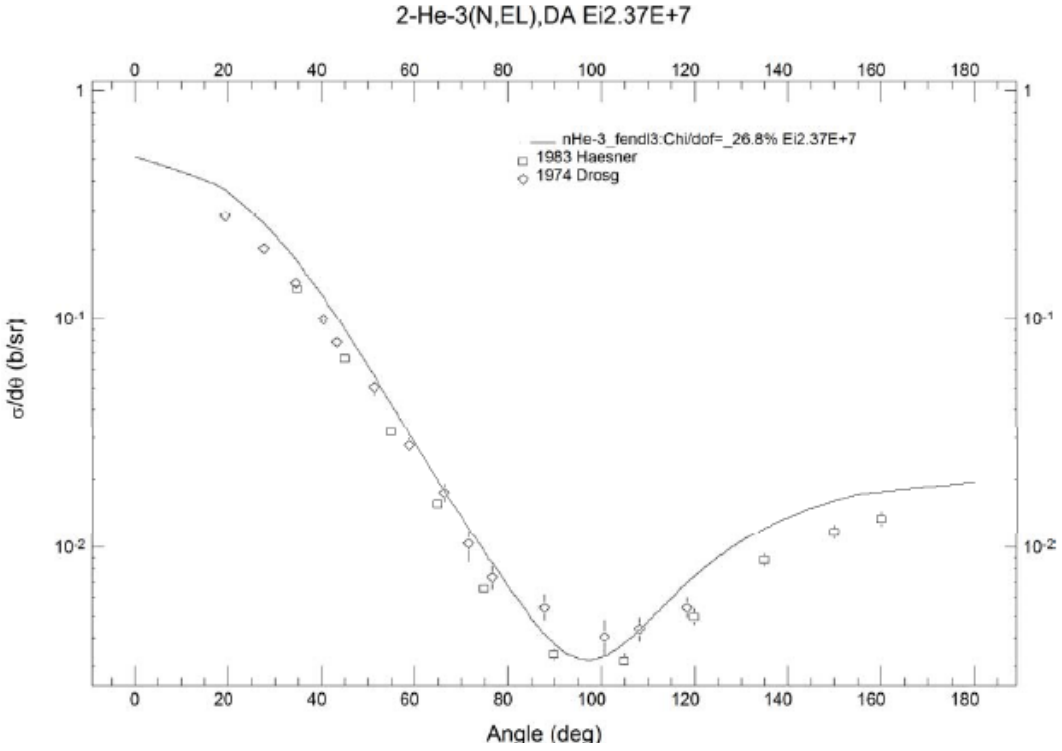

FIG. 4. Differential elastic cross section of ^{3}He for incident neutrons of 23.7 MeV.

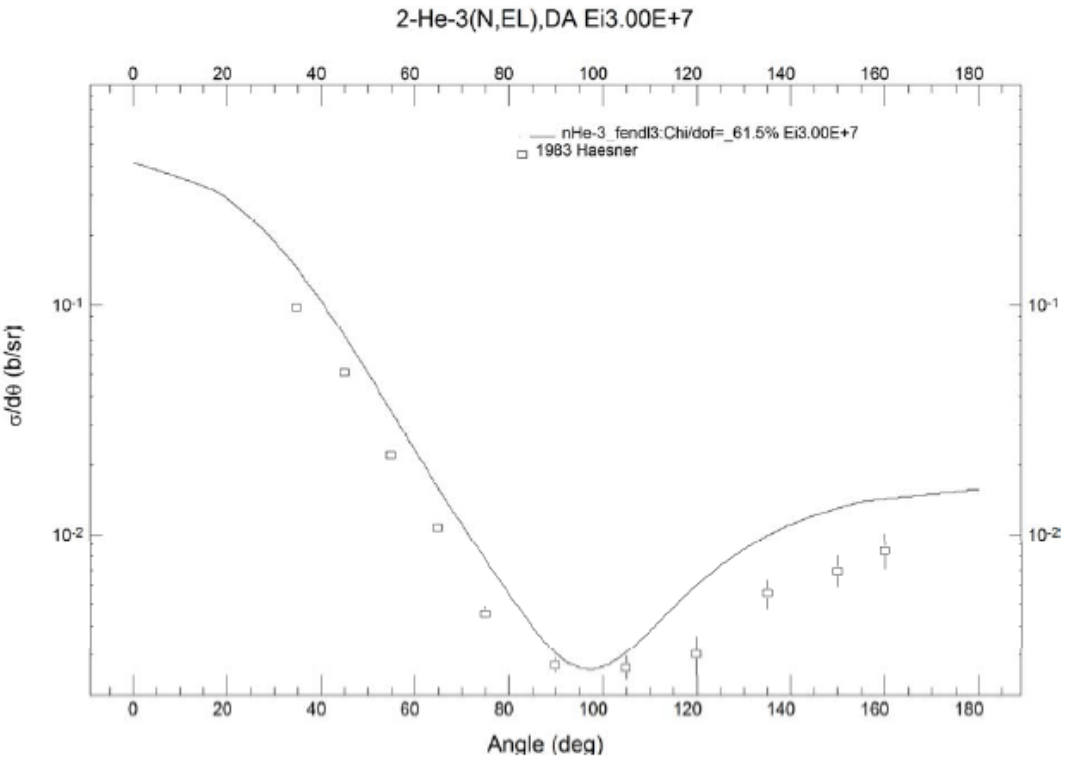

FIG. 5. Differential elastic cross section of ^{3}He for incident neutrons of 60 MeV

10.6 NON-ELASTIC CROSS SECTION

The non-elastic cross section is redundant and can be reconstructed from the cross sections of the constituting reactions. It is sometimes needed to describe the gamma-emission data, but this is not the case for ^{3}He. Therefore, the reaction was deleted from the original file.

10.7 RADIATIVE CAPTURE CROSS SECTION

The radiative capture cross sections in the JENDL-4 library differ considerably from those in the ENDF/B-VII.1b4 library, which tend to be supported by the data of Komar and some other measurements, which are not in EXFOR. It is possible that the ENDF/B-VII.1b4 data are closer to the truth for this reaction in this energy region, but for the sake of consistency the JENDL-4 cross sections are retained. Extrapolation to 60 MeV is done assuming approximately a 1/*v* shape. The plot is shown on Fig. 6.

10.8 PROTON EMISSION CROSS SECTION

The proton emission cross section in JENDL-4 follows the data of Haesner [1] near 20 MeV. The same experimental data extend to 30 MeV. Extrapolation to 60 MeV is performed assuming linear behaviour in log-log scale with a gradient to match the Haesner data. The plot of the cross sections is shown in Fig. 7. No emission spectra or angular distributions of protons are given.

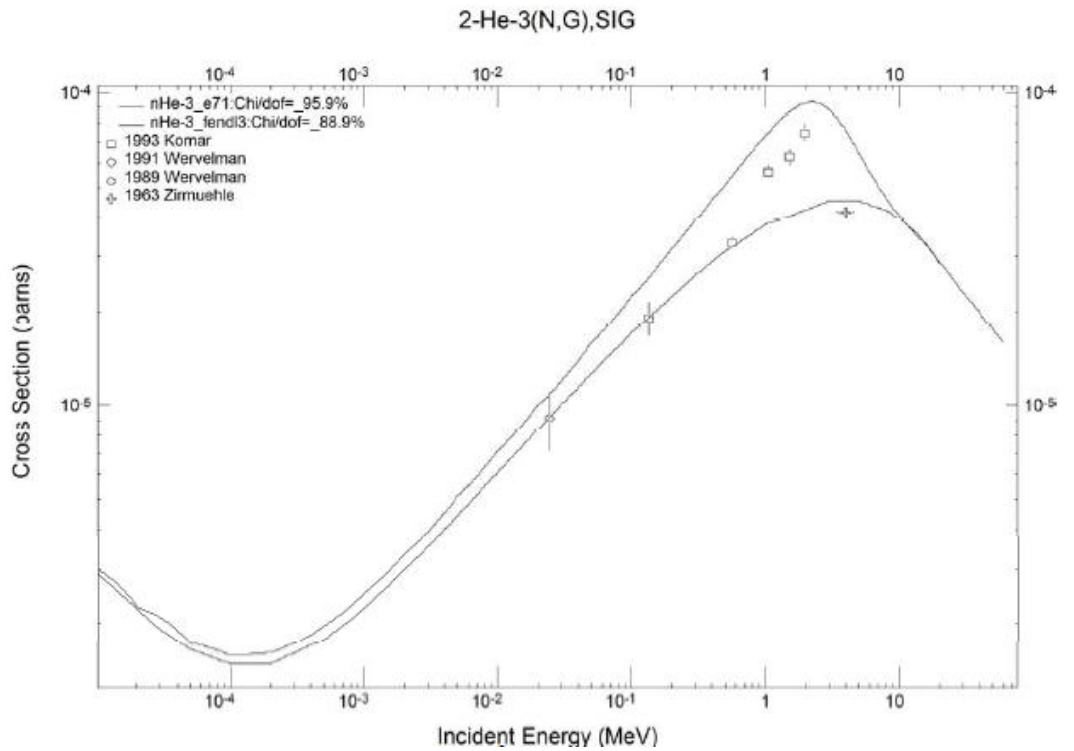

FIG. 6. Radiative capture cross section of ^{3}He .

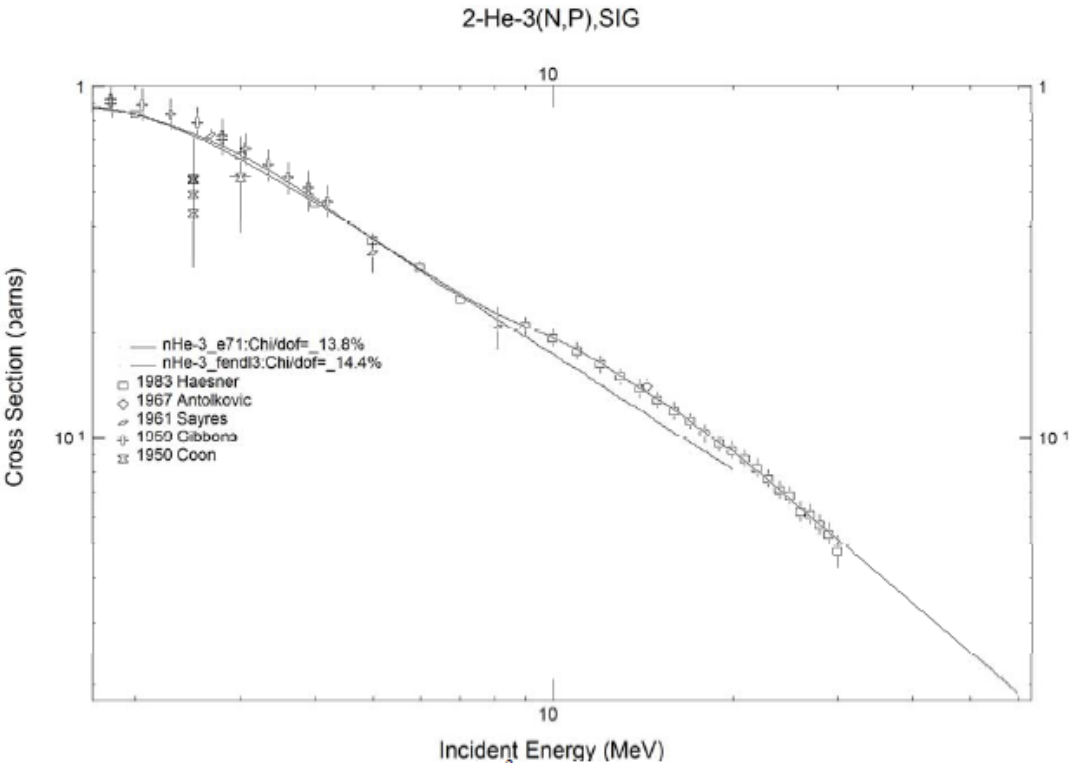

FIG. 7. The (n,p) reaction cross section of ^{3}He.

10.9 DEUTERON EMISSION CROSS SECTION

Deuteron emission cross section has a threshold at 4.36 MeV. Above 10 MeV the data of Haesner [1] are available. The JENDL-4 evaluation seems to follow the data better than the ENDF/B-VII.1b4 evaluation. The measured data are available up to 30 MeV. Extrapolation to 60 MeV is performed assuming linear behaviour in log-log scale with a gradient to match the Haesner data. The cross section plot is shown in Fig. 8. No emission spectra or angular distributions of deuterons are given.

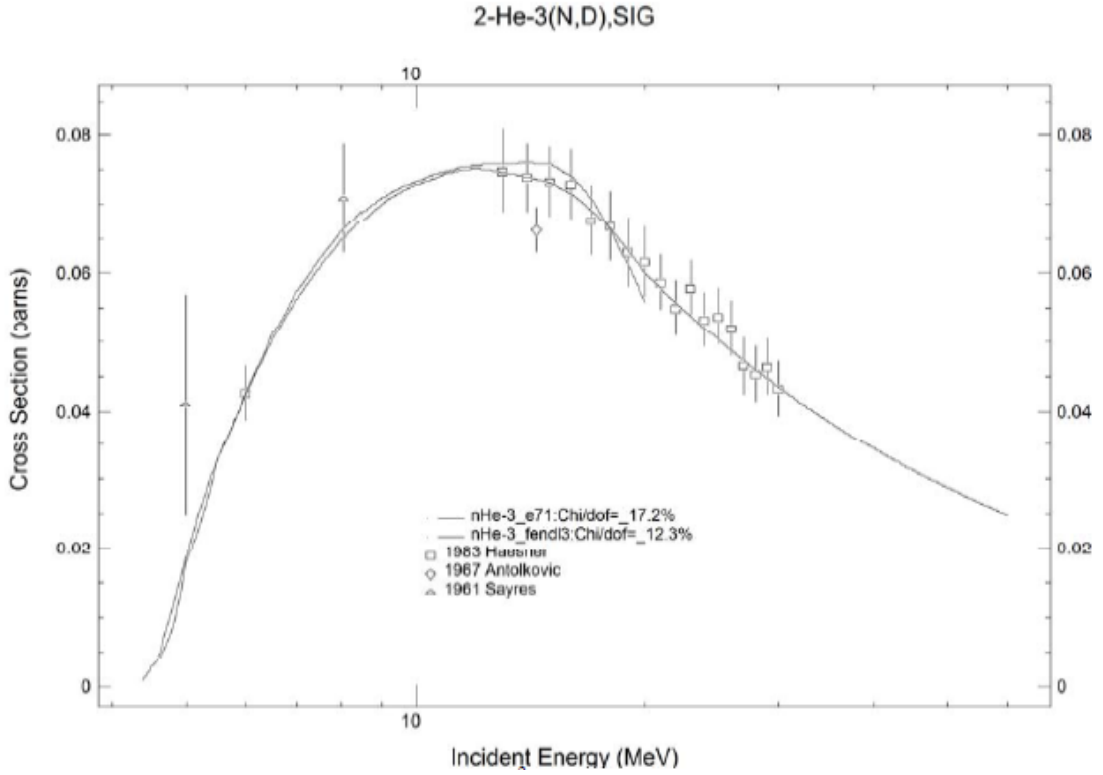

FIG. 8. The (n,d) reaction cross section of 3He.

10.10 VERIFICATION

Neither the CHECKR nor the FIZCON codes reported any problems. PSYCHE reports that the scattering radius of 0.3 is not in the range between 0.1011 and 0.2456, but this is the evaluator's choice.

Processability of the file is checked by running the codes of the PrePro-2010 series including LINEAR, RECENT, SIGMA1 and FIXUP. Further testing is done by running NJOY to generate an ACE library for Monte Carlo codes like MCNP and a MATXS library for deterministic codes. The heating curve generated by the HEATR module is useful for checking potential energy-balance problems and is shown in Figure 9. The figure did not reveal any problems. The plots produced by the ACER module also showed nothing suspicious and are not presented.

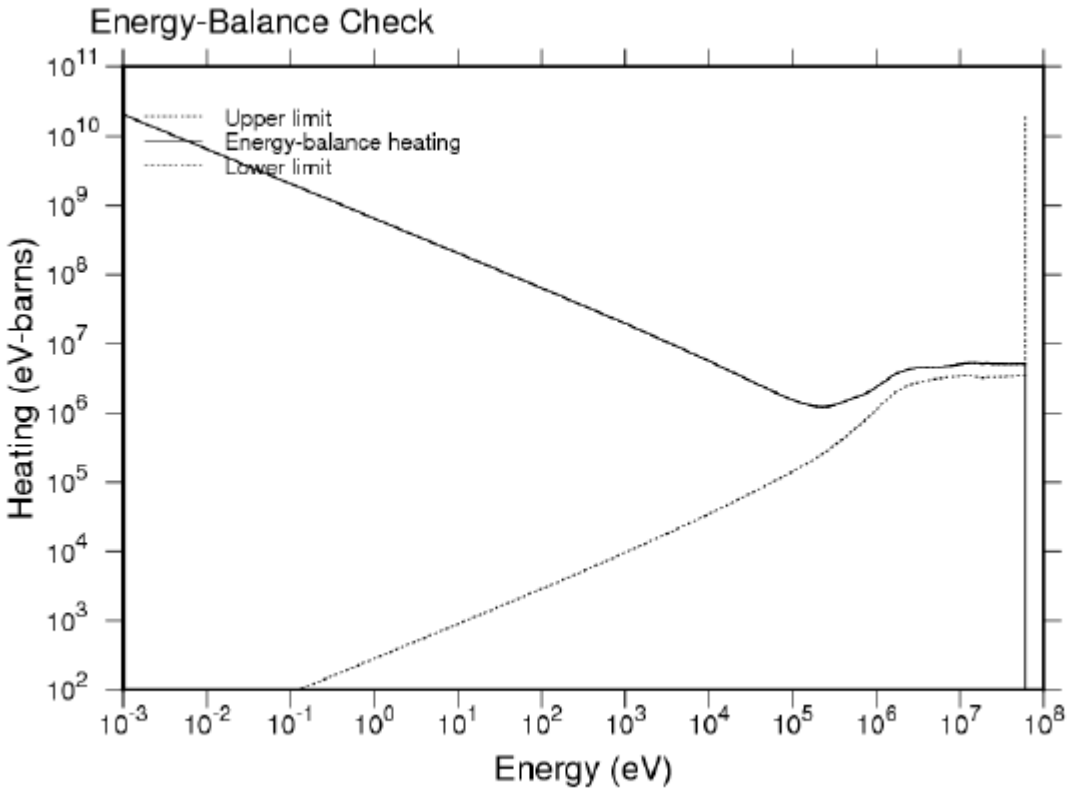

FIG. 9. Plot of the heating calculated by the HEATR module of NJOY.

10.11 CONCLUSIONS

A viable evaluated nuclear data file for ^{3}He for incident neutron energies up to 60 MeV was produced for inclusion in the FENDL-3 library by extending the JENDL-4 evaluation. The extension is based on ad-hoc methods and cannot compete with evaluations based on rigorous R-matrix analysis such as announced by G. Hale from the Los Alamos National Laboratory, but the data from that evaluation above 20 MeV have not been released and are not likely to be available before the release of FENDL-3.

References for Section 10

[1] B. Haesner, W. Heeringa, H.O. Klages, H. Dobiasch, G. Schmalz, P. Schwarz, J. Wilczynski, B. Zeitnitz, F. Kappeler, Phys. Rev. **C 28** (1983) 995, EXFOR 21883.
[2] C.A. Goulding, P. Stoler, J.D. Seagrave, Nucl. Phys. **A215**, (1973) 253, EXFOR 10278.
[3] M.E. Battat, R.O. Bondelid, J.H. Coon, L. Cranberg, R.B. Day, F. Edeskuty, A.H. Frentrop, R.L. Henkel, R.L. Mills, R.A. Nobles, J.E. Perry, D.D. Phillips, T.R. Roberts, S.G. Sydoriak, Nucl. Phys. **12** (1959) 291, EXFOR 11021.

11. Extension of the He-4 Evaluation to 60 MeV for FENDL-3 (A. Trkov)

11.1 INTRODUCTION

One of the objectives of the IAEA CRP on the FENDL-3 library is to provide evaluated nuclear reaction data for all materials relevant for fusion-related neutronics calculations up to incident neutron energies of 60 MeV. Starter evaluations were selected and in case they did not extend up to the desired incident neutron energies, the Japanese colleagues extended the range to at least 60 MeV using data from the TENDL-2010 library. Unfortunately this was not possible for the light nuclides because TENDL-2010 is based on nuclear model calculations, which are not applicable for the lightest nuclides. The evaluations in the new ENDF/B-VII.1b4 library for ^{1}H and ^{2}H cover the desired energy range, but no evaluation extends beyond 20 MeV for ^{3}H, ^{3}He and ^{4}He. In the present work the extension of the ^{4}He evaluation to 60 MeV is described.

11.2 PROCEDURES

The ENDF/B-VII.1b4 evaluation is taken as a starting point. The evaluation was checked against the experimental data in the EXFOR database. Extension to each reaction was made as described below.

11.3 TOTAL CROSS SECTION

The data of Haesner [1], Shamu [2] and Battat [3] were considered. A curve was fitted manually through the data points, applying some ad-hoc smoothing. The data were extrapolated to 60 MeV such that the general trends of the cross section behaviour at lower energies were preserved. The total cross section plot is shown on Figure 1.

11.4 ELASTIC CROSS SECTION

The competing (n,d) reaction is significant only at the 22.2 MeV peak and the (n,2n) reaction has a threshold at about 25 MeV and is much smaller than the elastic cross section, therefore the elastic cross section is practically equal to the total cross section.

11.5 ELASTIC ANGULAR DISTRIBUTIONS

Above 20 MeV measurements by Shamu [2] are available and they extend up to 23.7 MeV. The plots of the angular differential cross sections are shown on Figures 2 and 3. At 60 MeV the measured data by Arnold [4] are available. Legendre Polynomial expansion was fitted to the data. The fit is shown in Fig. 4. The evaluated angular differential cross sections between 20 MeV and 60 MeV were obtained by linear interpolation. The agreement with measured data at 23.7 MeV can be seen on Fig. 3.

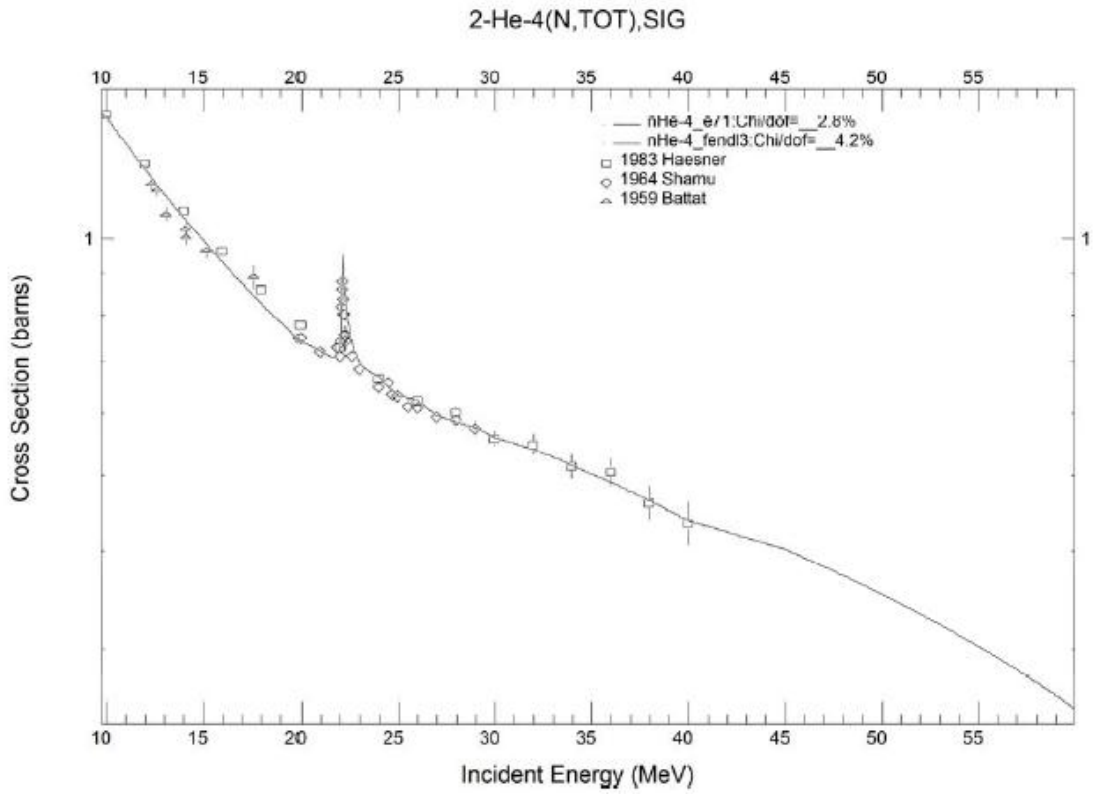

FIG. 1. Total cross section of ^{4}He extended to neutron incident energies up to 60 MeV.

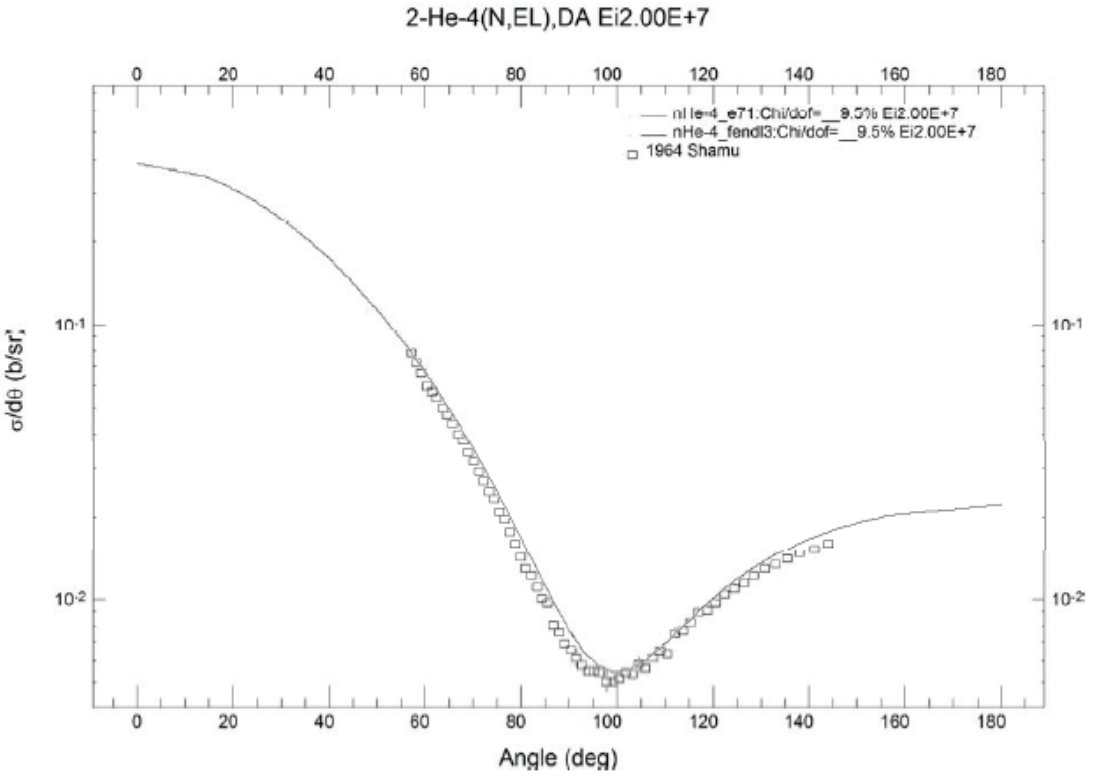

FIG. 2. Differential elastic cross section of ^{4}He for incident neutrons of 20 MeV.

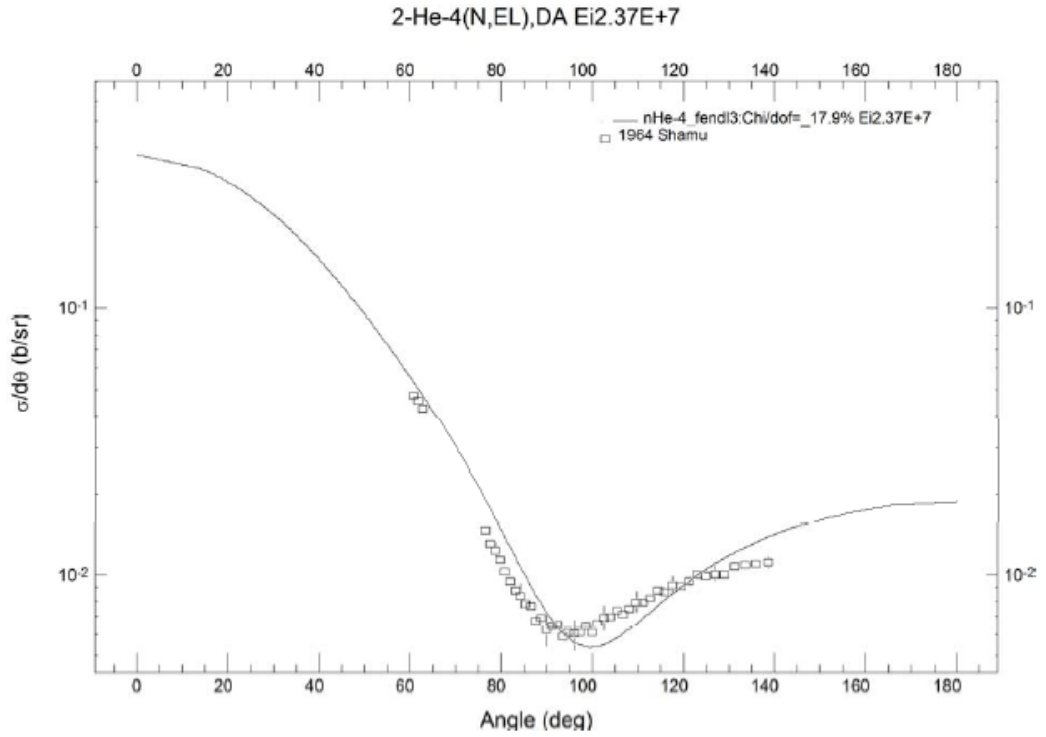

FIG. 3. Differential elastic cross section of ^{4}He for incident neutrons of 23.7 MeV.

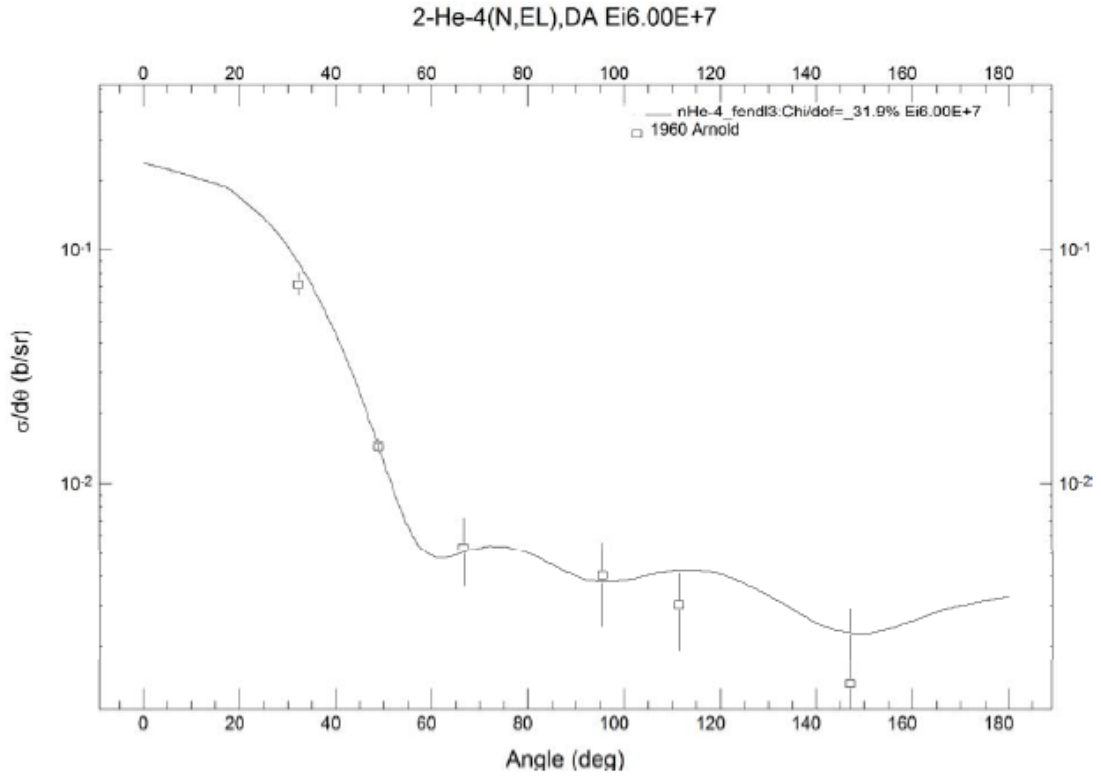

FIG. 4. Differential elastic cross section of ^{4}He for incident neutrons of 60 MeV

11.6 TWO-NEUTRON EMISSION CROSS SECTION

The two-neutron emission cross section has a threshold of 25.67 MeV and is not present in any of the evaluated nuclear data libraries, except the special library for activation EAF-2010 [5]. The cross sections from this library were adopted, which have a peak of 3.5 mb at around 54 MeV. The angular distributions of the emitted neutrons were assumed isotropic in the laboratory system. The emitted neutrons were assumed to follow the distribution of an evaporation spectrum with an effective temperature of 900 keV.

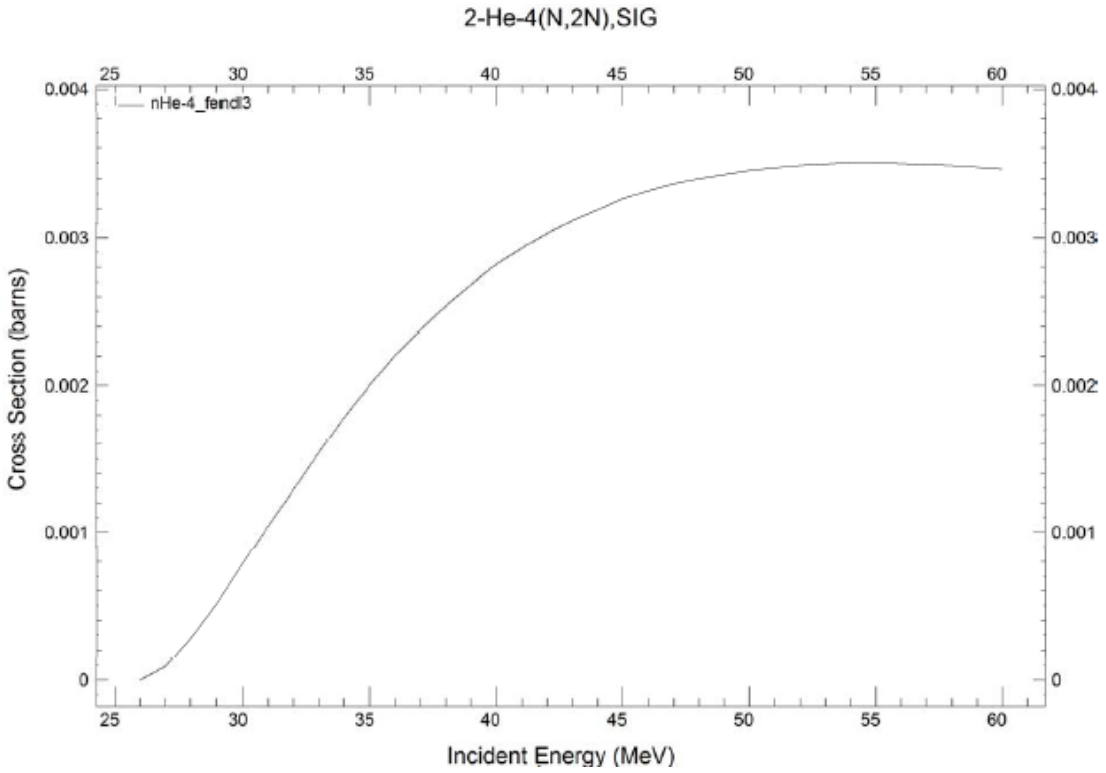

FIG. 5. The (n,2n) reaction cross section of ^{4}He.

11.7 DEUTERON EMISSION CROSS SECTION

Deuteron emission cross section has a threshold of 22.02 MeV and is not present in any of the evaluated nuclear data libraries, including EAF-2010. However, the experimental data by Shamu [2] include the $^{4}He(n,d)^{3}H$ reaction in the peak of the resonance at 22.2 MeV. The data were entered into the ENDF file, extrapolating the cross section to 60 MeV by following the trend of the last four measured points on log-log scale. The cross section is shown in Fig. 6. No emission spectra and angular distributions of deuterons and tritons are given.

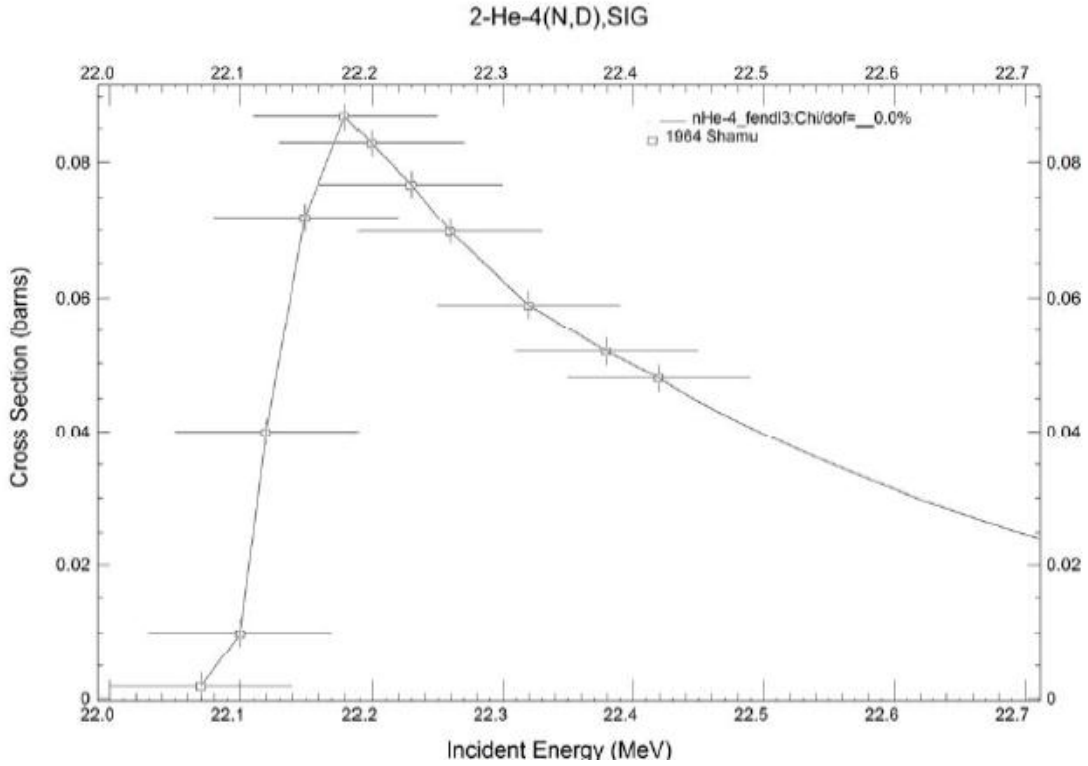

FIG. 6. The (n,d) reaction cross section of ^{4}He.

11.8 VERIFICATION

The CHECKR code reported no problems. Fizcon reports that for MT=15 in MF=5 the value of U is not consistent. It seems likely that this is a false message because FIZCON compares (Q+U)/Q to a tolerance of 10^{-3}, but U is given in the laboratory system while the Q-value is defined in the centre-of-mass system. The PSYCHE code does not report problems either.
Processability of the file is checked by running the codes of the PrePro-2010 series including LINEAR, RECENT, SIGMA1 and FIXUP. Further testing is done by running NJOY to generate an ACE library for Monte Carlo codes like MCNP and a MATXS library for deterministic codes. The heating curve generated by the HEATR module is useful for checking potential energy-balance problems and is shown in Fig. 7. The figure did not reveal any problems. The plots produced by the ACER module also showed nothing suspicious and are not presented.

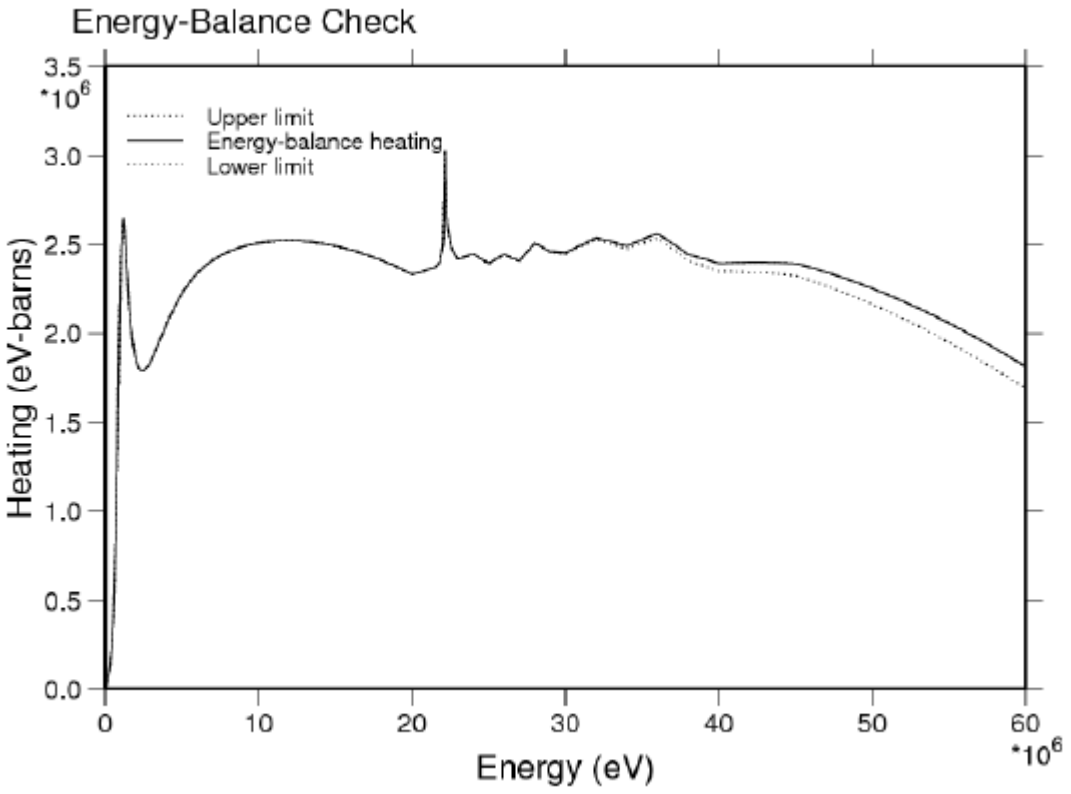

FIG. 7. Plot of the heating calculated by the HEATR module of NJOY.

11.9 CONCLUSIONS

A viable evaluated nuclear data file for ^{4}He for incident neutron energies up to 60 MeV was produced for inclusion in the FENDL-3 library by extending the ENDF/B-VII.1b4 evaluation. The extension is based on ad-hoc methods and cannot compete with evaluations based on rigorous R-matrix analysis such as announced by G. Hale from the Los Alamos National Laboratory, but the data from that evaluation above 20 MeV have not been released and are not likely to be available before the release of FENDL-3.

References for Section 11

[1] B. Haesner, W. Heeringa, H.O. Klages, H. Dobiasch, G. Schmalz, P. Schwarz, J. Wilczynski, B. Zeitnitz, F. Kappeler, Phys. Rev. **C 28** (1983) 995, EXFOR 21883.
[2] R.E. Shamu, J.G. Jenkin, Phys. Rev. **135** (1964) B99, EXFOR 30405.
[3] M.E. Battat, R.O. Bondelid, J.H. Coon, L. Cranberg, R.B. Day, F. Edeskuty, A.H. Frentrop, R.L. Henkel, R.L. Mills, R.A. Nobles, J.E. Perry, D.D. Phillips, T.R. Roberts, S.G. Sydoriak, Nucl. Phys. **12** (1959) 291, EXFOR 11021.
[4] M. Arnold, P.E. Hodgson, D.F. Shaw, D.M. Skyrme, Nucl. Phys. **19** (1960) 500, EXFOR 21152.
[5] EAF-2010 European Activation Library.

12. Validation of FENDL-3/A Library Using Integral Measurements (J. Kopecky)

A full description of the validation of the activation part of FENDL-3 has already been published [1].

[1] J. Kopecky, "Validation of FENDL-3/A Library using Integral Measurements", INDC(NED)-011, IAEA Nuclear Data Section, August 2012.

13. Benchmarking of FENDL-3A Library (U. Fischer et al.)

A full description of the benchmarking is under preparation and will be published in the near future [1].

[1] U. Fischer, *et al*., "FENDL-3 Benchmarking report", INDC(NDS)-631, IAEA Nuclear Data Section, In preparation.

14. LIST OF PARTICIPANTS IN THE COORDINATED RESEARCH PROJECT (CRP)

Dr Ulrich FISCHER	Institute for Neutron Physics and Reactor Technology, Karlsruhe Institute of Technology, Germany
Dr Ferenc TÀRKÀNYI	Institute for Nuclear Research, Hungarian Academy of Sciences, Hungary
Dr Paola BATISTONI	Centro Ricerche Energia Frascati, ITaly
Dr Yukinobu WATANABE	Interdisplinary Graduate School of Engineering Sciences, Kyushu University, Japan
Dr Hyeong KIM	Korea Atomic Energy Research Institute, Korea, Republic of
Dr Jiri KOPECKY	JUKO Research, Netherlands
Dr Arjan KONING	NRG Nuclear Research and Consultancy Group, Netherlands
Dr Marilena AVRIGEANU	Institut de Fizica si Inginerie Nucleara "Horia Hulubei, Romania
Dr Anatoly IGNATYUK	Institute for Physics and Power Engineering, Russian Federation
Dr Andrej TRKOV	Jozef Stefan Institute, Slovenia
Dr Jean-Christophe SUBLET	Culham Centre for Fusion Energy, United Kingdom
Dr Toshihiko KAWANO	Los Alamos National Laboratory, United States of America
Dr Constance KALBACH WALKER	Duke University, United States of America
Dr Mohamed SAWAN	Fusion Technology Institute, University of Wisconsin, United States of America

Nuclear Data Section
International Atomic Energy Agency
Vienna International Centre, P.O. Box 100
A-1400 Vienna, Austria

E-mail: nds.contact-point@iaea.org
Fax: (43-1) 26007
Telephone: (43-1) 2600 21725
Web: http://www-nds.iaea.org